



UNIVERSIDAD  
DE GRANADA



**CSIC**  
CONSEJO SUPERIOR DE INVESTIGACIONES CIENTÍFICAS

CHEMOTAXIS IN  
*Pectobacterium*  
*atrosepticum* SCRI1043

FUNCTIONAL AND STRUCTURAL STUDIES ON CHEMOTAXIS  
ADAPTATION PROTEINS AND CHEMORECEPTORS

Félix Velando Soriano

Tesis Doctoral

2023

Editor: Universidad de Granada. Tesis Doctorales  
Autor: Félix Velando Soriano  
ISBN: 978-84-1195-067-1  
URI: <https://hdl.handle.net/10481/85094>

**CHEMOTAXIS IN *Pectobacterium atrosepticum*  
SCRI1043: FUNCTIONAL AND STRUCTURAL  
STUDIES ON CHEMOTAXIS ADAPTATION PROTEINS  
AND CHEMORECEPTORS**

Doctoral Thesis  
Granada, 2023

Programa de Doctorado en Biología Fundamental y de  
Sistemas

*Doctorate Program of Fundamental and Systems Biology*



**UNIVERSIDAD  
DE GRANADA**

**Doctoral Candidate**  
**Félix Velando Soriano**

**Thesis Supervisors**  
**Prof. Tino Krell**  
**Dr. Miguel A. Matilla**

Estación Experimental del Zaidín  
Consejo Superior de Investigaciones Científicas - *Spanish*  
*National Research Council*



**CSIC**

CONSEJO SUPERIOR DE INVESTIGACIONES CIENTÍFICAS



**KRELL  
LABORATORY**

---

## Agradecimientos

---

A pesar de todo, parece que he llegado al final. Durante el tiempo que he estado en el laboratorio trabajando para sacar esta tesis adelante, he perdido a mi padre y esto ha marcado profundamente mi vida. Por eso, me gustaría agradecerle a él todo el apoyo que me dio mientras estuvo aquí, y cómo me sigue demostrando que está de algún modo. Esta tesis, tal como le dije aquel día, está dedicada a él. Espero que esté orgulloso.

A mi madre, quiero darle gracias infinitas por todo lo que ha hecho y hace siempre por mi y por nuestra familia. Creo que he pasado muchos años sin notar que la vocación y la ciencia siempre han formado parte de ella, que publicó su tesis con tres hijos, ni más, ni menos. A mis hermanos, gracias por estar siempre, por nuestras semejanzas, y por nuestras diferencias.

Gracias, Elena, por aparecer, volver o venir a mi vida, por tu forma de ser, tu punto de vista y tus emociones y pensamientos, y por tus ganas. Por hacer un futuro, un principio y un proyecto. Y a mi pequeña Marina, porque ahora las cosas se ven de otra manera, y esto no es más que el principio.

Y gracias a toda la gente con la que he compartido horas, alegrías y penas, en los laboratorios, en la cafetería, jardines y salas de la EEZ, y que han puesto su granito de arena para ayudarme a llegar a este momento. Seguro que me dejo gente, pero quiero nombrar agradecido a María, Joaquín, Pacheco, Sophie, Patri, Alicia, Paul, Eli, Jesús, David, Miriam, Roberta, Ana, Cristina y Rafa.

Finalmente, gracias también a mis directores de tesis, Tino y Miguel, por su ayuda estos cinco años que he pasado en el mundo de las proteínas.

# TABLE OF CONTENT

---

Figure Index.....	v
Table Index.....	vii
Supplementary Figures Index.....	vii
Supplementary Tables Index.....	viii
List of Abbreviations.....	xi
General Abstract .....	xiv
<b>INTRODUCTION .....</b>	<b>1</b>
1. Bacterial signal transduction systems .....	1
2. Chemoreceptors.....	5
3. The <i>E. coli</i> chemosensory pathway as paradigm in the field .....	11
4. Adaptation mechanisms in bacterial chemotaxis .....	13
5. Sensing mechanisms in chemoreceptors .....	17
6. Physiological roles of chemotaxis .....	21
7. Soft Rot <i>Pectobacteriaceae</i> (and <i>Pectobacterium atrosepticum</i> ) .....	27
<b>OBJECTIVES .....</b>	<b>33</b>
<b>METHODOLOGY .....</b>	<b>35</b>
<b>RESULTS .....</b>	<b>39</b>
<b>Chapter 1. Evidence for pentapeptide dependent and independent CheB methylesterases....</b>	<b>41</b>
Abstract.....	41
Introduction .....	43
Materials and Methods.....	46
Results.....	49
Discussion.....	56
Supplementary Material .....	59
<b>Chapter 2. Differential occupation of chemoreceptors with CheR as a potential mechanism to bias chemotactic responses. ....</b>	<b>71</b>
Abstract.....	71
Introduction .....	72
Materials and Methods.....	73
Results.....	77
Discussion.....	82
Supplementary Material .....	84

<b>Chapter 3. The chemoreceptor PacA of <i>Pectobacterium atrosepticum</i> is homologous to PctD of <i>Pseudomonas aeruginosa</i> PAO1 and mediates taxis to quaternary amines.....</b>	<b>89</b>
Abstract .....	89
Introduction .....	92
Materials and methods .....	94
Results .....	97
Discussion.....	105
Supplementary Material .....	109
<b>Chapter 4. Identification of three chemoreceptors for amino acids in <i>Pectobacterium atrosepticum</i>SCRI1043. Basis for broad-spectrum amino acid chemotaxis .....</b>	<b>120</b>
Abstract .....	120
Introduction .....	122
Materials and Methods.....	124
Results .....	126
Discussion.....	134
Supplementary material .....	137
<b>Chapter 5. Identification of a receptor family that recognizes specifically phosphorylated compounds. ....</b>	<b>142</b>
Abstract .....	142
Introduction .....	143
Materials and Methods.....	144
Results .....	146
Discussion.....	152
Supplementary material .....	154
<b>GENERAL DISCUSSION .....</b>	<b>158</b>
<b>CONCLUSIONS .....</b>	<b>172</b>
<b>REFERENCES .....</b>	<b>174</b>

## Figure Index

---

Figure 1. Overview of bacterial signaling systems.....	4
Figure 2. Molecular architecture of a canonical chemoreceptor. ....	6
Figure 3. Members of some ligand binding domain families present in bacterial chemoreceptors.....	8
Figure 4. The <i>E. coli</i> chemosensory signaling arrays.....	12
Figure 5. Chemotactic behavior and signaling pathway.....	13
Figure 6. The adaptation mechanism in chemotaxis.....	14
Figure 7. 3D structure of CheR from <i>Salmonella enterica</i> ser. Typhimurium bound to S-adenosylmethionine (SAM) and the carboxy-terminal NWETF pentapeptide sequence of the Tar chemoreceptor. ....	16
Figure 8. The diversity of repellent and attractant sensing mechanisms in <i>B. subtilis</i> and <i>E. coli</i> chemoreceptors.....	20
Figure 9. The relevance of chemotaxis for plant pathogens.....	24
Figure 10. Bacterial blackleg and tuber soft rot symptoms caused by SRP on potato, including <i>P. atrosepticum</i> .....	28
Figure 11. Schematic representation of the chemotaxis system of <i>P. atrosepticum</i> SCRI1043.....	31
Figure 12. Gene clusters encoding chemosensory signaling proteins in <i>P. aeruginosa</i> PAO1 and <i>P. atrosepticum</i> SCRI1043.....	45
Figure 13. Specificity of the interaction between four CheB homologs of <i>P. aeruginosa</i> and the terminal pentapeptide GWEEF of the McpB chemoreceptor. ....	50
Figure 14. Quantitative capillary chemotaxis assays of wild type and mutant strains of <i>P. atrosepticum</i> SCRI1043 towards 0.1% (w/v) casamino acids.....	51
Figure 15. The chemoreceptor repertoire of <i>P. atrosepticum</i> SCRI1043. ....	52
Figure 16. C-terminal pentapeptides at <i>P. atrosepticum</i> chemoreceptors.....	53
Figure 17. The three-dimensional structure of <i>P. atrosepticum</i> CheB.....	54
Figure 18. Structural and sequence features related to the capacity of CheB to recognize C-terminal pentapeptides.....	56
Figure 19. C-terminal pentapeptides at <i>P. atrosepticum</i> SCRI1043 chemoreceptors.....	78
Figure 20. Binding of S-adenosylmethionine (SAM) and S-adenosylhomocysteine (SAH) to <i>P. atrosepticum</i> CheR.....	79
Figure 21. Interaction between <i>P. atrosepticum</i> pentapeptides with CheR.....	80
Figure 22. Quantitative capillary chemotaxis assays of wild type <i>P. atrosepticum</i> SCRI1043 and a mutant in <i>cheR</i> towards different chemoattractants.....	81
Figure 23. Determination of the cellular CheR concentration of <i>P. atrosepticum</i> SCRI1043 by immunoblot using polyclonal anti CheR antibodies. ....	82
Figure 24. Chemotaxis of <i>P. aeruginosa</i> PAO1 toward acetylcholine and related compounds. ....	97

Figure 25. Isothermal titration calorimetry study of the binding of different ligands to the ligand-binding domain of chemoreceptor PctD.....	99
Figure 26. Characterization of responses mediated by a PctD-Tar hybrid using FRET measurements in <i>E. coli</i> .....	100
Figure 27. The three-dimensional structures of the ligand binding domains of the PctD chemoreceptor of <i>P. aeruginosa</i> PAO1 in complex with acetylcholine and the PacA chemoreceptor of <i>P. atrosepticum</i> SCRI1043 in complex with betaine. ....	102
Figure 28. Isothermal titration calorimetry study of the binding of different ligands to the LBD of the <i>P. atrosepticum</i> SCRI1043 chemoreceptor ECA_RS10935 (PacA). ....	103
Figure 29. The molecular detail of signal recognition by the PctD and PacA chemoreceptors.....	104
Figure 30. Chemotaxis to acetylcholine in different bacterial species. ....	105
Figure 31. The three dCache_1 domain containing chemoreceptors of <i>P. aeruginosa</i> PAO1 that mediate chemotaxis to important neurotransmitters. ....	108
Figure 32. The chemoreceptor repertoire of <i>Pectobacterium atrosepticum</i> SCRI1043. ....	124
Figure 33. PacB is a broad ligand range chemoreceptor. ....	127
Figure 34. Quantitative capillary chemotaxis assays of <i>Pectobacterium atrosepticum</i> SCRI1043 and mutants deficient in the PacB and PacC chemoreceptors. ....	130
Figure 35. Isothermal titration calorimetry study of the binding of L-proline to the LBD of <i>Pectobacterium atrosepticum</i> SCRI1043 chemoreceptor PacA ....	131
Figure 36. PacC is a Tsr ortholog. ....	133
Figure 37. The Tsr ortholog PacC binds aspartate and asparagine but not serine. ....	134
Figure 38. Thermal shift assays of ECA_RS12390 (PacP-LBD) with the compounds of the Biolog array PM4A (phosphorous and sulfur sources). ....	146
Figure 39. Microcalorimetric titration of PacP-LBD with different phosphorylated compound .....	147
Figure 40. Summary of binding studies to PacP-LBD.....	148
Figure 41. Capillary chemotaxis assays of <i>P. atrosepticum</i> SCRI1043 containing the empty plasmid pBBR1MCS-2_START and its derivative pBBR1-PacP causing expression of chemoreceptor ECA_RS12390 (PacP).....	149
Figure 42. PacP homologs. ....	150
Figure 43. Microcalorimetric titration of the Ligand Binding Domain of chemoreceptor WP_158281851.1 from <i>Rivicola pingtungensis</i> with its different phosphorylated compounds.....	151
Figure 44. Sector diagram with the percentage of predicted sequences with the dCache_1AM motif according to their taxonomic classification. ....	162
Figure 45. Bayesian phylogenetic tree of amine and amino acid receptor sensory domains. ....	163
Figure 46. Sector diagram showing the percentage of the 85 identified SBPs in <i>P. atrosepticum</i> SCRI1043 genome predicted to recognize each class of ligands .....	166
Figure 47. Histogram representing some compounds that <i>P. atrosepticum</i> SCRI1043 can use as sole nitrogen source.....	168



## Table Index

---

Table 1. Summary of signals directly recognized by chemoreceptors. ....	18
Table 2. Binding parameters for the interaction of <i>P. atrosepticum</i> CheR with S-adenosylmethionine (SAM), S-adenosylhomocysteine (SAH) and pentapeptides. ....	80
Table 3. Thermodynamic parameters for the titration of <i>P. aeruginosa</i> PctD-LBD and <i>P. atrosepticum</i> PacA-LBD with different ligands.....	101
Table 4. Binding parameters derived from microcalorimetric titrations of the ligand binding domains of chemoreceptors PacA, PacB and PacC with different signal molecules. ....	129
Table 5. Results of microcalorimetric binding studies of phosphorylated compounds to the LBDs of different chemoreceptors.....	147
Table 6. Ligands identified for proteins with substitutions in the phosphorylated C3 compounds binding motif. ....	152

## Supplementary Figures Index

---

Figure S 1. Sequence alignment of CheB from <i>E. coli</i> K-12 substrain MG1655 and <i>S. enterica</i> serovar Typhimurium str. LT-2.....	59
Figure S 2. Microcalorimetric binding studies of the CheB2 D55E mutant with the McpB-derived pentapeptide GWEEF.....	60
Figure S 3. Alignment of the linker sequences of the 19 chemoreceptors from <i>Pectobacterium atrosepticum</i> containing terminal pentapeptides. ....	60
Figure S 4. Secondary structure prediction of the C-terminal segment of pentapeptide containing chemoreceptors of <i>P. atrosepticum</i> . ....	64
Figure S 5. Analysis of the structure of <i>P. atrosepticum</i> CheB. ....	64
Figure S 6. B-factors of Ca atoms of <i>P. atrosepticum</i> chain B. ....	65
Figure S 7. Structural superimposition of chain A of <i>P. atrosepticum</i> CheB with CheB of <i>S. enterica</i> sv. Typhimurium (pdb ID 1A2O).....	65
Figure S 8. Alignment of the linker sequences of the 19 chemoreceptors from <i>Pectobacterium atrosepticum</i> containing terminal pentapeptides ....	84
Figure S 9. Charge distribution at the cytosolic fragments of <i>P. atrosepticum</i> chemoreceptors.....	84
Figure S 10. Electron microscopy images of <i>Pectobacterium atrosepticum</i> SCRI1043 grown on minimal medium for approximately 5 hours (OD <sub>660</sub> =0.5).....	85
Figure S 11. Immunoblot of <i>P. atrosepticum</i> SCRI1043 samples and purified CheR using polyclonal antibodies against CheR.....	86
Figure S 12. Immunoblot calibration curve showing the integrated band densities for different amounts of purified <i>P. atrosepticum</i> CheR. ....	86
Figure S 13. Growth experiments with <i>P. aeruginosa</i> PAO1 .....	109

Figure S 14. Sequence alignments of the ligand binding domains of <i>P. aeruginosa</i> PAO1 chemoreceptor PctD (PA4633) with <i>S. meliloti</i> McpX (A), <i>P. atrosepticum</i> SCRI1043 ECA_RS05475 (B) and <i>P. atrosepticum</i> SCRI1043 chemoreceptor ECA_RS10935 (PacA)(C) .....	110
Figure S 15. Quantitative capillary chemotaxis assays of <i>P. aeruginosa</i> PAO1, a mutant in PA4633 ( <i>pctD</i> ) (A-D) and the mutant in PA4633 harboring different plasmids for complementation (E) .....	111
Figure S 16. FRET measurements of the Tar response to PctD chemoeffectors. ....	112
Figure S 17. Microfluidic assay of the chemotactic response of <i>E. coli</i> strain UU1250 expressing PctD-Tar as the sole receptor. ....	112
Figure S 18. Capillary chemotaxis assays of <i>P. atrosepticum</i> SCRI1043 to 1 mM choline, betaine, L-carnitine and acetylcholine.....	113
Figure S 19. Capillary chemotaxis assays of <i>P. atrosepticum</i> SCRI1043 containing the empty plasmid pBBR1MCS-2_START and its derivative pBBR_ECA_RS10935 causing expression of chemoreceptor ECA_RS10935 (PacA).....	113
Figure S 20. Sequence of the ECA_RS05475 (PacB) chemoreceptor of <i>P. atrosepticum</i> SCRI1043. ....	137
Figure S 21. Quantitative chemotaxis capillary assays of <i>P. atrosepticum</i> SCRI1043 containing the empty plasmid pBBR1MCS-2_START and plasmid pBBR_ECA_RS10935 (harboring the <i>pacA</i> gene) towards 1 mM L-proline. ....	137
Figure S 22. Sequence alignment of the ligand binding domains of the <i>E. coli</i> Tar and <i>P. atrosepticum</i> PacC (ECA_RS08370) chemoreceptors .....	138

## Supplementary Tables Index

---

Table S 1. Strains and plasmids used in Chapter 1. ....	66
Table S 2. <i>P. atrosepticum</i> SCRI1043 chemoreceptors with a C-terminal pentapeptide. ....	67
Table S 3. Structural alignment of chains A to E of <i>P. atrosepticum</i> CheB amongst each other and with related structures. ....	68
Table S 4. Oligonucleotides used in Chapter 1. ....	69
Table S 5. Data collection and refinement statistics of the 3D structure of <i>P. atrosepticum</i> CheB. ....	70
Table S 6. The sequence-derived pI values of linker and pentapeptide sequences of the 19 pentapeptide containing chemoreceptors of <i>P. atrosepticum</i> .....	87
Table S 7. Strains and plasmids used in Chapter 2. ....	88
Table S 8. Oligonucleotides used in Chapter 2. ....	88
Table S 9. Results from structural alignments of the PctD-LBD structure (in complex with acetylcholine) and the PacA-LBD structure (in complex with betaine) with structures deposited in the Protein Data Bank .....	114
Table S 10. Strains, plasmids and oligonucleotides used in Chapter 3. ....	116
Table S 11. Crystallization conditions, data collection and refinement statistics of the PctD-LBD and PacA-LBD three-dimensional structures. ....	118
Table S 12. Strains and plasmids used in Chapter 4. ....	139

Table S 13. Oligonucleotides used in Chapter 4 .....	140
Table S 14. Strain, plasmids and oligonucleotides used in Chapter 5. ....	154
Table S 15. Composition and pH of purification and analysis buffers used for the different LBDs analysed in this study.....	155
Table S 16. Amino acid sequence of the proteins purified for calorimetric studies, consisting of the LBDs predicted as PacP homologs plus a His Tag. ....	156



## List of Abbreviations

<b>4HB</b>	Four (4) helix bundle
<b>Acf</b>	Alternative cellular functions
<b>Aer</b>	Aerotaxis
<b>AI-2</b>	Autoinducer 2
<b>Cache</b>	Ca <sup>2+</sup> channels and chemotaxis
<b>cAMP</b>	Cyclic adenosine monophosphate
<b>CCW</b>	Counter-clockwise
<b>c-di-GMP</b>	Cyclic-di-guanosine monophosphate
<b>Cfu</b>	Colony-forming unit
<b>CHASE</b>	Cyclases/Histidine kinases associated sensory extracellular
<b>Che</b>	Chemotaxis
<b>CheB_Pec</b>	CheB of <i>Pectobacterium atrosepticum</i> SCRI1043
<b>CheR_Pec</b>	CheR of <i>Pectobacterium atrosepticum</i> SCRI1043
<b>Chp</b>	Chemosensory pili
<b>C-terminal</b>	Carboxy-terminal
<b>Cryo-EM</b>	Cryo-Electron Microscopy
<b>CW</b>	Clockwise
<b>CZB</b>	Chemoreceptor zinc-binding
<b>DHMA</b>	3,4-dihydroxymandelic acid
<b>EDTA</b>	Ethylenediaminetetraacetic acid
<b>FAD</b>	Flavin adenine dinucleotide
<b>Fla</b>	Flagellar
<b>FMN</b>	Flavin mononucleotide
<b>G2P</b>	Glycerol 2-phosphate
<b>G3P</b>	Glycerol 3-phosphate
<b>GABA</b>	γ-amino butyric acid
<b>GAF</b>	cGMP-specific phosphodiesterases, adenyl cyclases and FhIA
<b>Gal3P</b>	Glyceraldehyde 3-phosphate
<b>GPCR</b>	G-protein-coupled receptor
<b>HAI</b>	Horizontally acquired island
<b>HAMP</b>	Histidine kinases, adenylate cyclases, methyl-accepting proteins and phosphatases
<b>HBM</b>	Helical bimodular
<b>HTH</b>	Helix-Turn-Helix
<b>HK</b>	Histidine kinase (Sensor kinase)
<b>IPTG</b>	Isopropyl-β-D-1-thiogalactopyranoside
<b>ITC</b>	Isothermal titration calorimetry
<b>LBD</b>	Ligand binding domain
<b>Mcp</b>	Methyl-accepting chemotaxis protein
<b>NAD</b>	Nicotinamide adenine dinucleotide
<b>NIT</b>	Predicted nitrate and nitrite sensing
<b>N-terminal</b>	Amino-terminal
<b>OCS</b>	One-Component System
<b>PAB</b>	Plant-associated bacteria
<b>PAS</b>	Per-Arnt-Sim
<b>Pba</b>	<i>Pectobacterium atrosepticum</i>
<b>PCR</b>	Polymerase chain reaction
<b>PCWDEs</b>	Plant cell wall degrading enzymes

<b>PDB</b>	<u>Protein Data Bank</u>
<b>PilJ</b>	Type IV Pili methyl-accepting chemotaxis transducer
<b>Rcsv</b>	<u>Rugose small-colony variants</u>
<b>REC</b>	<u>Receiver</u>
<b>Rmsd</b>	<u>Root mean square deviation</u>
<b>RR</b>	<u>Response regulator</u>
<b>SAM</b>	<u>S-adenosylmethionine</u>
<b>SAH</b>	<u>S-adenosylhomocysteine</u>
<b>SBP</b>	<u>Solute binding protein</u>
<b>SRP</b>	<u>Soft-Rot <i>Pectobacteriaceae</i></u>
<b>T1SS</b>	<u>Type-1 secretion system</u>
<b>T6SS</b>	<u>Type-6 secretion system</u>
<b>TarH</b>	<u>Tar homologue</u>
<b>Tca</b>	<u>Tricarboxylic acid</u>
<b>TCS</b>	<u>Two-Component System</u>
<b>Tfp</b>	<u>Type-IV pili</u>
<b>T<sub>m</sub></b>	<u>Denaturation midpoint temperature</u>
<b>TM</b>	<u>Trans-membrane</u>
<b>Wsp</b>	<u>Wrinkly spreader phenotype</u>
<b>Wt</b>	<u>Wild type</u>



## General Abstract

---

Bacteria possess different systems to sense and respond to environmental signals. One-component systems, two-component systems and chemosensory pathways are the most commonly found. While one- and two-component systems mainly control gene expression and are present in all bacteria we currently know, chemosensory pathways are approximately found in half of the bacterial genomes described to date and primarily mediate chemotaxis.

The core of a chemosensory pathway is the ternary complex formed by chemoreceptors, the CheA autokinase and the CheW coupling proteins. Chemoreceptors sense ligands and modulate CheA activity, leading to transphosphorylation of the response regulator CheY. CheY-P interacts with the flagellar motor, and this results in chemotaxis, or movement towards or away of compounds. In this process, adaptation proteins are important to enable bacteria to react appropriately to physicochemical gradients. These adaptation proteins, CheR and CheB, are tasked with methylation and demethylation of chemoreceptors, respectively; a mechanism that causes changes in their sensitivity to their cognate ligands.

A canonical chemoreceptor typically consists of: (i) a periplasmic ligand binding domain; (ii) a transmembrane module; and (iii) a cytoplasmic signaling domain. Chemoreceptor genes are easy to predict bioinformatically, but the function and signals recognized for most of them remain unknown. Plant-associated bacteria have a higher number of chemoreceptors than bacteria inhabiting other niches, and exploring the function of these receptors can help to understand the evolutionary pressures that have driven chemoreceptor evolution in this particular ecological niche.

In this thesis, the enterobacterium *Pectobacterium atrosepticum*, a phytopathogen of global relevance, was used as a model to explore chemotaxis. Strain SCRI1043 has a single chemosensory pathway and 36 chemoreceptors. Interestingly, 19 of them present carboxy-terminal pentapeptides, which, in *Escherichia coli* and other species, were found to function as docking sites for the adaptation enzymes, CheB and CheR.

I demonstrated that the chemosensory pathway of *P. atrosepticum* SCRI1043 regulates chemotaxis and characterised the interaction between CheR/CheB and the chemoreceptors and identified the function of four chemoreceptors that were termed PacA, PacB, PacC and PacP. I found that CheR of SCRI1043 (CheR\_Pec) binds, with different affinities, all 9 different C-terminal pentapeptides present in the chemoreceptors of this strain. In addition, I showed that the cellular concentration of CheR\_Pec is subject to changes during growth and is in the range of the  $K_d$  values for the interaction of CheR with the different pentapeptides, suggesting a new mechanism of regulation of the chemotactic output. Contrary to these results, CheB of SCRI1943 (CheB\_Pec) is unable to bind pentapeptides, and solving the three-dimensional structure of CheB\_Pec by X-ray crystallography revealed that the region corresponding to the pentapeptide binding site in the *E. coli* CheB is disordered in CheB\_Pec, which most likely accounts for the lack of pentapeptide binding. These results supported that CheB methylsterases can be divided into pentapeptide dependent and independent enzymes.

PacA was functionally described as a chemoreceptor with a dCache ligand binding domain that binds and mediates chemotaxis towards quaternary amines (e.g. choline, betaine, L-carnitine) and the amino acid L-proline. During this thesis, the three-dimensional structure of the sensor



domain of PacA was solved. Through comparison with that of the sensor domain of the PctD chemoreceptor of *Pseudomonas aeruginosa*, a receptor that has a similar profile of ligands, but which also recognizes the neurotransmitter acetylcholine, progress was made towards understanding quaternary amines binding by dCache domains.

Along with PacA, I described two additional chemoreceptors of SCRI1043 that recognize amino acids, indicating that amino acids are important signals for bacteria. PacB has a dCache ligand binding domain that recognizes a wide range of proteinogenic and non-proteinogenic amino acids. Instead, PacC, the sole chemoreceptor encoded in the chemotaxis gene cluster, was shown to be homologous to the Tsr chemoreceptor of *E. coli*, but was shown to bind and mediate taxis to D- and L- aspartate and L-asparagine. Its evolutionary history was described in this thesis. Finally, PacP, the only chemoreceptor with a sCache domain in SCRI1043, was described as the first identified chemoreceptor for phosphorylated compounds. PacP binds compounds related to the glycolysis as well as glycerol 3-phosphate and glycerol 2-phosphate. It is shown here that it is part of a family of chemoreceptors that primarily recognize glycerol 3-phosphate - a potential stress signal in plants. Evolutionary analyses revealed that this subfamily of chemoreceptors originated from sCache domains that recognize organic acids. It was concluded that the recognition of families of homologous proteins with similar ligand binding capabilities from *in silico* docking analyses is a promising tool to rapidly increase knowledge about sensing capabilities of all kinds of bacterial receptors.

Overall, the findings in this thesis have led to significant advances in the knowledge of the chemotactic capacities of the important phytopathogen *P. atrosepticum*, including the function of several chemoreceptors and how the adaptation enzymes CheR and CheB recognize chemoreceptors. The role of chemotaxis in plant colonization and disease development by *P. atrosepticum* is now open for scientific experimentation, and insights gleaned on this thesis can be applied to other soft rot *Pectobacteriaceae* species. Collectively, soft rot *Pectobacteriaceae* phytopathogens have a great impact on a wide range of crops and plants worldwide. Future work will allow the characterization of new chemoreceptor proteins of *P. atrosepticum*, as well as describe their homologue families in other species, thereby facilitating progress in the study of bacterial sensing and signaling mechanisms.



# INTRODUCTION

---

## 1. **Bacterial signal transduction systems**

Live organisms are entities composed of cells that maintain homeostasis and undergo metabolism, have a life cycle, adapt to their environment, respond to stimuli, reproduce and evolve. Bacteria and archaea are unicellular organisms that appeared as the first forms of life on Earth, roughly 4350 million years ago. Nowadays, every ecological niche available in our planet harbors bacterial life. This includes all the parts of the biosphere, including soil, hot springs, the ocean floor, acid lakes, deserts, geysers, rocks, plants and animals and to some extent in the troposphere (Whitman *et al.*, 1998; Flemming and Wuertz, 2019). As they started to proliferate, bacteria evolved different signal transduction systems to fulfill their need to sense stimuli and adapt to specific environments. Signal transduction, also known as cell signaling, is the transmission of information (in the form of molecular signals or other physicochemical stimuli) through a cell, triggering appropriate physiological responses. The basis for signal transduction is the transformation of a certain stimulus, that can be extracellular cues or intracellular events, into a biochemical signal (Galperin, 2004). Bacteria, in this way, are able to interact with their surroundings, exchanging information with other cells, from the same or different species, interacting with organisms from other life kingdoms in very diverse ways, exploring optimal growth conditions and sensing and responding to various biotic or abiotic stresses (Ostovar *et al.*, 2020).

While eukaryotic signal transduction involves more complex cascades initiated by G-protein coupled receptors and ion channels, prokaryotes employ simpler signal transduction systems. This sensing is achieved in bacteria through an array of proteins that can be conceptually conceived as molecular antennas that sense intracellular and environmental signals. Proteins then translate this information to a molecular response. Sensor and output proteins can be domains of the same polypeptide or separated diffusible proteins that interact specifically (Imelio *et al.*, 2021). Signaling systems described in bacteria comprise three main families, namely cytosolic transcriptional regulators (also known as one-component systems), two-component systems and chemosensory pathways. In addition, there are additional systems like phosphoenolpyruvate:sugar phosphotransferase systems, adenylate cyclases and cAMP phosphodiesterases, diguanylate cyclases and c-di-GMP phosphodiesterases, extracytoplasmic function sigma factors as well as Ser/Thr/Tyr protein kinases and phosphatases (Galperin, 2018; Matilla *et al.*, 2022a). A comprehensive knowledge of all these signal transduction systems may be at our reach: human cells encode more than 600 protein kinases and 800 G-protein-coupled receptors (GPCRs), but bacteria have far fewer signaling proteins, and progress in elucidating their functions is steady and incremental (Galperin, 2018).

### 1.1. **One-Component Systems**

Most of these systems are so-called transcriptional regulators composed of at least two functional elements, an input and an output domain. The input domain is tasked with binding intracellular ligands (and those that are extracellular but can diffuse across the membrane). On

the other hand, the output domain has DNA binding activity, achieved by a motif called Helix-Turn-Helix (HTH) (Figure 1). The output of this binding is a temporary change in transcription activity of target genes as these proteins are the major regulators of transcription in bacteria (Ulrich *et al.*, 2005). However, there are also One-Component Systems (OCS) whose output is another regulatory action (e.g., protein phosphorylation, regulation of intracellular second messenger levels). OCS are considered ancestral signaling systems and are present in Bacteria and Archaea, displaying a huge diversity of ligand binding domains (LBDs) – diversity that is richer than in Two-Component Systems (Ulrich *et al.*, 2005).

### 1.2. Two-Component Systems

Two-Component Systems (TCS) based signaling is the primary mechanism of transmembrane signaling in bacteria (Wuichet and Zhulin, 2010). They have been found in the genomes of nearly all sequenced bacteria, with the majority of species encoding dozens, and sometimes hundreds, of TCSs (Capra and Laub, 2012; Gumerov *et al.*, 2020). These systems are also present in Archaea and Eukarya (Kabbara *et al.*, 2019), but to a lesser degree, suggesting a latter appearance than transcriptional regulators. A canonical TCS is composed of a histidine sensor kinase (HK) and a response regulator (RR). The canonical sensor kinase is a transmembrane protein with an extracytosolic LBD in between two transmembrane regions and an autokinase domain able to interact with the RR located in the cytoplasm (Figure 1). Typically, signal binding to the LBD of the HK modulates the auto-phosphorylation of a specific histidine residue that modulates in turn the transphosphorylation kinetics to the receiver domain of the cognate RR. This phosphorylation occurs on an aspartate residue and results in the modulation of the activity of the output domain of the RR (Zschiedrich *et al.*, 2016). Frequently, HKs can also act as phosphatases for their cognate RRs (Igo *et al.*, 1989). In most cases, a HK will phosphorylate a single cognate RR, forming an exclusive one-to-one signaling pair. However, in other cases, cells exhibit many-to-one and one-to-many relationships, like the multiple HKs that phosphorylate the Spo0F RR to drive the initiation of *Bacillus subtilis* sporulation, or in *Vibrio harveyi*, where multiple HKs converge on the histidine phosphotransferase LuxU, a hybrid RR that can transfer the phosphoryl group in additional reactions to regulate the quorum sensing response (Laub, 2010).

The majority of output domains in RRs are predicted to regulate DNA transcription (Galperin, 2006; Gumerov *et al.*, 2020). Other RRs directly carry out enzymatic reactions like synthesis/hydrolysis of cAMP or c-di-GMP (Gao and Stock, 2009; Galperin, 2010). Furthermore, there are many variations to the domain composition and mechanism of canonical TCSs; such as HKs with multiple LBDs or located entirely in the cytosol, TCSs that employ multi-step phosphorelays or phosphorylation among sensor kinases (Stephenson and Hoch, 2002; López-Redondo *et al.*, 2010; Zschiedrich *et al.*, 2016).

### 1.3. Chemosensory Pathways

In bacteria, three principal functional groups of chemosensory pathways have been described based on genomic studies (Wuichet and Zhulin, 2010): those that evolve to control flagellar motility (Fla), Type IV pili-based motility (Tfp) and alternative (non-motility) cellular functions (ACF), for example, controlling second messenger (e.g., c-di-GMP, cAMP) levels. The Fla group seems very diverse, with seventeen distinct classes (F1-F17), constituting by far the most

abundant group, while each of the other two groups contained a single class (Gumerov *et al.*, 2021). However, the family of chemosensory systems carrying ACFs is heterogeneous as shown by the diversity of domain arrangements of CheY proteins that mediate the response output (Wuichet and Zhulin, 2010).

Chemotaxis allows motile bacteria to migrate towards environments that are favorable for growth and survival (Hazelbauer, 2012; Colin *et al.*, 2021). Physiologically favorable conditions are sensed as spatial gradients of chemical compounds, pH, osmolarity, redox potential or temperature. Temporal sensing allows bacteria to move through these gradients to the most desirable location (Macnab and Koshland Jr, 1972). In *Escherichia coli*, the primary model species to investigate chemotaxis, this is achieved by a biased random walk that arises from alternating straight swimming with brief directional changes (Berg and Brown, 1972). The signaling pathway that mediates this chemotactic behavior is largely conserved among prokaryotes and is present in approximately half of the known genomes, with *E. coli* chemotaxis system being one of the simplest and the best studied, representing an ideal model that illustrates fundamental principles of biological signaling processes.

Chemotaxis systems are one of the most complex bacterial signaling systems and it has been proposed that they evolved from TCSs (Wuichet and Zhulin, 2010). In fact, intermediate systems between chemotaxis systems and TCSs have been discovered (Hazelbauer and Lai, 2010). Chemotaxis systems can be described as a TCS whose performance is enhanced by additional signaling components providing features of signal amplification, sensory adaptation, molecular memory and a wide dynamic range (Bi and Lai, 2015). Moreover, chemoreceptors and other types of transmembrane receptors share at times a same LBD that recognize the same ligand, indicating that a given stimulus can be sensed through different signal transduction pathways (Zhulin *et al.*, 2003). For example, the NarQ HK and the McpN chemoreceptor both have a nitrate binding PilJ domain. The effect of nitrate binding to NarQ and McpN is either transcriptional regulation or nitrate chemoattraction, respectively (Gushchin *et al.*, 2017; Martín-Mora *et al.*, 2019).

Approximately half of bacterial genomes have chemosensory signaling proteins (Wuichet and Zhulin, 2010). Chemoreceptors, CheA, and CheW are present in >95% of genomes that contain at least one chemotaxis gene. Additionally, CheB and CheR are found in ~90% of genomes with chemotaxis components. This set of conserved proteins from the core chemosensory pathway is also likely to include CheY, which could not be included in this analysis because it cannot be distinguished from other single-domain response regulators on the basis of sequence alone (Wuichet and Zhulin, 2010). Although it is also well established that chemosensory systems typically mediate chemotaxis, as previously mentioned, they can also feed into systems with alternative functions, such as type IV pili-based motility or the control of second messenger levels (Hickman *et al.*, 2005; Willett and Kirby, 2011; Matilla *et al.*, 2021a). For example, in *Pseudomonas* species, the Wsp chemosensory pathway senses cell-envelope stress and activates the diguanylate cyclase WspR to ultimately increase intracellular c-di-GMP levels promoting cell aggregation and biofilm formation (Ferrández *et al.*, 2002; O'Neal *et al.*, 2022). Homologous cluster to the *wsp* cluster are also present in other species (Xu *et al.*, 2022), suggesting that mechanosensing can be of relevance in other bacterial species.

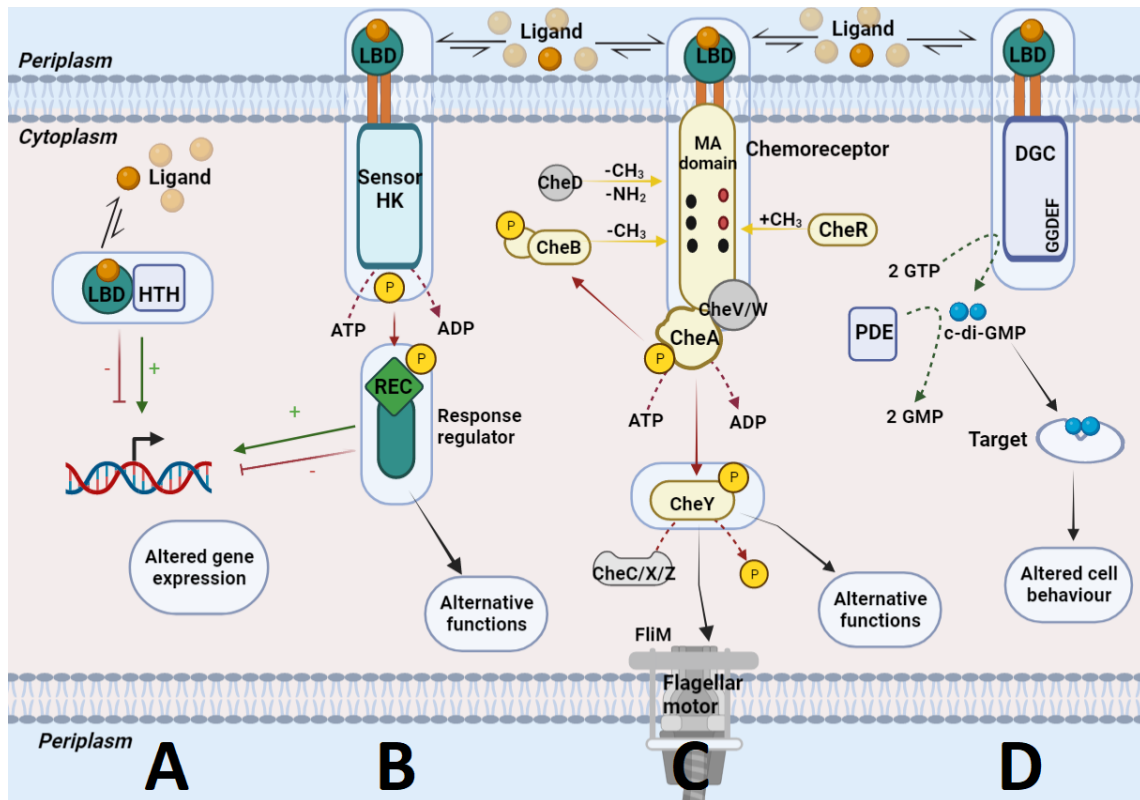


**Figure 1. Overview of bacterial signaling systems.** (A) One-Component Systems (OCSs); (B) Two-Component Systems (TCSs); (C) Chemosensory pathways; (D) Diguanylate cyclases and phosphodiesterases. For TCSs, chemosensory pathways and diguanylate-cyclases, membrane-bound sensor proteins are depicted, but also soluble sensor proteins exist. In OCS and TCS, the transcriptional regulator/response regulator binds to DNA to modulate gene expression, and alternative functions include c-di-GMP and c-AMP signaling for TCSs and type IV pili motility for chemosensory systems. For diguanylate cyclase and phosphodiesterases, ligand binding can up- or downregulate the function of the GGDEF domain of the diguanylate cyclase (DGC), which generates c-di-GMP from two GTP molecules. c-di-GMP can then binds to target proteins to modulate cellular behavior, e.g., biofilm formation, motility or cellular development. c-di-GMP is degraded by phosphodiesterases (PDE). Color code: Ligand binding domains (LBD) are in green, core chemosensory proteins in yellow and alternative chemosensory proteins in grey. Proteins of OCSs, TCSs and DGC/PDEs are in different shades of blue/green. Phosphorylation reactions are represented as red arrows, while yellow arrows represent methylation/demethylation and deamidation reactions. Other reactions and outputs are represented in black lines. Red T-lines and green arrows represent transcriptional repression and activation, respectively. Adapted from (Martín-Mora *et al.*, 2018a) and from (Watts *et al.*, 2019). Image created with BioRender.com.

Chemosensory pathways have been studied experimentally in approximately 30 bacterial species (Gumerov *et al.*, 2021). These organisms represent only eight bacterial phyla out of more than one hundred currently described. Experimentally studied systems are mostly present in Proteobacteria and systems from several major classes, namely F5, F6, F7, and F9, have only been found in this phylum. A number of chemosensory pathways show a narrow phylogenetic distribution. For example, F1 system is found in Firmicutes, Thermotogota and Archaea, but not in Proteobacteria, whereas F6 system is found exclusively in Proteobacteria (Gumerov *et al.*, 2021). Thus, there are different mechanistic and evolutionary pressures acting over these

chemosensory circuits in different taxonomic groups and pending research will help elucidate similarities and differences in their functioning and roles in currently unexplored taxonomic groups (Briegel *et al.*, 2015; Sharma *et al.*, 2018; Yang and Briegel, 2020; Gumerov *et al.*, 2021; Mo *et al.*, 2022).

Many species contain more than one chemosensory system per genome, and cross-talk between chemosensory pathways governing different functions, like chemotaxis and biofilm formation, has been described, with components of one pathway modulating or interacting with components of additional pathways (Cerna-Vargas *et al.*, 2019; Matilla *et al.*, 2021a). This cross-talk may play a role in coordination of complex behaviors in bacteria (Huang *et al.*, 2019b).

## 2. Chemoreceptors

Chemoreceptors are at the beginning of the cascade and are proteins that sense effectors activating the chemosensory signaling cascade. The five chemoreceptors from *E. coli* have served as traditional models in the study of this protein family. Genome analyses have revealed that across bacteria broader sensory capabilities are widespread, with many bacteria encoding many more chemoreceptors (Ortega *et al.*, 2017a; Gumerov *et al.*, 2020). A canonical chemoreceptor is composed of several domains: (i) a sensing domain, usually periplasmic, also known as ligand binding domain (LBD), typically sandwiched between two transmembrane regions; (ii) a cytoplasmic signal conversion HAMP (present in Histidine kinases, Adenylate cyclases, Methyl accepting proteins and Phosphatases) domain; and (iii) a cytoplasmic methyl-accepting signaling domain that can be subdivided into several conserved subdomains (Figure 2).

Almost three quarters of available sequences of chemoreceptors possess an extracytoplasmic amino-terminal LBD (Ortega *et al.*, 2017a). There are other known topologies for chemoreceptors. For example, those which have two transmembrane regions and a cytosolic LBD, like the *E. coli* Aer receptor (Amin *et al.*, 2006) and those that lack transmembrane regions and thus are completely cytosolic, like the TlpD receptor from *H. pylori* (Schweinitzer *et al.*, 2008). Indeed, around 14% of chemoreceptors are predicted to be cytosolic proteins with no transmembrane regions (Ortega *et al.*, 2017a). Moreover, some species contain chemoreceptors with the LBD located at the carboxy-terminal part. In fact, it has been predicted bioinformatically that about 5% of LBDs in microbial chemoreceptors are located at the C-terminal extension (Ortega *et al.*, 2017a).

Chemoreceptors without dedicated sensory domains represent around 18% of the total (Ortega *et al.*, 2017a), and their function is mostly unknown. There are examples, however, that demonstrate they have specific functions, such as the McpA chemoreceptor of *P. aeruginosa* that was shown to mediate positive taxis to trichloroethylene (Kim *et al.*, 2006). Split-gene chemoreceptors, in which a cytosolic protein that includes a HAMP and a signaling domain interacts with an individual LBD to form a fully functional chemoreceptor, have been identified, such as for example the CetA/CetB pair in *Campylobacter jejuni* (Elliott and Dirita, 2008).

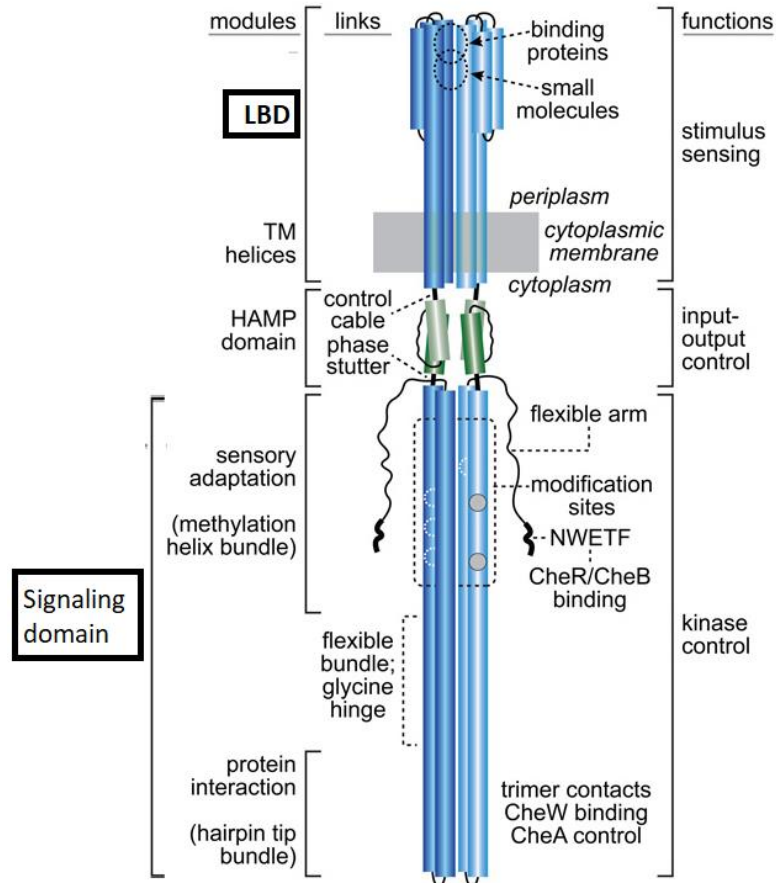


**Figure 2. Molecular architecture of a canonical chemoreceptor.** Cylindrical segments represent  $\alpha$ -helical secondary structures, drawn approximately to scale. The two protomers of the homodimer are shown in different shades of blue. Each protomer contains four methylation sites (gray and white circles) as identified in the *E. coli* Tar and Tsr chemoreceptors. White rectangles in the flexible bundle region represent glycine hinge residues. The four-helix bundle of the cytoplasmic kinase-control domain ends with an unstructured linker segment at the C-terminus of each subunit (thin wavy line). A pentapeptide sequence (NWETF) at the very C-terminus provides a binding site for the CheR- and CheB-modification enzymes of the sensory adaptation system. Adapted from (Parkinson *et al.*, 2015).

### 2.1. LBDs for stimulus sensing

Chemoreceptors show a significant structural diversity in their LBDs. More than 80 different LBD types have been detected with sizes ranging from 120 to 340 amino acids (Ortega *et al.*, 2017a). These differences have been the basis for an initial classification of most known LBDs into two clusters, with cluster 1 comprising those domains with sizes between 120 and 210 amino acids (four-helix bundle are the prototype LBD family in this cluster) and cluster II those that have between 220 to 340 amino acids (Lacal *et al.*, 2010b). There is growing evidence that most cluster II LBDs have originated from two cluster I domains following gene duplication events (Upadhyay *et al.*, 2016).

From all the LBD types recognized in bioinformatics analyses, there is experimental information about some of them, with the most abundant families being:

- **Four-helix bundle (4HB) domain:** Since present in more than 17% chemoreceptors (Sanchis-López *et al.*, 2021), it is the most abundant family. Four out of the five chemoreceptors from



*E. coli* have 4HB domains. 4HB LBDs were found to form homodimers that bind ligands on their dimer interface and amino acids from both monomers participate in ligand binding, as shown by the Tar structure (Milburn *et al.*, 1991). In these chemoreceptors, ligand recognition typically shifts the monomer-dimer equilibrium towards the dimeric state and stabilizes the LBD conformation (Martín-Mora *et al.*, 2016a; Martín-Mora *et al.*, 2016b). Recent data suggest a significant amount of structural and functional diversity in 4HB domains, including different ligand binding sites at 4HB domains (Hong *et al.*, 2019; Gavira *et al.*, 2021).

- **Per-Arnt-Sim (PAS) domain:** this family forms the third most abundant LBD family (Sanchis-López *et al.*, 2021). PAS domains are always present in the cytosolic cell compartment and never present extracellularly (Upadhyay *et al.*, 2016). PAS domains can be classified into a significant number of subfamilies which are ubiquitous sensors in bacterial signal transduction systems and in eukaryotic proteins (Henry and Crosson, 2011). Some of these domains contain co-factors like heme for gas sensing, FAD and NAD<sup>+</sup> for redox sensing or FMN for light sensing, whereas others bind a variety of different signals directly, such as aromatic hydrocarbons, Zn(II), dodecanoic acids, aromatic amino acids or compounds with autoinducer function (Matilla *et al.*, 2022a). Cache and PAS are homologous domains and share important structural similarities but are distinct types of domains. In contrast to PAS domains, Cache domains are predominantly of extracytosolic location (Upadhyay *et al.*, 2016).
- **The Ca<sup>2+</sup> channels and chemotaxis (Cache) domains:** This LBD include single Cache (sCache) and double Cache (dCache) domains. dCache are the second most abundant LBD family and have a bimodular arrangement, comprising two  $\alpha/\beta$  fold modules that may have arisen following gene duplication and fusion (Upadhyay *et al.*, 2016; Ortega *et al.*, 2017a). These two modules are structurally different and typically ligands bind to the membrane-distal module, with the proximal module allowing at times the binding of additional ligands (Rico-Jiménez *et al.*, 2013b; Zhang *et al.*, 2020; Johnson *et al.*, 2021; Boyeldieu *et al.*, 2022; Feng *et al.*, 2022). The sCache domains have a PAS-like fold and were consequently initially defined as extracellular PAS-like domains prior to the establishment of the sCache domain family (Upadhyay *et al.*, 2016).

Most Cache domains have been described as monomeric proteins with no evidence for oligomerization upon signal recognition (Goers Sweeney *et al.*, 2012; Rico-Jiménez *et al.*, 2013a; Rico-Jiménez *et al.*, 2013b; Nishiyama *et al.*, 2016; Machuca *et al.*, 2017; Gavira *et al.*, 2018). Although sometimes, as can be seen in Figure 3, these proteins crystalize as dimers, ligands bind to the domain monomer establishing contacts with only one protein chain.

- **Helical bimodular (HBM) domain:** In analogy to 4HB domains, HBM LBDs form dimers that recognize signal molecules at the dimer interface with the signal establishing contacts with both monomers of the dimer (Ortega and Krell, 2014). The best-studied family member is the LBD of the McpS chemoreceptor from *Pseudomonas putida* KT2440, where both modules, distal and proximal, bind different ligands (e.g., malate and acetate) and a chemotactic response is elicited to both ligands in an additive way (Pineda-Molina *et al.*, 2012). The conservation of amino acids in the ligand binding sites of both modules suggests that HBM family members recognize similar ligands (Ortega and Krell, 2014).

It must be noted that although dCache and 4HB/HBM domains differ in their sensing mechanisms, the corresponding receptors appear to employ the same mechanism of transmembrane signaling. This has been demonstrated by generating chimeric receptors with dCache domains and the cytosolic fragment of Tar, which were functional and able to generate a normal signal output in response to the ligand recognized by the sensor domain (Bi *et al.*, 2016).

- **Additional LBDs families:** families less abundant in chemoreceptors are PilJ (Type IV Pili methyl-accepting chemotaxis transducer) which has been shown to function as a dimer (Martín-Mora *et al.*, 2019), NIT (predicted nitrate and nitrite sensing domain), CZB (chemoreceptor zinc-binding), GAF (cGMMP-specific phosphodiesterases, adenylyl cyclases and FhIA) and CHASE (Cyclases/Histidine kinases associated Sensory Extracellular) domains, among others. Taken together, they account for less of 20% of known LBDs (Ortega *et al.*, 2017a).

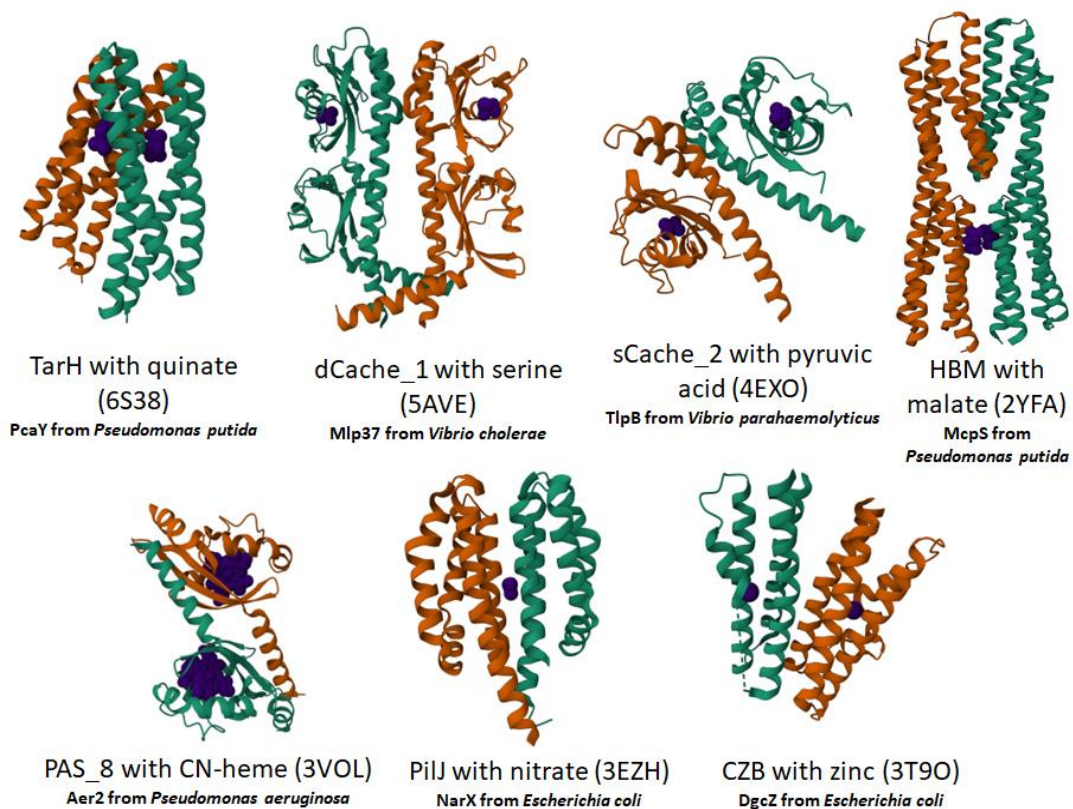


**Figure 3. Members of some ligand binding domain families present in bacterial chemoreceptors.** LBD monomers are shown in green or orange and bound ligands in dark blue. Protein Data Bank (PDB) accession codes are provided in parentheses for each structure. In the case of PilJ and CZB domains, although they can be found in chemoreceptors, shown in this figure are structures solved from Histidine Kinases.

Another emergent classification of chemoreceptors has been derived from structural information available. Resolving an increasing number of LBD structures has made patent that they can be classified into two groups depending on the major fold they adopt. 4HB and other less prominent families like HBM, PilJ and NIT adopt an antiparallel  $\alpha$ -helix bundle without

significant  $\beta$ -folds in their structure. On the other hand, Cache, PAS and GAF domains adopt an  $\alpha/\beta$ -fold that has been described as PAS-like  $\alpha/\beta$ -fold (Matilla *et al.*, 2022a).

## 2.2. Transmembrane regions for stimulus transduction into the cytosol

In roughly three quarters of chemoreceptors, like in the canonical Tar chemoreceptor, two  $\alpha$ -helical transmembrane regions flank the LBD (Parkinson *et al.*, 2015). In addition, the second transmembrane region has an extension of several residues, termed control cable, as a linker with the cytoplasmic domains of the protein (Kitanovic *et al.*, 2011). Despite the structural diversity of LBDs, there is evidence for a common mechanism of transmembrane signaling. This mechanism, first identified for the *E. coli* chemoreceptors, consists of chemoeffector-induced, piston-like shift, accompanied by a rotational movement, of the second transmembrane helix (Chervitz and Falke, 1996; Yu *et al.*, 2015; Ames *et al.*, 2016). A report identified similar types of movements in the sensory domain of a histidine kinase, further strengthening the argument for a common mechanism for transmembrane signaling in bacteria (Gushchin *et al.*, 2017). Whether there are different molecular mechanisms involved in transmembrane signaling depending on the type of LBDs is still an unsolved question, with examples of specific chemoreceptors with alternative molecular movements described (Szurmant *et al.*, 2004; Gavira *et al.*, 2021). However, different studies have generated chimeric receptors fusing the cytosolic fragment of the Tar chemoreceptor with different types of LBDs derived from chemoreceptors and sensor histidine kinases, resulting in functional constructs that responded to their corresponding chemoeffectors, supporting the notion of an universal transmembrane signaling mechanism (Reyes-Darias *et al.*, 2015b; Bi *et al.*, 2016).

## 2.3. HAMP domain for converting input into output

The 50-residue HAMP (histidine kinases, adenylate cyclases, methyl-accepting proteins, and phosphatases) domain converts input signal into output response in a variety of transmembrane signal transduction proteins, including chemoreceptors and HKs (Dunin-Horkawicz and Lupas, 2010). Cytosolic chemoreceptors also contain HAMP domains (Garcia *et al.*, 2016). It is composed of two amphiphilic helices (AS1 and AS2) linked by a flexible, non-helical region. The two HAMP domains from a receptor dimer adopt a membrane-proximal parallel four-helix bundle arrangement (Hulko *et al.*, 2006; Airola *et al.*, 2013) (Figure 2). This HAMP bundle receives conformational input from the sensing domain and exerts conformational control over the receptor's signaling tip. Contacts between HAMP helices AS1 and AS2 at the subunit interface play a critical role in modulating receptor on-off switching (Swain and Falke, 2007; Watts *et al.*, 2011).

HAMP signaling mechanisms have been widely investigated and different hypothesis have been proposed. However, all these signaling models postulate changes in the packing stability or geometry of the four-helix HAMP bundle induced by the stimuli. HAMP signaling, in turn, appears to modulate the packing interactions or orientation of the N-terminal helices of the adjoining methylation bundle, which are coupled in structural opposition to the C-terminal HAMP helices through a phase stutter formed by 4 amino acids (Parkinson *et al.*, 2015). This oppositional coupling may poise receptors so that small changes in free energy upon ligand binding can propagate meaningful conformational or dynamics changes throughout the molecule (Flack and Parkinson, 2018).

## 2.4. Signaling domain

The whole region is composed of two parallel helices containing a hairpin turn at the membrane-distal end. In the chemoreceptor homodimers, this module adopts a quaternary structure that can be described as a four-helix anti-parallel coiled-coil (Kim *et al.*, 1999). There is a high degree of conservation in this part of chemoreceptors, allowing for *in silico* identification of chemoreceptors (Alexander and Zhulin, 2007). Mutations in this area of the protein are highly detrimental for the signal transduction to CheA and for the formation of the high ordered clusters observed in chemotactic bacteria (Hazelbauer *et al.*, 2008). For these reasons, a strong evolutionary pressure against sequence variability in this area can be inferred from the number of protein interactions that it must establish. Thus, current research reveal that there are two evolutionary speeds in chemoreceptor sequences; while LBDs rapidly evolve to acquire new capabilities/functions, the signaling domains are highly conserved and evolutionarily fixed (Matilla and Krell, 2017).

The signaling domain is composed of three different subdomains, as can be observed in Figure 2:

- Methylation helix bundle: It contains the methylation sites, 1 to 4 residues in each helix that can be amidated or methylated by the corresponding enzymes. These methylation sites have a medium conservation (Alexander and Zhulin, 2007; Swain *et al.*, 2009). In this part, a heptad-repeat structural motif (LLF) has also been described at the membrane-proximal end that is critical for HAMP output control. Studies in the Tsr receptor have shown that this motif may function like a leucine zipper to promote stable association of the C-terminal signaling helices, with substitutions in any of these LLF residues abrogating chemotactic responses to serine (Flack and Parkinson, 2018). Also, HAMP bundle conformations have been related with recognition of methylation sites by the adaptation enzymes, with HAMP deletion mutants not responding to adaptive control (Ames *et al.*, 2014).
- Flexible bundle: A poorly conserved region identified between the methylation helix bundles and the protein interaction hairpin turn. In the middle of this bundle, six conserved glycine residues form a molecular hinge that is important for CheA docking or activation/inactivation (Coleman *et al.*, 2005).
- Protein interaction region: A hairpin U-turn between the two parallel helices that is highly conserved. CheW and CheA bind to this region (Mehan *et al.*, 2003). The CheA kinase-regulatory module and adaptor protein CheW interact through conserved hydrophobic surfaces at the ends of their  $\beta$ -barrels to form pseudo 6-fold symmetric rings in which the two proteins alternate around the circumference, as shown by crystal structures (Muok *et al.*, 2020a). This means in signaling arrays, every protein interaction region can interact with either a CheA protein, a CheW or another receptor (Li *et al.*, 2013).

Seven major and five additional minor classes of chemoreceptors have been defined by the number of coiled-coil heptad repeats of the corresponding signaling domains (Alexander and Zhulin, 2007). Heptad repeats contain seven consecutive amino acid residues that correspond to two  $\alpha$ -helical turns. *E. coli* receptors belong to the 36-heptad class, with 18 heptads in the N-helices and 18 in the C-helices. Not all the positions in these heptads have the same importance, as certain positions form part of conserved sockets with knob residues that constitute inter-helix connecting structures allowing for proper signal transmission along the enlarged hairpin (Swain

*et al.*, 2009). The assembly of membrane-bound receptors of different specificities into mixed clusters is dictated by the length-class (number of heptads) to which the receptors belong (Herrera Seitz *et al.*, 2014).

### **3. The *E. coli* chemosensory pathway as paradigm in the field**

The mechanisms and molecular components of chemotaxis have been most profoundly scrutinized in the model bacterium *E. coli*. Conceptually, bacterial chemotaxis pathways consist of two modules, one for rapid signal transduction and another for slower adaptation processes (Colin *et al.*, 2021). The canonical chemotactic system of *E. coli* is composed of 5 membrane-embedded chemoreceptors and six soluble chemotaxis (Che) proteins. The chemotaxis signaling proteins as well as the Tar and Tap chemoreceptors are encoded in a single gene cluster. The rest of the chemoreceptor genes are scattered throughout the genome (Zhulin, 2016).

In *E. coli*, chemoreceptors form homodimers in the membrane that group into heterotrimers (involving chemoreceptors that recognize different ligands, like Tar or Tsr) and interact with the adaptor protein CheW and the histidine kinase CheA (Studdert and Parkinson, 2005). As a result, clusters of signaling complexes are formed, resembling hexagonal lattices, with CheA interacting with different heterotrimers at the same time (Briegel *et al.*, 2009; Liu *et al.*, 2012), as can be seen in Figure 4. This structure is conserved across chemotactic bacteria and has been observed for both, membrane-bound and cytoplasmic chemoreceptor arrays. Super-lattices resembling these have also been found largely conserved in chemotactic Archaea, which received the chemotactic apparatus through lateral gene transfer events (Briegel *et al.*, 2015). Cryo-electron microscopy (cryo-EM) and tomography have already provided a wealth of information, showing signaling clusters assembled in patches that for the most part have a polar localization in the cells (Yang *et al.*, 2018; Burt *et al.*, 2021). The patches contain closely packed, needle-like receptors extending from the membrane with a layer of CheA and CheW at their cytoplasmic, membrane-distal tips (Hazelbauer *et al.*, 2008) (Figure 4).

Chemoeffector binding to chemoreceptors modulate the autophosphorylation activity of CheA. In *E. coli*, and most studied bacteria, repellent binding or attractant removing activate CheA, which is achieved through conformational changes that are relayed from the chemoreceptors to the signaling complexes (Cassidy *et al.*, 2020; Muok *et al.*, 2020a). Although single chemoreceptor dimers can bind ligand and signal across the membrane, efficient activation of CheA requires more than one receptor dimer (Li *et al.*, 2011). The phosphorylated CheA (kinase-ON state) transfers its phosphoryl group to CheY. CheY, when phosphorylated, diffuses and interacts with the flagellar motor, changing the direction of flagellar rotation, inducing clockwise (CW) rotation of one or several flagella (Minamino *et al.*, 2019) In *E. coli*, 4–6 peritrichous flagella, each driven by a rotary motor powered by proton motive force, form a bundle that propels the cell in long runs when rotating counter-clockwise (CCW) (Figure 5). Destabilization of this bundle when CheY-P binds the motor causes the cell to tumble, or reorient randomly (Turner *et al.*, 2000) (Figure 5). Bacteria that are polarly flagellated, on the other hand, have several different cell motility states, so their reorientation when chemotactically swimming are more complex and have diversified putatively to adapt to their distinct ecological niches (Grognot and Taute, 2021).

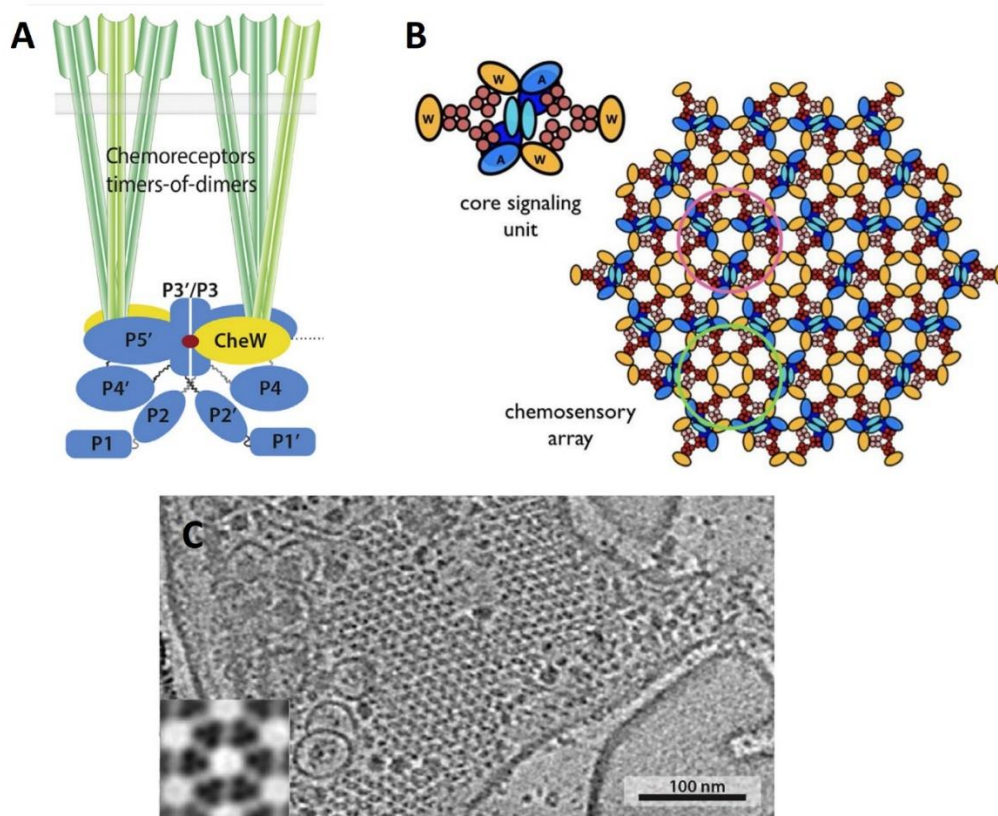


**Figure 4. The *E. coli* chemosensory signaling arrays.** (A) Side view of a signaling core unit. The chemoreceptor homodimers form trimers-of-dimers through the interaction at their cytoplasmic tips. To form the signaling core units, receptor trimers bind both the kinase CheA and coupling protein CheW following a strict stoichiometry of 6 receptor trimers-of-dimers: 1 dimeric CheA: 2 monomeric CheWs (Studdert and Parkinson, 2004; Li and Hazelbauer, 2004; Erbse and Falke, 2009). Among the five domains (P1-P5) of CheA, the P5 domain directly binds to the receptor trimers. (B) Top view of the chemoreceptor array at the level of the array baseplate. Receptor trimers-of-dimers can be seen interconnected by rings of CheA and CheW (pink circle) and CheW only (green circle). On the left, a single core signaling unit, containing two trimers of dimers that interact with CheA and CheW, that are depicted with two additional CheW molecules. Chemoreceptors are shown in red and pink, representing two different chemoreceptors in this schematic array, CheA in shades of blue (dark blue and light blue represent the different domains of CheA), and CheW in gold. (C) Tomographic image of the chemosensory array in the side view near a flagellar motor in a lysed *E. coli* cell. Images taken from (Hadjidemetriou *et al.*, 2022) and (Yang and Briegel, 2020).

The cell's swimming behavior reflects the proportion of receptor signaling complexes in the kinase-ON and kinase-OFF states (Parkinson *et al.*, 2015). An additional protein, the phosphatase CheZ rapidly dephosphorylates CheY-P, regulating its concentration and being essential for rapid responses to stimuli (Zhao *et al.*, 2002). The steady-state kinase activity of CheA is subject to cell-to-cell variations that, given the ultrasensitive response of the flagellar motor to changes in CheY-P concentration, would disturb chemotaxis that is, however, suppressed by the interaction between CheZ and CheY-P (Liu *et al.*, 2022a).

Well-described additional proteins of the chemotaxis systems of other species include CheC, CheX and CheV. CheC or CheX are alternative phosphatases that can replace CheZ in controlling the CheY phosphorylation state (Silversmith, 2010). Furthermore, some bacterial chemotaxis



systems replace CheW with CheV, a bimodular protein with a CheW-like domain fused to a CheY-like receiver domain that can be phosphorylated by CheA. CheV proteins conserve CheW residues crucial for coupling, and phosphorylation of the receiver domain might adjust the efficiency of its coupling and thus allow the system to modulate the response to chemical stimuli in an adaptation process (Alexander *et al.*, 2010). However, currently the relevance of the presence of CheV instead of CheW is not fully understood.

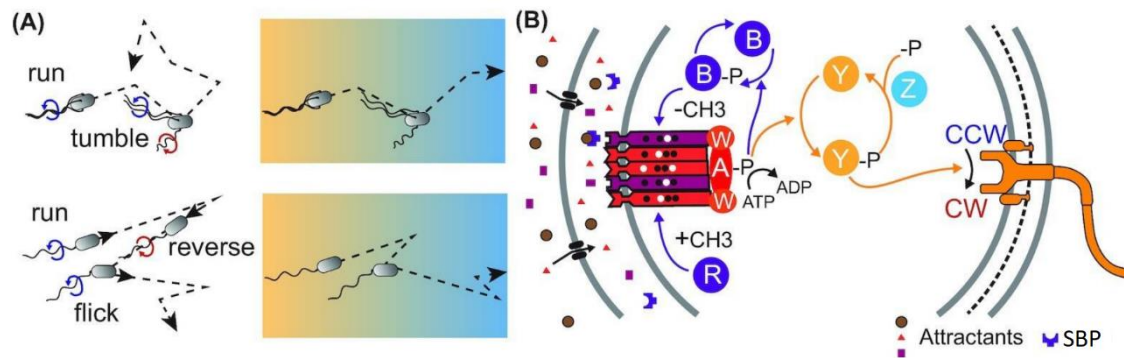


**Figure 5. Chemotactic behavior and signaling pathway.** (A) Shown are two types of bacterial motility patterns arising from flagellar function. In the upper panel, the run-tumble mode which is well-described in *E. coli* and, in the lower panel, the run-reverse-flick swimming, described in monoflagellated *Vibrio alginolyticus* (Xie *et al.*, 2011). Chemotaxis can alter both kinds of swimming to follow gradients. (B) The chemotaxis pathway of *E. coli* features chemotactic clusters composed of chemoreceptors, the CheA HK and the adaptor protein CheW, among others involved in adaptation (CheB, CheR and additional proteins). Chemoreceptors modulate CheA activity (red) upon signal recognition. CheA phosphorylates CheY (yellow) that diffuses to dock to the flagellar baseplate modulating the direction of motor rotation. CheZ is a phosphatase (light blue) that reverts the CheY to the unphosphorylated state. CheR and CheB (dark blue) adapt the sensitivity of the system to the present signal concentration, as detailed further below. CheW is shown also in red. Two different kinds of chemoreceptors are depicted as red or purple forms. SBP: periplasmic solute binding protein, proteins that bind and present ligands to some chemoreceptors, further expanding their ligand range; CCW: counterclockwise flagellar rotation; CW: clockwise flagellar rotation. Image taken from (Colin *et al.*, 2021).

#### 4. Adaptation mechanisms in bacterial chemotaxis

Bacterial size is insufficient to spatially sense concentration gradients at swimming speeds so, instead, concentrations must be compared temporally. An additional layer of regulation, the adaptation process, warrants that time-dependent changes of ligand concentration are readily detected, by adjusting pathway sensitivity to present signal levels and comparing to those encountered later. This is based on methylation or demethylation of the chemoreceptors at specific glutamyl residues on their cytoplasmic signaling domain (Kehry *et al.*, 1985). These modifications are carried out by the methyltransferase CheR and the methylesterase CheB (Figs. 1 and 5), but they can only do so at a slower pace than chemoeffector binding to LBDs. This results in a molecular cell memory that compares past and present ligand concentrations. The memory length of the organism should fit its lifestyle. In *E. coli* a typical run-time in adapted state lasts approximately 1 second (s), and the optimal memory resulted to be between 1 and 10 s (Koshland, 1974; Koshland, 1981). A longer memory will make the cell 'remember' the past conditions for a too long amount of time. A substantially shorter memory will make the cell

'forget' the gradient too fast, which means a drop of response accuracy (Vladimirov and Sourjik, 2009).

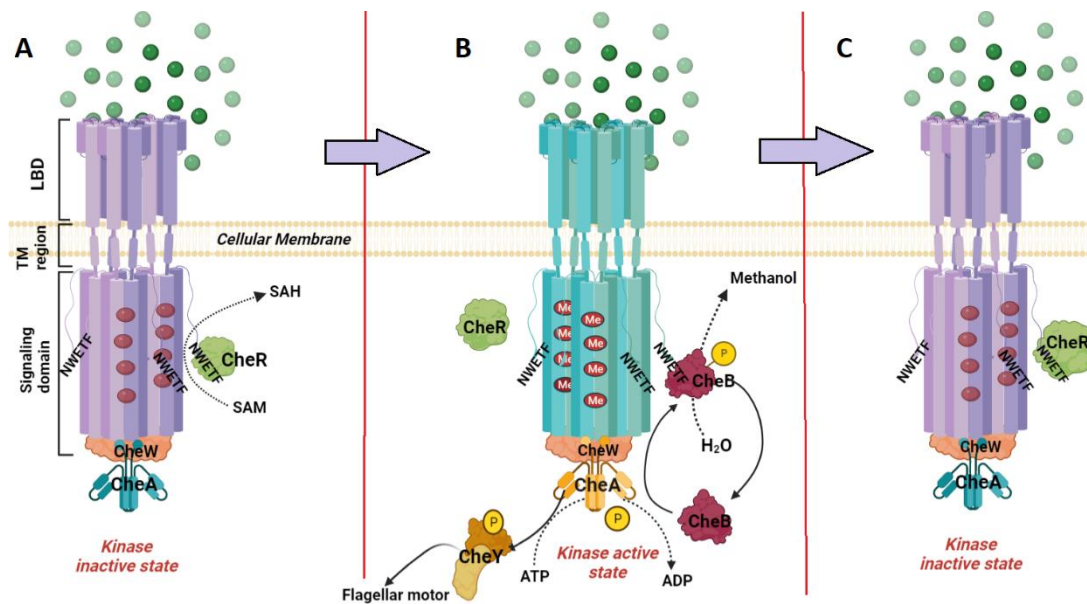


**Figure 6. The adaptation mechanism in chemotaxis.** (A) Ligands (green spheres) bind to the periplasmic chemoreceptor LBD, lowering CheA autophosphorylation (in *E. coli*). The chemoreceptors have been depicted as heterotrimeric dimers. CheA in this OFF state does not interact with CheY and CheB. CheR, which is shown bound to the NWETF pentapeptide, methylates the signaling domain of chemoreceptors. It uses S-adenosylmethionine (SAM) as a substrate and generates S-adenosyl-L-homocysteine (SAH) as a product. CheR prefers this inactivated form of the receptor and methylation makes the chemoreceptor less sensitive to ligands. (B) CheA then can become activated and trans-phosphorylates its response regulators CheY and CheB. Phosphorylated CheB also binds chemoreceptors at their pentapeptide (e.g. NWETF) to demethylate the signaling domain, thereby reestablishing the basal level of ligand sensitivity. CheY-P interacts with the flagellar motor and the length of straight runs in turn decreases in this kinase ON state. (C) As a result of both, the decrease in CheR activity and the increase in CheB output, chemoreceptors reach again the minimum level of methylation. Image created with BioRender.com. TM region: Trans-membrane region.

While attractant binding (or absence of repellent) in *E. coli* inhibits CheA kinase activity, compensatory methylation increases kinase activity. Attractant occupancy thus has two direct effects: enhances the propensity for chemoreceptor methylation and reduces the kinase activity of CheA (Figure 6). We must note that there are two feedback mechanisms: the first is provided by the substrate specificity of CheR and CheB, which are able to recognize the inactive or active conformations of the receptors, respectively, resulting in a receptor adaptation that is controlled by its own activity/conformation (Parkinson *et al.*, 2015). The second feedback is provided by CheB phosphorylation (mediated by CheA). Inactive CheA has an inhibitory effect on CheB, making CheR-mediated receptor methylation the prominent adaptation feature. In turn, methylated receptors increase CheA activity, and phosphorylated CheA can phosphorylate CheB. CheB-P suffers a conformational change that increases the methyltransferase activity of the catalytic domain (Anand *et al.*, 1998). It demethylates receptors at the methylation sites, which causes CheA activity to reduce to baseline levels (Figure 6). Thus, this feedback loop maintains kinase activity at an intermediate level that provides the cellular concentration of



phosphorylated CheY needed to generate a functional swim-tumble ratio (Falke and Hazelbauer, 2001). Overall, these two feedback mechanisms permit *E. coli* cells to react to small changes in ligand concentration over a range of several orders of magnitude, permitting, for example, responses of *E. coli* cells to aspartate concentrations from 10 mM to 3.2 nM (Mao *et al.*, 2003). Other less frequent, methylation-independent mechanisms of adaptation in bacterial chemotaxis have been described. For example, in *E. coli*, analyzing mutants lacking the methylation machinery demonstrated that they could adapt and follow gradients to some extent (Segall *et al.*, 1986). The underlying mechanism of control may be via CheY acetylation catalyzed by the enzyme acetyl-CoA synthetase (Baron *et al.*, 2017), but more research is needed to advance this knowledge and determine whether this is a general mechanism in other bacterial species.

#### 4.1. Carboxy-terminal pentapeptides at chemoreceptors

One feature of the interaction between the chemoreceptors and adaptation proteins is the recognition by CheR and CheB of specific sequences at the carboxy terminal end of receptors. In the two high-abundant *E. coli* chemoreceptors, Tar and Tsr, which mediate chemotaxis primarily towards aspartate and serine, respectively, the five amino terminal residues conform a pentapeptide that binds the methyltransferase CheR with high affinity ( $K_D \sim 2 \mu\text{M}$ ), an affinity that is much higher than the one this enzyme has for the methylation sites (100-200  $\mu\text{M}$ ) (Li and Hazelbauer, 2020). This pentapeptide, NWETF, is anchored to the rest of the signaling domain through a linker of 30-35 residues (Bartelli and Hazelbauer, 2011). The CheR of *Salmonella enterica* ser. Typhimurium has been crystalized and the 3D structure solved bound to this pentapeptide and the methyltransferase reaction substrate, S-adenosylmethionine (SAM) (Djordjevic and Stock, 1998). CheR is a two-domain protein, with a smaller N-terminal helical domain linked through a linker to a larger C-terminal  $\alpha/\beta$  domain. In this C-terminal domain, an insertion of a  $\beta$ -subdomain, not common to other methyltransferases, is responsible for recognizing the C-terminal pentapeptide. The interaction involves a number of hydrogen bonds, hydrophobic interactions of non-polar residues and a salt bridge. The NWETF pentapeptide binding site has a positive surface charge, whereas the pentapeptide is negatively charged (Figure 7). The most important residues for this binding are the aromatic residues at positions 2 and 5 of the pentapeptide (Djordjevic and Stock, 1998).

One important observation was that mutation or removal of the pentapeptide from Tar and Tsr in *E. coli* was sufficient to abolish aspartate and serine chemotaxis (Okumura *et al.*, 1998; Li and Hazelbauer, 2006). Adaptation through methylation ceased to happen and gradients of chemoeffectors could not effectively be sensed (Okumura *et al.*, 1998; Li and Hazelbauer, 2006). However, not all chemoreceptors contain this pentapeptide sequence (Ortega and Krell, 2020). For example, in *E. coli*, Tap, Trg and Aer chemoreceptors all mediate efficient taxis without the need of these pentapeptides. All of them are low-abundance chemoreceptors that are present in mixed chemotaxis signaling arrays with the high-abundance Tar and Tsr (Li and Hazelbauer, 2004; Parkinson *et al.*, 2015). In this view, CheR is recruited to a receptor dimer via pentapeptide docking and catalyzes methylation of neighboring chemoreceptors in the signaling arrays. The length of the C-terminal tail of the receptor, in an extended conformation ( $\sim 70 \text{ \AA}$ ), would allow for CheR bound to one receptor dimer to carry out methylation at an adjacent, but not more distant, receptor dimer (Djordjevic and Stock, 1998). The sequence of the *E. coli* Tar C-terminal

tail is particularly Pro-rich, supporting the notion that it may exist in an extended conformation lacking secondary structure elements, which has been experimentally demonstrated (Li *et al.*, 1997).

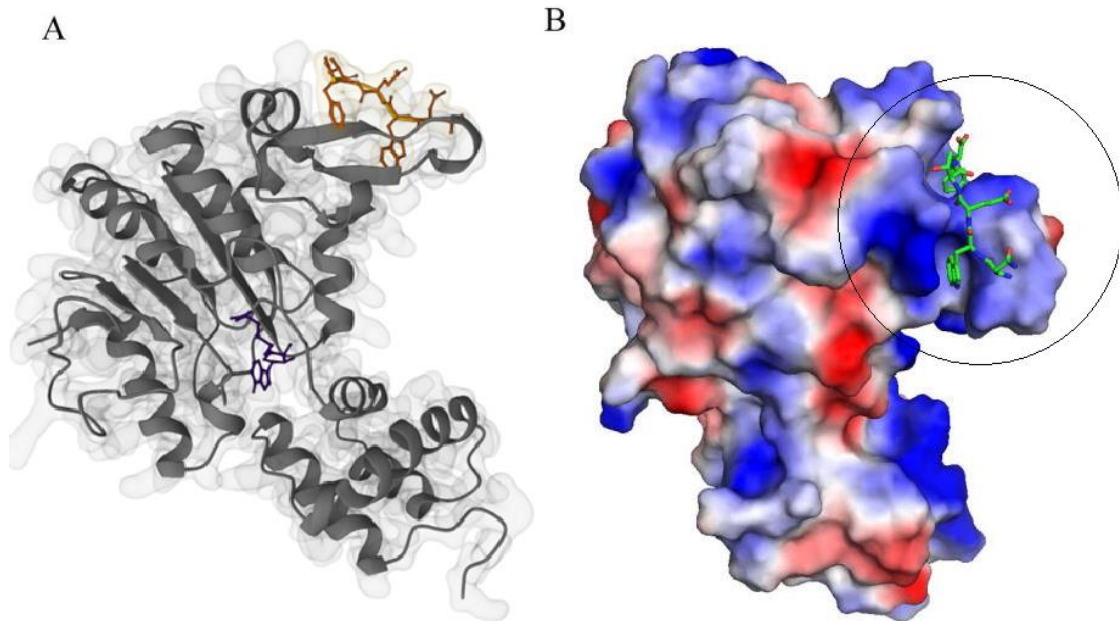


**Figure 7. 3D structure of CheR from *Salmonella enterica* ser. Typhimurium bound to S-adenosylmethionine (SAM) and the carboxy-terminal NWETF pentapeptide sequence of the Tar chemoreceptor. (A)** The CheR protein is shown as a ribbon diagram with the ligand (SAM) colored in purple. The Tar pentapeptide is in backbone representation colored in orange. **(B)** The same structure showing net surface charge. Red: negative charge, blue: positive charge. Pentapeptide is in backbone representation colored in green, and the black circle highlights how the pentapeptide binding site shows a predominantly positive charge. This image corresponds to PDB entry 1BC5. Part B is from (Ortega and Krell, 2020).

Alternatively, many species lack completely the pentapeptides in all of their chemoreceptors and a study in *Thermotoga maritima* showed that there are CheRs that can efficiently methylate without pentapeptide binding (Perez and Stock, 2007). Thus, CheR proteins from different species have been classified into two groups depending on sequence features on their pentapeptide binding site and it has been suggested that tethering of CheR to chemoreceptors is a relatively recent event in evolution and that the pentapeptide-independent methylation system is more common than the pentapeptide-dependent methylation system (Perez and Stock, 2007; Ortega and Krell, 2020).

The CheB methyltransferase is a two-domain RR in which phosphorylation of the C-terminal receiver domain (REC) enhances activity of the N-terminal methyltransferase domain. In addition, CheB deamidates glutamine residues creating methyl-accepting glutamyl groups. In *E. coli*, CheB binds the same pentapeptide sequence in Tar and Tsr chemoreceptors, which acts as a docking site for posterior modification of the signaling domain (Barnakov *et al.*, 1999). By clever biochemical studies of pentapeptide binding of CheB fragments and protection of CheB from proteolysis by pentapeptide, among others, the corresponding binding site of CheB was

localized. It spans the C-terminal end of the receiver domain and the start of the subsequent linker with the catalytic domain (Barnakov *et al.*, 2001). It must be noted that CheB has a lower affinity to the pentapeptide than CheR ( $K_D = 130$  to  $160 \mu\text{M}$ ), that is too low for increasing local CheB concentration. The CheB-pentapeptide interaction, on the other hand, stimulates methylesterase activity, additive to the direct effect of REC domain phosphorylation (Barnakov *et al.*, 2002). In addition, phosphorylation of CheB enhances pentapeptide binding as much as 18-fold tighter, with affinities measured of  $3 \pm 0.3 \mu\text{M}$ , and the pentapeptide selects the activated conformation of the enzyme, as could be demonstrated by using a stable phosphorylation mimic (Li *et al.*, 2021).

There are additional functions that have been demonstrated for these C-terminal pentapeptides. *P. aeruginosa* PAO1 has four chemosensory pathways, each one with a CheR and CheB homolog, and it has been shown that McpB, the only chemoreceptor that feeds into the Che<sub>2</sub> pathway, is also the only one with a pentapeptide. Furthermore, CheR2, which belongs to the Che<sub>2</sub> pathway, is the only of the four homologue CheR proteins able to bind this pentapeptide, in an interaction that ensures specificity between a chemoreceptor and its specific CheR (García-Fontana *et al.*, 2014).

Genome analyses have demonstrated that approximately 10% of chemoreceptors have pentapeptides (Ortega and Krell, 2020). Different pentapeptide sequences have been described and they are always fused to the C-terminus of a chemoreceptor, regardless of whether the last domain is an LBD or signaling domain. Pentapeptides are abundant in chemoreceptors that contain the four-helix bundle type LBDs (e.g., 4HB, TarH and CHASE3), being present in about half of the TarH domain-containing chemoreceptors. The pentapeptide is especially abundant in the order of Enterobacterales and in bacteria that interact with a host, although the relevance of this finding remains unclear (Ortega and Krell, 2020). Taken together, pentapeptides function as tethering sites that increase local concentration of adaptation enzymes, CheR and phosphorylated CheB, or provide specificity of CheR-chemoreceptor interaction in species that contain multiple CheR proteins. Questions on this field still remain, as the molecular detail of the competition of CheR and phosphorylated/unphosphorylated CheB to these sequences as well as the mode of CheR/CheB interaction with chemoreceptors lacking the pentapeptide in arrays containing different chemoreceptors. Species containing chemoreceptor pentapeptides with divergent sequences could help decipher additional regulatory layers involving these sequences (i.e. how are they differentially recognized by adaptation proteins) and their importance for chemotaxis in complex environments. As previously mentioned, Enterobacterales species, with their high percentage of pentapeptide-bearing proteins, are very interesting models to explore these questions (Ortega and Krell, 2020).

## **5. Sensing mechanisms in chemoreceptors**

Biochemical studies have identified the signals for a significant number of chemoreceptors. A comparison of signals recognized by chemoreceptors, sensor histidine kinases and transcriptional regulators shows that the very large majority of chemoreceptor ligands are of metabolic value and serve for growth as carbon or nitrogen sources (Matilla *et al.*, 2022a). The canonical mechanism is direct ligand binding at the LBD, that comprises a binding pocket for coordinating ligands through key amino acids. Recent advances have been made in predicting key motifs that enable direct binding of different signal molecules. For example, the AA\_motif

in dCache\_1 domains has permitted the prediction of thousands of amino acids responsive dCache domains and, in a number of cases, these predictions have been verified experimentally (Gumerov *et al.*, 2022).

Signal molecules that were found to directly interact with chemoreceptors are provided in Table 1. Amino acids constitute by far the family of ligands with the highest number of dedicated chemoreceptors, and species where these proteins have been identified show a wide phylogenetic spread. This suggests that chemoattraction to amino acids is of particular relevance for bacteria, a hypothesis that has motivated part of this thesis.

**Table 1. Summary of signals directly recognized by chemoreceptors.**

Name (Pfam)	Ligands	# of proteins
<b>Signal recognition at LBD</b>		
<b>dCache_1 (PF02743)</b>	Proteinogenic amino acids	19
	$\gamma$ -aminobutyric acid (GABA)	3
	Histamine and polyamines	2
	Decanoic acids (R)	2
	Autoinducer-2	2
	Purine derivatives	1
	Quaternary amines	1
	Citrate	1
	Taurine	1
	Ile, Asp, purine, malic acid, $\alpha$ -ketoglutarate, Lys (R), glucosamine (R), succinic acid (R), Arg (R), thiamine (R)	1
	Galactose	1
	Benzoate and derivatives	1
	L-lactate	1
K <sub>2</sub> CrO <sub>4</sub>	1	
<b>sCache_2 (PF17200)</b>	Pyruvate	4
	Acetate	4
	Propionate	3
	Glycolate	2
	L-lactate	1
	Acetoacetate	1
	Urea, hydroxyurea, acetamide, formamide	1
	L-malate, citramalate, bromosuccinate, methylsuccinate (NR) citraconic acid (NR)	1
	L-malate	1
	Malonate	1
<b>TarH (PF02203)</b>	Proteinogenic amino acids	4
	Methyl-DL-aspartate	2
	Phthalic acid (NR)	1
	Malic acid	1
	3,4-dihydroxymandelic acid	1
	Citrate	1
	Benzoate and derivatives, protocatechuate, vanillate, quinate, shikimate, dehydroshikimate	1
	Citrate and TCA cycle intermediates	1

<b>4HB_MCP_1 (PF12729)</b>	Cis-aconitate	1
	Boric acid	1
	Phenanthrene, pyrene, benzopyrene	1
<b>HBM (PF16591)</b>	Multiple TCA cycle intermediates	1
	Citrate	1
	$\alpha$ -Ketoglutarate	1
<b>DAHL (PF19443)</b>	Asp, Ile, purine, fumarate, malate, $\alpha$ -ketoglutarate, mannose, rhamnose, fucose, sialic acid, Arg (R), thiamine (R), galactose (R)	1
<b>CHASE3 (PF05227)</b>	Pyrene	1
<b>PilJ (PF13675)</b>	Nitrate	1
<b>PAS_8 (PF13188)</b>	O <sub>2</sub> , CO	2
<b>Hemerythrin (PF01814)</b>	O <sub>2</sub>	1
<b>CZB (PF13682)</b>	HOCl [Zn(II)] <sub>3</sub>	1
<b>PilZ (PF07238)</b>	C-di-GMP	1
<b>Not annotated, TarH-like</b>	Inorganic phosphate, pyrophosphate, ADP	1
	Citrate, gentisate, benzoate and derivatives	1
	Oxalate, malonate, glyoxylate, succinate, malate	1
<b>Not annotated, globin-like</b>	O <sub>2</sub> , ethanol	3
<b>Not annotated, dCache-like</b>	As(III)	1

R: repellent; NR: no response. Information taken from (Matilla *et al.*, 2022a), of which this PhD candidate is co-author.

Indirect binding is another well-known mechanism of chemoreceptor activation. In this case, a solute binding protein (SBP) recognizes the ligand(s) and the SBP/ligand complex is then sensed by the chemoreceptor (Matilla *et al.*, 2021b). The primary function of SBPs is to present substrates to transmembrane permeases to initiate compound uptake. In addition, SBPs can stimulate different receptors like HKs, chemoreceptors, diguanylate cyclases or Ser/Thr protein kinases coordinating this way transport with signal transduction (Ortega *et al.*, 2022). This mechanism allows for regulation of the perception of a specific ligand through changes in the expression levels of the SBP without compromising the perception of other ligands sensed by the chemoreceptor (Neumann *et al.*, 2010). As compared to direct sensing, SBP-mediated receptor stimulation has a narrower range for signal perception since the adaptation system is not functional with SBPs.

In Gram-negative bacteria, SBPs are present as diffusible proteins in the periplasm, and in Gram-positive bacteria and archaea they are tethered to the external face of the cytoplasmic membrane (Matilla *et al.*, 2021b). Although SBPs vary largely in size, from 20 to 65 kDa, they share the same overall topology that consists of two lobes linked by a hinge region (Dwyer and Hellinga, 2004). Examples of chemotaxis mediated by indirect signal binding include taxis to sugars, dipeptides and the autoinducer AI-2 in *E. coli* (Manson *et al.*, 1986; Björkman *et al.*, 1994; Zhang *et al.*, 1999; Hegde *et al.*, 2011). In *P. aeruginosa*, low inorganic phosphate concentrations

are sensed by the chemoreceptor CtpL in concert with the SBP PstS, which is part of the PstABC phosphate transporter (Rico-Jiménez *et al.*, 2016). Other responses mediated by SBPs, including repellent responses to AI-2 in *H. pylori*, have been identified to date (Rader *et al.*, 2011a).

LBD-independent signal perception is another mechanism that depends on ligand-induced perturbations in the transmembrane and cytoplasmic regions of chemoreceptors (Figure 8). Current data supports that direct binding of a signal molecule to a chemoreceptor LBD causes chemoattraction, whereas repellent chemotaxis appears to be caused by alternative sensing mechanisms, as exemplified by phenol repellence (Pham and Parkinson, 2011). Membrane-diffusible chemoeffectors such as phenol may stimulate a chemoreceptor by perturbing its structural stability or position of the transmembrane bundle helices (or other elements), which ultimately causes a modulation of kinase activity. It has been suggested that behavioral responses to cytoplasmic pH and temperature may also alter transmembrane regions of chemoreceptors, which is in agreement with a significant body of evidence showing that the temperature-sensing histidine kinases employ similar mechanisms (Aguilar *et al.*, 2001; Umemura *et al.*, 2002; Inda *et al.*, 2014). Other stimuli sensed without the need of LBDs comprise Ni<sup>2+</sup>, that can be sensed by a region between the transmembrane and the HAMP domain (Bi *et al.*, 2018), osmolarity being sensed by the HAMP domain (Vaknin and Berg, 2006) and ethanol, that was shown to directly bind to the signaling domain (Tohidifar *et al.*, 2020).

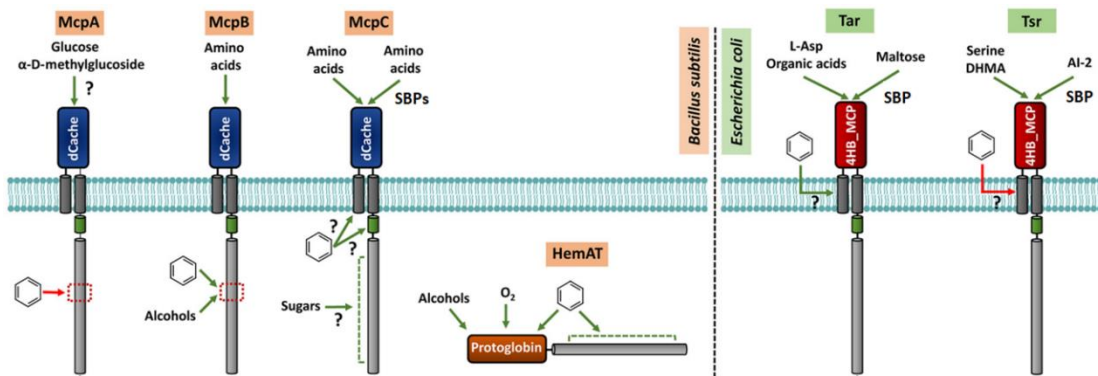


**Figure 8. The diversity of repellent and attractant sensing mechanisms in *B. subtilis* and *E. coli* chemoreceptors.** The HAMP domains are in green, signaling domains are colored in light gray; green arrows represent attractant responses; red arrows in turn are repellent responses. DHMA, 3,4-Dihydroxymandelic acid; AI-2, autoinducer-2. SBPs: solute binding proteins. The question mark highlights sensing mechanisms that have not been verified by direct binding studies. Image modified from (Matilla and Krell, 2022).

Sometimes, chemoreceptor activation can be a result of protein processing. For example, a well-known example is the BdlA chemoreceptor in *P. aeruginosa*, which requires phosphorylation and, subsequently, the proteolytic cleavage of one of its sensor domains. This protein regulates biofilm dispersion in response to different signals like carbohydrates, heavy metals, and nitric oxide, exerting control over phosphodiesterase activity and thus c-di-GMP levels (Petrova *et al.*, 2015). In addition, there are mechanisms that are completely independent of chemoreceptors, but result in a chemotactic response. For example, in *E. coli*, sugar-taxis is connected to sugar-uptake by the phosphotransferase system. Sugar uptake through these systems results in

lowering the level of phosphorylated phosphotransferase system proteins. These unphosphorylated proteins interact with CheA, triggering chemotactic responses that become integrated and undergo downstream processing including methylation-dependent adaptation (Neumann *et al.*, 2012; Somavanshi *et al.*, 2016). Future research will show whether other receptors employ similar mechanisms and likely reveal other ways to stimulate chemoreceptors.

## 6. Physiological roles of chemotaxis

Although a costly cellular behavior, chemotaxis provides bacteria with a physiological advantage by enhancing access to nutrient and energy sources in non-homogenous environments where toxins and nutrients can occur at the same time (Wadhams and Armitage, 2004). The cellular budget enabling chemotaxis can be divided into an energetic and proteomic cost. At high growth rates, energetic costs of chemotaxis are relatively low (around 2% of cell's energy undergoing active divisions), but this percentage becomes elevated in the absence of growth (Battley, 1988). However, bacteria still perform chemotaxis under these scenarios because it is a high-cost high-reward investment. It can potentially help pinpoint nutrient hotspots or optimal ecological niches, as well as to avoid adverse conditions (Keegstra *et al.*, 2022). The proteomic costs of chemotaxis establish a trade-off between growth rate and chemotaxis, and it has been shown that expression levels of motility proteins decrease linearly with increasing growth rates, with cells investing more in motility (and chemotaxis) when conditions are not optimal and thus growth rate is lower (Ni *et al.*, 2020).

Beyond enabling motile bacteria access nutrients and optimal growth conditions, in what has been called “informed foraging” (Keegstra *et al.*, 2022), chemotaxis is also involved in other important processes that are detailed below.

- **Promotion of range expansion (migration).** Motile bacteria, when growing with a nutritional source, can create a travelling band as the nutrient is consumed. The presence of chemoattractants in these nutrient-replete media can increase the velocity of expansion of the travelling band (Cremer *et al.*, 2019). The primary carbon source can be used for growth and a subpopulation of cells will start to chase the chemoattractant establishing new populations as they replicate during their movement. This way, migration occurs before nutrients become limiting, representing a fitness advantage enabling the detection of “virgin territories”. This can be extrapolated to complex media where both nutrient sources and different chemoattractants may be present and produce division of labor within populations, with chemotaxis allowing for environmental exploration of the whole accessible surroundings. This may also in fact explain why bacteria often show high chemotactic sensitivities for sub-optimal growth substrates such as serine or aspartate in *E. coli* (Keegstra *et al.*, 2022).
- **Coexistence and diversity promotion.** In environments such as the gut, characterized by a non-continuous arrival of nutrients, or for patchy environments such as the ocean, bacterial diversity can be promoted through trade-offs between motility and other traits, such as growth rates. In *E. coli*, phenotypic heterogeneity is observed for behaviors of individual cells even in genetically homogeneous microbial populations. Cell-to-cell non-genetic heterogeneity has been found in different elements of chemotactic behavior (Dufour *et al.*,

2016; Keestra *et al.*, 2017; Salek *et al.*, 2019), and in the flagellar number (Mears *et al.*, 2014). Stable coexistence of strains with different motility has been illustrated by growth-motility trade-offs between coexisting wild type strains of *E. coli* isolated from a single host (Gude *et al.*, 2020). This means faster moving strains often show slower growth and *vice-versa*. Different strains coexist because they are spatially segregated within their habitats. Chemotaxis enhances this segregation by enabling cells to climb self-generated gradients and colonize the newly available environment faster.

- **Promote interaction with hosts.** The acquisition of environmental symbionts often requires colonization through motility and chemotaxis (Raina *et al.*, 2019). For example, in plant-associated bacteria (PAB), it is crucial to sense compounds from root exudates or secreted from stomatal pores in order to effectively colonize hosts (Matilla and Krell, 2018). Chemotaxis allows PAB to actively swim towards plant exudates and produces a competitive advantage for host colonization (Colin *et al.*, 2021). For example, rhizobacteria typically possess different chemoreceptors capable of detecting components of root exudates that are frequently of nutritional value (Aroney *et al.*, 2021; Compton and Scharf, 2021). Remarkably, there are several examples of chemoreceptors in PAB that detect compounds present in plant exudates, such as auxins (Rico-Jiménez *et al.*, 2022), polyamines (Webb *et al.*, 2017b; Gavira *et al.*, 2018), amino acids (Oku *et al.*, 2012; Webb *et al.*, 2017b) and organic acids (García *et al.*, 2015; Martín-Mora *et al.*, 2016b). Overall, responses to gradients of small molecules excreted by animals, plants or other microbes, irrespective of the nutritional value, might be common in host–bacteria interactions and enable bacteria to orient themselves relative to their hosts or cooperation partners and also to locate specific niches (Colin *et al.*, 2021).
- **Biofilm formation.** Growth in a surface can help bacteria to survive in harsh environmental conditions and perform division of labor within bacterial communities (Rather *et al.*, 2021), and many bacteria are capable of switching between motile or sessile lifestyles. Typically, genes required for biofilm production and motility are antagonistically regulated (Besharova *et al.*, 2016; Condinho *et al.*, 2022). Despite this generally antagonistic regulation, chemotaxis towards chemoattractants on surfaces or quorum sensing signals have been described as necessary requirements for effective biofilm formation, particularly during the first stage of autoaggregation (Berke *et al.*, 2008; Hegde *et al.*, 2011; Laganenka *et al.*, 2016; Laganenka and Sourjik, 2018; Suchanek *et al.*, 2020). More complex links between chemotaxis and biofilm formation are present in species with several chemosensory pathways, where some of them can be especially devoted to controlling biofilm formation or dispersal (Morgan *et al.*, 2006; Petrova and Sauer, 2012).
- **Pathogenesis.** Chemotaxis, notably by helping bacteria to detect specific host signals, has been shown to be vital for host invasion and infectivity both in plant and animal pathogens (Matilla and Krell, 2018). A key example are gastrointestinal pathogens, which often possess chemosensory capabilities important for their host colonization (Matilla and Krell, 2018). This feature appears to be of special relevance in plant pathogens since these microbes possess an elevated number of chemoreceptor genes as compared to the bacterial average,



including human/animal pathogens (Matilla and Krell, 2018; Sanchis-López *et al.*, 2021). This issue will be dealt with in more detail in another section.

Several chemoreceptors that detect specific host signals have been described and their importance for host invasion and infection was demonstrated shown in different bacterial pathogens (Matilla and Krell, 2018; Perkins *et al.*, 2019; Takahashi *et al.*, 2019; Khan *et al.*, 2020; Elgamoudi *et al.*, 2021; Johnson *et al.*, 2021; Dhodary *et al.*, 2022; Matilla *et al.*, 2022a; Shu *et al.*, 2022; Taha *et al.*, 2022). Among these compounds, some might have a double function as nutrient and host signal molecules (Matilla and Krell, 2018).

### **6.1. Chemotaxis in plant pathogenic bacteria**

The field of chemotaxis has expanded to encompass the study of species which show significant variations on the canonical model identified in *E. coli*. In particular, important advances have been made in understanding the relevance of chemotaxis in PAB, either those establishing mutualistic or pathogenic relationships. Thus, in beneficial phytobacteria, mutant strains in flagellar motility and chemotaxis have reduced colonization capacities or are unable to establish endophytic populations at roots (Barahona *et al.*, 2010; Buschart *et al.*, 2012; Fernández-Llamosas *et al.*, 2021; Knights *et al.*, 2021). In analogy, phytopathogens were also found to have reduced colonization phenotypes when flagella dependent motility is abolished or when they are defective in chemosensory genes, including chemoreceptors (Haefele and Lindow, 1987; Antúñez-Lamas *et al.*, 2009; Ichinose *et al.*, 2013; Allard-Massicotte *et al.*, 2016; Matilla and Krell, 2018; Feng *et al.*, 2019).

Bacterial phytopathogens have complex life cycles (Leonard *et al.*, 2017). Frequently, they need to survive as saprophytes or epiphytes in the soil, on plant debris or plant surface. In these habitats, their capacity to sense and react to changing environmental parameters and to detect potential hosts for fine-tuning regulatory programs controlling survival and/or virulence is crucial (Leonard *et al.*, 2017). Consequently, these bacteria have a broad capacity for sensing and responding to environmental and plant-associated stimuli. Particularly, the soil provides a unique challenge for microbial motility, since water films on surfaces are not always continuous, especially in drier conditions. The reduction in microbial motility as a result of reduced water availability induces bacterial sessility (Tecon and Or, 2017). However, when water conditions are optimal, the soil can support stable long-range gradients of nutrients and signaling molecules. Since it is a nutrient-scarce medium, swimming motility and chemotaxis become a good strategy for niche localization of soil bacteria (Figure 9). Theoretical models have indicated that in heterogeneous environments, a more motile bacterium can outgrow a metabolically superior species (Lauffenburger *et al.*, 1982).

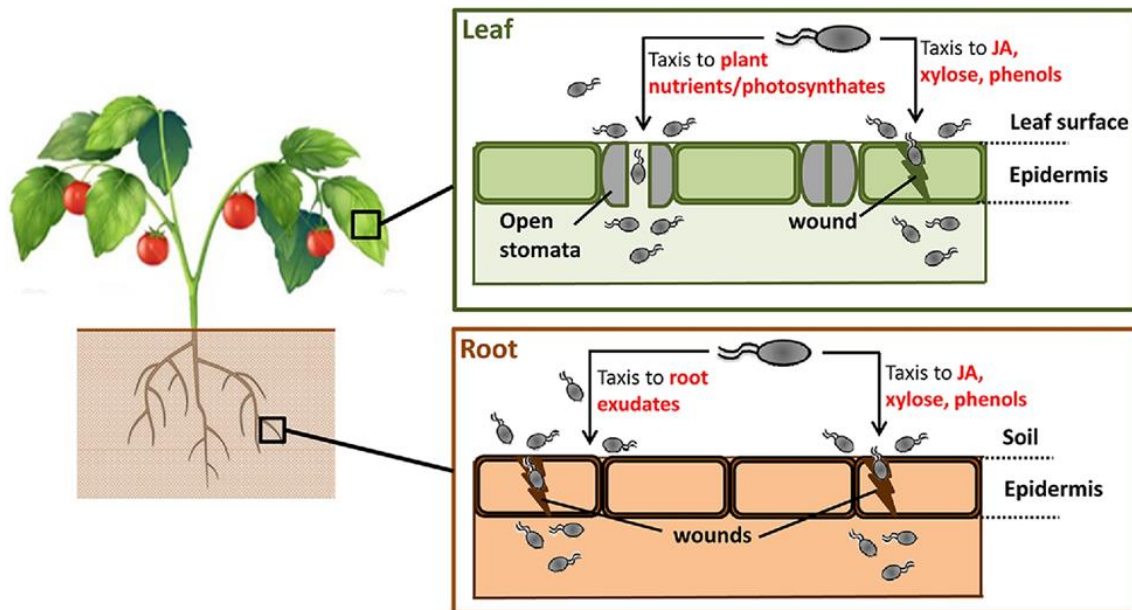


**Figure 9. The relevance of chemotaxis for plant pathogens.** Chemotaxis towards multiple plant-derived compounds facilitates the bacterial entry through natural openings or wounds. Once inside the plant, bacteria can proliferate at the infection site or disperse via de vascular system. Image taken from (Matilla and Krell, 2018).

The phyllosphere, the above-ground part of the plant, also offers some challenges to its bacterial inhabitants. Some pathogens need to endure these conditions in epiphytic stages prior to plant entry and infection (Figure 9). Leaves offer a hostile environment for microbial life since they represent a physicochemical barrier in the form of diverse cuticles and secreted compounds that impact bacterial performance (Koskella, 2020). Difficult physicochemical conditions that comprise temperature fluctuations, ultraviolet radiations, nutrient stress, relative humidity, and desiccation are also encountered by bacteria in the phyllosphere (Bashir *et al.*, 2022). Thus, chemotaxis help bacterial phytopathogens to localize plant entry points, such as wounds or open stomata (Figure 9). This is reflected in the fact that the median number of chemoreceptors in phytopathogenic bacteria (27.29) is significantly higher than in animal pathogens (12.94), but also than in beneficial phytobacteria (22.86) (Matilla and Krell, 2018; Sanchis-López *et al.*, 2021). The types of LBDs present in the chemoreceptors coded in a given genome are related to the lifestyle specialization, with plant symbionts and phytopathogens showing the highest number of niche-specific LBDs (Sanchis-López *et al.*, 2021). It was found that there are LBD subfamilies that are highly enriched in PAB but show a wide phylogenetic spread, indicating that not a phylogenetic closeness but a similar lifestyle accounts for these PAB specific LBDs (Sanchis-López *et al.*, 2021). Many PAB-specific clusters are formed by proteins of unknown LBD type, and excluding unknown LBD families, the most common domains in PAB are 4HB\_MCP\_1 (26%), TarH (4.5%), and HBM (4%). In contrast, despite being the second most abundant LBD in bacteria, the dCache\_1 domain was not very abundant in PAB (Sanchis-López *et al.*, 2021).

The key role of chemotaxis for efficient virulence has been determined for a number of phytopathogens of economic importance, which has been reviewed by (Matilla and Krell, 2018). It is a thriving research field, with some examples of characterized chemoreceptors and their implication in virulence from several model phytopathogens detailed below.

- ***Ralstonia pseudosolanacearum*** is able to infect a vast group of plant species through radical tips and wounds (Mansfield *et al.*, 2012). In this pathogen, the chemoreceptors McpA and McpM mediate attraction towards amino acids and L-malate/D-malate, with McpM being necessary for root localization and effective infection (Hida *et al.*, 2015; Tunchai *et al.*, 2017b). The inactivation of chemotaxis by masking signal gradients by the supplementation of D- or L-malate to sand, reduced plant infection because it suppresses the bacterial entry into tomato roots, probably through McpM-mediated signaling (Tunchai *et al.*, 2021). In addition, two aerotaxis chemoreceptors, Aer1 and Aer2, were also implicated in tomato root colonization (Yao and Allen, 2007). A specific chemoreceptor for boric acid, McpB, was shown to directly bind this compound, but it was not important in virulence. However, the presence of McpB orthologues is limited to plant pathogenic bacteria, and borate is a ubiquitous constituent of higher plants (Hida *et al.*, 2017). Another chemoreceptor McpP, mediates attraction towards inorganic phosphate and repulsion to maleate (Tunchai *et al.*, 2017a), whereas McpT was found to constitute a chemoreceptor for L-tartrate and D-malate, although neither McpP nor McpT-mediated chemotaxis play an important role in tomato plant infection (Tunchai *et al.*, 2017b). Finally, it has been demonstrated that phosphate receptor McpP also recognizes citrate in concert with chemoreceptor McpC (Hida *et al.*, 2019).

- ***Pseudomonas syringae*** is the etiological agent of diverse bacterial spot and blight diseases in several important crops (Mansfield *et al.*, 2012). Strains can be grouped into different pathovars depending on their host range (Xin and He, 2013). *P. syringae* pv tomato DC3000 has 48 chemoreceptors. PsPto-PscA, presenting a dCache\_1 LBD domain, binds D-Asp, L-Asp and L-Glu, and mutation of this gene abolishes chemoattraction to these ligands. Ligand perception by PsPto-PscA controls DC3000 virulence, as well as biofilm formation and swarming motility via c-di-GMP level regulation. It was shown that the addition of D-Asp to *P. syringae* pv. tomato DC3000 culture prior to plant inoculation reduces bacterial virulence by 3 orders of magnitude. The addition of this compounds masked existing gradients on the leaf surface, hence causing inefficient entry resulting in reduced virulence, which could be an alternative strategy to fight phytopathogens (Cerna-Vargas *et al.*, 2019). PsPto-PscC is a chemoreceptor with a dCache\_1 LBD domain that directly binds L-Pro and GABA, compounds that are produced in tomato plants upon pathogen infection and are involved in the regulation of the plant defense response. Chemotaxis to these compounds through PsPto-PscC was also shown to participate in plant entry and virulence (Santamaría-Hernando *et al.*, 2022). Similarly to the *P. aeruginosa* receptors PctA, PctB and PctC, PsPto-PscA and PsPto-PscC are part of a trio of paralogous chemoreceptors that bind amino acids with complementary ligand specificities (Rico-Jiménez *et al.*, 2013a; Gavira *et al.*, 2020a).

Similarly, in *P. syringae* pv. *actinidiae* (Psa), the causative agent of kiwifruit canker, the homologue receptors PscA, PscB and PscC bind 3, 10 and 3 amino acids respectively (McKellar *et al.*, 2015). Notably, PscA-LBD is a narrow-range chemoreceptor that only binds L-Asp, D-Asp and L-Glu (McKellar *et al.*, 2015). In the same strain, PscD mediating chemotaxis to four carboxylate ligands, glycolate, acetate, propionate and pyruvate, has been identified (Brewster *et al.*, 2016). Another *P. syringae* pathovar whose chemoreceptors have been investigated is *P. syringae* pv. *tabaci* 6605. The function of several chemoreceptors containing dCache\_1 type

LBDs has been investigated. Whereas McpG specifically binds GABA, chemoreceptors PscA, PscB and PscC2 bind 14, 14 and 12 amino acids, respectively. Ligands recognized by PscC1, could not be identified. These chemoreceptors are homologous to the PctA, PctB, PctC chemoreceptors of *P. aeruginosa*. Mutants in *mcpG*, *pscB*, *pscC1* and *pscC2*, but not *pscA*, had reduced virulence in the host tobacco plant (Tumewu *et al.*, 2020; Tumewu *et al.*, 2021).

- ***Agrobacterium tumefaciens*** causes crown gall tumour disease, producing overgrowths at plant wound sites which affect woody crops limiting productivity worldwide (Mansfield *et al.*, 2012). Chemotaxis towards phenolic plant compounds, shoot lysates, opines produced in crown galls and root exudates has been demonstrated (Parke *et al.*, 1987:19; Ashby *et al.*, 1988; Chesnokova *et al.*, 1997; Kim and Farrand, 1998).

Genomic analyses of different *Agrobacterium* strains showed they encode a major chemotactic cluster (Xu *et al.*, 2020). In the strain *Agrobacterium fabrum* C58 the deletion of the chemoreceptor encoded in this chemotaxis cluster significantly weakened the chemotactic response to four chemicals, namely sucrose, valine, citric acid and acetosyringone, but direct ligand binding to this receptor has not been demonstrated (Ye *et al.*, 2021).

- The ***Xanthomonas*** genus include, among twenty described species, three that have been classified among the top 10 plant pathogens. Typically, *Xanthomonas* spp. cause diseases in aerial parts of plants and are associated with enormous economic losses (Mansfield *et al.*, 2012). *X. oryzae* pv. *oryzae* has a complex chemotaxis system consisting of several paralogues of the core chemotaxis components, auxiliary proteins and several putative chemoreceptors. The chemoreceptor Mcp2 was identified to mediate taxis to the xylem sap components methionine, serine and histidine (Kumar Verma *et al.*, 2018).

The chemoattractants recognized by *X. arboricola* pv. *pruni* were compared between one non-pathogenic strain and two pathogenic strains, and despite high similarity in the chemoreceptor content, both pathogenic strains showed chemoattraction to a higher number of compounds than the non-pathogenic strain (Garita-Cambronero *et al.*, 2016). In a similar study, different chemotactic responses for carbon sources and apoplastic fluids were found for wide and narrow-host-range strains of *X. citri* pv. *citri*, *X. euvesicatoria* pv. *citrumelonis* and *X. campestris* pv. *campestris* (Sena-Vélez *et al.*, 2022).

- ***Dickeya dadantii*** is responsible for soft rot disease in several plant species and some crops of interest (Mansfield *et al.*, 2012). The SBP TogB, which is part of the TogMNAB transporter with a major role in pectin catabolism, was found to be required for chemotaxis towards oligogalacturonides. It is likely that TogB interacts with a yet un-identified chemoreceptor (Hugouvieux-Cotte-Pattat *et al.*, 2001). Jasmonic acid has been identified as a strong chemoattractant for *D. dadantii* 3937, as well as xylose, a plant-cell-wall-derived compound that is released after plant tissue damage (Antunez-Lamas *et al.*, 2009). Two candidate chemoreceptors for this response have been identified through screening of chemoreceptor mutants (Río-Álvarez *et al.*, 2015). Both receptors are necessary for plant entry and colonization, and, consistently, a mutant of *A. thaliana* defective in jasmonic acid production was more resistant to bacterial entry through wounds (Antunez-Lamas *et al.*, 2009). A NIT-containing chemoreceptor was recently identified and direct nitrate and nitrite binding to its LBD

demonstrated. Plant wound entry and virulence assays using potato plants showed that this chemoreceptor was involved in these processes (Gálvez-Roldán *et al.*, 2022).

- In contrast to the phytopathogens discussed above, *Xylella fastidiosa* constitutes a clear exception. *X. fastidiosa* is obligatorily transmitted by xylem sap-feeding insects that inject the bacterium into xylem vessels. Unlike most phytopathogens, it is non flagellated and to efficiently colonize and expand inside xylem vessels it depends on twitching motility, mediated by its only chemosensory pathway (Chatterjee *et al.*, 2008). Thus, this lack of flagellum-based chemotaxis in *X. fastidiosa* is probably the result of insect-mediated direct injection into the xylem, avoiding the need to enter plant tissues by finding natural openings or wounds (Matilla and Krell, 2018).

In this doctoral thesis, we have established *Pectobacterium atrosepticum* as a new model to study chemotaxis in phytopathogens, as a preliminary step to analyze the involvement of this process in the virulence of this important plant pathogen.

### **7. Soft Rot *Pectobacteriaceae* (and *Pectobacterium atrosepticum*)**

The Soft Rot *Pectobacteriaceae* (SRP) are Enterobacterales responsible of crop diseases of global importance, including common tuber soft rot, blackleg, wilt and aerial stem rot. It is composed of the *Pectobacterium* and *Dickeya* genera (Davidsson *et al.*, 2013). SRP differ in their host range, with some species affecting a variety of plants and other specialized in a single host (Czajkowski *et al.*, 2015; Ma *et al.*, 2018; Toth *et al.*, 2021). The effects of these diseases can be very important in agriculture, representing losses of several million dollars worldwide each year (Pérombelon, 2002). For example, the annual loss for the European potato market due to SRP is estimated at 46 million € (Dupuis *et al.*, 2021). For this reason, both *Dickeya* and *Pectobacterium* genera rank among the top 10 most important plant pathogenic bacteria (Mansfield *et al.*, 2012). In general, SRP enter the plant host via natural openings, wounds or via contaminated propagation material (Van Gijsegem *et al.*, 2021). On plant surfaces, SRP are flagellated motile cells and chemoattraction to entry sites has been reported (Antúnez-Lamas *et al.*, 2009). Inside plants, SRP reach the apoplast compartment (Van Gijsegem *et al.*, 2021). Temperature is considered as one of the most important factors affecting disease development caused by SRPs (Figure 10) (du Raan *et al.*, 2016). SRPs can rot plant tissues by disintegrating plant cell walls using different Plant Cell Wall Degrading Enzymes (PCWDEs) and can feed on these plant components (Van Gijsegem *et al.*, 2021). Plant cell walls are mainly composed of a cellulose/hemicellulose network embedded in pectin, a matrix of acidic polysaccharides (Cosgrove, 1997; Caffall and Mohnen, 2009). SRPs have adapted to the complexity of pectin by producing a vast array of enzymes including pectinases (e.g. pectate lyases, pectin lyases, pectin sterases, rhamnogalacturonate lyase, and polygalacturonases), with additional PCWDEs secreted for further degradation of cell walls, such as cellulases and proteases (Van Gijsegem *et al.*, 2021). These and other excreted factors are pumped out through different protein secretion systems (T1SS to T6SS), whose presence vary between SRP species (Van Gijsegem *et al.*, 2021).

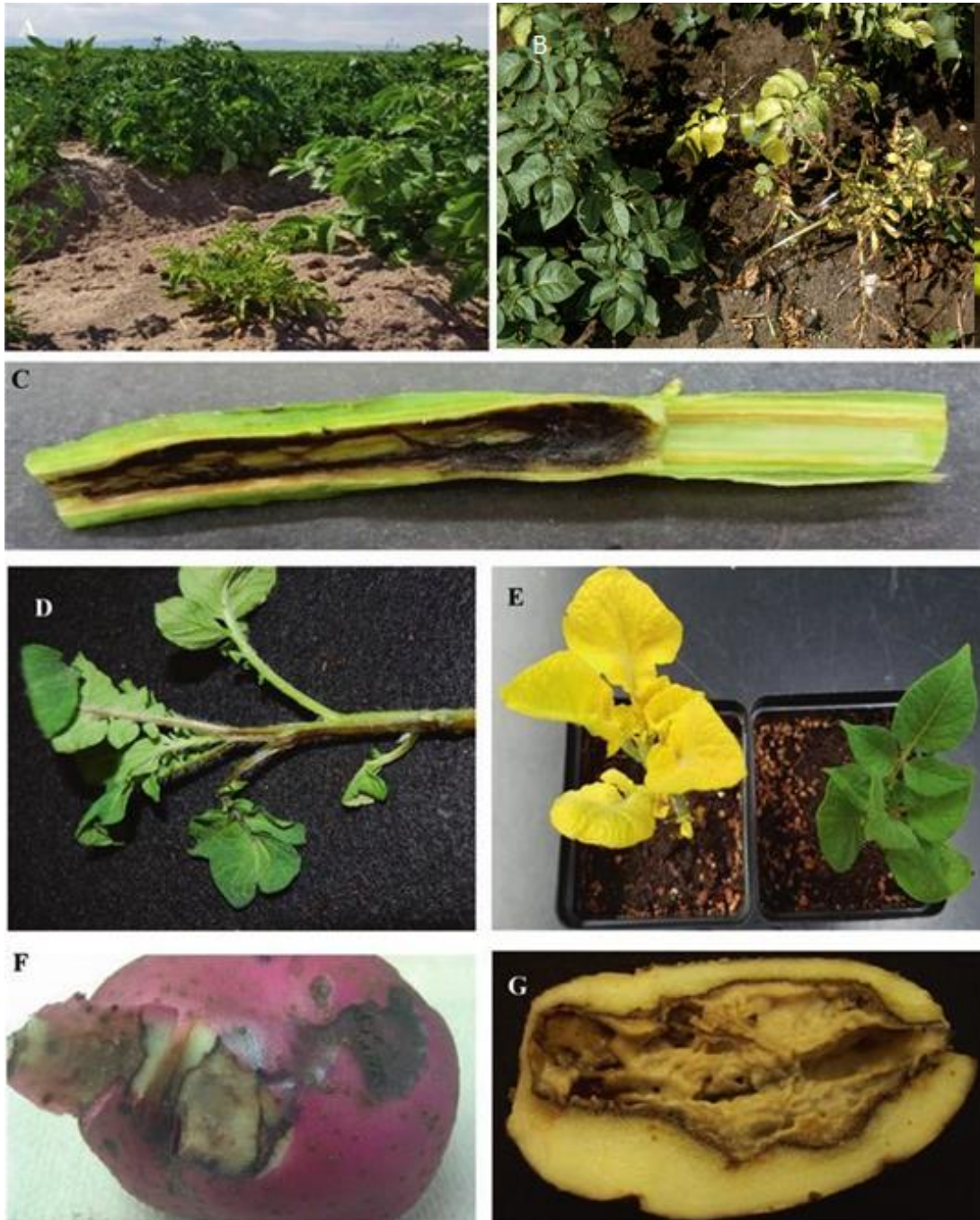


**Figure 10. Bacterial blackleg and tuber soft rot symptoms caused by SRP on potato, including *P. atrosepticum*.** (A,B) Plants with blackleg are shorter and have curled leaves. (C) The stem is blackened on the outside and the inside is decayed with brown xylem. (D) Brown or black decay may spread into leaves (E) or leaves may turn bright yellow. Tubers may have swollen lenticels and sunken lesions. (F, G) Decay in the macerating tuber characteristically spreads from the stolon end. Image modified from (Charkowski *et al.*, 2020).

The taxonomic classification of the *Pectobacterium* genus has changed over time (Arizala and Arif, 2019). It was first characterized as part of the *Erwinia* genus, until 16S rDNA analyses prompted the establishment of an independent phylogenetic cluster (Hauben *et al.*, 1998). Nowadays, it contains several species, from which only *P. carotovorum* subsp. *carotovorum* and *P. brasiliense* (Charkowski *et al.*, 2014; Huang *et al.*, 2019a) are characterized by a wide host



range, including solanaceous and non-solanaceous hosts. The other species are specialized pathogens for one or a few related plant species, including *P. atrosepticum*, *P. parmentieri*, *P. peruviense*, *P. polaris* and *C. P. maceratum* (Bell *et al.*, 2004). *P. atrosepticum* is not further divided into subspecies or pathovars. In 2021, a pangenome analysis of 197 *Pectobacterium* strains, including 19 species, showed that as much as the 52.3% of the average *Pectobacterium* genome is accessory, 46.9% compose the core genome and 0.9% represent unique genes (Jonkheer *et al.*, 2021). Different virulence determinants have been described in *Pectobacterium* species that are employed to downregulate plant defenses and produce disease. They include flagella-based motility and chemotaxis, production of PCWDE, phytotoxins and other effector molecules that are exported by multiple secretion systems, polysaccharides, cell attachment proteins and the type IV pilus, and additional elements jointly regulated by virulence associated promoters (Toth *et al.*, 2006a; Davidsson *et al.*, 2013). Some *Pectobacterium* spp. produces broad spectrum antimicrobials like carbapenem and phenazine, or narrow spectrum, including carotovorcin and carocins (Nguyen *et al.*, 1999; Toth *et al.*, 2006a; Chuang *et al.*, 2007; Chan *et al.*, 2009). Latent infections by *Pectobacterium* have also been reported extensively, and mutants of *Pectobacterium* that do not cause disease but actively propagate in the host plant have been characterized (Fagard *et al.*, 2007; Yang *et al.*, 2008; Jahn *et al.*, 2008; Kim *et al.*, 2011).

Strains belonging to the *Pectobacterium atrosepticum* (*Pba*) species are facultative anaerobes with peritrichous flagella, with an optimal growth temperature of 27 °C (Toth, 2022). *Pba* strain SCRI1043 was the first fully sequenced *Pectobacteriaceae*, containing a genome of 5.06 Mbp, with 4491 protein encoding genes and a G+C content of 50.97 % (Bell *et al.*, 2004). The genome contains 17 putative horizontally acquired islands (HAIs), and protein secretion systems (T1SS to T6SS) are all present in *Pba* (Van Gijsegem *et al.*, 2021). Within the HAIs, fewer than 50% of the genes are shared with other related enterobacteria that are animal pathogens, like *E. coli*, *Yersinia* or *Shigella* species, in contrast to the core genome where many genes are shared between all enterobacteria irrespective of their lifestyle. Moreover, genes within HAIs are often more closely related to genes from other, phylogenetically distant plant pathogens, suggesting an acquisition during development in the same plant niche (Toth *et al.*, 2006a). As indicated above, the main crop infected by *Pba* is potato (*Solanum tuberosum*), a globally important crop plant (Beals, 2019). *Pba* was once the major cause of potato disease in Europe and is probably an indigenous, root dwelling, epiphyte when not causing disease (Toth, 2022). However, its disease range has been much constrained in Europe since the 1970s with 'new' *Pectobacterium* and *Dickeya* species (Toth, 2022). *Pba* still remains the dominant species causing potato blackleg and soft rot in specific temperate regions, including the United Kingdom, Norway, and Canada (Dees *et al.*, 2017; Skelsey *et al.*, 2018; van der Wolf *et al.*, 2021). *Pba* is consistently found in different water sources, suggesting that the main way of spreading of *P. atrosepticum* is water-borne, particularly during irrigation of crops (McCarter-Zorner *et al.*, 1984; Maddox and Harrison, 1988; van Doorn *et al.*, 2011). When *Pba* reaches the plant, it enters the apoplast but can also colonize and spread actively through xylem vessels, leading to systemic infection (Gorshkov *et al.*, 2014). *Pba* are thus pathogens with a subtlety regulated virulence, and that depends of yet unknown signals, resulting in either pronounced virulence or asymptomatic infection. Pathogen and host co-existence without negative effects for plant or bacteria can take place in these latent infections, and understanding this process may help find ways to control this pathogen (Toth and Birch, 2005; Czajkowski *et al.*, 2011; Davidsson *et al.*, 2013).

### 7.1. Chemotaxis in *Pectobacterium atrosepticum* SCRI1043

*Pectobacterium atrosepticum* SCRI1043 (*Pba* SCRI1043) is the model strain in this species and constitutes a widely used model for investigating plant virulence and molecular microbiology of phytopathogenic bacteria (Hinton *et al.*, 1989; Toth *et al.*, 1999; Bell *et al.*, 2004). This thesis has contributed to lay the groundwork on the use of this strain as a model to study the role of chemotaxis in plant pathogenicity. Chemotaxis is suspected to be important when bacteria persisting in their environmental reservoirs need to localize their hosts and aggregate around potential entry sites, as has been demonstrated before for *Dickeya* species (Antunez-Lamas *et al.*, 2009). These reservoirs where chemotaxis may be vital include water, soil, the rhizosphere and plant surfaces. Supporting this hypothesis, expression of chemoreceptor genes has been found up-regulated in nutrient deprived conditions that lead to resistance phenotypes, a phenomenon called “cross-protection” that may help bacteria to survive in different environments including soil, water, insect-vectors, etc. (Gorshkov *et al.*, 2017). We currently ignore which effectors can be recognized by *Pectobacterium* spp. and help cells navigate their environment towards plant hosts.

Flagella proteins were described as important virulence determinants of *Pba* SCRI1043 in the early 1990s (Mulholland *et al.*, 1993). More recently, motility and biofilm formation in *Pba* SCRI1043 were shown to be regulated by c-di-GMP levels (Tan *et al.*, 2014). In addition, flagella and chemotaxis genes were shown to be strongly down-regulated in *P. atrosepticum* infecting tobacco versus *in vitro*. Down-regulating flagellar motility and chemotaxis during endophytic infection agrees with the notion that flagella are a widely known trigger plant immune reactions (Kwenda *et al.*, 2016), but also with the fact that chemotaxis is particularly important during early stages of host infection (Matilla and Krell, 2018). Active movement of *Pba* inside the plant and migration through the xylem vessels has been observed (Gorshkov *et al.*, 2014). This may be explained by the fact that *Pba* SCRI1043 is using pili/fimbriae-based motility inside the host. In fact, the phylogenetically related *P. carotovorum* ssp. *brasiliense* was shown to exhibit twitching motility *in planta* (Moleleki *et al.* 2017). Further details on the role *Pectobacterium* spp. motility and chemotaxis inside different plant tissues are needed and infection studies of mutants in flagellar genes and genes involved in twitching motility may help to define their precise roles in bacterial spread inside plant hosts and their relationship with virulence.

The genome of SCRI1043 codes for a single chemotactic cluster and 36 chemoreceptors (Figure 11). This elevated number of chemoreceptors suggests that this strain is able to perform chemotaxis to a wide range of environmental signals. The cluster contains genes coding for the CheA, CheW, CheR, CheB, CheY, CheZ and a single chemoreceptor (Figure 11A), whereas the rest of the chemoreceptor genes are scattered through the genome. At the beginning of this thesis, no chemoreceptor had been characterized within the *Pectobacterium* genus, and only a couple of them had been identified in the SRP *Dickeya dadanti* (Antunez-Lamas *et al.*, 2009; Río-Álvarez *et al.*, 2015). In the case of SCRI1043, we only could infer weak evidence of their putative ligands based on sequence homology for some of them. This way, the chemoreceptor encoded within the chemotaxis cluster, ECA\_RS08370, has a 4HB LBD with 44% identity to the Tsr chemoreceptor LBD that mediates responses towards cysteine and energy taxis in *Salmonella typhimurium* (Lazova *et al.*, 2012; Rivera-Chávez *et al.*, 2013) or chemotaxis to serine in *E. coli* (Kim *et al.*, 1999). Furthermore, the gene ECA\_RS05475 encodes a receptor containing a dCache



domain with 48% identity to McpA-LBD from *Ralstonia solanacearum*, a sensor for several amino acids (Hida *et al.*, 2015). In addition, the dCACHE domain of the protein ECA\_RS10935 has low identify (22%) to the quaternary amine chemoreceptor McpX from *Sinorhizobium meliloti* (Webb *et al.*, 2017b), whereas ECA\_RS18000 has a 4HB domain sharing 36% identity to Mcp\_2201, an organic acids receptor from *Comamonas testosteroni* (Ni *et al.*, 2013).

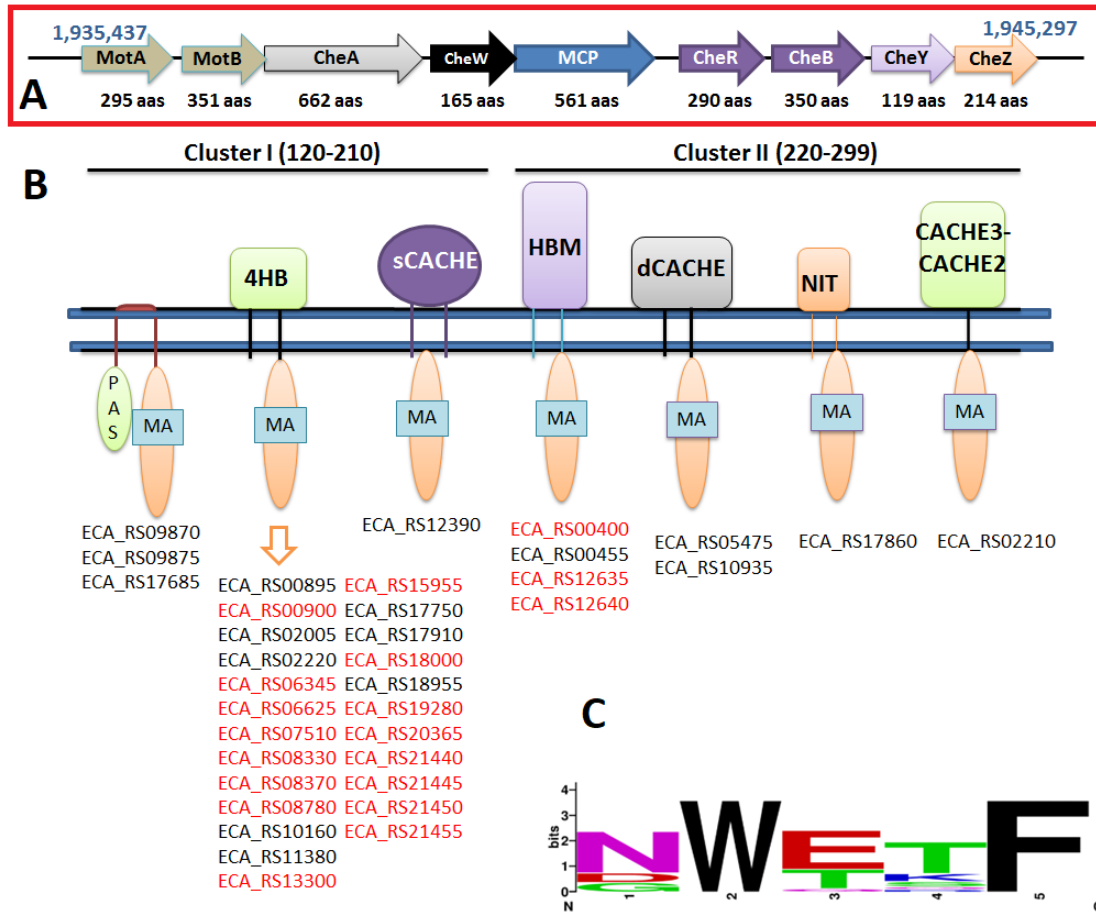


**Figure 11. Schematic representation of the chemotaxis system of *P. atrosepticum* SCRI1043.** (A) The only chemotactic gene cluster of SCRI1043 is represented with the size in amino acids of the predicted proteins. The start and the end coordinates of the cluster are included in blue. (B) The chemoreceptors encoded in the genome are classified with respect to their predicted LBD type. Chemoreceptors with C-terminal pentapeptides are highlighted in red. According to the MIST3 database, there are two dCache\_1 (PF02743) containing chemoreceptors, twelve containing the domain 4HB\_MCP\_1 (PF12729), twelve containing the TarH domain (PF02203), three PAS\_3 domain (PF08447) containing proteins, 2 proteins with HBM (PF16591) domains, one with a Cache\_3-Cache\_2 fusion domain (PF17201), one with a sCACHE\_2 domain (PF17200) and finally one containing the NIT domain (PF08376). In two additional chemoreceptors that we predict to have HBM domains, namely ECA\_RS12640 and ECA\_RS00400, MIST3 can't predict a sensing domain (Gumerov *et al.*, 2020). (C) Consensus sequence of the C-terminal pentapeptides present in 19 of the chemoreceptors.

During the course of this thesis, four chemoreceptors were characterized in the strain *Pectobacterium brasiliense* 1692, whose genome encodes 34 chemoreceptors (Tanui *et al.*, 2021). The authors first identified chemoeffectors for this strain and then selected four chemoreceptor genes that were up-regulated during potato tuber infection. Using mutational

deletion, the function of these chemoreceptors was inferred: two of them, MCP<sub>cit2</sub> and MCP<sub>cit1</sub> responded to citrate, MCP<sub>xyl</sub> responded to xylose and MCP<sub>asp</sub> to aspartate. Trans-complementation of the corresponding mutants restored chemotactic responses towards the compounds identified, although direct binding of the proteins to the ligands was not demonstrated. The authors also showed that these chemoreceptors were not involved in plant virulence, but the mutants were deficient in the capacity to attach to potato leaves. These findings imply a role of these chemoreceptors in the epiphytic phase of pathogen-host interaction (Tanui *et al.*, 2021).

Another question that can be addressed using the chemotactic system of the strain SCRI1043 is the role of the complex set of C-terminal pentapeptides on its chemoreceptors. *P. atrosepticum* SCRI1043 has 19 chemoreceptors with C-terminal pentapeptides that can be grouped into 10 families according to their sequence (Figure 11C). In fact, *Pectobacterium* constitutes the genus where there are more pentapeptide-containing chemoreceptors on average (Ortega and Krell, 2020). In contrast, the better-known system of *E. coli*, where they are involved in chemoreceptor adaptation as has been described before, only has 2 chemoreceptors with a pentapeptide (NWETF), and 3 without pentapeptide. Almost the totality of knowledge on CheR and CheB interactions with C-terminal pentapeptides involves binding to the *E. coli* NWETF sequence. It remains unclear whether all the 10 different pentapeptides in *P. atrosepticum* SCRI1043 bind CheR and CheB, and if so, with what affinity, which is an issue addressed in this thesis.

## OBJECTIVES

---

The main objective of this thesis is to describe the chemosensory pathway and the chemoreceptors present in *P. atrosepticum* SCRI1043, at the functional and structural level, in order to understand the chemotactic abilities of this phytopathogen.

The specific objectives are:

1. Characterization of the binding of the C-terminal pentapeptides present in chemoreceptors to *P. atrosepticum* CheR and CheB and explore the relation of these affinities to the cellular concentration of the adaptation enzymes.
2. Functional and structural analysis of PacA, a quaternary amine binding chemoreceptor of *P. atrosepticum*.
3. Characterization of the various chemoreceptors of *P. atrosepticum* that mediate chemotaxis towards amino acids, at the functional and evolutionary levels.
4. Annotation and description of a new sub-family of sensor domains that specifically recognizes phosphorylated compounds.



## METHODOLOGY

---

This section briefly summarizes the different experimental procedures that have been consistently employed during this thesis. More detailed protocols are described for each chapter in their respective methodology sections.

---

### **Bacterial strains, culture media and growth conditions**

During this doctoral thesis the bacterial strain used was *P. atrosepticum* SCRI1043 along with its mutants and derivative strains generated. Cloning procedures were generally carried out using *E. coli* DH5 $\alpha$ , while protein overexpression was done using *E. coli* BL21 (DE3) or *E. coli* BL21-AI. Typically, *E. coli*  $\beta$ -2163 was employed for generating mutant strains in *P. atrosepticum* SCRI1043. Additional strains specified in the different chapters were used to a lesser extent. General use growth media used were Lisogeny Broth (5 g/l yeast extract, 10 g/l bacto tryptone, 5 g/l NaCl) or minimal medium (0.41 mM MgSO<sub>4</sub>, 7.56 mM (NH<sub>4</sub>)<sub>2</sub>SO<sub>4</sub>, 40 mM K<sub>2</sub>HPO<sub>4</sub>, 15 mM KH<sub>2</sub>PO<sub>4</sub>) supplemented with 0.2% (w/v) glucose as carbon source. *P. atrosepticum* SCRI1043 and its derivative strains were routinely grown at 30 °C while *E. coli* strains were grown at 37 °C. When appropriate, antibiotics were used at different final concentrations that can be found in each chapter. Detailed information about strains used can be found in Tables 2, S6, S9, S11 and S13.

### **Growth experiments**

A Bioscreen Microbiological Growth Analyser (Oy Growth Curves Ab Ltd, Helsinki, Finland) was used to test compounds as potential carbon and nitrogen sources. The assays were conducted in 100-well polystyrene plates containing 200  $\mu$ l of bacterial suspension at an OD<sub>600</sub> of 0.02-0.05 as well as 0.5-10 mM of the compound to be tested. Typically, growth was followed over a time of 24 hours and growth rates were calculated from three independent experiments conducted at least in triplicate.

### **Plasmid construction for LBD overexpression**

Plasmids containing the LBD of the chemoreceptors that were studied were either generated on the laboratory or purchased from Genescript (Piscataway, NJ,). The DNA fragments cloned in the laboratory were amplified by polymerase chain reaction (PCR) using *P. atrosepticum* SCRI1043 genomic DNA as template. The resulting products were then cloned into the expression plasmid pET28(b). The plasmids generated were then verified by sequencing the insert and flanking regions and transformed into *E. coli* DH5a for storage at -80 °C.

### **Generation of *P. atrosepticum* mutant strains**

A modified version of the unmarked non-polar deletion mutant procedure was used for the replacement of wild type genes in the chromosome (Schweizer, 1992). The plasmids for the construction of the deletion mutants were generated by amplifying the up- and downstream flanking regions of the gene to be mutated. The resulting PCR products were digested with enzymes specified in each chapter and cloned into PUC18NotI (Herrero *et al.*, 1990). The

resulting plasmids were then digested with NotI and then the fusion of both fragments was subcloned into the marker exchange suicide vector pKNG101 (Ramos-González and Molin, 1998). Subsequently, plasmids for mutagenesis were transferred into *P. atrosepticum* by biparental conjugation using *E. coli*  $\beta$ -2163. Cells were plated in LB with 50  $\mu$ g/ml streptomycin but lacking 300 mM 2, 6-diaminopimelic acid, necessary for *E. coli*  $\beta$ 2163 growth, for selection of plasmid cointegration. For the construction of the final mutant, sucrose was added to a final concentration of 10% (w/v) to select derivatives that had undergone a second cross-over event during marker exchange mutagenesis. Streptomycin sensitive colonies were screened by PCR analyses and the resulting mutants were confirmed by DNA sequencing. When this procedure didn't produce clear mutant strains, the kanamycin resistance cassette Km3 from the plasmid p34S-km3 was inserted into the BamHI site of the pUC18Not-derivative plasmids, and the steps described above were performed using kanamycin selection as an additional pressure for mutant generation. Kanamycin resistant strains were also confirmed by PCR screening and sequencing.

### **Construction of overexpression plasmids**

Genes for chemoreceptors that didn't show wild type chemotactic phenotypes in the experimental conditions assayed (Chapters 2 and 4) were overexpressed using plasmid pBBRMCS-2\_START (Obranić *et al.*, 2013). The DNA-sequences for the desired genes were amplified using appropriate primers from genomic DNA of *P. atrosepticum* SCRI1043 and cloned into pBBRMCS-2\_START using restriction enzymes detailed in the corresponding chapters. These plasmids were verified by PCR and sequencing the inserts and flanking regions. The resulting plasmid was transformed into *P. atrosepticum* SCRI1043 by electroporation and these strains were used for phenotypic analyses.

### **Protein overexpression**

*E. coli* BL21 (DE3) or BL21-AI was transformed with each of the expression plasmids. The resulting strains were cultured at 30 °C in LB supplemented with kanamycin under continuous shaking. At an OD 600 of 0.5-0.6 protein overexpression was induced by the addition of 0.1 mM isopropyl-B-D-1- thiogalactopyranoside (IPTG). When using BL21-AI, L-arabinose 2% (w/v) was also added to the culture at this point. After 14 - 16 h of further growth at 16 °C and continuous shaking, cells were harvested by centrifugation at 10000 x *g* and 4°C for 30 min.

### **Protein purification**

Cells pellets containing overexpressed polyHis-tagged protein, were resuspended in buffer and broken by French press treatment at a gauge pressure of 62.5 lb/in. After centrifugation at 20000 x *g* and 4 °C for 30-60 min, the supernatant was filtered and loaded onto an immobilized metal ion affinity chromatography column (HisTrap, Amersham Bioscience), connected to a ÄKTA P- 920/UPC-900 fast liquid protein chromatography instrument. After a wash step with buffer containing 35 mM imidazole, the protein was eluted by a gradient of buffer containing 35 - 500 mM imidazole. Protein-containing fractions were pooled and dialysed into analysis buffer for immediate analysis.

### **Differential scanning fluorimetry based high throughput ligand screening**

High-throughput ligand screening was performed by Differential Scanning Fluorimetry based thermal shift assays, using commercially available compound arrays (Biolog, Hayward, CA, USA). Each well of a 96-well plate was filled with a 25  $\mu$ l aliquot containing 10-50  $\mu$ M of protein, 5x SYPRO Orange (Life Technologies) and 1 - 2 mM of the compound to be tested. One of the wells (control) contained only the protein and 5 x SYPRO. Plates were inserted into a MyIQ2 Real-Time PCR instrument (Bio-Rad) and heated from 23  $^{\circ}$ C to 85  $^{\circ}$ C at a scan rate of 1  $^{\circ}$ C/min, during which time fluorescence changes were monitored.  $T_m$  values were calculated analyzing the minima of the first derivatives of the raw data.

### **Isothermal titration calorimetry**

Experiments were carried out on a VP microcalorimeter (Microcal, Amherst, MA, USA) at a temperature of 15 - 35  $^{\circ}$ C. Protein solutions, typically between 10 - 100  $\mu$ M, were placed into the sample cell and titrated with 6.4 - 19.2  $\mu$ l aliquots of ligand solutions at a concentration of 0.25 -20 mM. The mean enthalpy changes arising from the titration of buffer with ligand solution were subtracted from the protein raw titration data prior to data analysis. Unless otherwise is stated, data analysis was performed with the "One binding site model" of the MicroCal version of ORIGIN.

### **Protein crystallization**

Optimal conditions for protein crystallization were screened using the capillary counter-diffusion technique using the set of conditions prepared *ad hoc* that have been reported in (González-Ramírez *et al.*, 2017). Purified protein was incubated with saturating ligand concentrations at 4 -25  $^{\circ}$ C and the excess of ligand was removed by centrifugation using 3 kDa cutoff Amicon concentrators. The apo-protein and protein-ligand complex were loaded into capillaries with an inner diameter of 0.2-mm. Crystals were extracted from the capillaries, flash cooled in liquid nitrogen and stored until data collection.

### **Structure resolution**

Crystals were diffracted at the European Synchrotron Radiation Facility or the Spanish Synchrotron ALBA. In Chapter 1 data generated was indexed, reduced and scaled using the default data processing with EDNA (Incardona *et al.*, 2009) within the MXCuBE data collection interface (Gabadinho *et al.*, 2010). In Chapter 2, data were indexed and integrated with XDS (Kabsch, 2010) and scaled and reduced with AIMLESS (Evans and Murshudov, 2013) of the CCP4 program suite (Collaborative Computational Project, Number 4, 1994). Attempts to solve the phase problem were undertaken using molecular replacement techniques and homology models, including by implementing the deep learning-based method, AlphaFold, within the Rosetta predictor software run in the Robetta server (RoseTTAFold) (Baek *et al.*, 2021). The coordinates and the experimental structure factors for the crystallized proteins from *P. atrosepticum* SCRI1043 have been deposited at the Protein Data Bank (PDB) (wwPDB consortium *et al.*, 2019).

### **Swimming plate motility assay**

Overnight cultures from single colonies of bacteria were grown at the appropriate temperature. Two-microliter aliquots of bacterial suspension were transferred to the center of swim agar plates (0.25 % (w/v) agar in minimal medium supplemented with 10 % (w/v) LB. Plates were inspected after growth for 14-18 h.

### **Quantitative capillary chemotaxis assay**

Bacterial chemotaxis was quantified in a modified version of the capillary assay (Adler, 1973). Unless otherwise indicated, flasks containing 20 ml of minimal medium supplemented with 15 mM D-glucose were inoculated with overnight cultures grown in minimal medium to an initial  $OD_{600}$  of 0.05-0.075. The cultures were grown until an  $OD_{600}$  of 0.4-0.5 and washed twice by a 5-minute centrifugation at  $1667 \times g$ , followed by resuspension in chemotaxis buffer (50 mM potassium phosphate, 20  $\mu$ M EDTA, 0.05% (v/v) glycerol, pH 7.0) and dilution with the same buffer to an  $OD_{600}$  of 0.1. The wells of 96- well plates were filled with 230  $\mu$ l of the resulting bacterial suspension. Capillaries (Microcaps, Drummond Scientific) were heat-sealed on one end and filled by heating the capillary over a flame and subsequent placement of the open end of the capillary into buffer or chemoeffector solution. The open end of the capillaries were submerged into the bacterial suspension for 30 min, after which time the capillary content was emptied into Eppendorf tubes containing 1 ml of chemotaxis medium (see chemotaxis media composition details in "Methodology" section of each chapter). Serial dilutions were plated on minimal medium plates supplemented with 15 mM D- glucose. Colonies were counted after 48 h incubation.



## RESULTS

---



## Chapter 1. Evidence for pentapeptide dependent and independent CheB methylesterases

---

*Published article*

### **Evidence for pentapeptide dependent and independent CheB methylesterases**

**Félix Velando**<sup>1</sup>, José A. Gavira<sup>2</sup>, Miriam Rico-Jiménez<sup>1</sup>, Miguel A. Matilla<sup>1</sup> and Tino Krell<sup>1</sup>

<sup>1</sup>Department of Environmental Protection, Estación Experimental del Zaidín, Consejo Superior de Investigaciones Científicas; <sup>2</sup>Laboratory of Crystallographic Studies, IACT, (CSIC-UGR)

**International Journal of Molecular Sciences** (Published 11 November 2020); vol. 21, 8459.  
doi:10.3390/ijms21228459

---

### **Abstract**

---

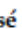


Many bacteria possess multiple chemosensory pathways that are composed of homologous signaling proteins. These pathways appear to be functionally insulated from each other, but little information is available on the corresponding molecular basis. We report here a novel mechanism that contributes to pathway insulation. We show that, of the four CheB paralogues of *Pseudomonas aeruginosa* PAO1, only CheB<sub>2</sub> recognizes a pentapeptide at the C-terminal extension of the McpB (Aer2) chemoreceptor ( $K_D=93 \mu\text{M}$ ). McpB is the sole chemoreceptor that stimulates the Che2 pathway and CheB<sub>2</sub> is the methylesterase of this pathway. *Pectobacterium atrosepticum*SCRI1043 has a single CheB, CheB<sub>Pec</sub>, and 19 of its 36 chemoreceptors contain a C-terminal pentapeptide. Deletion of *cheB<sub>Pec</sub>* abolished chemotaxis but, surprisingly, none of the pentapeptides bound to CheB<sub>Pec</sub>. To determine the corresponding structural basis we solved the 3D structure of CheB<sub>Pec</sub>. Its structure aligned well with that of the pentapeptide dependent enzyme from *Salmonella enterica*. However, no electron density was observed in the CheB<sub>Pec</sub> region corresponding to the pentapeptide binding site in the *Escherichia coli* CheB. We hypothesize that this structural disorder is associated with the failure to bind pentapeptides. Combined data show that CheB methylesterases can be divided into pentapeptide dependent and independent enzymes.

---



Article

# Evidence for Pentapeptide-Dependent and Independent CheB Methyltransferases

Félix Velando <sup>1,†</sup>, José A. Gavira <sup>2,†</sup> , Miriam Rico-Jiménez <sup>1,†</sup>, Miguel A. Matilla <sup>1,\*</sup>  and Tino Krell <sup>1,\*</sup> 

<sup>1</sup> Department of Environmental Protection, Estación Experimental del Zaidín, Consejo Superior de Investigaciones Científicas, Prof. Albareda 1, 18008 Granada, Spain; felix.velando@eez.csic.es (F.V.); miriamrj@gmail.com (M.R.-J.)

<sup>2</sup> Laboratory of Crystallographic Studies, IACT, (CSIC-UGR), Avenida de las Palmeras 4, 18100 Armilla, Spain; jgavira@iact.ugr-csic.es

\* Correspondence: miguel.matilla@eez.csic.es (M.A.M.); tino.krell@eez.csic.es (T.K.); Tel.: +34-958-181600 (M.A.M. & T.K.); Fax: +34-958-135740 (M.A.M. & T.K.)

† Authors contributed equally.

Received: 21 October 2020; Accepted: 9 November 2020; Published: 11 November 2020



**Abstract:** Many bacteria possess multiple chemosensory pathways that are composed of homologous signaling proteins. These pathways appear to be functionally insulated from each other, but little information is available on the corresponding molecular basis. We report here a novel mechanism that contributes to pathway insulation. We show that, of the four CheB paralogs of *Pseudomonas aeruginosa* PAO1, only CheB<sub>2</sub> recognizes a pentapeptide at the C-terminal extension of the McpB (Aer2) chemoreceptor ( $K_D = 93 \mu\text{M}$ ). McpB is the sole chemoreceptor that stimulates the Che2 pathway, and CheB<sub>2</sub> is the methyltransferase of this pathway. *Pectobacterium atrosepticum* SCRI1043 has a single CheB, CheB<sub>Pec</sub>, and 19 of its 36 chemoreceptors contain a C-terminal pentapeptide. The deletion of *cheB<sub>Pec</sub>* abolished chemotaxis, but, surprisingly, none of the pentapeptides bound to CheB<sub>Pec</sub>. To determine the corresponding structural basis, we solved the 3D structure of CheB<sub>Pec</sub>. Its structure aligned well with that of the pentapeptide-dependent enzyme from *Salmonella enterica*. However, no electron density was observed in the CheB<sub>Pec</sub> region corresponding to the pentapeptide-binding site in the *Escherichia coli* CheB. We hypothesize that this structural disorder is associated with the failure to bind pentapeptides. Combined data show that CheB methyltransferases can be divided into pentapeptide-dependent and independent enzymes.

**Keywords:** bacterial signal transduction; chemosensory pathways; chemoreceptor; X-ray structure; C-terminal pentapeptide; CheB; methyltransferase

## 1. Introduction

Chemosensory pathways are among the most abundant prokaryotic signal transduction mechanisms [1]. Apart from mediating flagellum based chemotaxis, chemosensory pathways carry out alternative cellular functions like the control of second messenger levels or type IV pili-based motility [1–3]. The key element of a chemosensory pathway is the ternary complex formed by chemoreceptors, the CheA autokinase and the CheW coupling protein. Signaling is typically initiated by signal recognition at the chemoreceptor ligand-binding domain (LBD) that creates a molecular stimulus modulating CheA autophosphorylation and, subsequently, transphosphorylation to the CheY response regulator. The ratio of CheY to phosphorylated CheY (CheY-P) defines the pathway output [4].

The pathway sensitivity is adjusted by the coordinated action of the CheR methyltransferase and the CheB methyltransferase that catalyze methylation and demethylation, respectively, of several

## Introduction

---

Chemosensory pathways are among the most abundant prokaryotic signal transduction mechanisms (Wuichet and Zhulin, 2010). Apart from mediating flagellum based chemotaxis, chemosensory pathways carry out alternative cellular functions like the control of second messenger levels or type-IV pili based motility (Whitchurch *et al.*, 2004; Hickman *et al.*, 2005; Wuichet and Zhulin, 2010). The key element of a chemosensory pathway is the ternary complex formed by chemoreceptors, the CheA autokinase and the CheW coupling protein. Signalling is typically initiated by signal recognition at the chemoreceptor ligand binding domain (LBD) that creates a molecular stimulus modulating CheA autophosphorylation and subsequently transphosphorylation to the CheY response regulator. The ratio of CheY to phosphorylated CheY (CheY-P) defines the pathway output (Parkinson *et al.*, 2015).

The pathway sensitivity is adjusted by the coordinated action of the CheR methyltransferase and the CheB methyl-esterase that catalyse methylation and demethylation, respectively, of several glutamate residues at the chemoreceptor signaling domain. It was shown that poorly methylated chemoreceptors have high chemoeffector affinity and high propensity for methylation (Parkinson *et al.*, 2015; Bi and Sourjik, 2018). Genome analyses revealed that genes encoding both enzymes are present in the large majority of chemosensory pathways and are thus among the 6 core pathway proteins (Wuichet and Zhulin, 2010).

In *Escherichia coli*, CheR was found to bind to the methylation site of the Tar chemoreceptor with a rather modest affinity, ranging between 100 to 200  $\mu\text{M}$  depending on experimental conditions (Li and Hazelbauer, 2020). However, Tar possesses a C-terminal pentapeptide that is tethered to the C-terminal end of the chemoreceptor signaling domain via an unstructured linker (Bartelli and Hazelbauer, 2011). This pentapeptide, NWETF, represents an additional binding site for CheR and CheB (Perez and Stock, 2007; Ortega and Krell, 2020). CheR from *E. coli* bound NWETF with a  $K_D$  value affinity of approximately 2  $\mu\text{M}$ , an affinity that is around 100-fold higher than the affinity for the methylation site (Wu *et al.*, 1996; Li and Hazelbauer, 2020). It was proposed that CheR binding to the pentapeptide enhanced the local CheR concentration leading to optimal adaptation (Le Moual *et al.*, 1997; Li and Hazelbauer, 2005). Remarkably, genome analyses indicated that approximately 10% of chemoreceptors possess a C-terminal pentapeptide (Ortega and Krell, 2020) and experimental studies as well as sequence analyses of CheR from different species have shown that this protein family can be subdivided into pentapeptide dependent and independent enzymes that are either able or unable to bind these pentapeptides (Perez and Stock, 2007; García-Fontana *et al.*, 2014). The structure of the CheR-pentapeptide complex has been solved (Djordjevic and Stock, 1998) and several sequence features at or close to the pentapeptide binding site have been identified to be specific for each CheR subfamily (Perez and Stock, 2007; García-Fontana *et al.*, 2014).

Compared to CheR, less information is available on CheB function. Much of what we know on this protein family is due to the studies of the enzymes from *E. coli* (Barnakov *et al.*, 1999; Barnakov *et al.*, 2001; Barnakov *et al.*, 2002; Li and Hazelbauer, 2004; Li and Hazelbauer, 2006) and *Salmonella enterica* sv. Typhimurium (West *et al.*, 1995; Anand *et al.*, 1998; Djordjevic *et al.*, 1998; Anand and Stock, 2002) that share 95 % of amino acid sequence identity (Figure S1). Both species possess a single chemosensory pathway, a single pentapeptide dependent CheB and two chemoreceptors, Tar and Tsr, that contain a C-terminal pentapeptide. CheB from *E. coli* bound

this pentapeptide with much lower affinity ( $K_D= 130$  to  $160 \mu\text{M}$ , depending on method used) (Barnakov *et al.*, 2002) as compared to CheR. The affinity of CheB for the pentapeptide is thus too low as to increase the local concentration, but the CheB-pentapeptide interaction was found to stimulate methylesterase activity (Barnakov *et al.*, 2002). CheB is composed of a phosphorylgroup accepting receiver domain (REC) and a methylesterase domain (Djordjevic *et al.*, 1998) and it was shown that REC domain phosphorylation stimulates the catalytic activity of CheB (Barnakov *et al.*, 2002).

The mutation or removal of the NWETF pentapeptide from the *E. coli* Tar and Tsr chemoreceptors largely reduced methylation and demethylation *in vivo* and *in vitro* and abolished chemotaxis (Li *et al.*, 1997; Le Moual *et al.*, 1997; Okumura *et al.*, 1998; Barnakov *et al.*, 1999; Li and Hazelbauer, 2006). This results in the paradoxical situation where C-terminal pentapeptides are essential for the functioning of some receptors, like Tar and Tsr, but are absent from many other chemoreceptors that mediate strong chemotactic responses (Luu *et al.*, 2015; Matilla and Krell, 2017; Corral-Lugo *et al.*, 2018; Compton *et al.*, 2018; Martín-Mora *et al.*, 2019). Consequently, the physiological relevance of pentapeptide depending chemosignaling remains to be established, but we have recently shown that pentapeptide containing chemoreceptors are more abundant in bacteria that maintain host interactions (Ortega and Krell, 2020). In addition, it is little clear to which degree there are pentapeptide independent CheB. To address this latter issue, we report here studies of CheB homologs from the human and plant pathogenic bacterial strains, *Pseudomonas aeruginosa* PAO1 (Stover *et al.*, 2000) and *Pectobacterium atrosepticum* SCRI1043 (Bell *et al.*, 2004).

*P. aeruginosa* PAO1 has five gene clusters encoding signaling proteins that assemble to four chemosensory pathways (Figure 11) (Ortega *et al.*, 2017b). These pathways differ in function: whereas the Che pathway mediates chemotaxis (Masduki *et al.*, 1995; Kato *et al.*, 1999), the Wsp pathway controls c-di-GMP levels (Hickman *et al.*, 2005), the Chp pathway was associated with type-IV pili mediated motility and cAMP levels (Whitchurch *et al.*, 2004; Fulcher *et al.*, 2010), whereas the function of the Che<sub>2</sub> pathway is unknown. As shown in Figure 12, each chemosensory pathway contains a CheR and CheB homolog. Experimental and bioinformatic studies indicate that of the 26 chemoreceptors, McpB (synonym Aer2) (Figure 11) is the sole chemoreceptor that feeds into the Che<sub>2</sub> pathway (Ortega *et al.*, 2017b; Orillard and Watts, 2021). Furthermore, it is the only chemoreceptor with a C-terminal pentapeptide (García-Fontana *et al.*, 2014). We previously showed that of the four CheR homologs, the methyltransferase of the Che<sub>2</sub> pathway, CheR<sub>2</sub>, was the only homolog that bound the McpB pentapeptide (García-Fontana *et al.*, 2014). Furthermore, binding to this pentapeptide was essential for the CheR<sub>2</sub> interaction and methylation of McpB (García-Fontana *et al.*, 2014). We have concluded that the specific pentapeptide-CheR<sub>2</sub> interaction is a mechanism that permits the targeting a particular chemoreceptor with a specific CheR (García-Fontana *et al.*, 2014).

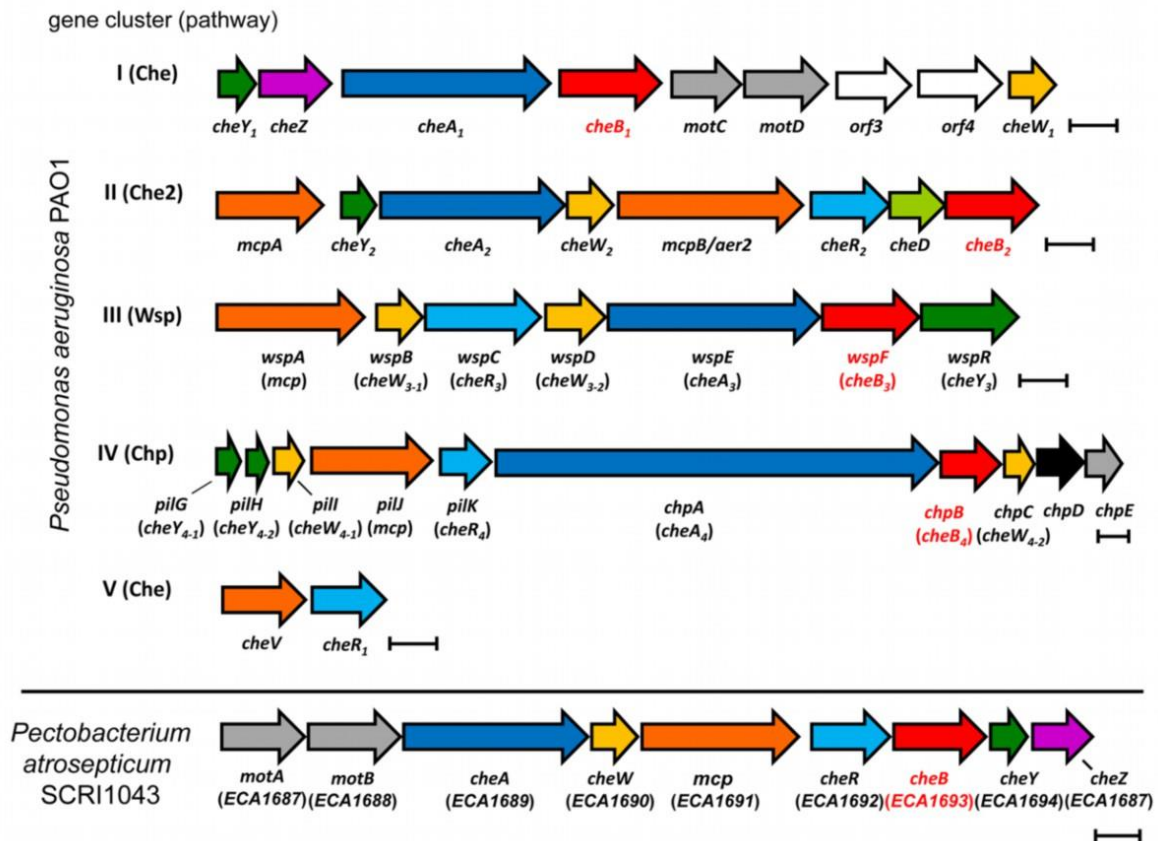


**Figure 12. Gene clusters encoding chemosensory signaling proteins in *P. aeruginosa* PAO1 and *P. atrosepticum* SCRI1043.** Genes of the same family are coloured in the same colour. The genes of the proteins studied in this article are shown in red. Bars, 0.5 kbp.

The 4 CheB homologs of *P. aeruginosa* were found to play important physiological roles. A *cheB*<sub>1</sub> mutant was non chemotactic (Ferrández *et al.*, 2002) and screening of a 2,200-member mutant library for virulence defects in a cystic fibrosis airway *P. aeruginosa* isolate revealed that a *cheB*<sub>2</sub> mutant showed one of the strongest phenotypes in *Caenorhabditis elegans*; a finding that was confirmed by experimentation on mice (Garvis *et al.*, 2009). A *cheB*<sub>3</sub>/*wspF* mutant caused elevated c-di-GMP levels and enhanced biofilm formation (Hickman *et al.*, 2005), due to locking this pathway into an active state. Interestingly, cystic fibrosis airway infections frequently produce rugose small-colony variants (RSCV) and this phenotype could be reverted by the *in trans* expression of *cheB*<sub>3</sub>/*wspF*, indicating that *cheB*<sub>3</sub>/*wspF* mutations are a very frequent mechanism for generating RSCV morphotypes (Starkey *et al.*, 2009). As for the *cheB*<sub>4</sub> gene, its mutation caused hyper-piliation (Whitchurch *et al.*, 2004), prevented swarming and formed more robust biofilms by stimulating matrix production (Caiazza *et al.*, 2007). Considering the pentapeptide mediated specific interaction of CheR<sub>2</sub> and McpB, we have studied here the interaction of the McpB pentapeptide with the four CheB homologs.

Since *P. aeruginosa* has 4 CheB paralogs and a single pentapeptide containing chemoreceptor, we aimed at studying the inverse situation, i.e. a bacterium with a single CheB but multiple chemoreceptors with pentapeptides of different sequences. To this end, we have chosen *P. atrosepticum* SCRI1043 as model that has a single CheB and 19 chemoreceptors with a pentapeptide (Bell *et al.*, 2004). *P. atrosepticum* is among the top 10 plant pathogens (Mansfield *et al.*, 2012) and the causative agent of soft rot diseases in many agriculturally relevant crops

(Toth *et al.*, 2003). This species belongs, like *E. coli* and *S. enterica*, to the *Enterobacteriaceae* family. Combined data from both strains allows distinguishing between pentapeptide dependent and independent CheB proteins.

## Materials and Methods

---

**Bacterial strains and growth conditions:** Bacterial strains used in this study are listed in Table S1. *P. atrosepticum* SCRI1043 and its derivative strains were routinely grown at 30 °C in Lisogeny Broth (5 g/l yeast extract, 10 g/l bacto tryptone, 5 g/l NaCl) or minimal medium (0.41 mM MgSO<sub>4</sub>, 7.56 mM (NH<sub>4</sub>)<sub>2</sub>SO<sub>4</sub>, 40 mM K<sub>2</sub>HPO<sub>4</sub>, 15 mM KH<sub>2</sub>PO<sub>4</sub>) supplemented with 0.2% (w/v) glucose as carbon source. *E. coli* strains were grown at 37 °C in LB. *E. coli* DH5α was used as a host for gene cloning. Media for propagation of *E. coli* β2163 were supplemented with 300 mM 2,6-diaminopimelic acid. When appropriate, antibiotics were used at the following final concentrations (in µg ml<sup>-1</sup>): kanamycin, 50; tetracycline, 10, streptomycin, 50, ampicillin, 100. Sucrose was added to a final concentration of 10% (w/v) when required to select derivatives that had undergone a second cross-over event during marker exchange mutagenesis.

**Generation of protein expression plasmids:** Plasmids used in this study are listed in Table S1. Genes encoding *P. aeruginosa* PAO1 CheB<sub>1</sub> (PA1459), CheB<sub>2</sub> (PA0173), CheB<sub>3</sub> (PA3703), CheB<sub>4</sub> (PA0414) and *P. atrosepticum* SCRI1043 CheB (ECA1693) were amplified by PCR using the oligonucleotides indicated in Table S4 and genomic DNA as template. The latter PCR product was digested with NheI and Sall, whereas the remaining products were digested with NdeI and BamHI. The resulting DNA fragments were cloned into pET28b(+) linearized with the respective endonucleases. The generated plasmids were verified by DNA sequencing.

**Site-directed mutagenesis:** The Hemsley method (Hemsley *et al.*, 1989) was used to generate the CheB<sub>2</sub> D55E mutant. The pair of overlapping mutagenic primers pET28\_CheB<sub>2</sub>\_D55E\_f and pET28\_CheB<sub>2</sub>\_D55E\_r (Table S4) were used to amplify the entire plasmid pET28b-CheB<sub>2</sub> using the *Pfu* Turbo DNA polymerase (Agilent Technologies). Following the elimination of template DNA by a digestion with DpnI, the resulting mixture was transformed into *E. coli* DH5α and colonies were selected on LB agar plates supplemented with kanamycin. Plasmid inserts and flanking regions were sequenced.

**Protein overexpression and purification:** Plasmids for the overexpression of the wt and mutant CheB proteins of PAO1 were transformed into *E. coli* BL21 (DE3). Alternatively, pET28b-CheB\_Pec was transformed into *E. coli* BL21-AI™. The resulting strains were grown under continuous stirring (200 rpm) at 30 °C in 2-liter Erlenmeyer flasks containing 500 ml of LB medium supplemented with 50 µg/ml kanamycin. At an OD<sub>660</sub> of 0.6, protein expression was induced by the addition of 0.1 mM isopropyl β-D-1-thiogalactopyranoside. In addition, L-arabinose was added to *E. coli* BL21-AI™ cultures to a final concentration of 0.2% (w/v). Growth was continued at 16 °C overnight prior to cell harvest by centrifugation at 10 000 x g for 30 min. Cell pellets for the purification of CheB proteins of *P. aeruginosa* were resuspended in buffer A (20 mM Tris/HCl, 500 mM NaCl, 5% (v/v) glycerol, 10 mM imidazole, 0.1 mM EDTA, 5 mM β-mercaptoethanol, pH 8.0), whereas pellets for the purification of CheB\_Pec were resuspended in buffer B (20 mM Tris/HCl, 150 mM NaCl, 10 mM imidazole, 0.1 mM EDTA, 10% (v/v) glycerol, 10 mM β-mercaptoethanol, pH 8.0). Subsequently, cells were broken by French press treatment at 62.5 lb/in<sup>2</sup>. After centrifugation at 20 000 x g for 30 min, supernatants were loaded onto 5-ml



HisTrap HP columns (Amersham Biosciences) equilibrated with the corresponding buffer A or B and eluted with an imidazole gradient of 40–500 mM in the corresponding buffer. When necessary, the His-tag was removed by treatment with bovine thrombin (Sigma-Aldrich, Buchs, Switzerland) at 2 U/ml and 16 °C for 2 h. For crystallization, CheB\_Pec was dialysed into 5 mM Tris/HCl, 5 mM Pipes, 5 mM Mes, 2 mM dithiothreitol, 150 mM NaCl, 10 % (v/v) glycerol, pH 7.4 and purified by size-exclusion chromatography using a HiPrep™ 26/60 Sephacryl™ S200 HR gel filtration column (GE Healthcare) at a flow rate of 1 ml/min. All proteins were purified at 4 °C. Purified proteins were dialysed overnight into the corresponding analysis buffers for immediate analysis.

*Isothermal titration calorimetry (ITC):* All experiments were conducted on a VP-microcalorimeter (Microcal, Amherst, MA) at 25 °C. For the analysis of the CheB homologs of *P. aeruginosa*, 15–40 µM of protein (dialysed into 5 mM Tris/HCl, 5 mM Pipes, 5 mM Mes, pH 7.0) were placed into the sample cell and titrated with 1–7 mM solutions of the GWEEF peptide (synthesized by Biomedal S.L., Spain). For the analysis of CheB\_Pec, protein was dialysed into 5 mM Tris/HCl, 5 mM PIPES, 5 mM MES, 10% (v/v) glycerol, 2 mM dithiothreitol, 150 mM NaCl, 0.1 mM EDTA, pH 7.4, adjusted to 15–50 µM and titrated with 4.8–14.4 µl aliquots of 1–5 mM peptide solutions (synthesized by GenScript®). All ligand solutions were prepared in dialysis buffer immediately before use. The mean enthalpies measured from the injection of the peptide into the buffer were subtracted from raw titration data prior to data analysis with the ‘One binding site model’ of the MicroCal version of ORIGIN.

*Chemoreceptor sequence analysis:* Sequences were retrieved from the MIST 3.0 database (Gumerov *et al.*, 2020), transmembrane regions identified using DAS (Cserző *et al.*, 1997) and ligand binding domains annotated according to Pfam (El-Gebali *et al.*, 2019). Pentapeptides at chemoreceptors were identified as reported in (Perez and Stock, 2007). These peptides matched the xZxxZ motif (where Z represents either F, W or Y) and are separated from the chemoreceptor signaling domain by a linker sequence of at least 10 amino acids.

*Derivatization of CheB\_Pec by beryllium fluoride:* A modified version of the protocol described in (Guhaniyogi *et al.*, 2006) was employed. Briefly, 0.1 M BeSO<sub>4</sub>, 10 mM NaF and 10 mM MgCl<sub>2</sub> (all final concentrations) were added to CheB\_Pec dialysed into 5 mM Tris/HCl, 5 mM PIPES, 5 mM MES, 10% (v/v) glycerol, 2 mM dithiothreitol, 150 mM NaCl, 0.1 mM EDTA, pH 7.4. The resulting mixture was incubated at 25 °C for 3 h.

*Construction of mutants deficient in cheA and cheB:* Chromosomal mutants of SCRI1043 were constructed by homologous recombination using a derivative plasmid of the suicide vector pKNG101. These plasmids were confirmed by DNA sequencing and carried deletion mutant alleles for the replacement of wild type genes in the chromosome. In all cases, plasmids for mutagenesis were transferred to *P. atrosepticum* SCRI1043 by biparental conjugation using *E. coli* β2163. The plasmids for the construction of the deletion mutants were generated by amplifying the up- and downstream flanking regions of the gene to be mutated. The resulting PCR products were digested with enzymes specified in Table S1 and ligated in a three-way ligation into pUC18Not, producing plasmids pUC18Not\_ΔcheB and pUC18Not\_ΔcheA. Subsequently, the kanamycin resistance cassette Km3 from the plasmid p34S-km3 was inserted into the BamHI of pUC18Not\_ΔcheA, resulting in plasmid pUC18Not\_ΔcheA-Km3. The ΔcheB and ΔcheA-km3 deletion constructs were then sub-cloned into the marker exchange vector

pKNG101 using NotI. Mutant strains defective in *cheA* and *cheB* were generated using plasmids pKNG101\_Δ*cheA*-km3 and pKNG101\_Δ*cheB*, respectively.

*Quantitative capillarity chemotaxis assays:* Overnight cultures of *P. atrosepticum* were grown at 30 °C in minimal medium. At an OD<sub>660</sub> of 0.35–0.4, the cultures were washed twice with chemotaxis buffer (50 mM K<sub>2</sub>HPO<sub>4</sub>/KH<sub>2</sub>PO<sub>4</sub>, 20 μM EDTA and 0.05% (v/v) glycerol, pH 7.0) and diluted to an OD<sub>660</sub> of 0.1 in the same buffer. Subsequently, 230 μl of the resulting bacterial suspension were placed into the wells of 96-well plates. One-microliter capillary tubes (P1424, Microcaps; Drummond Scientific) were heat-sealed at one end and filled with either the chemotaxis buffer (negative control) or chemotaxis buffer containing casamino acids. The capillaries were immersed into the bacterial suspensions at their open ends. After 30 min at room temperature, the capillaries were removed from the bacterial suspensions, rinsed with sterile water and the content expelled into 1 ml of minimal medium salts. Serial dilutions were plated onto minimal medium supplemented with 15 mM glucose as carbon source. The number of colony forming units was determined after incubation at 30 °C for 36 h. In all cases, data were corrected with the number of cells that swam into buffer containing capillaries.

*Crystallization and resolution of the three-dimensional structure of CheB\_Pec:* CheB\_Pec was dialyzed into 5 mM Tris/HCl, 150 mM NaCl, 2 mM dithiothreitol, 10% (v/v) glycerol, pH 7.4 and concentrated to 2.35 mg/ml using 3 kDa cut-off centricon concentrators (Amicon). Crystallization conditions were screened using the capillary counter-diffusion technique and a set of conditions prepared *ad hoc* that have been reported in (González-Ramírez *et al.*, 2017). CheB\_Pec was loaded into capillaries of 0.2 mm inner diameter and crystals appeared in several conditions, namely C4 (1.25 M sodium citrate, 0.1 M Na/Hepes, pH 7.5), C5 (1.7 M ammonium sulphate, 3.5% (w/v) PEG 400, 0.1 M Na/Hepes, pH 7.5) and C7 (2.0 M ammonium sulphate, 0.1 M Tris/HCl pH 8.0 and 8.5). Crystals were extracted from the capillary and equilibrated in mother solution supplemented with 15% (v/v) glycerol. Individual crystals were placed into LithoLoops (Molecular Dimensions), flash-frozen in liquid nitrogen and stored until data collection at the Xaloc beamline of the Spanish Synchrotron Radiation Source Alba. Several full data sets were obtained and automatically indexed, reduced and scaled using the default data processing with EDNA (Incardona *et al.*, 2009) within the MXCuBE (Gabadinho *et al.*, 2010) data collection interface. The automatically determined space groups, I422 or F422, did not permit phasing using molecular replacement. Data were manually inspected, indexed and merged with iMOSFLM (Battye *et al.*, 2011) in space group I4, scaled and reduced using Aimless (Evans and Murshudov, 2013) of the CCP4 program suite (Winn *et al.*, 2011). The structure was determined by molecular replacement in Phaser (Bunkóczi *et al.*, 2013) using a homology model (Kelley *et al.*, 2015) based on the CheB structure of *S. enterica* sv. Typhimurium (pdb ID 1A2O) and after lowering the symmetry of the space group to I4. Five polypeptide chains were placed into the unit cell giving rise to a Matthews coefficient (Matthews, 1968) of 2.85 and a water content of 57%. Refinement was done by phenix.refine of the PHENIX suite (Afonine *et al.*, 2012) including Titration-Libration-Screw (TLS) parameterization (Painter and Merritt, 2006b). Cycles of manual building and inspection were done in Coot (Emsley *et al.*, 2010). The final refined model was verified with Procheck (Laskowski *et al.*, 1993), Molprobity (Williams *et al.*, 2018) and PDBe validation server (Berman *et al.*, 2003). Table S5 summarizes crystallographic data statistics and final model characteristics. The coordinates and the experimental structure factors for the CheB methyltransferase from *P. atrosepticum* SCRI1043 have been deposited at the Protein Data Bank with ID 6YMZ.

## Results

---

### ***P. aeruginosa* CheB<sub>2</sub> is the only CheB homolog that binds to the McpB chemoreceptor pentapeptide.**

We have reported previously that CheR<sub>2</sub> is the only of the four *P. aeruginosa* CheR homologs that binds the terminal pentapeptide of the McpB chemoreceptor (García-Fontana *et al.*, 2014). To verify which CheB homolog interacts with this peptide, the four CheB homologs were overexpressed in *E. coli*, purified and submitted to microcalorimetric titrations with the pentapeptide of the McpB receptor, GWEEF. The titration of CheB<sub>1</sub>, CheB<sub>3</sub> and CheB<sub>4</sub> with the peptide caused small and uniform heat changes that were similar to ligand dilution heats (Figure 13). In contrast, exothermic binding heats were observed for the titration of CheB<sub>2</sub> and a dissociation constant ( $K_D$ ) of  $93 \pm 15 \mu\text{M}$  was derived.

This indicated that the CheR and CheB homologs of the Che<sub>2</sub> pathway specifically interact with the only chemoreceptor that feeds into this pathway, McpB (Figure 12). The measured affinity was approximately 180-fold lower than that for the peptide binding to CheR<sub>2</sub> (García-Fontana *et al.*, 2014) ( $K_D=0.52 \mu\text{M}$ ), implying that CheR<sub>2</sub> largely outcompetes CheB<sub>2</sub> for binding at the GWEEF pentapeptide. Next, it was investigated whether CheB<sub>2</sub> phosphorylation alters the affinity for the pentapeptide. Because the phosphorylation half-life of CheB proteins is typically very short (Porter and Armitage, 2002), we generated stable beryllium fluoride adducts that mimic phosphorylation (Guhaniyogi *et al.*, 2006); however, protein precipitation made any biochemical study impossible. Previous studies showed that the replacement of the phosphorylgroup accepting aspartate with glutamate in receiver domains mimics protein phosphorylation (Rapun-Araiz *et al.*, 2020). We have generated the CheB<sub>2</sub> D55E mutant protein that was titrated with the GWEEF peptide resulting in a  $K_D$  of  $56 \pm 14 \mu\text{M}$  (Figure S2), representing a modest increase in affinity as compared to the native protein.

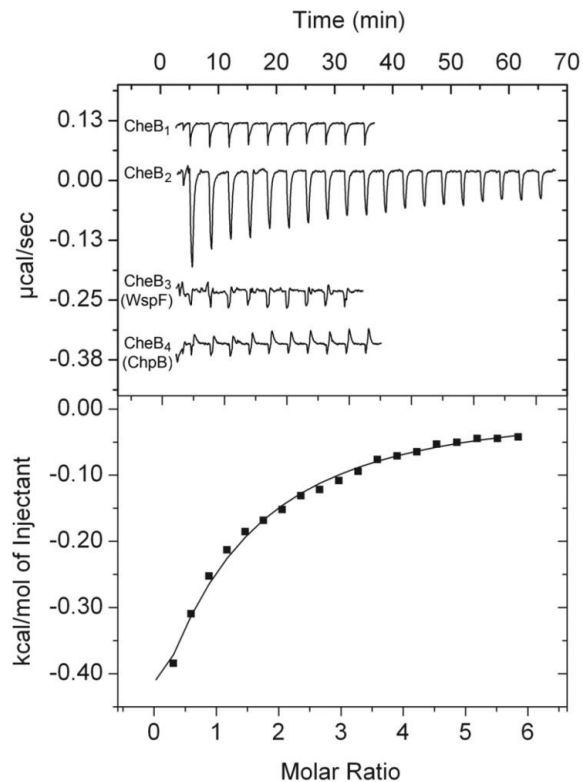


**Figure 13. Specificity of the interaction between four CheB homologs of *P. aeruginosa* and the terminal pentapeptide GWEEF of the McpB chemoreceptor.** Microcalorimetric titrations of the four CheB homologs (15 to 40  $\mu$ M) with 14  $\mu$ l aliquots (1 to 7 mM) of the GWEEF pentapeptide. Upper panel: raw titration data; lower panel: integrated, dilution heat-corrected and concentration-normalized peak areas of the titration data for CheB<sub>2</sub>. Data were fitted using the 'One binding site model' of the MicroCal version of ORIGIN.

**The signaling gene cluster of *P. atrosepticum* SCRI1043 encodes a chemosensory pathway that mediates chemotaxis.**

Chemosensory pathways can exert a number of different functions like chemotaxis, modulating second messenger levels and type-IV pili based movement (Wuichet and Zhulin, 2010). To explore the function of the sole chemosensory gene cluster in *P. atrosepticum* SCRI1043 (Figure 12), we created deletion mutants of the *cheA* and *cheB* genes. Subsequently, we conducted quantitative capillary chemotaxis assays of the wild type (wt) and mutant strains towards casamino acids. As shown in Figure 14, the wt strain showed strong chemotactic responses whereas the *cheA* and *cheB* mutants failed to respond, indicating that the chemosensory pathway mediates chemotaxis.

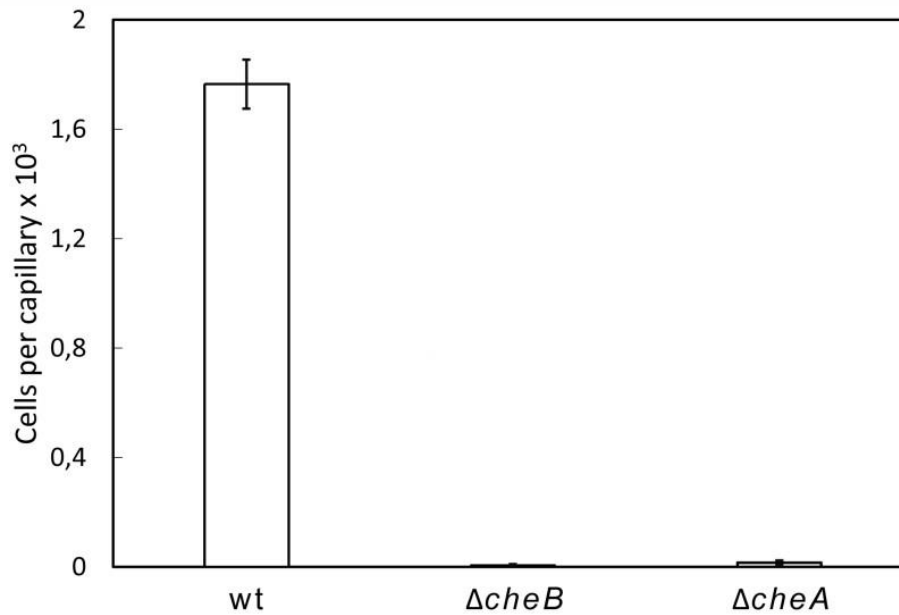


**Figure 14. Quantitative capillary chemotaxis assays of wild type and mutant strains of *P. atrosepticum* SCRI1043 towards 0.1% (w/v) casamino acids.** Data were corrected with the bacteria that migrated into buffer containing capillaries ( $225 \pm 35$ ). Data are means and standard deviations from three experiments conducted in triplicate.

***P. atrosepticum* SCRI1043 contains a large number of chemoreceptors with a C-terminal pentapeptide.**

The chemoreceptor reservoir of *P. atrosepticum* SCRI1043 is illustrated in Figure 15. Previous studies have shown that approximately 14% of bacterial chemoreceptors lack transmembrane regions and are thus involved in the sensing of cytoplasmic signals (Collins *et al.*, 2014). No such receptors are present in *P. atrosepticum* SCRI1043 since all 36 chemoreceptors are membrane bound and possess two transmembrane regions (Figure 15).

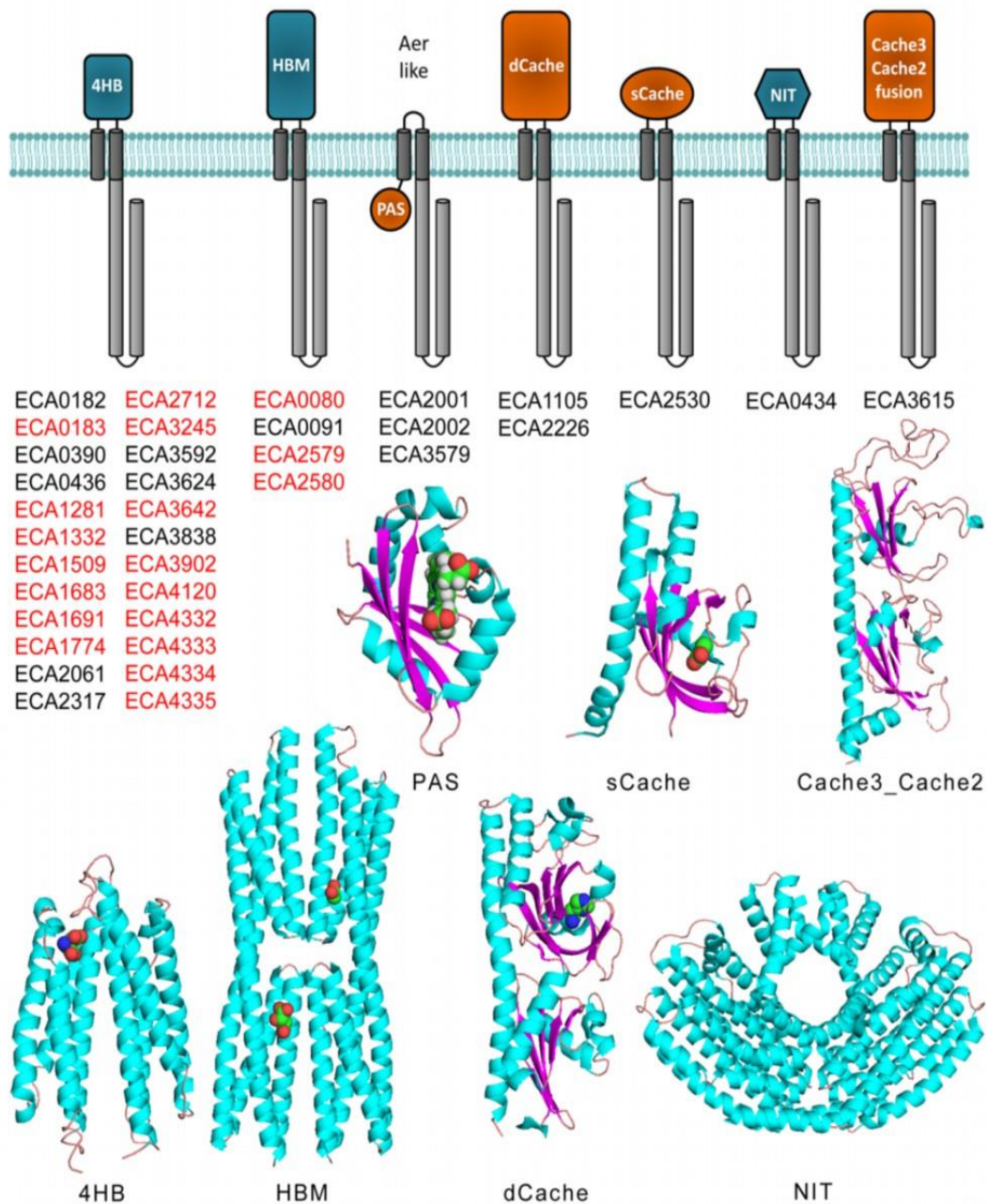


**Figure 15. The chemoreceptor repertoire of *P. atrosepticum* SCRI1043.** Ligand binding domains with  $\alpha/\beta$  folds or parallel helices are shown in orange or blue, respectively. Shown below are representative 3D structures of these domains, namely the structure of Tar-LBD (4HB) in complex with aspartate (pdb ID: 1vlt), McpS-LBD (HBM) in complex with malate and acetate (pdb ID: 2yfa), Aer2-LBD (PAS) in complex with heme (pdb ID: 4hi4), TlpQ-LBD (dCache) in complex with histamine (pdb ID: 6Fu4), PscD-LBD (sCache) in complex with propionate (pdb ID: 5G4Z), NasR-LBD (NIT) (pdb ID: 4AKK) and a homology model of the ECA3615-LBD (Cache3\_Cache2 fusion) generated by SwissModel (Waterhouse *et al.*, 2018) using pdb ID 4avf as template.

There are three receptors that possess the typical topology and domain arrangement of Aer receptors (Taylor *et al.*, 1999) that mediate aerotaxis (Figure 15). Only two receptors possess a dCache type LBD that are highly abundant sensor domains in chemoreceptors and sensor

kinases (Upadhyay *et al.*, 2016) and respond mainly to different amines (Matilla and Krell, 2017). In addition, the repertoire contains one and four receptors with sCache or HBM LBDs, respectively, that are typically organic acid sensors (Matilla *et al.*, 2020). The alignment of the C-terminal segment of *P. atrosepticum* SCRI1043 chemoreceptors revealed that 19 of them possess a terminal pentapeptide that is tethered to the signaling domain via linker sequences of 29 to 39 amino acids (Figure 16).

A

```

ECA0182 ...LADAVSAFKIPSYSHGNAGSYESVPMSTPTLSLALARKE
ECA0183 ...LAEAVSTFKLLSYGNGKTASYASAPTRTPTLSLAPAAAKNQSNNDNWETF
ECA1774 ...LARTVSVFNLGASYKSAALNRKTETPALAAPKNNRAEKTSAGKELADWETF
ECA2061 ...LSHAVAAFRI
ECA3642 ...LAETVQSFRLGNHGHIARTPAAAAASLTLRPAALAPGKSGISAGEGDWTSF
ECA4332 ...LVELMKVFIVEGGSSQRIAPPLKRPSSAKFSLANPKGSAGSNNQNWEQF
ECA4333 ...LVELMKVFIVEGGSSQRTTPELKRPSAKLSLASPKGRTKSDSQNWETF
ECA4120 ...LVTLMNHFHRLRGTPAARPAAPMAKKAQTARLALAPVGNTQDNWEKF
ECA4334 ...LLELMGVFKLNGIQTKAPRLTSQVKQPAAPRLALASKSGHTSSDNWETF
ECA4335 ...LVELMGVFKIDGTQSQRAVPQVTTLSRPKLALAGNSSNTNWETF
ECA2530 ...LNEQAQELSRTEVQFRVDESAGSYLALGAR
ECA0436 ...LRDAVRFFKVNQDHLRLRH
ECA1281 ...LQNAVEVFKINQAVAQEHRAASASSLALPKSLLPKPTSAGSSNNWETF
ECA1691 ...LNQAVAVFRLSEDTGSFRRTTQATAGQKPVLLAPSVNGGKKAKEGSSTDNWETF
ECA1683 ...LTRAVATFKLSSHLSSGHSAPARPNALAAKGRSSLALPRQANTENGNWETF
ECA3902 ...LTQAVAVFKLSGIVQVRSLSLPSAPQPRALPAMAIAGSSKGNSNQNWETF
ECA3838 ...LNLGVSFRFHLM
ECA1332 ...LNQTVSLFQLSDTQSALQVAAKPVRKAQAIAPRAGKALPTSSDNWEKF
ECA1509 ...LSAVVDVFNLDSDSDQQTAFSRPAIAAPVHRAVAQSTTPLLSVHGRHGEWKEF
ECA2712 ...LTEAVSVFQLSAAEAPRRPQRLAEKAPAAQKPMLLAAAGGKKNANDNWETF
ECA2579 ...LESMVANFRLSENEGRKPKANISGLPPQOKYLPPAAKQTQDSGWTF
ECA2580 ...LEKLLHFVRVQSQDNRVASRASSIIPRHTLPKSVSAKAASSESDWTSF
ECA0080 ...LATLMSVFRISDKDVARLQGSNTGNPNSGNKATARLPTLASRDNGDNWETF
ECA0091 ...LKQAVSVFRLANAQHDDTPAGIAFNNQPHRLHAPR
ECA2226 ...LAQTIEHFRLEQQHALPHALLR
ECA3592 ...LAESMVQFKVQSQEFAAIGRF
ECA3624 ...LMRSMALFQVEPRLS
ECA0390 ...LQQSVSRFQIARENREMDNVLPGLRQNTLADAR
ECA3245 ...LSQLVGQFIVGQIASSSLIPALASVPSGLSAPRLASAKNKNALAQDEAGWQRF
ECA1105 ...LNSVVGAFRV
ECA0434 ...MESLVSHFKVDDSAPOQLQHALLSR
ECA2001 ...MSEAVSVFSIPR
ECA2002 ...MVQAASVFSLSR
ECA3579 ...LNSAINVYGS
ECA3615 ...LSELVSVFRI
ECA2317 ...LNTSVSLFILPSTEADVNPMDQREMTQRIPMMG

```

B

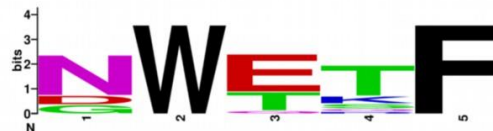


**Figure 16. C-terminal pentapeptides at *P. atrosepticum* chemoreceptors. (A)** C-terminal section of the sequence alignment of *P. atrosepticum* SCRI1043 chemoreceptors. Pentapeptides are in boldface and the linker sequences are underlined. **(B)** Sequence logo of the 19 pentapeptides. The figure was generated using Weblogo (<https://weblogo.berkeley.edu/logo.cgi>).

In total, there were 9 different pentapeptide sequences among which NWETF, the pentapeptide of the *E. coli* and *S. enterica* sv. Typhimurium receptors, was most abundant and present in 8 chemoreceptors (Table S2). Interestingly, the 19 pentapeptide containing chemoreceptors possess either 4HB or HBM type LBDs that correspond to either single- or double-module four helical bundle domains, respectively (Figure 15). The linkers showed no apparent sequence similarities (Figure S3) and were predicted to be mainly unstructured (Figure S4).



### ***P. atrosepticum* SCRI1043 CheB fails to recognize pentapeptides.**

We subsequently overexpressed and purified *P. atrosepticum* CheB (CheB\_Pec) to study its interaction with the pentapeptides present in SCRI1043 chemoreceptors. However, microcalorimetric titrations conducted with all nine pentapeptides (Table S2) and at different analysis temperatures did not show any sign of binding. This was an unexpected finding since CheB\_Pec shares 86% sequence identity with the *E. coli* CheB that was shown to bind in its unphosphorylated form the free or receptor-born NWETF pentapeptide (Barnakov *et al.*, 1999; Barnakov *et al.*, 2001; Barnakov *et al.*, 2002). To verify whether the N-terminal His-tag at CheB\_Pec may potentially prevent binding, the His-tag was enzymatically removed from CheB, but no binding was observed in ITC. Since phosphorylation of *E. coli* CheB greatly enhanced its methyltransferase activity (Barnakov *et al.*, 2002), we hypothesized that phosphorylation may be a necessary prerequisite for pentapeptide binding to CheB\_Pec. To verify this hypothesis we generated purified CheB\_Pec containing a beryllium fluoride adduct that mimics phosphorylation (Cho *et al.*, 2001; Guhaniyogi *et al.*, 2006). However, microcalorimetric titrations did not evidence binding.

### **Three-dimensional structure of a pentapeptide independent CheB methyltransferase**

The above results suggest that the single CheB in a strain that harbours 19 chemoreceptors with a pentapeptide is unable to bind any of these pentapeptides. One possible explanation may be that the protein is unfolded or present in an inactive conformation. To address this issue, we crystallized CheB\_Pec and solved its three-dimensional structure at a resolution of 2.3 Å (Figure 17).

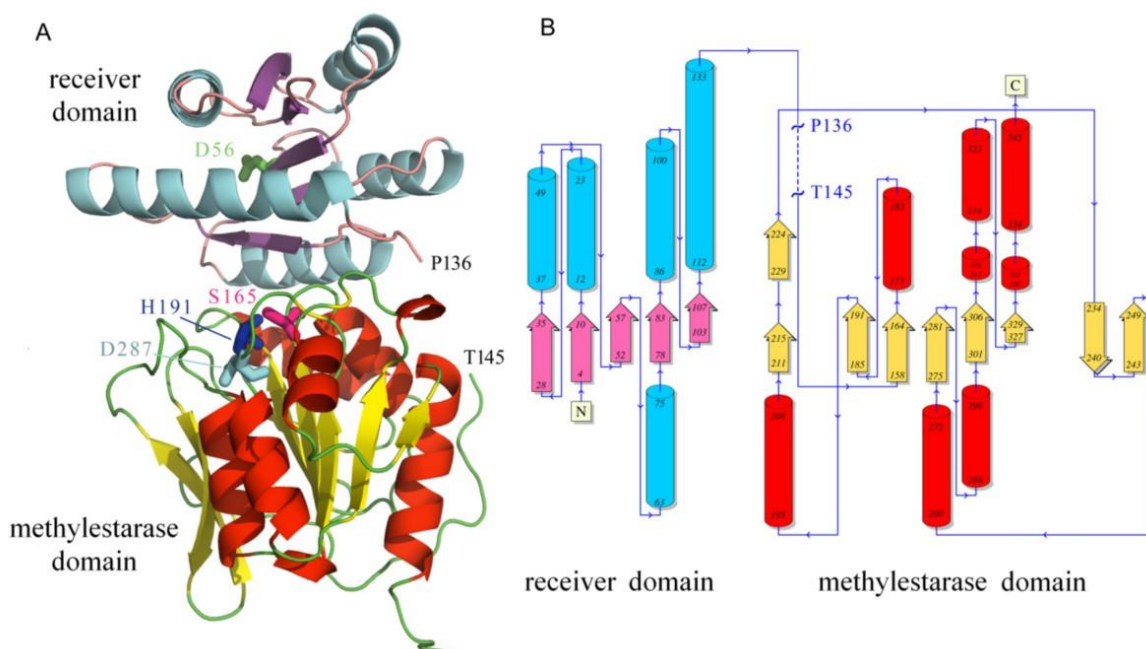


**Figure 17. The three-dimensional structure of *P. atrosepticum* CheB.** (A) Ribbon diagram of the structure. The gap observed due to lacking electron density is indicated (P136 to T145). The phosphorylgroup accepting aspartate (D56) as well as the residues that form the methyltransferase catalytic triad (S165-H191-D287) are shown in stick mode. (B) Secondary structure elements: tubes:  $\alpha$ -helix; arrows:  $\beta$ -strand. The Figure was produced using PDBsum (Laskowski *et al.*, 2018).



The enzyme is composed of an N-terminal REC domain and a C-terminal methyltransferase domain that are connected by a linker of approximately 25 amino acids (Figure 17). The asymmetric unit contains 5 CheB\_Pec chains that can be closely superimposed onto each other resulting in C $\alpha$  root mean square deviation (rmsd) values of 0.23 to 0.61 Å (Figure S5, Table S3). These 5 chains can also be closely aligned with the structure of *S. enterica* sv. Typhimurium CheB (West *et al.*, 1995; Djordjevic *et al.*, 1998), as evidenced by rmsd values of between 1.21 to 1.47 Å (Table S3), as well as onto the receiver and catalytic domains of *Thermotoga maritima* CheB (pdb ID: 3t8y and 3sft). In each CheB\_Pec chain there was a gap due to lacking electron density that, depending on the chain, extended from amino acids 137 to 144-150. Lacking electron density is generally attributed to the corresponding protein segment being disordered. The gap was flanked by a segment with high B-factor values, indicative of significant protein flexibility in this region (Sun *et al.*, 2019) (Figure S6).

There was a very satisfactory overall structural alignment of the CheB structures from *S. enterica* sv. Typhimurium and *P. atrosepticum* SCRI1043 (Figure 18A). Major deviations in this alignment showed a small region in the receiver domain as well as in both flanking regions of the gap (Figure S7). The segment in the *S. enterica* sv. Typhimurium structure corresponding to the gap in CheB\_Pec was characterized by low mean B-factors, namely  $20 \pm 7$  for chain A and  $30 \pm 9$  for chain B, indicative of a well-ordered structure.

#### **The region corresponding to the pentapeptide binding site in *E. coli* CheB is disordered in *P. atrosepticum* CheB.**

Having provided evidence that CheB\_Pec is a correctly folded protein that resembles closely the *S. enterica* sv. Typhimurium structure, the question as to why it does not bind pentapeptides remained. The answer to this question may be related to studies that have identified the pentapeptide binding site at *E. coli* CheB. This binding site was found to comprise amino acids 130 to 140 (coloured in red in Figure 18A and B) and is located on the C-terminal extension of the REC domain and N-terminal part of the linker (Barnakov *et al.*, 2001). The inspection of the sequence alignment of CheB from *E. coli* and *P. atrosepticum* SCRI1043 revealed a high degree of sequence divergence in the pentapeptide binding area (Figure 18B). Importantly, a large part of the *E. coli* CheB pentapeptide binding site overlaps with the gap observed in the CheB\_Pec structure (shaded in grey in Figure 18B). We therefore hypothesize that the structural disorder of CheB\_Pec in the region homologous to the pentapeptide binding site in *E. coli* may be related to the failure to bind pentapeptides. In the case of CheR, distinct sequence features have been identified for pentapeptide dependent and independent forms (Perez and Stock, 2007; García-Fontana *et al.*, 2014). In contrast, sequence alignment of pentapeptide dependent and independent CheB did not reveal any obvious conserved sequence features.

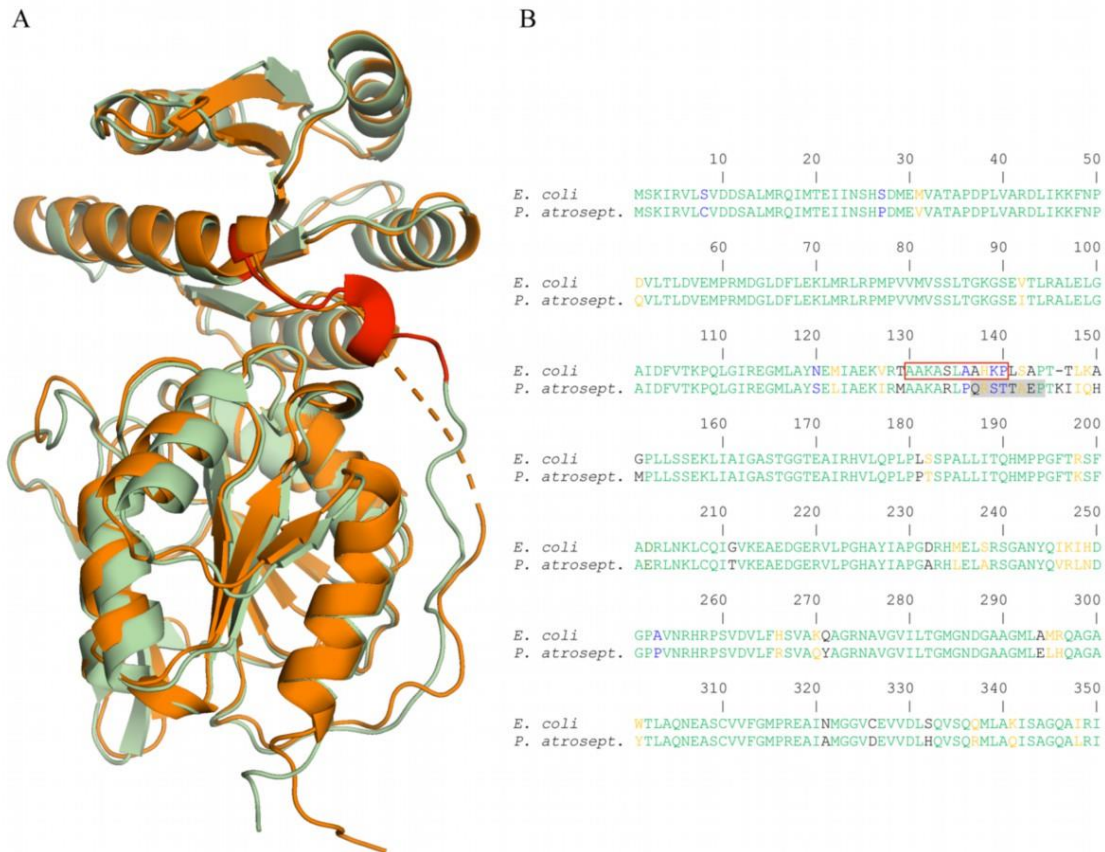


**Figure 18. Structural and sequence features related to the capacity of CheB to recognize C-terminal pentapeptides.** (A) Structural alignment of CheB from *P. atrosepticum* (orange) and *S. enterica* sv. Typhimurium (green, pdb ID: 1A2O). The amino acid segment identified to be the pentapeptide binding site (Barnakov *et al.*, 2001) is shown in red. (B) Sequence alignment of *E. coli* K-12 and *P. atrosepticum* SCRI1043 CheB. The amino acids that form the pentapeptide binding site in the *E. coli* enzyme are boxed in red. The gap in the CheB\_Pec structure is shaded in grey. The alignment was done using the CLUSTALW algorithm of the NPS@ software (Combet *et al.*, 2000). The Gonnet protein weight matrix was used; gap opening and gap extension penalties were 10.0 and 0.1, respectively. Residues in green are identical, orange highly similar, blue weakly similar and black dissimilar.

## Discussion

Many bacteria contain multiple paralogs of signaling proteins that form part of different chemosensory pathways (Wuichet and Zhulin, 2010). A central question is whether or to what degree there is specificity of interaction between the different homologs of signaling proteins and chemoreceptors. Furthermore, bacteria contain frequently a significant number of chemoreceptors of which some possess C-terminal pentapeptides that are generally considered additional binding sites for CheR and CheB (Ortega and Krell, 2020). *P. aeruginosa* has four chemosensory pathways and a single chemoreceptor that contains a C-terminal pentapeptide. We have shown previously that exclusively CheR<sub>2</sub> but not any of the remaining three CheR homologs of *P. aeruginosa* binds to the McpB pentapeptide (García-Fontana *et al.*, 2014). Here we show that the same holds for the 4 CheB homologs of *P. aeruginosa*, since CheB<sub>2</sub> was the only homolog that interacted with the McpB derived pentapeptide. Data thus show that

exclusively the CheR and CheB homologs encoded by the Che<sub>2</sub> gene cluster (Figure 12) bind to McpB, the only receptor predicted to stimulate the Che<sub>2</sub> pathway (Ortega *et al.*, 2017b). This pathway is essential for the full virulence of *P. aeruginosa* (Garvis *et al.*, 2009; García-Fontana *et al.*, 2019) but its precise function still needs to be determined (Orillard and Watts, 2021). McpB and Che<sub>2</sub> pathway homologs are widespread in pathogenic and non-pathogenic  $\gamma$ -Proteobacteria (Ortega *et al.*, 2020) suggesting a function that is not exclusively associated with virulence. Interestingly, this pentapeptide is present in most McpB homologs and it was concluded that this motif represents a fundamental feature of the McpB-like family (Ortega *et al.*, 2020). We propose that a major reason for the pentapeptide conservation is its capacity to bind the pathway specific CheB<sub>2</sub> and CheR<sub>2</sub> homologs (Ortega *et al.*, 2020), corresponding to a mechanism permitting pathway isolation. Pathway isolation of two-component systems has been extensively studied, particularly in the Laub laboratory (McClune *et al.*, 2019), but the corresponding knowledge for chemosensory pathways is scarce. Data available on *P. aeruginosa* indicate that these four pathways are isolated (Ortega *et al.*, 2017b) and the findings of our study may represent one of the corresponding mechanisms. Genome analyses of bacteria with pentapeptide containing chemoreceptors showed that strains containing a single pentapeptide containing chemoreceptor are most abundant (approx. 2 500 genomes) (Ortega and Krell, 2020). Future research will show whether the corresponding pentapeptides exert a similar function in these species.

The dissociation constant for the binding of CheB<sub>2</sub> to the McpB pentapeptide (93  $\mu$ M) is well below the corresponding value determined for the CheR<sub>2</sub>-pentapeptide interaction of 0.52  $\mu$ M (García-Fontana *et al.*, 2014). However, the values for the CheR and CheB binding to the *P. aeruginosa* pentapeptide GWETF are in the same range as those reported for the *E. coli* CheB and CheR binding to the NWETF pentapeptide, namely  $K_D$  values of 2  $\mu$ M (Wu *et al.*, 1996) and 130 to 160  $\mu$ M for the CheR (Barnakov *et al.*, 2002) and CheB, respectively. This may suggest that the much lower pentapeptide affinity of CheB as compared to CheR may be a more general feature. Studies have so far shown that there are pentapeptide-dependent and pentapeptide-independent CheR methyltransferases (Djordjevic and Stock, 1998; Li and Hazelbauer, 2006; Perez and Stock, 2007; García-Fontana *et al.*, 2014). Sequence and structural features in the CheR  $\beta$ -subdomain, responsible for the pentapeptide binding, were identified that account for the capacity or incapacity to bind pentapeptides (Perez and Stock, 2007; García-Fontana *et al.*, 2014). We show here that, in analogy to CheR, CheB methyltransferases also form pentapeptide dependent and independent subfamilies. The reason for the failure of CheB<sub>Pec</sub> to bind pentapeptide may be related to the structural disorder in the segment homologous to the pentapeptide binding site in *E. coli* CheB. Bioinformatic studies are required to establish the evolutionary history of CheB proteins in Enterobacteria to assess which sub-family has evolved first. However, in contrast to CheR, sequence analyses of this region in pentapeptide dependent and independent CheBs did not permit to identify a feature that can be associated with the capacity to bind pentapeptides.

Chemotaxis is particularly relevant for the virulence of plant pathogens (Matilla and Krell, 2018). This is also reflected at the genome level since more than 90% of plant pathogens, compared to 50 % for the bacterial average, possess chemosensory pathways (Matilla and Krell, 2018). In addition, the average number of chemoreceptors in plant pathogens, 33, is well superior to the bacterial average of 14 (Lacal *et al.*, 2010b; Matilla and Krell, 2018). In contrast to the relevance of chemotaxis in plant pathogens, there is little information on the corresponding molecular

mechanisms. *P. atrosepticum* is among the top 10 plant pathogens (Mansfield *et al.*, 2012) and a suitable model to study chemosensory signaling in a plant pathogen. The chemoreceptor repertoire of the strain SCRI1043 shows a number of unusual features: 1) Remarkably, 67 % of its chemoreceptors possess a 4HB LBD, which is well above the bacterial average of approx. 31 % (Ortega *et al.*, 2017a). This chemoreceptor family is characterized by its versatility as reflected in the broad range of ligands recognized (i.e. amino acids, boric acid, inorganic phosphate, aromatic acids, citrate, etc.), its capacity to recognize ligands with high (Rico-Jiménez *et al.*, 2016; Hida *et al.*, 2017) and low specificity (Luu *et al.*, 2015; Huang *et al.*, 2016) and its ability to bind ligands directly (Matilla *et al.*, 2020) or via ligand binding proteins (Gardina *et al.*, 1998). 2) Apart from the three Aer like receptors that possess cytosolic LBDs (Figure 15), there are no cytosolic chemoreceptors suggesting that primarily extracellular signals are sensed. 3) The abundance of chemoreceptors with a C-terminal pentapeptide. More than 50 % of *P. atrosepticum* SCRI1043 chemoreceptors contain pentapeptides, a number that is well above the bacterial average of 10% (Ortega and Krell, 2020), suggesting that pentapeptide function is important for signaling. However, CheB function does not require pentapeptide binding and future studies are necessary to elucidate to what degree CheR function requires pentapeptide recognition.

## Supplementary Material

	10	20	30	40	50	60
<i>E. coli</i>	MSKIRVLSVDDSAALMRQIMTEIINSHSDMEMVATAPDPLVARDLIKKFNPVLTLDVEMP					
<i>S. enterica</i>	MSKIRVLSVDDSAALMRQIMTEIINSHSDMEMVATAPDPLVARDLIKKFNPVLTLDVEMP					
	70	80	90	100	110	120
<i>E. coli</i>	RMDGLDFLEKLMRLRPMFVVMVSSLTGKGSEVTLRALELGAIIDFVTKPQLGIREGMLAYN					
<i>S. enterica</i>	RMDGLDFLEKLMRLRPMFVVMVSSLTGKGSEVTLRALELGAIIDFVTKPQLGIREGMLAYS					
	130	140	150	160	170	180
<i>E. coli</i>	EMIAEKVRTAAKASLAAHKPLSAPTTLKAGPLLSSEKLIAGASTGGTEAIRHVLQPLPL					
<i>S. enterica</i>	EMIAEKVRTAARARITAAHKPMAAPTTLKAGPLLSSEKLIAGASTGGTEAIRHVLQPLPL					
	190	200	210	220	230	240
<i>E. coli</i>	SSPALLITQHMPGFTFSFADRLNKLKQIGVKEAEDGEVLPGHAYIAPGDRHMELSRSG					
<i>S. enterica</i>	SSPAVLIITQHMPGFTFSFAERLNKLKQISVKEAEDGEVLPGHAYIAPGDKHMELARSG					
	250	260	270	280	290	300
<i>E. coli</i>	ANYQIKIHDGPAVNRHRPSVDVLFHSHVAKQAGRNAVGVILTGMGNDGAAGMLAMRQAGAW					
<i>S. enterica</i>	ANYQIKIHDGPPVNRHRPSVDVLFHSHVAKHAGRNAVGVILTGMGNDGAAGMLAMYQAGAW					
	310	320	330	340		
<i>E. coli</i>	TLAQNEASCVVFGMPREAINMGGVCEVVDLSQVSQQMLAKISAGQAIRI					
<i>S. enterica</i>	TIAQNEASCVVFGMPREAINMGGVSEVVDLSQVSQQMLAKISAGQAIRI					

**Figure S 1. Sequence alignment of CheB from *E. coli* K-12 substrain MG1655 and *S. enterica* serovar Typhimurium str. LT-2.** Protein accession numbers are NP\_416397.1 and NP\_460874.1, respectively. The alignment was made using the CLUSTALW algorithm of the NPS@ suite (Combet *et al.*, 2000) using the GONNET weight matrix, a gap opening penalty of 10 and a gap extension penalty of 0.2. Red: identical; green: highly similar; blue: weakly similar; black: dissimilar.

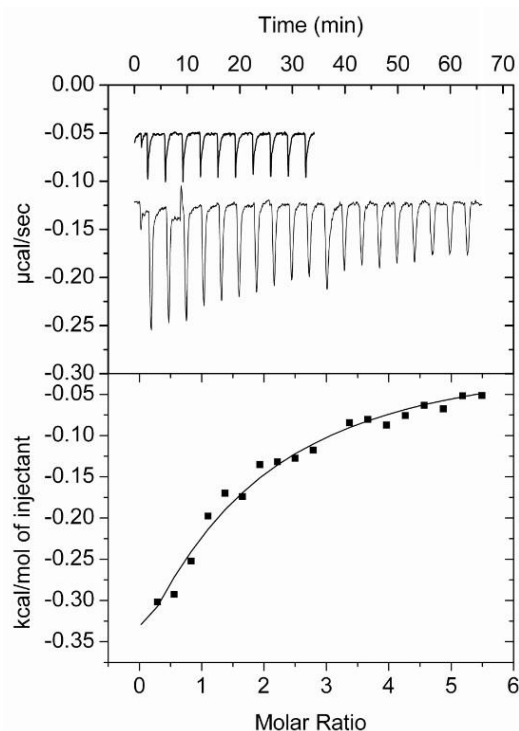


**Figure S 2. Microcalorimetric binding studies of the CheB2 D55E mutant with the McpB-derived pentapeptide GWEEF.** Upper panel: Raw data for the titration of buffer (upper curve) and the CheB<sub>2</sub> D55E mutant (38  $\mu$ M) with 14  $\mu$ l aliquots of the GWEEF pentapeptide (1 mM) at 25  $^{\circ}$ C. The lower panel shows the integrated, dilution heat-corrected and concentration-normalized peak areas of the protein titration data. Data were fitted using the ‘One binding site model’ of the MicroCal version of ORIGIN.

```

ECA0183      LSYGNGKTA-SYASAPTRTPTL-S-LAP--AAAKNQSNND--
ECA1774      ---GASYKS-AALNRKTETPAL-A-APKNRAEKTSAKGELA
ECA4120      -GTPAARPA-P-MAKKAQTAR----LALAPVG----NTQD--
ECA2712      AAEAPRRPQ-QRLAEKAPAAQK-P-MLLAAAGGKKNAND--
ECA4332      ---GGSSQ---RIAPPLKRPSS-AKFSLANPKGSAGSNNQ--
ECA4333      --ESGSSQ---RTTPELKRPS--AKLSLSPKGRTKSDSQ--
ECA4334      ---GIQTKA-PRLTSQVKQPAA-PRLALASKSGHTSSD----
ECA4335      ---GTQSQ---RAVPQVTLSR-PKLALAGNSSNT-----
ECA3642      ---GNHQI-ARTPAAAASTLRPALAAPGKSGISAGEG---
ECA3902      ---GIVQQVRSSLPKSAPQRLAPAMAIAGSS--KGNSNQ--
ECA3245      --QIASSSLIPALASVPSGLSA-PRLASAKNKNALAQDEA--
ECA1691      EDTGSFRR--TTQATAGQKPVLLAPSVNGGKKAKEGSSTD--
ECA1281      --QAVAQEH--RAASASSLAAL-PKSLLPKPTS-AGSSNA--
ECA1683      SHLSSGHS-APARNALAAKGR-SSLALPRQAN---TENG--
ECA2580      ---SQSDN---RVASRASSSI--PRHTLPKSVSAKAASSES-
ECA1332      ----DTQS---ALQVAAKPVVK-AQAIAPRAGKALPTSSD--
ECA1509      -SDSDQQTAFSRPAIAAPVHRAVAQSTTPLLS-VHGRHGE--
ECA2579      --ENGRK--PKANISGLPPQ--QKYLPPAAK---QTQDS--
ECA0080      -DKDVARLQ--GSNTGNPNSGNKATARLPTLAS-RDNGND-

```

**Figure S 3. Alignment of the linker sequences of the 19 chemoreceptors from *Pectobacterium atrosepticum* containing terminal pentapeptides.** The alignment was done using the CLUSTALW algorithm of the npsa suite [1] using the GONNET weight matrix, a gap opening penalty of 10 and a gap extension penalty of 0.2. No significant sequence conservation is observed.











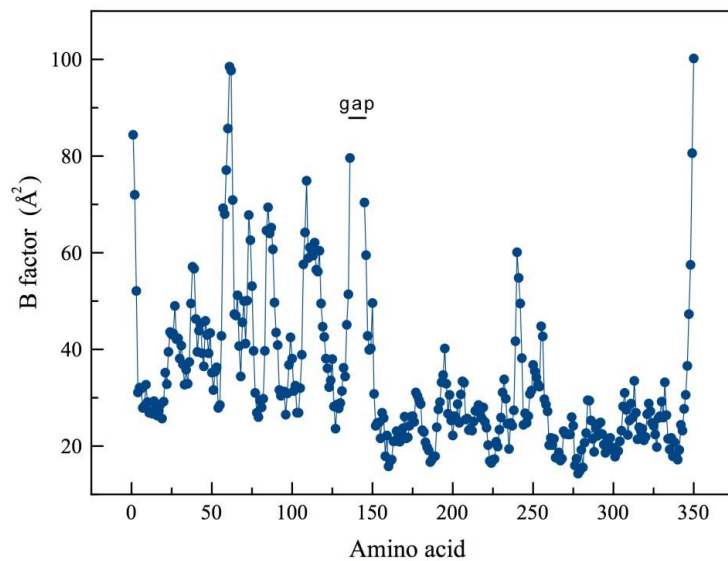


**Figure S 6. B-factors of C $\alpha$  atoms of *P. atrosepticum* chain B.** The gap caused by the low electron density in the crystal structure of CheB\_Pec is indicated.

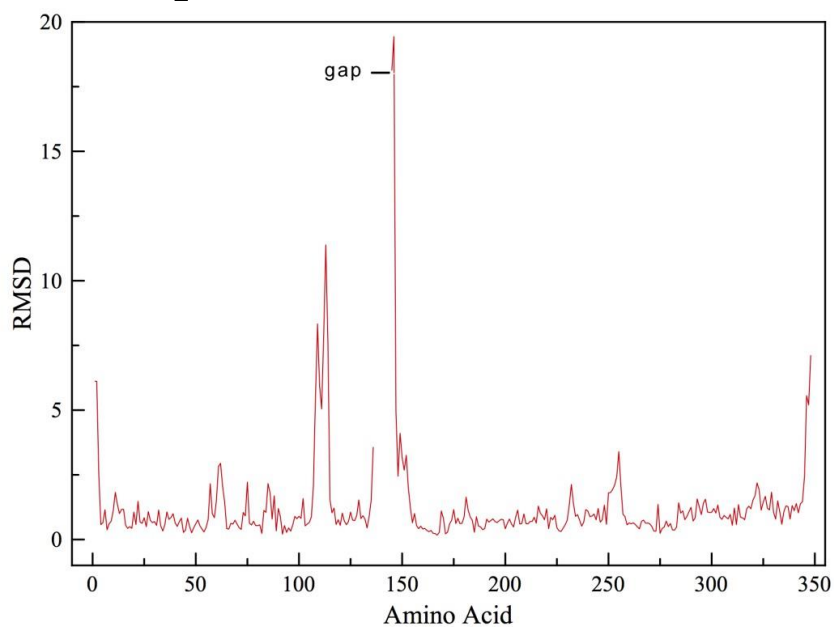


**Figure S 7. Structural superimposition of chain A of *P. atrosepticum* CheB with CheB of *S. enterica* sv. Typhimurium (pdb ID 1A2O).** Shown are rmsd of C $\alpha$  atoms.

**Table S 1. Strains and plasmids used in Chapter 1.**

Strains and plasmids	Genotype or relevant characteristics <sup>a</sup>	Reference
<b>Strains</b>		
<i>Escherichia coli</i> BL21(DE3)	F <sup>-</sup> <i>ompT gal dcm lon hsdS<sub>B</sub>(r<sub>B</sub><sup>-</sup>m<sub>B</sub><sup>-</sup>)</i> λ(DE3 [ <i>lacI lacUV5-T7p07 ind1 sam7 nin5</i> ]) [ <i>malB</i> <sup>+</sup> ] <sub>K-12</sub> (λ <sup>S</sup> )	(Jeong <i>et al.</i> , 2009)
<i>E. coli</i> BL21-AI	F <sup>-</sup> <i>ompT hsdS<sub>B</sub> (r<sub>B</sub><sup>-</sup>m<sub>B</sub><sup>-</sup>) gal dcm araB::T7RNAP-tetA</i>	Invitrogen
<i>E. coli</i> DH5α	F <sup>-</sup> <i>endA1 glnV44 thi-1 recA1 relA1 gyrA96 deoR nupG purB20 φ80dlacZΔM15 Δ(lacZYA-argF)U169, hsdR17(r<sub>K</sub><sup>-</sup>m<sub>K</sub><sup>+</sup>), λ<sup>-</sup></i>	(Woodcock <i>et al.</i> , 1989)
<i>E. coli</i> CC118λpir	<i>araD Δ(ara, leu) ΔlacZ74 phoA20 galk thi-1 rspE rpoB argE recA1 λpir</i>	(Herrero <i>et al.</i> , 1990)
<i>E. coli</i> β2163	F- RP4-2-Tc::Mu Δ <i>dapA</i> ::( <i>erm-pir</i> ); Km <sup>R</sup> , Em <sup>R</sup>	(Demarre <i>et al.</i> , 2005)
<i>Pectobacterium atrosepticum</i> SCRI1043	Wild type strain	(Bell <i>et al.</i> , 2004)
<i>P. atrosepticum</i> SCRI1043 Δ <i>cheB</i>	SCRI1043 in-frame deletion mutant of <i>cheB</i>	This study
<i>P. atrosepticum</i> SCRI1043 Δ <i>cheA</i>	SCRI1043 deletion mutant of <i>cheA</i> ; Km <sup>R</sup>	This study
<b>Plasmids</b>		
pET28b(+)	Protein expression plasmid; Km <sup>R</sup>	Novagen
pET28b-CheB <sub>1</sub>	Km <sup>R</sup> ; pET28b(+) derivative containing <i>P. aeruginosa cheB1</i> (PA1459)	This study
pET28b-CheB <sub>2</sub>	Km <sup>R</sup> ; pET28b(+) derivative containing <i>P. aeruginosa cheB2</i> (PA0173)	This study
pET28b-CheB <sub>2</sub> D55E	Km <sup>R</sup> ; pET28b(+) derivative containing <i>P. aeruginosa cheB2</i> D55E mutant	
pET28b-CheB <sub>3</sub>	Km <sup>R</sup> ; pET28b(+) derivative containing <i>P. aeruginosa cheB3</i> (PA3703)	This study
pET28b-CheB <sub>4</sub>	Km <sup>R</sup> ; pET28b(+) derivative containing <i>P. aeruginosa cheB4</i> (PA0414)	This study
pET28b-CheB_Pec	Km <sup>R</sup> ; pET28b(+) derivative containing <i>P. atrosepticum cheB</i> (ECA1693)	This study
pUC18Not	Ap <sup>R</sup> ; identical to pUC18 but with two NotI sites flanking pUC18 polylinker	(Herrero <i>et al.</i> , 1990)
pUC18Not_Δ <i>cheB</i>	Ap <sup>R</sup> ; 1.5-kb PCR product containing a 954 bp in frame deletion of <i>cheB</i> of SCRI1043 inserted into the SphI/NdeI sites of pUC18Not	This study
pUC18Not_Δ <i>cheA</i>	Ap <sup>R</sup> ; 1.5-kb PCR product containing a 1561 bp deletion of <i>cheA</i> (ECA1689) of SCRI1043 inserted into the EcoRI/HindIII sites of pUC18Not	This study
p34S-Km3	Km <sup>R</sup> , Ap <sup>R</sup> ; <i>Km3</i> antibiotic cassette	(Demarre <i>et al.</i> , 2005)
pUC18Not_Δ <i>cheA</i> -km3	Ap <sup>R</sup> , Km <sup>R</sup> ; 0.96-kb BamHI fragment containing <i>km3</i> cassette of p34S-Km3 was inserted into BamHI site of Δ <i>cheA</i> in pUC18Not_Δ <i>cheA</i>	This study
pKNG101	Sm <sup>R</sup> ; <i>oriR6K mob sacBR</i>	(Kaniga <i>et al.</i> , 1991)
pKNG101_Δ <i>cheB</i>	Sm <sup>R</sup> , Km <sup>R</sup> ; 1.5 kb NotI fragment of pUC18Not_Δ <i>cheB</i> was cloned at the same site in pKNG101	This study
pKNG101_Δ <i>cheA</i> -km3	Sm <sup>R</sup> , Km <sup>R</sup> ; 2.4-kb NotI fragment of pUC18Not_Δ <i>cheA</i> -km3 was cloned at the same site in pKNG101	This study

<sup>a</sup>Ap, ampicillin; Em, erythromycin; Km, kanamycin; Sm, streptomycin; Tc, tetracycline.

**Table S 2. *P. atrosepticum* SCRI1043 chemoreceptors with a C-terminal pentapeptide.** Shown are the pentapeptide sequence, the chemoreceptor locus tag and the LBD type of the receptor.

<b>Pentapeptide sequence</b>	<b>Receptor</b>	<b>LBD type</b>
GWQRF	ECA3245	4HB <sup>1</sup>
GWEKF	ECA1509	4HB
GWTF	ECA2579	HBM
DWTSF	ECA3642	4HB
	ECA2580	HBM
DWTF	ECA1774	4HB
NWTF	ECA0183	4HB
	ECA0080	HBM
NWEKF	ECA4120	4HB
	ECA1332	4HB
NWEQF	ECA4332	4HB
NWETF	ECA4333	4HB
	ECA4334	4HB
	ECA4335	4HB
	ECA1281	4HB
	ECA1691	4HB
	ECA1683	4HB
	ECA3902	4HB
	ECA2712	4HB

<sup>1</sup>4HB, four helix bundle domain; HBM, helical bimodular domain

**Table S 3. Structural alignment of chains A to E of *P. atrosepticum* CheB amongst each other and with related structures.** Data were calculated using MATRAS [2]. Pdb ID 1a2o: CheB from *S. enterica* sv. Typhimurium; pdb ID 1chd: methylesterase domain of *S. enterica* sv. Typhimurium CheB methylesterase; pdb ID 3sft: methylesterase domain of *Thermotoga maritima* CheB; pdb ID 3t8y: REC domain of *T. maritima* CheB.

	Ca rmsd (Å)								
	A	B	C	D	E	1a2o	1chd	3sft	3t8y
<b>Aligned amino acids</b>						347	198	198	138
CheB ( <i>P. atrosepticum</i> ) chain A	-	0.634	0.234	0.593	0.517	1.420	0.949	1.237	2.083
CheB ( <i>P. atrosepticum</i> ) chain B	0.634	-	0.607	0.252	0.522	1.468	0.878	1.163	2.775
CheB ( <i>P. atrosepticum</i> ) chain C	0.234	0.607	-	0.573	0.521	1.390	0.937	1.235	2.805
CheB ( <i>P. atrosepticum</i> ) chain D	0.593	0.252	0.573	-	0.527	1.397	0.896	1.168	2.758
CheB ( <i>P. atrosepticum</i> ) chain E	0.517	0.522	0.521	0.527	-	1.207	0.788	1.211	2.821
CheB ( <i>S. enter</i> ) pdb 1a2O	1.420	1.468	1.390	1.397	1.207	-	1.139	1.209	2.357
CheB cat. domain ( <i>S. enter</i> ) pdb 1chd	0.949	0.878	0.937	0.896	0.788	1.139	-	1.058	4.782
CheB cat. domain ( <i>T. mari</i> ) pdb 3sft	1.237	1.163	1.235	1.168	1.211	1.209	1.058	-	4.685
CheB REC domain ( <i>T. mari</i> ) pdb 3t8y	2.083	2.775	2.805	2.758	2.821	2.357	4.782	4.685	-

**Table S 4. Oligonucleotides used in Chapter 1.**

#	Name	sequence (5'-3')	Purpose
1	pET28_CheB <sub>1</sub> _f	GTCGCCCTCTGAGGAGTACATATGGCAGTC	Construction of pET28b-CheB <sub>1</sub>
2	pET28_CheB <sub>1</sub> _r	CATTCCTGCACGGATCCTTACTGGCACGCCTC	
3	pET28_CheB <sub>2</sub> _f	GGAGAGCCCCATATGCCCATCAGTGTCTT	Construction of pET28b-CheB <sub>2</sub>
4	pET28_CheB <sub>2</sub> _r	CCAGGATCCCGCTCAGAGG	
5	pET28_CheB <sub>3</sub> _f	CTGATCGGAGAAGCACACATATGAGGATCGGA	Construction of pET28b-CheB <sub>3</sub>
6	pET28_CheB <sub>3</sub> _r	GGAGTGGATCCCGGCTAATCGAATAC	
7	pET28_CheB <sub>4</sub> _f	CCTGGTCGGCCCATATGAGTGAG	Construction of pET28b-CheB <sub>4</sub>
8	pET28_CheB <sub>4</sub> _r	TCGGATCCTGGTTCATGTTTCGACTC	
9	pET28_CheB <sub>2</sub> _D55E_f	GACGTGATCAGCCTCGAAGTGGAAATGCCGGAATGGAC	Construction of pET28b-CheB <sub>2</sub> D55E
10	pET28_CheB <sub>2</sub> _D55E_r	GGCATTCCACTTCGAGGCTGATCACGTCCGGCGCGTGC	
11	pET28_CheB_Pec_f	TAATCATATGAAAAGTACACCATCGCAAATC	Construction of pET28b-CheB_Pec
12	pET28_CheB_Pec_r	TAATGGATCCCTCTTATCTTGCTCATTATCTTTCCTTAG	
13	pUC18Not_cheB_up_f	TAATGCATGCCTATTCTGACGCAGATGGTTGAC	Construction of pUC18Not_ΔcheB
14	pUC18Not_cheB_up_r	CAACATTCGCTGGCTCACGGATCCTAGGGCAGAATCATCAACGCA	
15	pUC18Not_cheB_down_f	GCGTTGATGATTCTGCCCGGATCCCAGGTGAGCCAGCGAATGTTG	Construction of pUC18Not_ΔcheB
16	pUC18Not_cheB_down_r	TAATCATATGAGCCTCTGCTGCTTCTGCTA	
17	pUC18Not_cheA_up_f	TAATGAATTCGCGAGATATCCTGCGTGCG	Construction of pUC18Not_ΔcheA
18	pUC18Not_cheA_up_r	CTCCGATGGATCCAACAATAATAAGTGTG	
19	pUC18Not_cheA_down_f	TAATGGATCCGACCTGTATCCGTTAGCTGGCG	Construction of pUC18Not_ΔcheA
20	pUC18Not_cheA_down_r	TAATAAGCTTCAATACGCTATCGACCAGCGC	

**Table S 5. Data collection and refinement statistics of the 3D structure of *P. atrosepticum* CheB.** Values in parentheses are for the highest-resolution shell.

<b>Protein</b>	<b>CheB</b>
<b>Pdb identifier</b>	6YMZ
<b>Data collection</b>	
Beamline	Xaloc (ALBA)
Space Group	I 4
Cell dimensions a=b, c (Å)	148.74, 206.34
Protein chains in ASU	5
Resolution (Å)	62.43 - 2.30 (2.38 - 2.30)
$R_{merge}$ (%)	78.78 (180)
$I/\sigma(I)$	40.01 (3.41)
Completeness (%)	98.12 (98.06)
Unique reflections	98138 (9778)
Multiplicity	26.2 (25.4)
CC(1/2)	0.83 (0.65)
<b>Refinement</b>	
Resolution (Å)	2.30
$R_{work}/R_{free}$ (%)	19.18/22.62
No. of atoms	13992
Protein	13433
Ligands	65
Water	494
B-factor (Å <sup>2</sup> )	43.92
R.m.s deviations	
Bond lengths (Å)	0.01
Bond angles (°)	1.15
Ramachandran (%)	
Favoured	98.44
Allowed	1.38
Outliers	0.18



## Chapter 2. Differential occupation of chemoreceptors with CheR as a potential mechanism to bias chemotactic responses.

---

*To be published*

Félix Velandó<sup>1</sup>, Miguel A. Matilla<sup>1</sup> and Tino Krell<sup>1</sup>

<sup>1</sup>Department of Biotechnology and Environmental Protection, Estación Experimental del Zaidín, Consejo Superior de Investigaciones Científicas.

### Abstract

---

Many chemoreceptors possess a pentapeptide that is tethered via a linker to the C-terminal extension of chemoreceptors. These pentapeptides are high-affinity binding sites for the CheR methyltransferase and the phosphorylated form of the CheB methylesterase. Binding of both enzymes to these pentapeptides causes an increase in their local concentration resulting in optimal pathway adaptation. The interaction of these enzymes with the NWETF pentapeptide of the *Escherichia coli* chemoreceptors Tar and Tsr has been studied extensively. Many other bacteria contain a large number of chemoreceptors with different pentapeptide sequences in which only the W and F residues are conserved. The functional relevance of multiple pentapeptides of different sequence is unknown and their elucidation is object of this study. Of the 36 chemoreceptors of *Pectobacterium atrosepticum* SCRI1043, 19 contain a pentapeptide that form 9 families according to their sequence. Using Isothermal titration calorimetry, we show that all 9 pentapeptides bound *P. atrosepticum* CheR with dissociation constants between 86 nM and 1.04  $\mu$ M. The pentapeptide with the highest affinity (GWTF) only differed in one amino acid from the pentapeptide with the lowest affinity (NWTTF). The replacement of the *cheR* gene abolished chemotaxis. The cellular CheR concentration of exponential and stationary phase cells were determined by quantitative immunoblot to be  $1.4 \pm 0.3 \mu$ M and  $0.73 \pm 0.1 \mu$ M, respectively. Since the cellular CheR concentration is close to the pentapeptide-CheR dissociation constants, we hypothesize that the differential occupation of chemoreceptors by CheR corresponds to a mechanism that permits to bias chemotactic responses.

---

## Introduction

---

Chemosensory pathways are among the most abundant prokaryotic signal transduction mechanisms (Wuichet and Zhulin, 2010; Gumerov *et al.*, 2020). Apart from mediating flagellum-based chemotaxis, chemosensory pathways also carry out alternative cellular functions like the control of second messenger levels such as cAMP or c-di-GMP, or were associated with type-IV pili based motility (Whitchurch *et al.*, 2004; Hickman *et al.*, 2005; Wuichet and Zhulin, 2010; Fulcher *et al.*, 2010). The key element of a chemosensory pathway is the ternary complex formed by chemoreceptors, the CheA autokinase and the CheW coupling protein. Signaling is typically initiated by signal recognition at the chemoreceptor ligand binding domains (LBD) that creates a molecular stimulus modulating CheA autophosphorylation activity leading subsequently to changes in the transphosphorylation activity to the CheY and CheB response regulators to control flagellar motor rotation and sensory adaptation, respectively. The ratio of CheY to phosphorylated CheY defines the pathway output (Parkinson *et al.*, 2015; Bi and Sourjik, 2018). The pathway sensitivity is adjusted by the coordinated action of the CheR methyltransferase and the CheB methylesterase, that catalyze methylation and demethylation, respectively, of several glutamyl residues at the chemoreceptor signaling domain, allowing chemosensory pathways to operate over a wide signal concentration range. It was shown that poorly methylated chemoreceptors have high attractant affinity and high propensity for methylation (Parkinson *et al.*, 2015; Bi and Sourjik, 2018). In this adaptation process, the activity of CheB is stimulated by the phosphorylation of its regulatory domain (Barnakov *et al.*, 2002; Hazelbauer *et al.*, 2008). Genome analyses indicated that chemoreceptors, CheA, CheW, CheY, CheR and CheB are core proteins for chemosensory pathway signaling (Wuichet and Zhulin, 2010). Furthermore, many chemosensory pathways contain additional signaling proteins, referred to as auxiliary proteins, that participate in some but not all pathways (Wuichet and Zhulin, 2010; Xu *et al.*, 2016).

The four *Escherichia coli* chemoreceptors contain four or five methylation sites that are located approximately in the middle of the long rod formed by the signaling domain and current data indicate that CheR binds with a relatively low affinity to these methylation sites (Li and Hazelbauer, 2020). Two of the four *E. coli* chemoreceptors, the high-abundant Tar and Tsr, possess a C-terminal pentapeptide, NWETF, that is tethered to the C-terminal end of the chemoreceptor signaling domain via an unstructured linker of approximately 35 amino acids (Bartelli and Hazelbauer, 2011). CheR binds to the individual NWETF pentapeptide with a dissociation constant of approximately 2  $\mu\text{M}$  (Wu *et al.*, 1996). Importantly, the same affinity was observed for the CheR binding to this pentapeptide when present at the C-terminal extension of receptors (Wu *et al.*, 1996). The affinity of CheR for the pentapeptide is thus about 100-fold higher than the affinity for the methylation sites at the chemoreceptor signaling domain (Li and Hazelbauer, 2020). In analogy to CheR, unphosphorylated CheB bound the individual pentapeptide and pentapeptide containing receptors with a similar affinity, which however, was with about 200  $\mu\text{M}$  lower as compared to CheR (Li *et al.*, 2021). However, Li *et al.* have shown that a stable phosphorylation mimic of CheB had a significantly higher affinity of about 13  $\mu\text{M}$ , suggesting that CheR and phosphorylated CheB compete for pentapeptide binding in the cell (Li *et al.*, 2021). Alterations in the chemoreceptor signaling state did not alter in significant manner the affinities of CheR and CheB for the pentapeptide (Wu *et al.*, 1996; Li and Hazelbauer, 2020; Li *et al.*, 2021).

It was proposed that the tethering of CheR and CheB-P to the C-terminal extension increases the local concentration of both enzymes leading to an optimal adaptation (Le Moual *et al.*, 1997; Li and Hazelbauer, 2005; Li *et al.*, 2021). The mutation or removal of the NWETF pentapeptide from the Tar and Tsr chemoreceptors largely reduced methylation and demethylation *in vivo* and *in vitro* preventing chemotaxis (Li *et al.*, 1997; Le Moual *et al.*, 1997; Okumura *et al.*, 1998; Barnakov *et al.*, 1999; Li and Hazelbauer, 2006). Since many other chemoreceptors that mediate strong chemotactic responses lack pentapeptides (Luu *et al.*, 2015; Compton *et al.*, 2018; Martín-Mora *et al.*, 2019), this observation results in the paradoxical situation where C-terminal pentapeptides are essential for some receptors, like Tar and Tsr, whereas other chemoreceptors do not require pentapeptides for their function (Ortega and Krell, 2020).

Apart from increasing the local concentration of CheB and CheR, studies of *Pseudomonas aeruginosa* suggested another reason for the existence of pentapeptides. *P. aeruginosa* PAO1 has four chemosensory pathways containing each a CheR and CheB homolog (Matilla *et al.*, 2021a). Of the 26 chemoreceptors, the oxygen-responsive McpB (synonym Aer2) (García *et al.*, 2017) is the only pentapeptide containing chemoreceptor (Matilla *et al.*, 2021a) and was predicted to be the sole chemoreceptor that feeds into the Che2 pathway (Ortega *et al.*, 2017b). We have shown that CheR<sub>2</sub>, the methyltransferase of the Che2 pathway, was the only CheR homologue that bound the McpB/Aer2 pentapeptide (García-Fontana *et al.*, 2014). Binding to this pentapeptide was essential for CheR<sub>2</sub>-mediated methylation of McpB/Aer2 (García-Fontana *et al.*, 2014) and it has therefore been concluded that the pentapeptide-CheR<sub>2</sub> interaction is a mechanism that permits the targeting of a particular chemoreceptor with a specific CheR (García-Fontana *et al.*, 2014).

Sequence analyses revealed that pentapeptides show a significant degree of sequence variability (Perez and Stock, 2007; Ortega and Krell, 2020). Whereas aromatic amino acids are conserved at positions 2 and 5, a number of different amino acids are found at the remaining places (Perez and Stock, 2007; Ortega and Krell, 2020). Whereas *P. aeruginosa* has a single pentapeptide containing chemoreceptor, other strains possess a large number of such receptors. Frequently, these strains contain a single chemosensory pathway indicating that their role has to differ from that observed in *P. aeruginosa* that consists in directing a given CheR homolog to a given chemoreceptor. To study pentapeptide function in these bacteria, we have chosen *Pectobacterium atrosepticum* SCRI1043 as a model organism. *P. atrosepticum* is among the top 10 plant pathogens (Mansfield *et al.*, 2012) and as the causative agent of soft rot diseases in several agriculturally relevant crops (Toth *et al.*, 2003). Strain SCRI1043 has 36 chemoreceptors of which many possess a C-terminal pentapeptide. Its single chemosensory pathway was shown to mediate chemotaxis (Velandó *et al.*, 2020). There is a significant sequence variability among terminal pentapeptides. So far, there is no information available on how pentapeptide sequence divergence modulates the affinity for CheR.

---

## Materials and Methods

---

*Bacterial strains and growth conditions:* Bacterial strains used in this study are listed in Table S7. *P. atrosepticum* SCRI1043 and its derivative strains were routinely grown at 30 °C in Lisogeny Broth (5 g/l yeast extract, 10 g/l bacto tryptone, 5 g/l NaCl) or minimal medium (0.41 mM MgSO<sub>4</sub>,

7.56 mM (NH<sub>4</sub>)<sub>2</sub>SO<sub>4</sub>, 40 mM K<sub>2</sub>HPO<sub>4</sub>, 15 mM KH<sub>2</sub>PO<sub>4</sub>) supplemented with 0.2% (w/v) glucose as carbon source. *E. coli* strains were grown at 37 °C in LB. *Escherichia coli* DH5α was used as a host for gene cloning. Media for propagation of *E. coli* β2163 were supplemented with 300 mM 2,6-diaminopimelic acid. When appropriate, antibiotics were used at the following final concentrations (in μg ml<sup>-1</sup>): kanamycin, 50; tetracycline, 10, streptomycin, 50, ampicillin, 100. Sucrose was added to a final concentration of 10% (w/v) when required to select derivatives that had undergone a second cross-over event during marker exchange mutagenesis.

*In vitro nucleic acid techniques:* Plasmid DNA was isolated using the NZY-Tech miniprep kit. For DNA digestion, the manufacturer's instructions were followed (New England Biolabs and Roche). Separated DNA fragments were recovered from agarose using the Qiagen gel extraction kit. Ligation reactions were performed as described in (Sambrook *et al.*, 1989). PCR reactions were purified using the Qiagen PCR Clean-up kit. PCR fragments were verified by DNA sequencing that was carried out at the Institute of Parasitology and Biomedicine Lopez-Neyra (CSIC; Granada, Spain). Phusion<sup>®</sup> high fidelity DNA polymerase (Thermo Fisher Scientific) was used in the amplification of PCR fragments for cloning.

*CheR overexpression and purification:* The DNA sequences encoding CheR of *P. atrosepticum* SCRI1043 (ECA\_RS08375) was amplified by PCR using the oligonucleotides indicated in Table S8 and genomic DNA as template. The PCR product was digested with NheI and Sall and cloned into pET28b(+) linearized with the same enzymes. The resulting plasmid pET28b-CheR was verified by DNA sequencing and transformed into *E. coli* BL21-AI<sup>TM</sup>. The strain was grown under continuous stirring (200 rpm) at 30 °C in 2-liter Erlenmeyer flasks containing 500 ml of LB medium supplemented with 50 μg/ml kanamycin. At an OD<sub>660</sub> of 0.6, protein expression was induced by the addition of 0.1 mM isopropyl β-D-1-thiogalactopyranoside (IPTG) and 0.2% (w/v) L-arabinose. Growth was continued at 16 °C overnight prior to cell harvest by centrifugation at 10 000 x *g* for 30 min. The cell pellet was resuspended in buffer A (40 mM KH<sub>2</sub>PO<sub>4</sub>/K<sub>2</sub>HPO<sub>4</sub>, 10 mM imidazole, 10% (v/v) glycerol, 1 mM β-mercaptoethanol, pH 7.5) and cells were broken by French press treatment at 62.5 lb/in<sup>2</sup>. After centrifugation at 20 000 x *g* for 30 min, the supernatant was loaded onto a 5-ml HisTrap HP columns (Amersham Biosciences) equilibrated with buffer A and eluted with an imidazole gradient of 40–500 mM in the same buffer. Protein-containing fractions were pooled, and dialyzed overnight against 40 mM KH<sub>2</sub>PO<sub>4</sub>/K<sub>2</sub>HPO<sub>4</sub>, 10% (v/v) glycerol, 1 mM 2-mercaptoethanol, pH 7.0. For the purification of CheR that was used for animal immunization or as standard in the immunoblot, protein was further purified by size exclusion chromatography on a HiPrep<sup>TM</sup> 26/60 Sephacryl<sup>TM</sup> S200 HR gel filtration column (GE Healthcare). Protein was eluted isocratically at a flow of 1 ml/min. All manipulations were carried out at 4 °C.

*Isothermal titration calorimetry (ITC):* All experiments were conducted on a VP-microcalorimeter (MicroCal, Amherst, MA) at 25 °C. CheR was dialyzed overnight against 40 mM KH<sub>2</sub>PO<sub>4</sub>/K<sub>2</sub>HPO<sub>4</sub>, 10% (v/v) glycerol, 1 mM β-mercaptoethanol, pH 7.0, adjusted to a concentration of 10–25 μM, placed into the sample cell and titrated with 3.2–4.8 μl aliquots of 0.1–1 mM peptide solutions (purchased from GenScript, Piscataway, NJ, USA), 2 mM SAM or 250 μM SAH. All solutions were prepared in dialysis buffer immediately before use. The mean enthalpies measured from the injection of the peptide into the buffer were subtracted from raw titration data prior to data analysis with the MicroCal version of ORIGIN. Data were fitted with the 'One binding site model' of ORIGIN.

*Construction of a mutant deficient in cheR:* A chromosomal *cheR* mutant of SCRI1043 was constructed by homologous recombination using a derivative plasmid of the suicide vector pKNG101. The up- and downstream flanking regions of *cheR* were amplified by PCR using the oligonucleotides listed in Table S8, which were subsequently digested with EcoRI/BamHI and BamHI/PstI, respectively, and ligated in a three-way ligation into the EcoRI/PstI sites of pUC18Not to generate plasmid pUC18Not\_Δ*cheR*. Subsequently, a 0.95-kb BamHI fragment containing the Km3 cassette of p34S-Km3 was inserted into the BamHI site of pUC18Not\_Δ*cheR*, giving rise to pUC18Not\_Δ*cheR*\_km3. Lastly, a 2.5-kb NotI fragment of pUC18Not\_Δ*cheR*\_km3 containing the *cheR* deleted gene was cloned at the same site into the suicide vector pKNG101, resulting in pKNG101\_Δ*cheR*. This plasmid was transferred to *P. atrosepticum* SCRI1043 by biparental conjugation using *E. coli* β2163. Cells were plated onto LB plates containing kanamycin at 50 μg/ml. Selected merodiploid colonies were transferred plated on LB plates containing sucrose 10 % (w/v) to select derivatives that had undergone a second cross-over event during marker exchange mutagenesis. All plasmids and mutations were confirmed by PCR and sequencing.

*Quantitative capillarity chemotaxis assays:* Overnight bacterial cultures of *P. atrosepticum* SCRI1043 were grown at 30 °C in minimal medium. At an OD<sub>660</sub> of 0.35-0.4, the cultures were washed twice with chemotaxis buffer (50 mM K<sub>2</sub>HPO<sub>4</sub>/KH<sub>2</sub>PO<sub>4</sub>, 20 μM EDTA and 0.05% (v/v) glycerol, pH 7.0) and diluted to an OD<sub>660</sub> of 0.1 in the same buffer. Subsequently, 230 μl aliquots of the resulting bacterial suspension were placed into 96-well plates. One-microliter capillary tubes (P1424, Microcaps; Drummond Scientific) were heat-sealed at one end and filled with either the chemotaxis buffer (negative control) or chemotaxis buffer containing the chemoeffectors to test. The capillaries were immersed into the bacterial suspensions at its open end. After 30 min at room temperature, the capillaries were removed from the bacterial suspensions, rinsed with sterile water and the content expelled into tubes containing 1 ml of minimal medium salts. Serial dilutions were plated onto minimal medium supplemented with 15 mM glucose as carbon source. The number of colony forming units was determined after 36 h incubation at 30 °C. In all cases, data were corrected with the number of cells that swam into buffer containing capillaries.

*Determination of the cellular CheR concentration by quantitative immunoblotting:*

Generation of the acetone powder: Sera of polyclonal antibodies were obtained from Genescript Biotech Corp (Piscataway, New Jersey, USA) by an immunisation of rabbit. To reduce non-specific antibody binding an acetone powder pre-absorption protocol similar to that described in (Li and Hazelbauer, 2004) was used to reduce antibody unspecific binding. To this end a 700 ml culture of *P. atrosepticum* SCRI1043 Δ*cheR* was grown in minimal medium until an OD<sub>660</sub> 0.8 and cells were harvested by centrifugation at 10 000 x *g* for 10 minutes (4°C). Cells were then resuspended in 4 ml of 0.9% NaCl (w/v) to which 16 ml acetone were added. After an incubation for 30 minutes, the sample was centrifuged at 10 000 x *g* for 10 minutes, the pellet resuspended in 20 ml acetone and kept on ice for 10 minutes. This solution was centrifuged as above and the pellet was dried and homogenized to a powder, prior to storage at -20 °C. The antibody solution was diluted three-fold with PBS, prior to the addition of this powder to a final concentration of 1% (w/v). This suspension was incubated at room temperature for 30 minutes and then centrifuged at 13000 *g* for 5 min. The supernatant was recovered and then diluted 200 fold with PBS to be used in the immunoblots as detailed below.

Cell culture and western blot analysis: The wt and  $\Delta cheR$  strains were grown in minimal medium as detailed above. Twenty ml samples were taken during exponential phase ( $OD_{660} = 0.5$ ) or late stationary phase (overnight culture with  $O.D_{660} > 2.5$ ) and cells harvested by centrifugation at 10000 g during 5 min. In parallel, the number of cells in both samples was determined by plating out serial dilutions and cell counting. Cell pellets were resuspended in a volume of buffer A (40 mM  $K_2HPO_4$ , 40 mM  $KH_2PO_4$ , 10 mM imidazole, 10 % (v/v) glycerol, 1 mM 2-mercaptoethanol, pH 7.0) containing the cOmplete™ EDTA-Free protease inhibitor at a 1 x concentration following manufacturer's instructions (Merck Millipore Corp, Burlington, Massachusetts, USA). The buffer volume was proportional to the cell density of the sample. This buffer was identified in buffer screening experiments with purified CheR and was found to maintain the protein stable and active. Cells were sonicated and Benzonase® Nuclease (Merck, Millipore Corp, Burlington, Massachusetts, USA) was added at a concentration of 1 U/ml. After an incubation at room temperature during 10 minutes, samples were adjusted to the same protein concentration prior to the addition of SDS sample buffer. Samples were incubated at 95 °C for 10 minutes and separated on 12 % w/v SDS-PAGE gels. The gel was also loaded with purified CheR as a standard (1 to 10 ng). SDS-PAGE electrophoresis was done at 120 V, prior to protein transfer onto 0.45  $\mu$ m-pore-size nitrocellulose membranes (Protram Premium; Amersham Pharmacia Biotech, Amersham, UK) at 100 V for 1-2 h. Nitrocellulose membranes were immersed in 10% (w/v) nonfat powdered milk in PBS and placed on an orbital shaker at 4 °C for 12 h. Subsequently, membranes were immersed in a 1/200 dilution of primary antiserum in PBS + 10% milk, placed on an orbital shaker at room temperature for 2 h. Membranes were then washed three times with PBS for 10 min, incubated with a 1/5000 dilution of secondary antibody (Goat anti-Rabbit IgG (H+L) Secondary Antibody, HRP, Thermofisher Scientific, Waltham, Massachusetts, USA) for 1-2 h, washed as above, and treated with Femto ECL Western blotting detection reagent (Amersham Pharmacia Biotech, Amersham, UK) according to the manufacturer's protocol and exposed to a chemiluminescent detector (Bio-Rad ChemiDoc™ XRS+ System, Bio-Rad, Hercules, California, USA). Chemiluminescent images were captured, and intensities were quantified using Quantity One software (Bio-Rad, Hercules, California, USA).

Calculation of the cellular CheR concentration: The amount of CheR present in samples was inferred from the standard curve. The determination of the cellular CheR concentration was based on the normalization of absolute values with the number of cells and the cell volume. The *P. atrosepticum* SCRI1043 cell volume was derived from electron microscopy studies. To this end cells were cultured as detailed above and fixed with a solution of 2.5 % (v/v) glutaraldehyde containing 100 mM sodium cacodylate. Subsequently a 0.1 % (w/v) solution of poly-L-Lys in water was deposited on a coverslip to which the fixed sample was added. A solution of 1% (w/v) in water of osmium tetroxide was then applied to the sample and incubated at 4 °C for 1 hour. The coverslip was then washed with distilled water and the sample was dehydrated by applying an ethanol gradient (50 %, 70 %, 90 % and 3 x 100 %), with 10 minutes per step. Finally, the samples were dried by the Critical Point Method (Anderson, 1951) in a desiccator Polaron CPD 7501. Finally, cells are covered with a carbon sheet (EMITECH K975X). Images were recorded using a Scanning Electron Microscope HITACHI, S-510. From the resulting images, the length and width of 200 individual, non-attached cells were determined using the ImageJ software (U. S. National Institutes of Health, Bethesda, Maryland, USA) for each of the two conditions. The cell volume was calculated by approximating the shape of cells to a spherocylinder, i.e. a cylinder with hemispherical caps, using  $V = \pi R^2 (L - 2R) + 4/3\pi R^3 = \pi R^2 (L -$

2/3R) (Trueba and Woldringh, 1980), where V= volume; R=radius and L=length. Cellular CheR concentrations are the means and standard errors of three biological replicates conducted in duplicates.

## Results

---

### ***Pectobacterium atrosepticum* has 19 chemoreceptors with a C-terminal pentapeptide**

The alignment of the C-terminal sections of the 36 *P. atrosepticum* SCRI1043 chemoreceptors is shown in Figure 18. Nineteen of them possess a terminal pentapeptide that is tethered to the signaling domain via linker sequences of 29 to 39 amino acids (Figure 19). In total, there were 9 different pentapeptide sequences (Table 2) among which the NWETF sequence, as found in the *E. coli* and *S. typhimurium* receptors, was most abundant and present at 8 chemoreceptors (Table 2, Figure 19). Three pentapeptide sequences, DWTSF, NWTTF and NWEKF, were present in two different chemoreceptors, whereas the remaining pentapeptides were found in only a sole chemoreceptor (Table 2, Figure 19). These pentapeptides form 9 families, each with a different sequence. Interestingly, all pentapeptide containing chemoreceptors possess a four-helix bundle arrangement, either in its monomodular (4HB) or bimodular arrangement (HBM) (Table 2). The alignment of the 19 linker sequences did not show any apparent sequence similarity (Figure S8). However, there was a clear charge pattern: whereas positively charged amino acids are abundant in the linker sequences, negatively charged amino acids are frequently found in the pentapeptides (Figure S8). As a result, the average sequence derived isoelectric point (pI) of linkers is  $10.3 \pm 1.3$ , whereas that of the pentapeptides is of  $4.8 \pm 1.5$  (Table S9). The signaling domain of chemoreceptors has typically a strong negative surface charge whereas the HAMP domain has neutral or positive net charge (Figure S9). The positively charged linker sequences are likely to maintain interactions with the negatively charged signaling domain.



**Figure 19. C-terminal pentapeptides at *P. atrosepticum* SCRI1043 chemoreceptors.** (A) Shown is the C-terminal section of the sequence alignment of *Pectobacterium atrosepticum* SCRI1043 chemoreceptors. Pentapeptides are shaded in grey. The linker sequences are underlined. Green: conserved residues in the signaling domain; red: Asp and Glu; blue: Lys and Arg. (B) The sequence logo of these pentapeptides. Image produced using Weblogo (Crooks *et al.*, 2004).

### ***P. atrosepticum* CheR binds to C-terminal pentapeptides with different affinities**

To study the binding of different pentapeptides to *P. atrosepticum* CheR, the protein was overexpressed in *E. coli* and purified from the soluble cell lysate. To verify the protein integrity, microcalorimetric titration with S-adenosylmethionine (SAM) and S-adenosylhomocysteine (SAH), the substrate and product of the methylation reaction, were conducted (Figure 20). Binding of SAM and SAH were characterized by  $K_D$  values of  $144 \pm 22 \mu\text{M}$  and  $478 \pm 19 \text{nM}$ , respectively (Table 2), revealing that the reaction product is recognized with large preference, which agrees with CheR from other species (Yi and Weis, 2002; García-Fontana *et al.*, 2013; García-Fontana *et al.*, 2014).



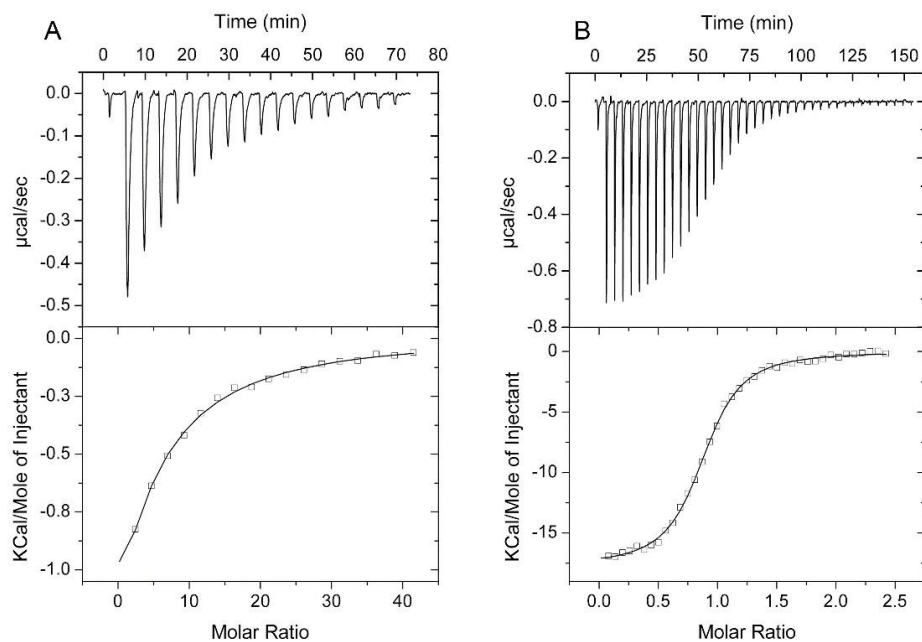


**Figure 20. Binding of S-adenosylmethionine (SAM) and S-adenosylhomocysteine (SAH) to *P. atrosepticum* CheR.** Shown are microcalorimetric titrations of 10 µM CheR with 16 µl aliquots of 2 mM SAM (A) and 14 µM CheR with 4.8 µl aliquots of 250 µM SAH (B). Upper panel: Raw titration data. Lower panel: Dilution heat corrected and concentration normalized integrated peak areas of raw titration data. Data were fitted with the “One binding site model” of the MicroCal version of ORIGIN.

In subsequent studies CheR was titrated with the nine different pentapeptides. In all cases, peptides were found to bind, but significant differences in affinity were observed (Figure 21, Table 2). Whereas the peptide GWTF bound with an affinity of 86 nM, peptides DWTF and NWTF that only differ in the amino acid at position 1, had  $K_D$  values of 226 and 1040 nM. The abundant pentapeptide NWETF bound with an intermediate affinity of 477 nM, which is higher than the affinity of 2 µM as determined for *E. coli* CheR (Wu *et al.*, 1996). In summary, there was an about 12-fold difference in the affinity of the most and least tightly binding peptide.

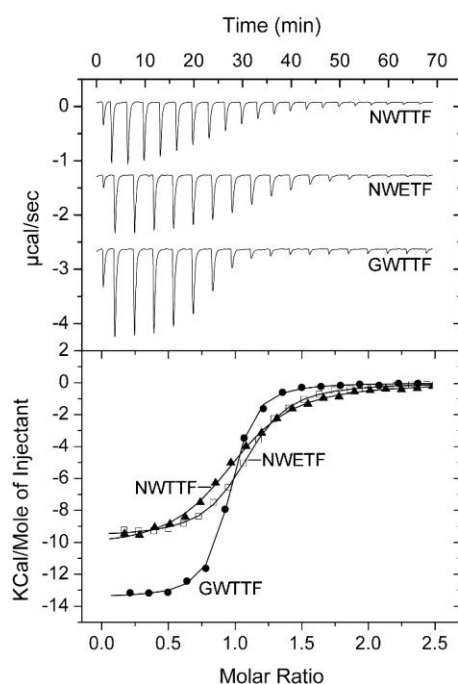


**Figure 21. Interaction between *P. atrosepticum* pentapeptides with CheR.** Upper panel: Microcalorimetric titrations of 16-20  $\mu\text{M}$  CheR with 1 mM pentapeptides NWTTF, NWETF and GWTF. Lower panel: Dilution heat corrected, and concentration normalized integrated peak areas of raw titration data. Data were fitted with the “One binding site model” of the MicroCal version of ORIGIN. Derived parameters are provided in Table 2.

**Table 2. Binding parameters for the interaction of *P. atrosepticum* CheR with S-adenosylmethionine (SAM), S-adenosylhomocysteine (SAH) and pentapeptides.**

Ligand	Chemoreceptor (LBD type)	$K_D^a$	$\Delta H$ (kcal/mol) <sup>a</sup>
SAM	-	144 $\pm$ 22 $\mu\text{M}$	-15.1 $\pm$ 3
SAH	-	478 $\pm$ 19 nM	-17.7 $\pm$ 0.3
GWQRF	ECA_RS15955 (4HB)	544 $\pm$ 107 nM	-9.8 $\pm$ 0.2
GWEKF	ECA_RS07510 (4HB)	197 $\pm$ 38 nM	-12.5 $\pm$ 1
GWTF	ECA_RS12635 (HBM)	86 $\pm$ 9 nM	-16.7 $\pm$ 2.5
DWTSF	ECA_RS18000 (4HB), ECA_RS12640 (HBM)	361 $\pm$ 61 nM	-10.7 $\pm$ 1
DWTF	ECA_RS08780 (4HB)	226 $\pm$ 39 nM	-12.9 $\pm$ 1
NWTF	ECA_RS00900 (4HB), ECA_RS00400 (HBM)	1.04 $\pm$ 0.23 $\mu\text{M}$	-12 $\pm$ 1
NWEKF	ECA_RS20365 (4HB), ECA_RS06625 (4HB)	788 $\pm$ 154 nM	-12.1 $\pm$ 0.5
NWEQF	ECA_RS21440 (4HB)	433 $\pm$ 23 nM	-16 $\pm$ 2
NWETF	ECA_RS21445 (4HB), ECA_RS21450 (4HB) ECA_RS21455 (4HB), ECA_RS06345 (4HB) ECA_RS08370 (4HB), ECA_RS08330 (4HB) ECA_RS19280 (4HB), ECA_RS13300 (4HB)	477 $\pm$ 37 nM	-11.5 $\pm$ 2

<sup>a</sup>Data were derived from microcalorimetric titrations (Figure 20). Shown are means and standard deviations from three experiments.

### The deletion of the *cheR* gene abolishes chemotaxis

To determine the function of CheR in *P. atrosepticum* chemotaxis we have constructed the corresponding deletion mutant. Quantitative chemotaxis capillary assays showed that this mutant is unable to perform chemotaxis to casamino acids, aspartate and malate (Figure 22). These data show that the *P. atrosepticum* adaptation system is essential to perform chemotaxis.

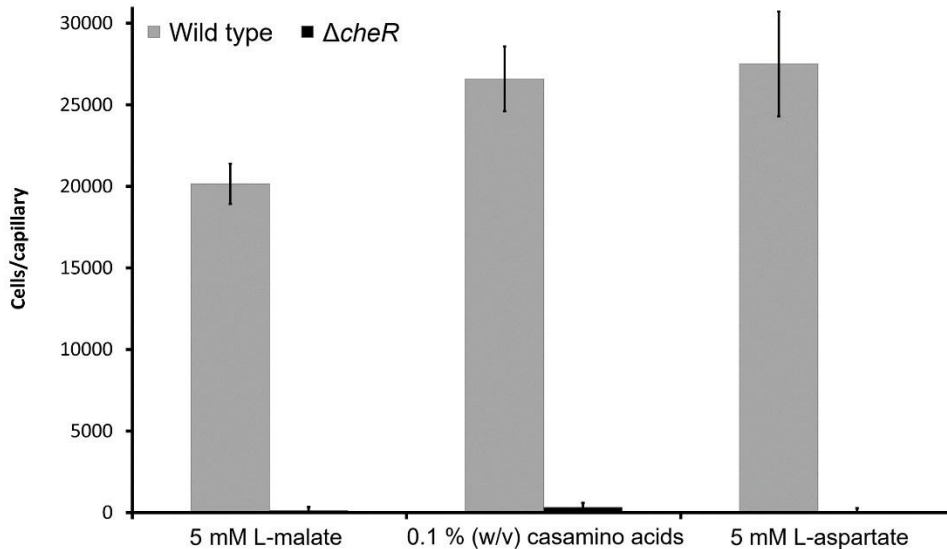


**Figure 22. Quantitative capillary chemotaxis assays of wild type *P. atrosepticum* SCRI1043 and a mutant in *cheR* towards different chemoattractants.** The data have been corrected by the number of cells that swam into buffer containing capillaries ( $113 \pm 19$  cells/capillary,  $370 \pm 64$  and  $305 \pm 49$  for malate, casamino acids and aspartate, respectively. CAA: casamino acids. Shown are means and standard deviations from three independent experiments conducted in triplicate.

### The cellular CheR concentration is in the same range as the dissociation constants determined for CheR-pentapeptide interactions.

As mentioned above, CheR bound pentapeptides with dissociation constants between 86 nM and 1.04  $\mu\text{M}$  (Table 2). We hypothesized that a differential occupation of chemoreceptor pentapeptides due to different affinities may be a potential mechanism to bias chemotactic responses. However, to assess the physiological relevance of the differential pentapeptide binding, information on the cellular CheR concentration is required. A further question resides in establishing whether this concentration is subject to changes such as for example during the different stages of growth. To this end we have determined the CheR concentration of cells in the exponential and stationary growth phase by quantitative immunoblotting.

In initial experiments we have studied cells by electron microscopy and representative images are shown in Figure S10. Based on the analysis of 200 cells for each sample we were able to determine cell volumes of  $0.71 \pm 0.04 \mu\text{m}^3$  and  $0.82 \pm 0.02 \mu\text{m}^3$  for cells in the exponential and stationary phase, respectively (see Materials and Methods for further detail). Using highly purified CheR, polyclonal antibodies were generated by immunization of rabbit. In initial experiments the specificity of the CheR-antibody interaction was assessed and optimized by the addition of a protein extract of the CheR mutant to the antibody solution. Immunoblotting of the wt and the  $\Delta cheR$  mutant strains demonstrated the specificity of CheR-antibody interaction (Figure S11).

Subsequently, the CheR concentrations were determined in exponential and stationary phase cultures from three biological replicates conducted in duplicates, of which a representative experiment is shown in Figure 23. Different amounts of highly purified CheR were submitted to immunoblotting (Figure 23A) and the resulting standard curve showed a linear relation between the integrated band density and the protein amount (Figure S12). In the *P. atrosepticum* samples, a signal for full-length CheR as well as for a proteolytic fragment were detected (Figure 23B). Since the size of this fragment was largely inferior to that of CheR, it was considered as inactive protein. For the *P. atrosepticum* samples used in immunoblots, the cell number was determined by plating out serial dilutions. Using this cell number and the cell volume as derived from electron microscopy, the cellular CheR concentration of exponential and stationary phase cultures were determined to be  $1.4 \pm 0.3 \mu\text{M}$  and  $0.73 \pm 0.1 \mu\text{M}$ , respectively. These data show that, (1) the cellular CheR concentration is within the range of  $K_D$  values for pentapeptide binding and (2) that the CheR concentration varies during growth. This is therefore consistent with the notion that the different pentapeptide containing chemoreceptors are occupied with different amounts of CheR. An alteration of the cellular CheR concentration, such as for example during growth, may alter chemoreceptor occupation by CheR.

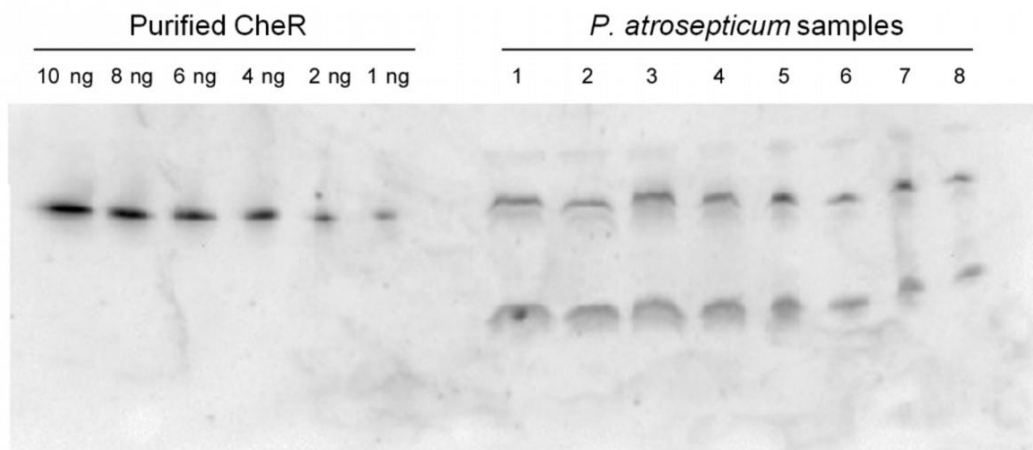


**Figure 23. Determination of the cellular CheR concentration of *P. atrosepticum* SCRI1043 by immunoblot using polyclonal anti CheR antibodies.** Left hand side: different amounts of purified CheR. Lanes 1 to 4: exponential phase culture: lanes 5 to 8: stationary phase cultures. Shown are duplicates (1 and 2, 3 and 4, 5 and 6, 7 and 8) of two biological replicates.

## Discussion

*Escherichia coli* is the traditional model organism in chemotaxis research. Since both high-abundance chemoreceptors contain the NWETF pentapeptide its interaction with CheR has been studied to some extent (Wu *et al.*, 1996; Feng *et al.*, 1999; Lai and Hazelbauer, 2005; Li and Hazelbauer, 2020). Pentapeptides differ largely in sequence and many species contain chemoreceptors fused to a multitude of different pentapeptides (Perez and Stock, 2007; Ortega and Krell, 2020). Here we present the first study evaluating the recognition of the complete set of different pentapeptides within a bacterial strain with CheR. All 9 pentapeptides were active and were recognized by CheR. The affinities of all *P. atrosepticum* pentapeptides were superior to the affinity of *E. coli* CheR for NWETF of about  $2 \mu\text{M}$  (Wu *et al.*, 1996; Li and Hazelbauer,

2020). Most measured affinities for *P. atrosepticum* pentapeptides are in the nanomolar range and are thus comparable to the affinity of about 500 nM for the interaction of *P. aeruginosa* CheR<sub>2</sub> with the GWEFF peptide of the McpB/Aer2 chemoreceptor (García-Fontana *et al.*, 2014). Molecular microbiology studies in the field of chemotaxis typically investigate responses to pure chemoeffector solutions. However, in their natural environment, bacteria are exposed to complex mixtures of compounds, of which many are chemoeffectors. In many bacteria, a multitude of chemoreceptors stimulate one or several chemotaxis signaling pathways resulting ultimately in changes in the phosphorylated levels of the response regulators CheY and CheB. There is currently a major need to identify the mechanisms that permit the definition of chemotactic responses in the presence of complex chemoeffector mixtures. What are the molecular features that define the weight of an individual chemoeffector/chemoreceptor in the definition of the final response? One such mechanism is related to the different affinities with which chemoeffectors are recognized by different chemoreceptors; a parameter that was shown to determine the onset of the tactic response (Reyes-Darias *et al.*, 2015c). Other mechanisms may be related to differences in the cellular abundance of chemoreceptors (Feng *et al.*, 1997; Zatakia *et al.*, 2018). Here, we report observations that suggest an additional mechanism that is based on the differential occupation of chemoreceptors with methyltransferases. We show here that the affinities of CheR for different pentapeptides differ more than 12-fold (Table 2). This implies that at a given cellular CheR concentration, chemoreceptors are differently occupied by CheR. Chemotaxis experiments with the *P. atrosepticum* cheR mutant have also shown that CheR is essential for chemotaxis (Figure 22). In this context, the dissociation of CheR from chemoreceptor is likely to have a major impact on downstream signaling. The differences in CheR-pentapeptide affinity may thus correspond to a mechanism to bias the chemotactic response to certain chemoreceptors. This hypothesis is supported by the determination of the cellular CheR concentration that was shown to be  $1.4 \pm 0.3 \mu\text{M}$  and  $0.73 \pm 0.1 \mu\text{M}$  for exponential and stationary phase cultures, respectively, being in the same range as the dissociation constant determined for the pentapeptide-CheR interaction. Interestingly, the three pentapeptides with highest affinity for CheR are only present on a single chemoreceptor, suggesting a potential bias for the binding of the methyltransferase to individual chemoreceptors. The function(s) of these chemoreceptors is unknown and future research will permit to determine their importance in the physiology and virulence of this important phytopathogen.

Although the linker sequences are of similar size, they do not share significant sequence similarities (Figure S8). However, they appear to share a charge pattern being both extremities frequently acidic and the linker core dominated by basic amino acids. Further studies are required to identify the physiological relevance of this pattern. Chemosensory arrays are highly ordered protein complexes and the positively charged linker may interact with the signaling domain that has a predominantly negative net charge as a means to limit the mobility of the linker and bound enzymes.

## Supplementary Material

```

ECA_RS00900      LSYGNGKTA-SYASAPTRTPTL-S-LAP--AAAKNQSNND--
ECA_RS08780      ---GASYKS-AALNRKTETPAL-A-APKNNRAEKTSAKGELA
ECA_RS20365      -GTPAARPA-P-MAKKAQTAR----LALAPVG----NTQD--
ECA_RS13300      AAEAPRRPQ-QRLAEKAPAAQK-P-MLLAAAGGKKNAND--
ECA_RS21440      ---GGSSQ---RIAPPLKRPSS-AKFSLANPKGSAGSNNQ--
ECA_RS21445      --ESGSSQ---RTTPELKRPSS-AKLSLASPKGRTKSDSQ--
ECA_RS21450      ---GIQTKA-PRLTSQVKQPAA-PRLALASKSGHTSSD----
ECA_RS21455      ---GTQSQ---RAVPQVTLSR-PKLALAGNSSNT-----
ECA_RS18000      ---GNQHQI-ARTPAAAASLTLRPALAAPGKSGISAGEG---
ECA_RS19280      ---GIVQQVRSSLPKSAPQPRLAPAMAIAGSS--KGNSNQ--
ECA_RS15955      --QIASSSLIPALASVPSGLSA-PRLASAKNKNALAQDEA--
ECA_RS08370      EDTGSFRR--TTQATAGQKPVLLAPSVNGGKKAKEGSSTD--
ECA_RS06345      --QAVAQEH--RAASASSLAAL-PKSLLPKPTS-AGSSNA--
ECA_RS08330      SHLSSGHS-A-PARPNALAAKGR-SSLALPRQAN---TENG--
ECA_RS12640      ---SQSDN---RVASRASSI--PRHTLPKSVSAKAASSES-
ECA_RS06625      ----DTQS---ALQVAAKPVRK-AQAIAPRAGKALPTSSD--
ECA_RS07510      -SDSDQQTAFSRPAIAAPVHRAVAQSTTPLL-S-VHGRHGE--
ECA_RS12635      --ENEGRK--PKANISGLPPQ--QKYLPPAAK---QTQDS--
ECA_RS00400      -DKDVARLQ--GSNTGNPNSGNKATARLPTLAS-RDNGND--
    
```

**Figure S 8.** Alignment of the linker sequences of the 19 chemoreceptors from *Pectobacterium atrosepticum* containing terminal pentapeptides. The alignment was done using the CLUSTALW algorithm of the npsa suite (Combet *et al.*, 2000) using the GONNET weight matrix, a gap opening penalty of 10 and a gap extension penalty of 0.2.

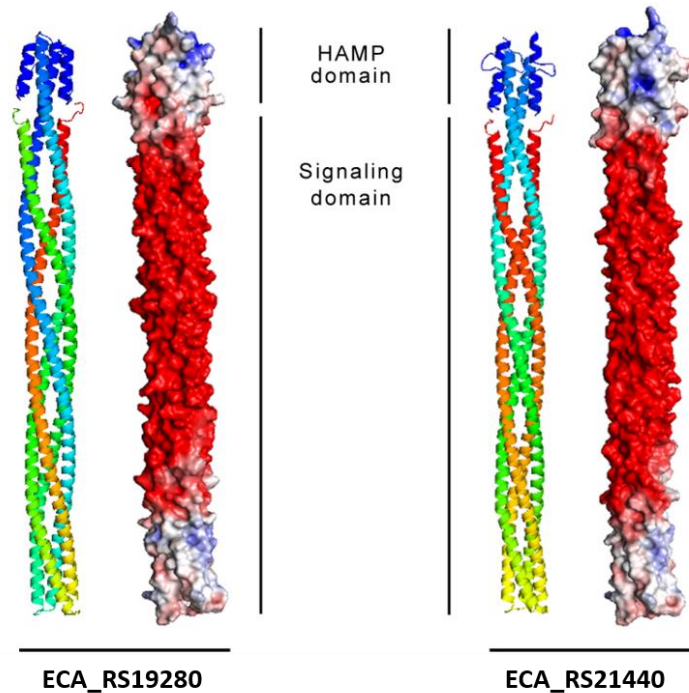


**Figure S 9.** Charge distribution at the cytosolic fragments of *P. atrosepticum* chemoreceptors. Homology models of the cytosolic fragments of the ECA\_RS19280 and ECA\_RS21440 receptors were produced using SwissModel (Waterhouse *et al.*, 2018). Ribbon diagrams are shown on the left and surface charges as calculated by PyMol (Schrödinger, 2010) are shown on the right. Red: negative charge, blue: positive charge. Two representative chemoreceptors are shown. Similar results were obtained for the remaining receptors.

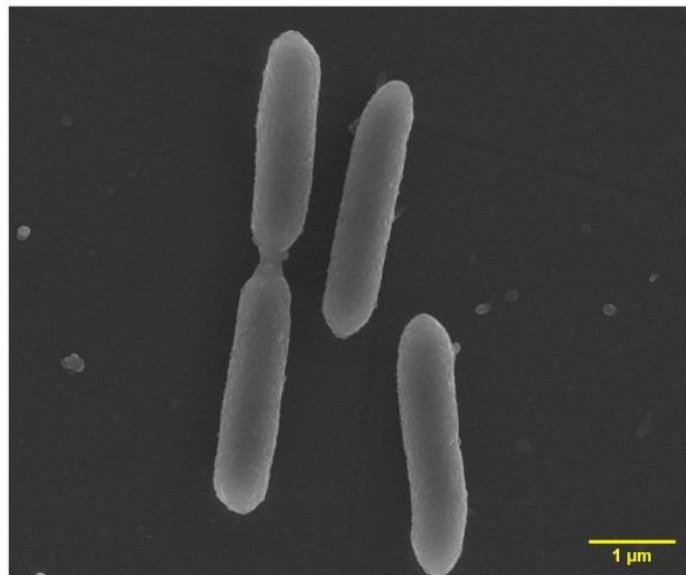
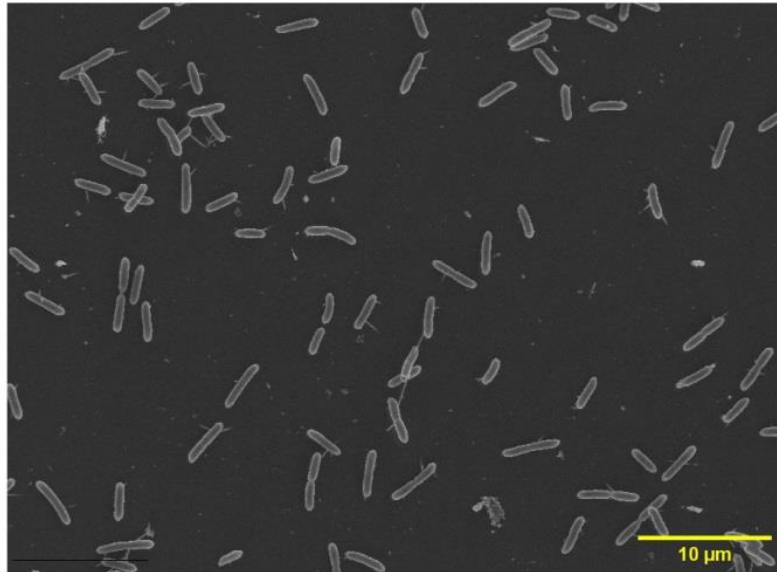


**Figure S 10.** Electron microscopy images of *Pectobacterium atrosepticum* SCRI1043 grown on minimal medium for approximately 5 hours ( $OD_{660}=0.5$ ).

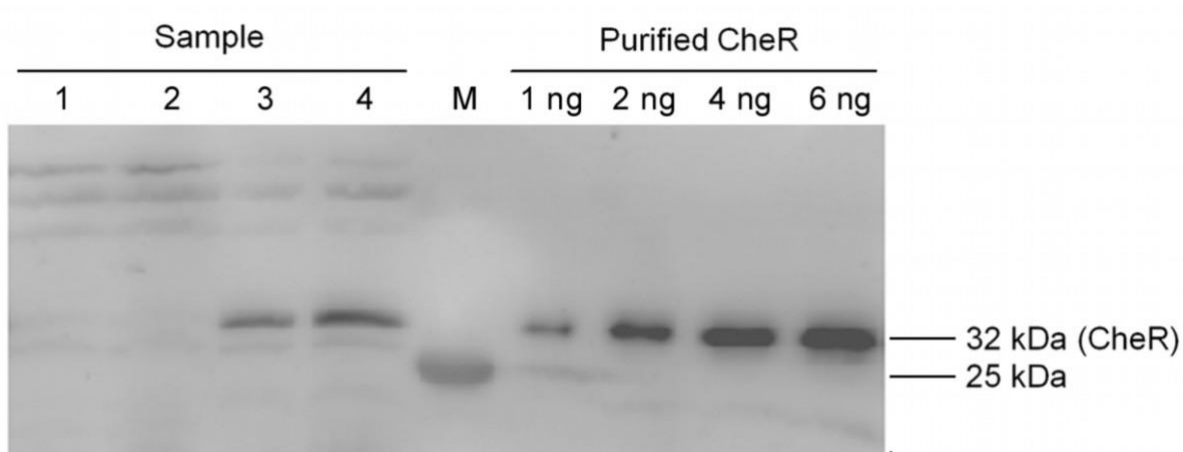


Figure S 11. Immunoblot of *P. atrosepticum* SCRI1043 samples and purified CheR using polyclonal antibodies against CheR. Lanes 1 and 2: two dilutions of *P. atrosepticum* SCRI1043  $\Delta cheR$ ; lanes 3 and 4: two dilutions of *P. atrosepticum* SCRI1043 (wt); M: molecular weight marker. The remaining four lanes contain different amounts purified *P. atrosepticum* SCRI1043 CheR.

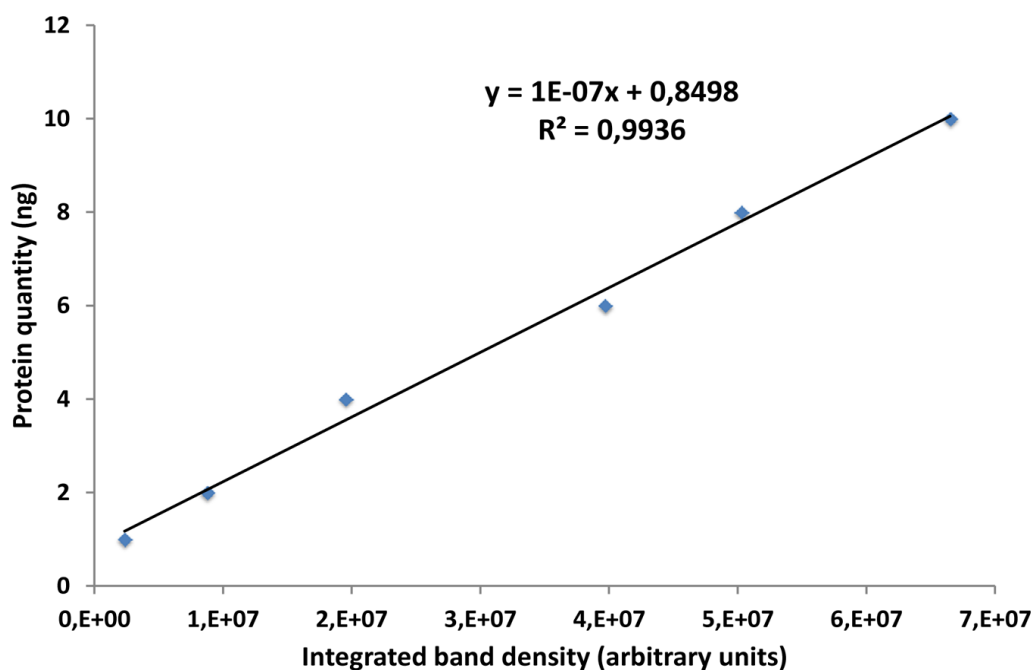


Figure S 12. Immunoblot calibration curve showing the integrated band densities for different amounts of purified *P. atrosepticum* CheR.



**Table S 6. The sequence-derived pI values of linker and pentapeptide sequences of the 19 pentapeptide containing chemoreceptors of *P. atrosepticum*.**

Receptor	Linker/ sequence <sup>a</sup>	pI linker	pI pentapeptide <sup>a</sup>
ECA_RS00900	LSYGN <b>G</b> KTASYASAPT <b>R</b> TP <b>T</b> LSLAPAA <b>K</b> NQSN <b>D</b> NW <b>T</b> TF	9.53	5.52
ECA_RS08780	GAS <b>Y</b> <b>K</b> SAAL <b>N</b> <b>R</b> <b>K</b> <b>T</b> ETPALAAP <b>K</b> NN <b>R</b> A <b>E</b> KT <b>S</b> A <b>K</b> EL <b>A</b> D <b>W</b> TT <b>F</b>	10.00	3.80
ECA_RS18000	GNGHQ <b>I</b> <b>A</b> <b>R</b> TPAAAAS <b>L</b> <b>R</b> PALAAP <b>G</b> <b>K</b> SGISAG <b>E</b> <b>G</b> D <b>W</b> TS <b>F</b>	10.84	3.80
ECA_RS21440	<b>E</b> GGSS <b>Q</b> <b>R</b> IAP <b>L</b> <b>K</b> <b>R</b> PSSA <b>K</b> FSLAN <b>P</b> <b>K</b> GSAGSNNQ <b>N</b> W <b>E</b> Q <b>F</b>	12.02	4.00
ECA_RS21445	<b>E</b> SGSS <b>Q</b> <b>R</b> TT <b>P</b> <b>E</b> <b>L</b> <b>K</b> <b>R</b> PSSA <b>K</b> LSL <b>A</b> SP <b>K</b> <b>G</b> <b>R</b> <b>T</b> <b>K</b> <b>S</b> D <b>S</b> Q <b>N</b> W <b>E</b> TF	10.43	4.00
ECA_RS20365	<b>R</b> GPAA <b>R</b> PAPMA <b>K</b> <b>K</b> AQTAR <b>L</b> ALAPV <b>G</b> NTQ <b>D</b> NW <b>E</b> K <b>F</b>	11.00	6.00
ECA_RS21450	NGI <b>Q</b> <b>T</b> <b>K</b> AP <b>R</b> LT <b>S</b> Q <b>V</b> <b>K</b> QPAAP <b>R</b> LALAS <b>K</b> SGHTSS <b>D</b> NW <b>E</b> TF	11.10	4.00
ECA_RS21455	<b>D</b> GT <b>Q</b> <b>S</b> <b>Q</b> <b>R</b> AV <b>P</b> Q <b>V</b> TT <b>L</b> <b>S</b> <b>R</b> <b>P</b> <b>K</b> LALAGN <b>S</b> NT <b>N</b> W <b>E</b> TF	12.01	4.00
ECA_RS06345	NQAVA <b>Q</b> <b>E</b> <b>H</b> <b>R</b> AASASSLAAL <b>P</b> <b>K</b> SLL <b>P</b> KPTSAGSS <b>N</b> ANW <b>E</b> TF	9.99	4.00
ECA_RS08370	<b>S</b> ED <b>T</b> <b>G</b> <b>S</b> <b>F</b> <b>R</b> <b>R</b> TTQATAG <b>Q</b> <b>K</b> PVLLAPSV <b>N</b> GG <b>K</b> <b>K</b> <b>A</b> EGS <b>S</b> <b>T</b> <b>D</b> NW <b>E</b> TF	9.53	4.00
ECA_RS08330	SSH <b>L</b> SSGH <b>S</b> AP <b>A</b> <b>R</b> <b>P</b> <b>N</b> ALAA <b>K</b> <b>G</b> <b>R</b> SSLAL <b>P</b> <b>R</b> QANTEN <b>G</b> NW <b>E</b> TF	11.71	4.00
ECA_RS19280	SGIV <b>Q</b> <b>Q</b> <b>V</b> <b>R</b> SSL <b>P</b> <b>K</b> SAP <b>Q</b> <b>P</b> <b>R</b> LAPAMAIAGSS <b>K</b> GNS <b>N</b> Q <b>N</b> W <b>E</b> TF	12.02	4.00
ECA_RS06625	<b>S</b> D <b>T</b> Q <b>S</b> ALQ <b>V</b> AA <b>K</b> P <b>V</b> <b>R</b> <b>K</b> AQ <b>A</b> IAP <b>R</b> AG <b>K</b> ALPTSS <b>D</b> NW <b>E</b> K <b>F</b>	10.28	6.00
ECA_RS07510	<b>D</b> <b>S</b> <b>D</b> <b>S</b> <b>D</b> Q <b>T</b> A <b>F</b> <b>S</b> <b>R</b> PAIAAP <b>V</b> <b>H</b> <b>R</b> AVAQ <b>S</b> TT <b>P</b> LLSV <b>H</b> <b>G</b> <b>R</b> <b>H</b> <b>G</b> <b>E</b> <b>G</b> <b>W</b> <b>E</b> <b>K</b> <b>F</b>	6.78	6.00
ECA_RS13300	SA <b>A</b> E <b>A</b> <b>P</b> <b>R</b> <b>R</b> <b>P</b> <b>Q</b> <b>Q</b> <b>R</b> L <b>A</b> <b>E</b> <b>K</b> APAA <b>Q</b> <b>K</b> PMLAAAG <b>G</b> <b>K</b> <b>K</b> GNAN <b>D</b> NW <b>E</b> TF	10.43	4.00
ECA_RS12635	<b>S</b> EN <b>E</b> <b>G</b> <b>R</b> <b>K</b> <b>P</b> KANISGL <b>P</b> <b>P</b> <b>Q</b> <b>Q</b> <b>K</b> Y <b>L</b> <b>P</b> <b>P</b> <b>A</b> <b>A</b> <b>K</b> <b>Q</b> <b>T</b> <b>Q</b> <b>D</b> <b>S</b> <b>G</b> <b>W</b> <b>T</b> <b>T</b> <b>F</b>	9.41	5.52
ECA_RS12640	<b>S</b> Q <b>S</b> <b>D</b> <b>N</b> <b>R</b> <b>V</b> AS <b>R</b> ASS <b>I</b> <b>P</b> <b>R</b> <b>H</b> <b>T</b> <b>L</b> <b>P</b> <b>K</b> SV <b>S</b> <b>A</b> <b>K</b> AASS <b>E</b> <b>S</b> D <b>W</b> TS <b>F</b>	10.90	3.80
ECA_RS00400	<b>S</b> <b>D</b> <b>K</b> <b>D</b> <b>V</b> <b>A</b> <b>R</b> LQGSNT <b>G</b> <b>N</b> <b>P</b> <b>N</b> <b>S</b> <b>G</b> <b>N</b> <b>K</b> AT <b>A</b> <b>R</b> <b>L</b> <b>P</b> <b>T</b> <b>L</b> <b>A</b> <b>S</b> <b>R</b> <b>D</b> <b>N</b> <b>G</b> <b>N</b> <b>D</b> <b>N</b> <b>W</b> <b>T</b> <b>T</b> <b>F</b>	8.59	5.52
ECA_RS15955	GQ <b>I</b> ASS <b>S</b> LIPALAS <b>V</b> PSGL <b>S</b> AP <b>R</b> LASA <b>K</b> <b>N</b> <b>K</b> NAL <b>A</b> <b>Q</b> <b>D</b> E <b>A</b> <b>G</b> <b>W</b> <b>Q</b> <b>R</b> <b>F</b>	8.59	9.75
<b>Average</b>		<b>10.3 ± 1.3</b>	<b>4.8 ± 1.5</b>

<sup>a</sup>Positively and negatively charged amino acids are highlighted in blue and red, respectively.

<sup>b</sup>Values were determined using the ProtParam algorithm (<https://web.expasy.org/cgi-bin/protparam/protparam>).

**Table S 7. Strains and plasmids used in Chapter 2.**

Strains and plasmids	Genotype or relevant characteristics <sup>a</sup>	Reference
<b>Strains</b>		
<i>Escherichia coli</i> BL21-AI	F- <i>ompT hsdS<sub>B</sub> (r<sub>B</sub><sup>-</sup>m<sub>B</sub><sup>-</sup>) gal dcm araB::T7RNAP-tetA</i>	Invitrogen
<i>E. coli</i> DH5α	F- <i>endA1 glnV44 thi-1 recA1 relA1 gyrA96 deoR nupG purB20 φ80dlacZΔM15 Δ(lacZYA-argF)U169, hsdR17(r<sub>K</sub><sup>-</sup>m<sub>K</sub><sup>+</sup>), λ<sup>-</sup></i>	(Woodcock <i>et al.</i> , 1989)
<i>E. coli</i> β2163	F- RP4-2-Tc::Mu Δ <i>dapA</i> ::( <i>erm-pir</i> ); Km <sup>R</sup> , Em <sup>R</sup>	(Demarre <i>et al.</i> , 2005)
<i>Pectobacterium atrosepticum</i> SCRI1043	Wild type strain	(Bell <i>et al.</i> , 2004)
<i>P. atrosepticum</i> SCRI1043 Δ <i>cheR</i>	SCRI1043 in-frame deletion mutant of <i>cheR</i>	This study
<b>Plasmids</b>		
pET28b(+)	Km <sup>R</sup> ; Protein expression plasmid	Novagen
pET28b-CheR	Km <sup>R</sup> ; pET28b(+) derivative containing <i>P. atrosepticum cheR</i> ( <i>ECA_RS08375</i> )	This study
pUC18Not	Ap <sup>R</sup> ; identical to pUC18 but with two NotI sites flanking pUC18 polylinker	(Herrero <i>et al.</i> , 1990)
pUC18Not_Δ <i>cheR</i>	Ap <sup>R</sup> ; 1.5-kb PCR product containing a 678 bp in frame deletion of <i>cheR</i> of <i>P. atrosepticum</i> inserted into the EcoRI/PstI sites of pUC18Not	This study
p34S-Km3	Km <sup>R</sup> , Ap <sup>R</sup> ; Km3 antibiotic cassette	(Dennis and Zylstra, 1998)
pUC18Not_Δ <i>cheR</i> _km3	Ap <sup>R</sup> , Km <sup>R</sup> ; 0.95-kb BamHI fragment containing Km3 cassette of p34S-Km3 was inserted into BamHI site of <i>cheR</i> in pUC18Not_Δ <i>cheR</i>	This study
pKNG101	Sm <sup>R</sup> ; <i>oriR6K mob sacBR</i>	(Kaniga <i>et al.</i> , 1991)
pKNG101_Δ <i>cheR</i>	Sm <sup>R</sup> , Km <sup>R</sup> ; 2.5-kb NotI fragment of pUC18Not_Δ <i>cheR</i> _Km3 was cloned at the same site in pKNG101	This study

<sup>a</sup>Ap, ampicillin; Em, erythromycin; Km, kanamycin; Sm, streptomycin.

**Table S 8. Oligonucleotides used in Chapter 2.**

Name	Sequence (5'-3')	Purpose
pET28_CheR_Pec_f	TAATGCTAGCATGAGCAAGATAAGAGTATTATGC GTTG	Construction of pET28b-CheR
pET28_CheR_Pec_r	TAATGTCGACGCTCACCGAGAGCTGCTTAT	
pUC18Not_cheR_up_f	TAATGAATTCGGTTCAGAAGAACGACACAGGC	Construction of pUC18Not_Δ <i>cheR</i>
pUC18Not_cheR_up_r	TAATGGATCCCCGGTCAACCATCTGCGTC	
pUC18Not_cheR_down_f	TAATGGATCCCCGTCGATTCGTCGCCGATGC	
pUC18Not_cheR_down_r	TAATCTGCAGGCGCAATATAGGCATGTCCAGG	

## Chapter 3. The chemoreceptor PacA of *Pectobacterium atrosepticum* is homologous to PctD of *Pseudomonas aeruginosa* PAO1 and mediates taxis to quaternary amines.

---

Published article

### Chemotaxis of the human pathogen *Pseudomonas aeruginosa* to the neurotransmitter acetylcholine

Miguel A. Matilla<sup>1</sup>, Félix Velando<sup>1</sup>, Ana Tajuelo<sup>2</sup>, David Martín-Mora<sup>1</sup>, Wenhao Xu<sup>3</sup>, Victor Sourjik<sup>3</sup>, José A. Gavira<sup>4</sup> and Tino Krell<sup>1</sup>

<sup>1</sup>Department of Environmental Protection, Estación Experimental del Zaidín, Consejo Superior de Investigaciones Científicas; <sup>2</sup>Intrahospital Infections Laboratory, National Centre for Microbiology, Instituto de Salud Carlos III (ISCIII), Madrid, Spain; <sup>3</sup>Max Planck Institute for Terrestrial Microbiology and Center for Synthetic Microbiology (SYNMIKRO), Marburg, Germany; <sup>4</sup>Laboratory of Crystallographic Studies, IACT, (CSIC-UGR).

mBio (Published 7 March 2022); vol. 13, No. 2: e0345821. doi:10.1128/mbio.03458-21

---

### Abstract

---

Acetylcholine is a central biological signal molecule present in all kingdoms of life. In humans, acetylcholine is the primary neurotransmitter of the peripheral nervous system; it mediates signal transmission at neuromuscular junctions. Here, we show that the opportunistic human pathogen *Pseudomonas aeruginosa* exhibits chemoattraction towards acetylcholine over a concentration range of 1  $\mu$ M to 100 mM. The maximal magnitude of the response was superior to that of many other *P. aeruginosa* chemoeffectors. We demonstrate that this chemoattraction is mediated by the PctD (PA4633) chemoreceptor. Using microcalorimetry, we show that the PctD ligand-binding domain (LBD) binds acetylcholine with a  $K_D$  of 23  $\mu$ M. It also binds choline and betaine, with lower affinity. Highly sensitive responses to acetylcholine, choline, and less sensitive responses to betaine and L-carnitine, were observed in *Escherichia coli* expressing a chimeric receptor comprising the PctD-LBD fused to the Tar chemoreceptor signaling domain. We also identified the PacA (ECA\_RS10935) chemoreceptor of the phytopathogen *Pectobacterium atrosepticum*, which binds choline and betaine but fails to recognize acetylcholine. To identify the molecular determinants for acetylcholine recognition, we report high-resolution structures of PctD-LBD (with bound acetylcholine and choline) and PacA-LBD (with bound betaine). We identified an amino acid motif in PctD-LBD that interacts with the acetylcholine tail. This motif is absent in PacA-LBD. Significant acetylcholine chemotaxis was also detected in the plant pathogens *Agrobacterium tumefaciens* and *Dickeya solani*. To the best of our knowledge, this is the first report of acetylcholine chemotaxis and extends the range of host signals perceived by bacterial chemoreceptors.

### Importance





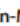



*P. aeruginosa* causes a significant number of deaths annually worldwide. For many pathogens, chemotaxis plays an important role in the initial stages of infection, and deciphering the key

chemoeffectors and their cognate chemoreceptors may permit the development of strategies to inhibit this process. Genome analyses have shown that many bacteria possess a large number of chemoreceptors. The chemoeffectors recognized by the large majority of chemoreceptors are unknown. However, identifying these chemoeffectors is crucial for deciphering the evolutionary forces that have shaped chemosensory signaling mechanisms in bacteria with different lifestyles. Our current understanding of the relationship between bacterial lifestyle and chemoreceptor repertoire is limited, and this work contributes to closing this gap in our knowledge. By expanding the list of known chemoeffectors and chemoreceptors, progress is made toward identifying functional receptor homologs in other bacteria.

---



# Chemotaxis of the Human Pathogen *Pseudomonas aeruginosa* to the Neurotransmitter Acetylcholine

 Miguel A. Matilla,<sup>a</sup>
 Félix Velando,<sup>a</sup>
 Ana Tajuelo,<sup>a\*</sup>
 David Martín-Mora,<sup>a</sup>
 Wenhao Xu,<sup>b</sup>
 Victor Sourjik,<sup>b</sup>
 José A. Gavira,<sup>c</sup>
 Tino Krell<sup>a</sup>

<sup>a</sup>Department of Environmental Protection, Estación Experimental del Zaidín, Consejo Superior de Investigaciones Científicas, Granada, Spain

<sup>b</sup>Max Planck Institute for Terrestrial Microbiology and Center for Synthetic Microbiology (SYNMIKRO), Marburg, Germany

<sup>c</sup>Laboratory of Crystallographic Studies, IACT (CSIC-UGR), Armilla, Spain

Tino Krell and José A. Gavira are joint senior authors. Tino Krell and José A. Gavira contributed equally to this work. Author order was determined by drawing straws.

**ABSTRACT** Acetylcholine is a central biological signal molecule present in all kingdoms of life. In humans, acetylcholine is the primary neurotransmitter of the peripheral nervous system; it mediates signal transmission at neuromuscular junctions. Here, we show that the opportunistic human pathogen *Pseudomonas aeruginosa* exhibits chemoattraction toward acetylcholine over a concentration range of 1  $\mu$ M to 100 mM. The maximal magnitude of the response was superior to that of many other *P. aeruginosa* chemoeffectors. We demonstrate that this chemoattraction is mediated by the PctD (PA4633) chemoreceptor. Using microcalorimetry, we show that the PctD ligand-binding domain (LBD) binds acetylcholine with an equilibrium dissociation constant ( $K_D$ ) of 23  $\mu$ M. It also binds choline and with lower affinity betaine. Highly sensitive responses to acetylcholine and choline, and less sensitive responses to betaine and L-carnitine, were observed in *Escherichia coli* expressing a chimeric receptor comprising the PctD-LBD fused to the Tar chemoreceptor signaling domain. We also identified the PacA (ECA\_RS10935) chemoreceptor of the phytopathogen *Pectobacterium atrosepticum*, which binds choline and betaine but fails to recognize acetylcholine. To identify the molecular determinants for acetylcholine recognition, we report high-resolution structures of PctD-LBD (with bound acetylcholine and choline) and PacA-LBD (with bound betaine). We identified an amino acid motif in PctD-LBD that interacts with the acetylcholine tail. This motif is absent in PacA-LBD. Significant acetylcholine chemotaxis was also detected in the plant pathogens *Agrobacterium tumefaciens* and *Dickeya solani*. To the best of our knowledge, this is the first report of acetylcholine chemotaxis and extends the range of host signals perceived by bacterial chemoreceptors.

**IMPORTANCE** *P. aeruginosa* causes a significant number of deaths annually worldwide. For many pathogens, chemotaxis plays an important role in the initial stages of infection, and deciphering the key chemoeffectors and their cognate chemoreceptors may permit the development of strategies to inhibit this process. Genome analyses have shown that many bacteria possess a large number of chemoreceptors. The chemoeffectors recognized by the large majority of chemoreceptors are unknown. However, identifying these chemoeffectors is crucial for deciphering the evolutionary forces that have shaped chemosensory signaling mechanisms in bacteria with different lifestyles. Our current understanding of the relationship between bacterial lifestyle and chemoreceptor repertoire is limited, and this work contributes to closing this gap in our knowledge. By expanding the list of known chemoeffectors and chemoreceptors, progress is made toward identifying functional receptor homologs in other bacteria.

**Invited Editor** Karen M. Ottemann, University of California, Santa Cruz

**Editor** Igor B. Zhulin, The Ohio State University

**Copyright** © 2022 Matilla et al. This is an open-access article distributed under the terms of the [Creative Commons Attribution 4.0 International license](https://creativecommons.org/licenses/by/4.0/).

Address correspondence to José A. Gavira, [jgavira@iact.ugr-csic.es](mailto:jgavira@iact.ugr-csic.es), or Tino Krell, [tino.krell@eez.csic.es](mailto:tino.krell@eez.csic.es).

\*Present address: Ana Tajuelo, Intrahospital Infections Laboratory, National Centre for Microbiology, Instituto de Salud Carlos III (ISCIII), Madrid, Spain.

The authors declare no conflict of interest.

**Received** 16 November 2021

**Accepted** 8 February 2022

**Published** 7 March 2022

## Introduction

---

Chemotaxis allows bacteria to move in chemical concentration gradients and facilitates the colonization of more-favorable ecological niches. Genome analyses indicate that about half of known bacterial species possess genes required for chemotaxis (Sanchis-López *et al.*, 2021). The molecular machinery for chemotaxis is highly complex and is among the best-studied bacterial signal transduction systems. Chemoeffectors are sensed by chemoreceptors that in turn stimulate chemosensory pathways that modulate the activity of the flagellar motor (Parkinson *et al.*, 2015; Bi and Sourjik, 2018).

A large number of different chemoeffectors have been identified (Matilla *et al.*, 2022a). Whereas some chemoeffectors serve as nutrients, including organic acids, amino acids, and sugars, other chemoeffectors provide information about the environment, as exemplified by chemotaxis to neurotransmitters (Pasupuleti *et al.*, 2014), quorum-sensing signals (Laganenka *et al.*, 2016), human hormones (Lopes and Sourjik, 2018), and plant signaling molecules (Antunez-Lamas *et al.*, 2009). Other chemoeffectors may have multiple functions, such as GABA (Reyes-Darias *et al.*, 2015a) and histamine (Corral-Lugo *et al.*, 2018), which are central signal molecules but also support bacterial growth.

A canonical chemoreceptor is composed of an extracytosolic ligand binding domain (LBD) and a cytosolic region that contains the signaling domain that interacts with other signaling proteins. Whereas the signaling domain is highly conserved in sequence, there is an enormous variety in the LBD type and sequence (Ortega *et al.*, 2017a). More than 80 different LBD types have so far been identified in chemoreceptors (Ortega *et al.*, 2017a), and new LBD families continue to be discovered (Elgamoudi *et al.*, 2021). The close correspondence in the affinities of full-length receptors and isolated LBDs (Milligan and Koshland, 1993; Lin *et al.*, 1994; Tajima *et al.*, 2011) indicates that all of the features necessary for chemoeffector recognition are contained within the LBD.

The chemotactic machinery represents an important metabolic burden to the cell. For example, the synthesis of the chemotaxis system and assembling and energizing the flagellar motors in *Escherichia coli* consumes several percent of total cellular protein and energy budget (Hosking *et al.*, 2006; Milo *et al.*, 2010; Colin and Sourjik, 2017). Another study has shown that the removal of the 70 kb flagellar operon from *Pseudomonas putida* resulted in several physiological advantages and increased fitness (Martínez-García *et al.*, 2014). This considerable metabolic burden has to be compensated by major benefits arising from chemotaxis. However, our understanding of these benefits for bacteria with different lifestyles is currently very limited, largely because the signals recognized by the majority of chemoreceptors is unknown.

The chemoeffector repertoire of a bacterium is a reflection of its lifestyle (Lacal *et al.*, 2010b; Colin *et al.*, 2021). Species that inhabit a specific ecological niche contain a reduced number of chemoreceptors. For example, *H. pylori* infects the gastric epithelium and is adapted to a highly specific niche. This species has 4 chemoreceptors which is a number significantly below the bacterial average of 14 (Sanchis-López *et al.*, 2021). Analysis of *H. pylori* chemoreceptor function has revealed a specialized spectrum of chemoeffectors that is closely linked to establishing an infection in the stomach. Furthermore, all four chemoreceptors were found to play a role in the

infection process (Ortega *et al.*, 2017b; Johnson and Ottemann, 2018; Perkins *et al.*, 2019; Hanyu *et al.*, 2019).

In contrast, bacteria with a versatile lifestyle that are able to survive in different ecological niches have a much higher number of chemoreceptors (Lacal *et al.*, 2010b). The opportunistic pathogen *Pseudomonas aeruginosa* serves as a model organism to study this category of bacteria. *P. aeruginosa* is omnipresent in the environment and has been detected in soil, water, human and animal-derived samples, different foods including vegetables and milk, and in plumbing systems and hospitals (Bédard *et al.*, 2016; Crone *et al.*, 2020; Bel Hadj Ahmed *et al.*, 2020). *P. aeruginosa* is also a highly versatile pathogen, able to infect almost all human tissues, including the respiratory tract, ear, eye, brain, heart, urinary tract, and it can cause a general bacteremia (Iglewski, 1996). *P. aeruginosa* is of great clinical relevance: (i) infections are associated with significant mortality; (ii) it is among the most frequent causes of nosocomial infections: and (iii) multidrug-resistant strains are rapidly emerging (Kang *et al.*, 2003; Morata *et al.*, 2012; Jean *et al.*, 2020; Sindeldecker and Stoodley, 2021). The ubiquity of this pathogen is also reflected in its capacity to infect different animals and plants (Rahme *et al.*, 2000; Walker *et al.*, 2004). Considering its omnipresence in the environment and the versatility of its lifestyle, it is of high importance to identify the environmental signals that are sensed by the *P. aeruginosa* chemoreceptors.

*P. aeruginosa* has 26 chemoreceptors that stimulate four different chemosensory pathways (Matilla *et al.*, 2021a). Whereas 23 chemoreceptors were predicted to stimulate the chemotaxis pathway (Ortega *et al.*, 2017b), a single receptor communicates with each of the remaining three pathways that carry out functions unrelated to chemotaxis (Matilla *et al.*, 2021a). A significant number of *P. aeruginosa* chemoreceptors have been functionally annotated. Among these are PctA, PctB and PctC, which are involved in chemotaxis to different proteinogenic amino acids and GABA (Taguchi *et al.*, 1997a; Rico-Jiménez *et al.*, 2013a; Gavira *et al.*, 2020); CtpL and CtpH, which sense inorganic phosphate (Wu *et al.*, 2000; Rico-Jiménez *et al.*, 2016); TlpQ, which senses histamine and polyamines (Corral-Lugo *et al.*, 2018); McpK, which senses  $\alpha$ -ketoglutarate (Martín-Mora *et al.*, 2016a); McpN, which senses nitrate (Martín-Mora *et al.*, 2019); CtpM, which senses malate and other C4 dicarboxylic acids (Alvarez-Ortega and Harwood, 2007; Martín-Mora *et al.*, 2018b); CttP, which senses chloroethylenes (Kim *et al.*, 2006); and Aer, which is involved in aerotaxis (Hong *et al.*, 2004). Furthermore, PctA and TlpQ were found to bind and mediate chemoattraction to the autoinducer-2 quorum sensing signal (Zhang *et al.*, 2020). The dCache domain is the predominant extracellular LBD in bacterial signal transduction systems, and it is present in about 15% of all chemoreceptors (Upadhyay *et al.*, 2016; Sanchis-López *et al.*, 2021). *P. aeruginosa* has five chemoreceptors that contain dCache LBDs, of which four - PctA, PctB, PctC and TlpQ - have been functionally annotated (Matilla *et al.*, 2021a).

Here, we show that the fifth dCache domain containing chemoreceptor, PA4633, binds the human neurotransmitter acetylcholine and induces a very strong attractant response to that compound. High-resolution 3D structures of its LBD and of a homologous domain that does not bind acetylcholine reveal the determinants for acetylcholine recognition. Acetylcholine chemotaxis has been observed in other bacteria, and its functional relevance is discussed.

## Materials and methods

---

*Strains, plasmids and culture conditions:* Bacterial strains, plasmids and oligonucleotides used are listed in Table S10. *E. coli* strains were grown in LB at 37 °C. *E. coli* DH5 $\alpha$  was used as a host for gene cloning. When necessary, antibiotics were used at the following concentrations: kanamycin, 25  $\mu$ g/ml (*E. coli* strains), ampicillin, 100  $\mu$ g/ml (*E. coli* strains), chloramphenicol, 17  $\mu$ g/ml (*E. coli* strains) and 100  $\mu$ g/ml (*P. aeruginosa* strains), tetracycline, 50  $\mu$ g/ml (*P. aeruginosa* strains).

*Construction of plasmids:* The DNA fragment encoding the LBD of *P. aeruginosa* PAO1 chemoreceptor PA4633 (amino acids 32 to 361) was amplified by PCR from genomic DNA and cloned into the NdeI and XhoI sites of pET28b(+) to generate plasmid pET28\_PA4633-LBD. The DNA fragment encoding the LBD of *P. atrosepticum* SCRI1043 chemoreceptor ECA\_RS10935 (amino acids 37-317) was amplified by PCR from genomic DNA. The resulting PCR fragment was then submitted to restriction free-cloning into pET28b(+) as described in (Bond and Naus, 2012). For the construction of the plasmid for complementation assays, the *pa4633* gene was PCR amplified and cloned into pBBR1MCS-2\_START. The resulting plasmid was transformed into *P. aeruginosa* PAO1-PA4633 by electroporation. The DNA sequence of gene *ECA\_RS10935* was amplified from the genomic DNA of *P. atrosepticum* SCRI1043 and cloned into plasmid pBBR1MCS-2\_START digested with NdeI and BamHI, resulting in pBBR\_ECA\_RS10935. The hybrid gene encoding PctD-Tar was constructed using PCR and inserted under the salicylate-inducible promoter into pKG116 using NdeI and BamHI sites to yield plasmid pVS1743. All plasmids were verified by sequencing the inserts and flanking regions.

*Protein overexpression and purification:* *E. coli* BL21-AI<sup>TM</sup> and *E. coli* BL21 (DE3) harboring plasmids pET28\_PA4633-LBD and pET28\_ECA\_RS10935-LBD, respectively, were grown in 2-l Erlenmeyer flasks containing 500 ml LB medium supplemented with kanamycin. Cultures were grown under continuous stirring (200 rpm) at 30 °C. At an OD<sub>660</sub> of 0.5, PA4633-LBD expression was induced by the addition of 0.2% (w/v) L-arabinose and 1 mM isopropyl- $\beta$ -D-thiogalactopyranoside (IPTG). Growth was continued at 30 °C for 5 h and cells were harvested by centrifugation at 20,000 x *g* for 20 min at 4 °C. ECA\_RS10935-LBD expression was induced by adding 0.1 mM IPTG at an OD<sub>660</sub> of 0.5 and growth was continued overnight at 18 °C, prior to cell harvest by centrifugation at 20,000 x *g* for 20 min. Proteins were purified by metal affinity chromatography. Briefly, the cell pellets of PA4633-LBD and ECA\_RS10935-LBD were resuspended in buffer A (30 mM Tris/HCl, 300 mM NaCl, 10 mM imidazole, 5% (v/v) glycerol, pH 8.0) or buffer B (40 mM KH<sub>2</sub>PO<sub>4</sub>/K<sub>2</sub>HPO<sub>4</sub>, 10 mM imidazole, 10% (v/v) glycerol, pH 7.0), respectively, containing cOmplete<sup>TM</sup> protease inhibitor (Roche) and benzonase (Merck). Cells were then broken by French press treatment at a gauge pressure of 62.5 lb/in<sup>2</sup>. After centrifugation at 10,000 x *g* for 1 h, the supernatant was loaded onto a 5-ml HisTrap column (Amersham Bioscience) equilibrated with buffers A or B. Proteins were eluted by a gradient of 40 to 500 mM imidazole in the same buffers.

*Isothermal titration calorimetry:* Measurements were made using a VP-ITC microcalorimeter (Microcal Inc., Northampton, Massachusetts) at 25 °C. PA4633-LBD was dialyzed into 5 mM Tris, 5 mM PIPES, 5 mM MES, 150 mM NaCl, 10% (v/v) glycerol, pH 7.5, whereas ECA\_RS10935-LBD was dialyzed into 40 mM KH<sub>2</sub>PO<sub>4</sub>/K<sub>2</sub>HPO<sub>4</sub>, 10% (v/v) glycerol, pH 7.0. Proteins at 15-22  $\mu$ M were placed into the sample cell and titrated with 9.6  $\mu$ l aliquots of 0.5-10 mM ligand solutions made



up in dialysis buffer. In the absence of binding, the experiment was repeated at 15 °C. The mean enthalpies from the injection of ligands into the buffer were subtracted from raw data prior to data fitting using the 'One binding site model' of the MicroCal version of the ORIGIN software.

*Chemotaxis assays:* Overnight cultures in M9 minimal medium supplemented with 6 mg/l Fe-citrate, trace elements (Abril *et al.*, 1989) and 15 mM glucose were used to inoculate fresh medium to an OD<sub>660</sub> of 0.05. Cells were cultured at 30 °C (*Pectobacterium atrosepticum*, *Pantoea agglomerans*, *Serratia plymuthica*, *Pseudomonas stutzeri*, *Agrobacterium tumefaciens*, *Dickeya solani*, *Pseudomonas savastanoi* pv. *savastanoi*) or 37 °C (*P. aeruginosa*, *E. coli*, *Salmonella enterica* sv. Typhimurium) until an OD<sub>660</sub> of 0.4 to 0.5. Subsequently, cells were washed twice by centrifugation (1,667 x *g* for 5 min at room temperature) and resuspension in chemotaxis buffer (50 mM KH<sub>2</sub>PO<sub>4</sub>/K<sub>2</sub>HPO<sub>4</sub>, 20 mM EDTA, 0.05% (v/v) glycerol, pH 7.0) and then resuspended in the same buffer at an OD<sub>660</sub> of 0.1. Aliquots (230 µl) of the resulting cell suspension were placed into the wells of 96-well microtiter plates. One microliter capillaries (Microcaps, Drummond Scientific) were heat-sealed at one end and filled with buffer (control) or chemoeffector solution prepared in chemotaxis buffer. The capillaries were rinsed with sterile water and immersed into the bacterial suspensions at their open ends. After 30 min, capillaries were removed from the wells, rinsed with sterile water, and emptied into 1 ml of chemotaxis buffer. Serial dilutions were plated onto M9 minimal medium plates supplemented with 20 mM glucose, incubated at 30 or 37 °C prior to colony counting. Data were corrected with the number of cells that swam into buffer containing capillaries. Data are means and standard deviations of three biological replicates conducted in triplicate.

*Protein crystallization and structure resolution:* Freshly purified PctD-LBD was dialyzed into 5 mM Tris/HCl, 5 mM MES, 5 mM Pipes, 150 mM NaCl, 10% (v/v) glycerol, pH 7.5 and concentrated to 20 mg/ml using 10 kDa cut-off centricon concentrators (Amicon). For the co-crystallization experiments, ligands were added to a final concentration of 10 mM and incubated on ice for 30 minutes. The excess of ligand was removed by rounds of concentration and dilution with the above buffer. Protein (20 mg/ml) was submitted to crystal screening using the hanging-drop vapor diffusion and the capillary counter-diffusion techniques. Vapor diffusion experiments were set up in 24-well crystallization plates VDX (Hampton Research) using the Hampton Research Screen I. Droplets were prepared by mixing protein with reservoir solution at a 1:1 ratio and equilibrated over 500 µl reservoir solution. Counter-diffusion experiments were set up by loading protein into 0.2 mm inner diameter capillaries and equilibrated against an excess of precipitant cocktails prepared *ad hoc* (González-Ramírez *et al.*, 2017). A similar procedure was employed to crystallize PacA-LBD, except that protein was at 35 mg/ml and in 5 mM Tris/HCl, 5 mM PIPES, 5 mM MES, pH 7.4. The conditions that resulted in crystals are given in Table S11. Crystals were equilibrated in mother solution supplemented with either 15% (v/v) glycerol or 20% (v/v) PEG 200, recovered by litholoops (Molecular Dimensions) and flash-frozen in liquid nitrogen. Data collection was done at beamlines ID30B, ID23-1 and ID30A-3 of the European Synchrotron Radiation Facility (Grenoble, France) and the Xaloc beamline of the Alba Spanish synchrotron radiation source (Barcelona, Spain). Data were indexed and integrated with XDS (Kabsch, 2010), scaled and reduced with AIMLESS (Evans and Murshudov, 2013) of the CCP4 program suite (Collaborative Computational Project, Number 4, 1994). PctD-LBD was phased by molecular replacement with Molrep (Vagin and Teplyakov, 2010) using a truncated version of the model predicted by RaptorX (Källberg *et al.*, 2012) that was based on templates with PDBs ID 6F9G, 6FU4 and 6PZJ. The molecular replacement solution of PacA-LBD was found by

implementing the deep learning based method, AlphaFold, within the Rossetta predictor software run in the Robetta server (RoseTTAFold) (Baek *et al.*, 2021) and top ranked in CAMEO (Robin *et al.*, 2021). Refinement was initiated with phenix.refine (Afonine *et al.*, 2010) and Refmac (Murshudov *et al.*, 2011) of the CCP4 program suite. Manual building, water inspection and ligand identification was done in Coot (Emsley *et al.*, 2010) and final refinement was assessed including Titration-Libration-Screw parameterization (Painter and Merritt, 2006a). Models were verified with Molprobit (Chen *et al.*, 2010) and the PDB validation server prior to deposition at the PDBe (Velankar *et al.*, 2012). The crystallographic data statistics and final model characteristics are provided in Table S11.

*Growth experiments:* PAO1 was grown overnight in M9 minimal medium containing 10 mM glucose. Cultures were then diluted to an OD<sub>600</sub> of 0.02 in either M9 or M8 medium (M9 minimal medium without NH<sub>4</sub>Cl) containing 10 mM glucose and medium supplemented with each of the compounds present in the Biolog Compound array PM2A (<https://www.biolog.com/wp-content/uploads/2020/04/00A-042-Rev-C-Phenotype-MicroArrays-1-10-Plate-Maps.pdf>). Two-hundred microliters of these cultures were transferred into microwell plates and growth at 37 °C was followed on a Bioscreen Microbiological Growth Analyzer (Oy Growth Curves Ab Ltd, Helsinki, Finland).

*FRET measurements:* FRET measurements were performed as described previously (Sourjik and Berg, 2002a; Sourjik *et al.*, 2007; Bi *et al.*, 2018). Cells of chemoreceptorless *E. coli* strain VS181 expressing PctD-Tar and the CheY-YFP/CheZ-CFP FRET pair were prepared by inoculating 200 µl of the overnight culture into 10 ml tryptone broth (TB; 1% (w/v) tryptone and 0.5% (w/v) NaCl) supplemented with ampicillin, chloramphenicol, 50 µM IPTG, and 2 µM sodium salicylate and grown in a rotary shaker at 34°C and 275 rpm. Cells were harvested at OD<sub>600</sub> of 0.5 by centrifugation, washed with tethering buffer (10 mM KH<sub>2</sub>PO<sub>4</sub>/K<sub>2</sub>HPO<sub>4</sub>, 0.1 mM EDTA, 1 µM methionine, 10 mM sodium lactate, pH 7.0), resuspended in 10 ml tethering buffer and kept at 4°C. For microscopy, the cells were attached to poly-lysine-coated coverslips for 10 min and mounted into a flow chamber that was maintained under constant flow of 0.3 ml/min of tethering buffer using a syringe pump (Harvard Apparatus) that was also used to add or remove compounds of interest. FRET measurements were performed on an upright fluorescence microscope (Zeiss Axiolmager.Z1) equipped with photon counters (Hamamatsu). The fluorescence signals were recorded and analyzed as described previously (Sourjik and Berg, 2002a; Sourjik *et al.*, 2007).

*Microfluidic assay:* The microfluidic assay was performed as previously described, using a chip with 24 parallel microchannels (Si *et al.*, 2012). In brief, cells of the receptorless *E. coli* strain UU1250 expressing GFP and PctD-Tar were grown at 34°C in TB supplemented with ampicillin, chloramphenicol, 100 µM IPTG, and 2 µM sodium salicylate until OD<sub>600</sub> of 0.5. Cells were harvested by centrifugation and washed twice with tethering buffer. Chemoeffectors were dissolved in tethering buffer at a concentration of 50 mM and the pH was adjusted to 7.0. The chemical source microchannels were filled with 4% (w/v) agarose gel to create a semi-permeable barrier. *E. coli* cells were added in the reservoir well and allowed to spread for 30 min into the channels. Compounds were added to the source well and allowed to form a concentration gradient. Cell fluorescence was recorded with a Nikon Ti-E inverted microscope system (Nikon Instruments Europe BV, Amsterdam, Netherlands) using a 20 x objective. Data were analyzed using ImageJ (Wayne Rasband, NIH, USA).

**Data availability:** The 3D structures reported have been deposited at the protein data bank with accession codes 7PRQ, 7PRR and 7PSG.

## Results

### Chemotaxis response of *P. aeruginosa* PAO1 to acetylcholine

The attraction to growth substrates is a major biological function of bacterial chemotaxis (Colin *et al.*, 2021). To identify the compounds that support the growth of *P. aeruginosa*, we conducted 96-well plate assays in which we screened *P. aeruginosa* growth in minimal media supplemented with the compounds from different Biolog arrays. As shown in Figure S13A, significant growth was observed for L-carnitine. To assess whether *P. aeruginosa* performs chemotaxis to L-carnitine, we conducted quantitative capillary chemotaxis assays that revealed chemoattraction (Figure 24).

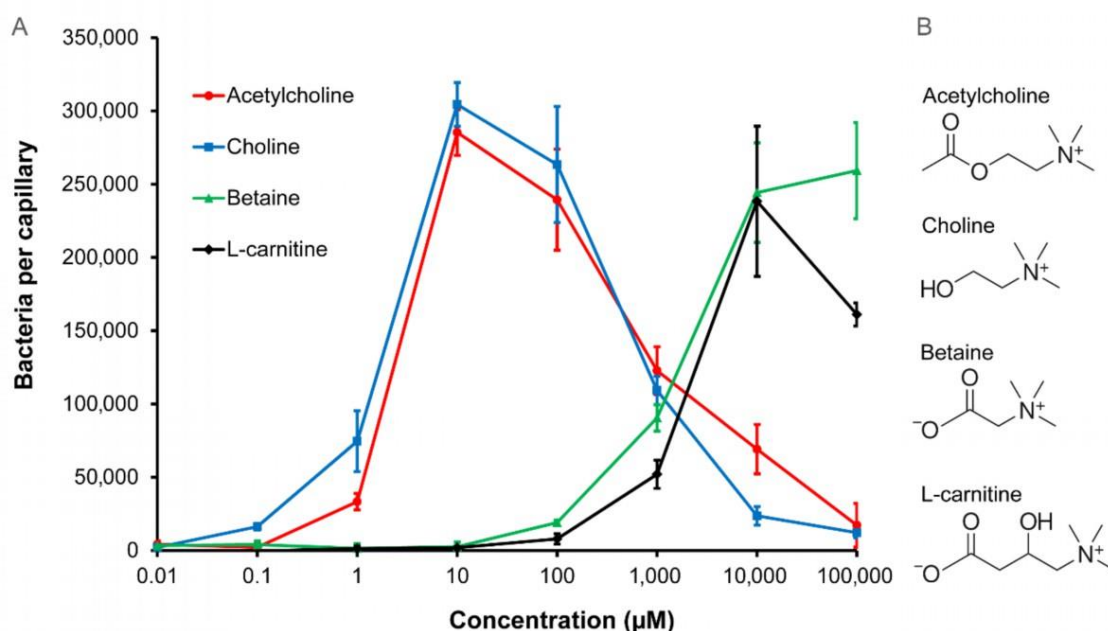


**Figure 24. Chemotaxis of *P. aeruginosa* PAO1 toward acetylcholine and related compounds.** A) Quantitative capillary chemotaxis assays. Data have been corrected for the number of bacteria ( $7825 \pm 623$ ) that swam into buffer-containing capillaries. Data are the means and standard deviations from three independent experiments conducted in triplicate. B) The structures of the chemoeffectors.

Responses were characterized by a rather high threshold of the response at 100 µM and a maximal response at 10 mM. We subsequently conducted experiments to find out whether structurally related compounds, such as other quaternary amines, also induced chemotaxis. We observed chemoattraction to betaine that was comparable to that of L-carnitine (Figure 24). Importantly, choline and acetylcholine also induced chemotaxis (Figure 24). In contrast to L-carnitine and betaine, responses to choline and acetylcholine occurred at much lower concentrations, with a response threshold of 0.1 µM for choline and 1 µM for acetylcholine. These response thresholds were at lower concentrations than for a number of other *P.*

*aeruginosa* chemoeffectors analysed with the same technique (Rico-Jiménez *et al.*, 2016; Martín-Mora *et al.*, 2018b; Martín-Mora *et al.*, 2019). Maximal responses induced by choline and acetylcholine were observed at 10  $\mu$ M, and the maximal accumulation of  $\sim$ 300,000 bacteria per capillary was significantly higher than the maximal accumulations in response to inorganic phosphate (Rico-Jiménez *et al.*, 2016), nitrate (Martín-Mora *et al.*, 2019), malate (Martín-Mora *et al.*, 2018b), and  $\alpha$ -ketoglutarate (Martín-Mora *et al.*, 2016a). The large magnitude of the chemotaxis response acetylcholine evokes, the low threshold concentration, and its important physiological role as a neurotransmitter motivated studies to identify the corresponding molecular mechanism of acetylcholine sensing.

### **Role of PctD (PA4633) in chemotaxis to acetylcholine**

The McpX chemoreceptor in *Sinorhizobium (Ensifer) meliloti* has been reported to mediate chemotaxis to quaternary amines (Webb *et al.*, 2017b). This chemoreceptor contains a dCache\_1 type LBD. Of the *P. aeruginosa* chemoreceptors with dCache\_1 LBDs, only PA4633 was of unknown function (Matilla *et al.*, 2021a). The LBD of this receptor shares only 17% sequence identity with the McpX-LBD (Figure S14A). To assess the role of PA4633 in chemotaxis to the four chemoeffectors, we have conducted quantitative capillary assays using a mutant defective in this chemoreceptor (Figure S15). Apart from some minor responses to high concentrations of betaine, the *pp4633* mutant failed to respond to these four quaternary amines – phenotypes that were reversed to wild-type responses by the *in trans* expression of PA4633 using a pBBR1MCS-based vector (Figure S15E). Taken together, these data indicate that PA4633 is the sole chemoreceptor that mediates chemotaxis to these four quaternary amines at physiologically relevant concentrations. Chemoreceptor PA4633 was thus renamed PctD (*Pseudomonas chemotaxis transducer D*).

### **Effect of acetylcholine binding on the activity of PctD**

There are a number of ways by which chemoeffectors stimulate chemoreceptors (Ortega *et al.*, 2017a). To verify whether the chemoeffectors activate PctD by direct binding, the LBD of PctD was produced as purified recombinant protein and submitted to microcalorimetric binding studies. Acetylcholine and choline bound with high affinity, with dissociation constants of 23 and 2.6  $\mu$ M, respectively (Figure 25, Table 3). Binding of betaine occurred with a much lower affinity ( $K_D = 990 \mu$ M). No response was observed with L-carnitine. This compound probably also binds, but the sensitivity of ITC experiments is limited by the heat produced simply by the injection of ligand into the buffer. Data are thus consistent with the notion that the binding affinity correlates with the onset of chemotaxis, as observed previously for PctA and PctB (Reyes-Darias *et al.*, 2015d).

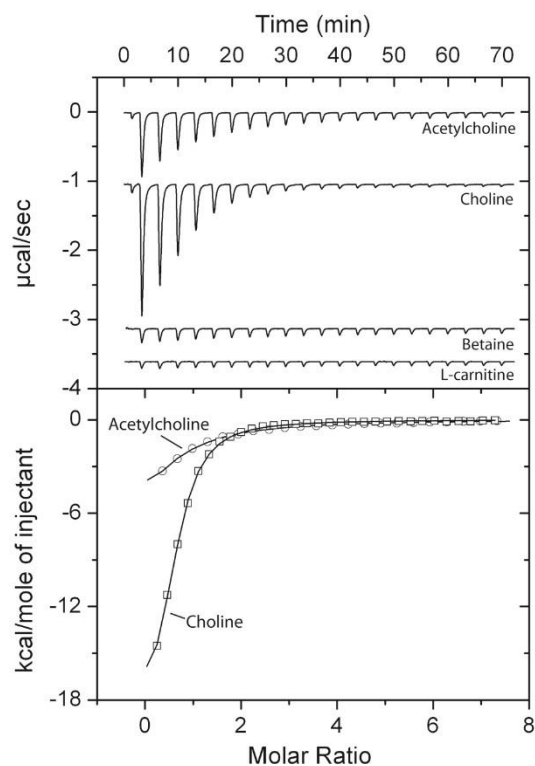


**Figure 25. Isothermal titration calorimetry study of the binding of different ligands to the ligand-binding domain of chemoreceptor PctD.** Upper panel: Raw data for the titration of 15-22  $\mu\text{M}$  protein with 9.6  $\mu\text{l}$  aliquots of 0.5-10 mM ligand solutions. Lower panel: Concentration-normalized and dilution heat-corrected raw data for the titration with acetylcholine and choline. The continuous line is the best fit with the “One binding site model” of the MicroCal version of ORIGIN.

In order to confirm that binding of these quaternary amines mediates the chemotaxis response, we constructed a chimeric receptor by fusing the PctD-LBD (including transmembrane helices and HAMP domain) to the signaling domain of the *E. coli* chemoreceptor Tar (Figure 26E). Similar chimeras were previously used to investigate chemotaxis signaling induced by binding of chemoeffectors to the LBDs of PctA, PctB, and PctC by measuring the responses that these hybrid receptors mediate in *E. coli* using Förster Resonance Energy Transfer (FRET) (Reyes-Darias *et al.*, 2015d; Reyes-Darias *et al.*, 2015a). These FRET measurements rely on stimulation-dependent interaction between the chemotaxis response regulator CheY fused to yellow fluorescent protein (CheY-YFP) and its phosphatase CheZ fused to cyan fluorescent protein (CheZ-CFP) (Sourjik and Berg, 2002a). The interaction between CheY and CheZ depends on the phosphorylation state of CheY. FRET measurements serve as a precise readout of pathway activity and were found to correlate linearly with physiological responses (Sourjik and Berg, 2002b; Sourjik *et al.*, 2007). When PctD-Tar was expressed as the sole chemoreceptor in the *E. coli* FRET strain VS181/pVS88, clear attractant responses were observed in the sub-micromolar concentration range for acetylcholine and choline (Figure 26A, B) and in the micromolar concentration range for betaine and L-carnitine (Figure 26C, D). The obtained EC50 values (Figure 26F) were generally consistent with the relative potency of these ligands as chemoeffectors for *P. aeruginosa* (Figure 24) and with the ITC results (Figure 25) when the signal amplification by the *E. coli* chemotaxis system is taken into account (Sourjik and Berg, 2002a). No responses to these quaternary amines were observed with the *E. coli* FRET strain expressing only full-length

Tar (Figure S16), confirming the specificity of signaling via the sensory domain of PctD. Choline and acetylcholine also elicited much stronger chemoattraction when the receptorless *E. coli* strain UU1250 (55) expressing PctD-Tar was tested in a microfluidic assay (Figure S17).

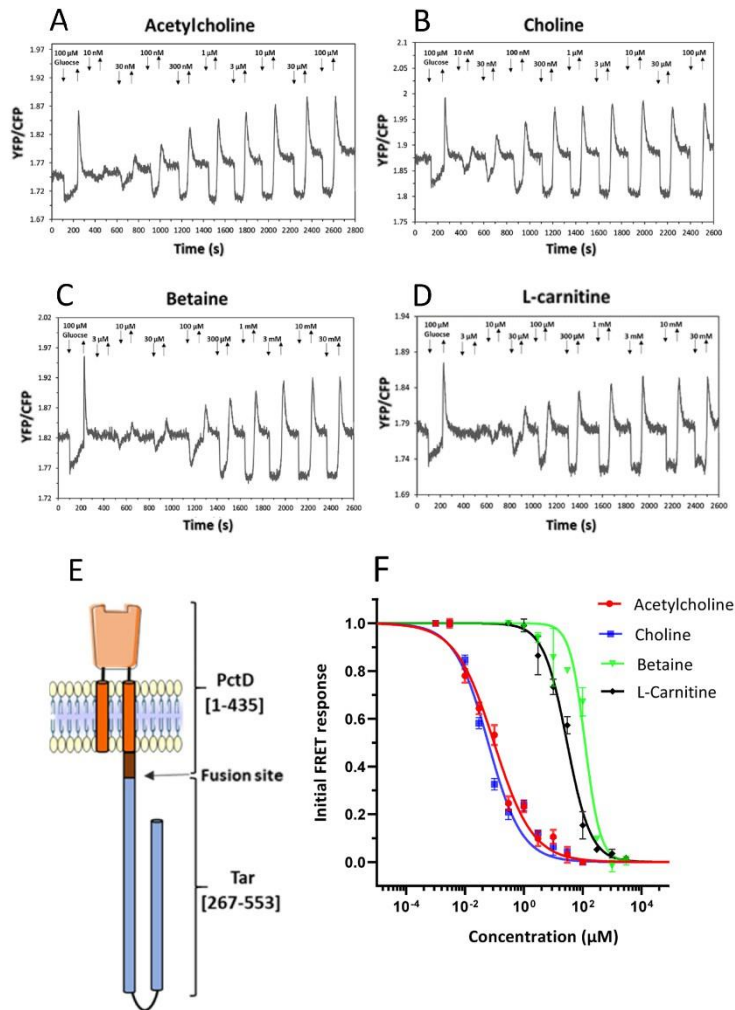


**Figure 26. Characterization of responses mediated by a PctD-Tar hybrid using FRET measurements in *E. coli*.** (A-D) FRET responses of buffer-adapted *E. coli* cells expressing PctD-Tar as the sole receptor upon stepwise addition (down arrow) and subsequent removal (up arrow) of the indicated concentrations of acetylcholine (A), choline (B), betaine (C), and L-carnitine (D). (E) Cartoon representation of the hybrid PctD-Tar. (F) Corresponding dose-response curves of responses mediated by PctD-Tar. The amplitudes of the initial FRET responses were calculated from changes in the ratio of YFP/CFP fluorescence after stimulation with indicated ligand concentrations and normalized to the saturated response. Error bars indicate the standard errors of three independent experiments; wherever invisible, error bars are smaller than the symbol size. Data were fitted using the Hill equation, with the EC50 (half-maximal effective concentration) fit values being  $0.07 \pm 0.02 \mu\text{M}$  for acetylcholine,  $0.04 \pm 0.01 \mu\text{M}$  for choline,  $150 \pm 25 \mu\text{M}$  for betaine and  $31 \pm 6 \mu\text{M}$  for L-carnitine.

**Table 3. Thermodynamic parameters for the titration of *P. aeruginosa* PctD-LBD and *P. atrosepticum* PacA-LBD with different ligands.** The corresponding titration data are shown in Figures 25 and 28, respectively.

Protein	Compound	$K_D$ ( $\mu\text{M}$ )	$\Delta H$ (kcal/mol)
PctD(PA4633)-LBD	Acetylcholine	$23 \pm 1$	$-12.2 \pm 1.0$
PctD(PA4633)-LBD	Choline	$2.6 \pm 0.1$	$-20.3 \pm 0.3$
PctD(PA4633)-LBD	Betaine	$990 \pm 59$	$-2.4 \pm 4.14$
PctD(PA4633)-LBD	L-carnitine	No binding	
PacA(ECA_RS10935)-LBD	Acetylcholine	No binding	
PacA(ECA_RS10935)-LBD	Choline	$113 \pm 16.4$	$-2.1 \pm 0.2$
PacA(ECA_RS10935)-LBD	Betaine	$7.5 \pm 0.1$	$-16.1 \pm 0.1$
PacA(ECA_RS10935)-LBD	L-carnitine	$20 \pm 2$	$-4.9 \pm 0.4$

### The three-dimensional structure of PctD-LBD in complex with acetylcholine and choline

To understand in molecular detail the mechanism of ligand recognition by PctD, we carried out crystallization trials of PctD-LBD in its ligand-free state and in complex with the identified ligands. Crystals formed in the presence of acetylcholine and choline, and atomic structures were determined and refined to a resolution of 1.8 and 2.0 Å, respectively. The structures showed the typical dCache fold (Figure 26), and alignments with all structures present in the protein data bank (Table S9) showed that it is most similar to the LBD of the TlpQ chemoreceptor from *P. aeruginosa* in complex with histamine (Corral-Lugo *et al.*, 2018), another neurotransmitter.

Among other similar structures are the McpX chemoreceptor for quaternary amines (Shrestha *et al.*, 2018), several amino acid sensing chemoreceptors (Machuca *et al.*, 2016; Ehrhardt *et al.*, 2021), and the DctB and KinD sensor kinases (Cheung and Hendrickson, 2008; Wu *et al.*, 2013) that bind organic acids. Well-defined electron density was observed for choline and acetylcholine, which permitted the precise placement of ligand structures (Figure 27A). As in the majority of dCache domains, the ligand was bound to the membrane-distal module (Figure 26). The quaternary amine moiety of both ligands is coordinated by hydrophobic interactions with a number of aromatic amino acids (Phe124, Phe188, Tyr206 and Trp155) and two methionine residues (Met169 and Met215) (Figure 27). However, the tails of both ligands point in opposing directions (Figure 27). The choline tail interacts with Ser217 and Asp235, whereas the acetylcholine tail interacts with Ala168, Asp171, and Ser172.

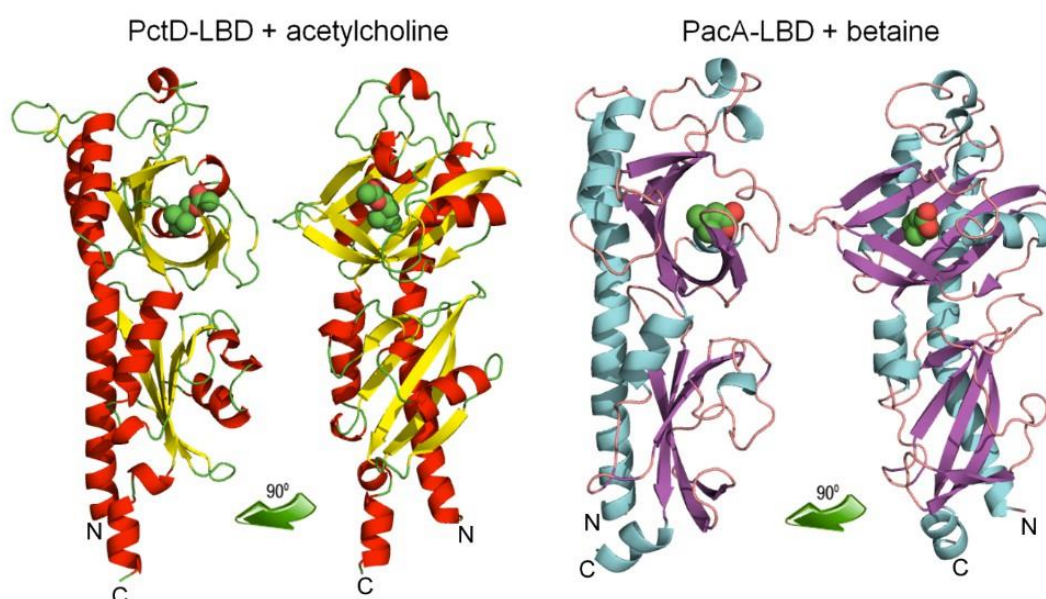


**Figure 27.** The three-dimensional structures of the ligand binding domains of the PctD chemoreceptor of *P. aeruginosa* PAO1 in complex with acetylcholine and the PacA chemoreceptor of *P. atrosepticum* SCRI1043 in complex with betaine. Structures are shown in two different orientations. Bound ligands are shown in space-filling mode.

#### **Identification of PacA from *P. atrosepticum* that binds quaternary amines but not acetylcholine**

We wanted to advance our understanding of the molecular mechanism for acetylcholine binding at dCache domains. *Pectobacterium atrosepticum* SCRI1043 is used in our laboratory to investigate chemotaxis of plant pathogens. This strain showed low but reproducible chemotaxis to betaine, choline, and L-carnitine, but it failed to respond to acetylcholine even at 1 mM (Figure S18). Of the 36 chemoreceptors of SCRI1043, two (ECA\_RS10935 and ECA\_RS05475) possess a dCache type LBD (Velando *et al.*, 2020). The LBDs of these receptors share only 20% and 17% sequence identity with PctD, respectively (Figure S14). We hypothesized that one of these receptors is responsible for the responses to quaternary amines.

To identify the corresponding chemoreceptor, we overexpressed and purified the LBD of ECA\_RS10935. Microcalorimetric titrations of the protein with 1 mM solutions of betaine, choline and L-carnitine showed binding in each case (Figure 28, Table 3). Betaine bound most tightly ( $K_D=7.5 \mu\text{M}$ ), followed by L-carnitine and choline with  $K_D$  values of 20  $\mu\text{M}$  and 113  $\mu\text{M}$ , respectively. Importantly, titration with 5 mM acetylcholine (Figure 28) did not produce any change in heat, indicating an absence of binding.

Given these results, we hypothesized that the observed weak chemotaxis of SCRI1043 to ligands bound by ECA\_RS10935 (Figure S18) may be due to a low level of receptor expression under the experimental conditions. To evaluate this, we constitutively expressed the ECA\_RS10935 gene from a pBBR1MCS-based multicopy vector. *P. atrosepticum* SCRI1043 harboring the resulting plasmid, pBBR\_ECA\_RS10935, exhibited up to an 8-fold increase in chemotaxis to the corresponding ligands as compared to the strain harboring the empty plasmid (Figure S19). The receptor was thus renamed PacA (Pectobacterium atrosepticum chemoreceptor A).



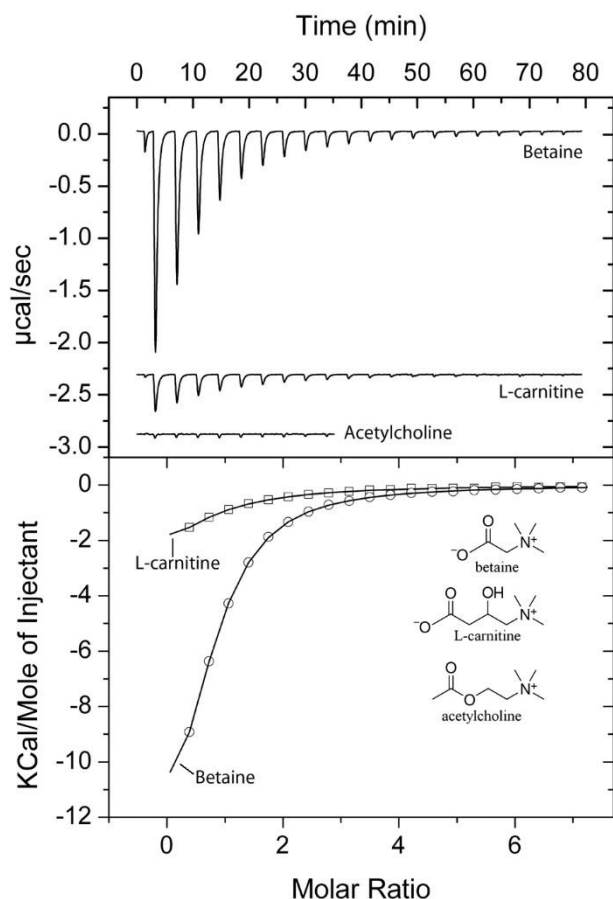


**Figure 28. Isothermal titration calorimetry study of the binding of different ligands to the LBD of the *P. atrosepticum* SCRI1043 chemoreceptor ECA\_RS10935 (PacA).** Upper panel: Raw data for the titration of 20  $\mu\text{M}$  protein with 9.6  $\mu\text{l}$  aliquots of 1 mM (betaine, carnitine) and 5 mM (acetylcholine) ligand solutions. Lower panel: Concentration-normalized and dilution heat-corrected raw data for the titration with acetylcholine and choline. The continuous line is the best fit with the “One binding site model” of the MicroCal version of ORIGIN.

#### Comparing the atomic structures of ligand-bound PacA-LBD and PctD-LBD

We crystallized the PacA-LBD and solved its 3D structure in complex with betaine to a resolution of 1.9  $\text{\AA}$  (Figure 27B). The overall structure is highly similar to that of PctD-LBD, with a root-mean-square deviation of 1.6  $\text{\AA}$  for the  $\text{C}\alpha$  atoms in a structural alignment. This similarity is also evidenced by the fact that the structural homologs of PctD-LBD correspond largely to those of PacA-LBD (Table S9). A well-defined electron density was observed for betaine bound to PacA-LBD (Figure 29A). The orientation of betaine corresponded to that of acetylcholine in PctD-LBD (Figure 29B), which was the opposite of the orientation of choline. Comparing the composition of the ligand-binding sites in the LBDs of PctD and PacA resulted in the identification of two conserved amino acids (Tyr and Asp, shown in red in Figure 29B) and two positions occupied by aromatic amino acids in both proteins (shown in blue in Figure 29B). The coordination of the quaternary amine moiety in PacA-LBD is very similar to that of PctD-LBD and primarily involves a number of aromatic amino acids. However, the amino acids that coordinate the acetylcholine tail in PctD-LBD (Ala168, Met169, Asp171, and Ser172) are not conserved in PacA-LBD (Figure

29B, Figure S14C). These four amino acids in PctD-LBD may thus correspond to a feature of acetylcholine binding dCache domains.

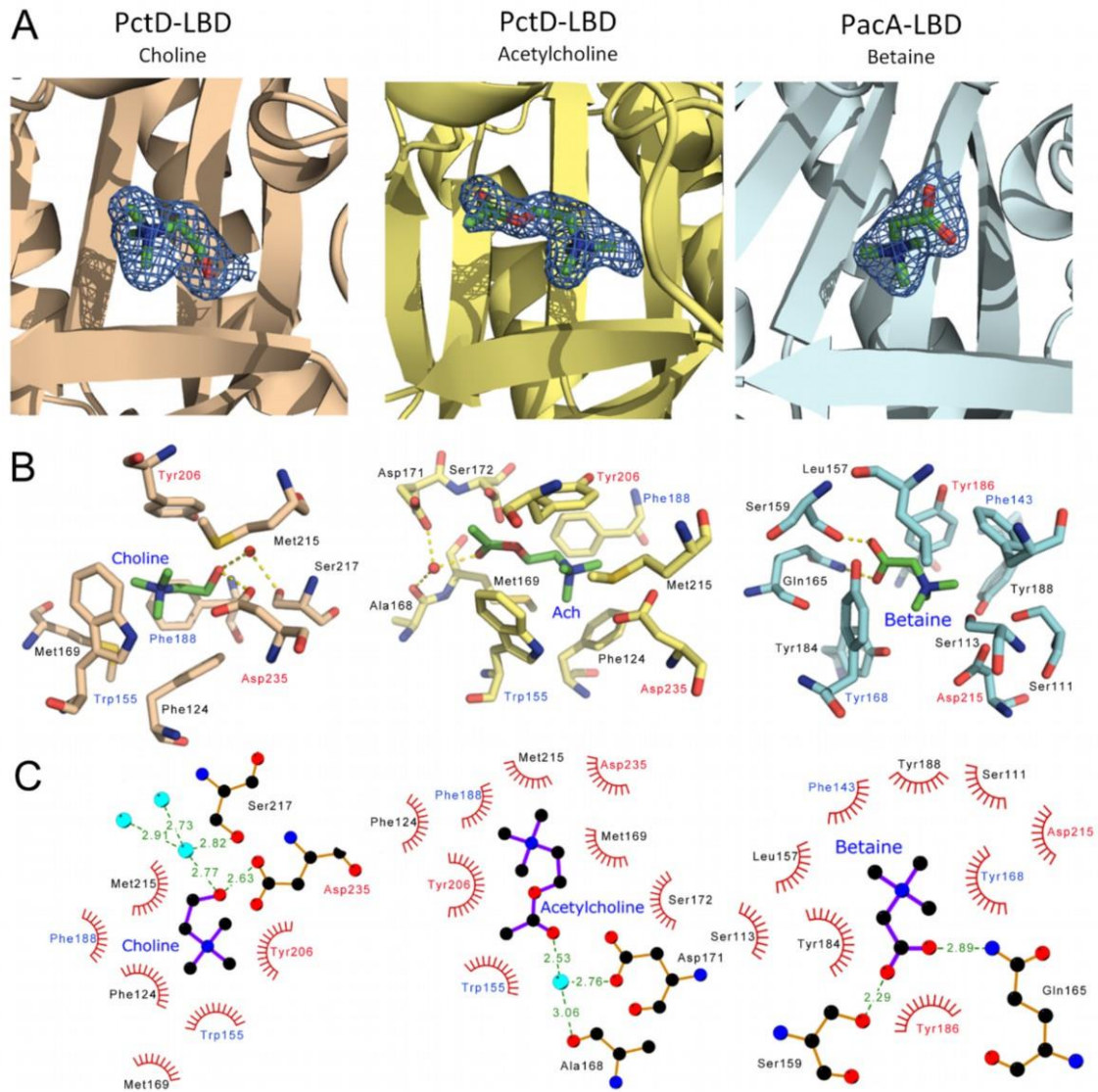


**Figure 29. The molecular detail of signal recognition by the PctD and PacA chemoreceptors. (A)** A zoom view of the ligand-binding sites. The mesh representation of the final  $|2F_o - F_c|$  electron density map is contoured at approx.  $1.0 \sigma$ . Ligands are shown in stick mode. **(B)** Amino acids involved in ligand binding. Hydrogen bonds are shown as dotted lines. Amino acids that are conserved in the ligand binding pockets of PctD and PacA are labelled in red (fully conserved) and blue (aromatic amino acid conserved). Ach: acetylcholine. **(C)** Schematic view of ligand binding as generated by the LigPlot software (Laskowski and Swindells, 2011). Hydrophobic interactions are shown as spoked arcs and hydrogen bonds as dashed green lines. Cyan spheres are water molecules. Amino acids that are conserved in the ligand-binding pockets of PctD and PacA are labelled in red (fully conserved) and blue (aromatic amino acid conserved).

### Acetylcholine chemotaxis in other species

Having obtained the first evidence for bacterial chemotaxis to acetylcholine, we investigated whether other strains show a similar behavior. To this end, we conducted capillary chemotaxis assays to 1 mM acetylcholine using a variety of strains with different lifestyles, including human pathogens, non-pathogenic plant-associated bacteria, soil bacteria, and plant pathogens. Two strains, *Agrobacterium tumefaciens* C58 and *Dickeya solani* MK10 showed acetylcholine chemotaxis (Figure 30). The magnitude in *A. tumefaciens* was comparable to that in *P. aeruginosa*, whereas that of *D. solani* was about a third of that observed in *P. aeruginosa*. Both strains are plant pathogens, indicating that bacteria with different lifestyles inhabiting dissimilar ecological niches are able to perform acetylcholine chemotaxis.

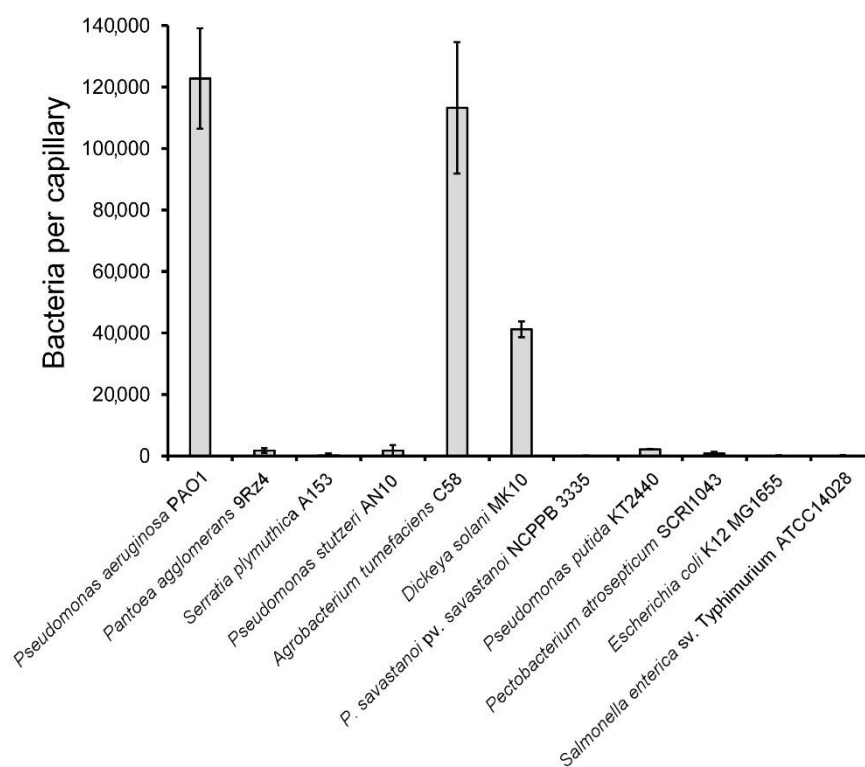


**Figure 30. Chemotaxis to acetylcholine in different bacterial species.** The results of quantitative capillary chemotaxis assays towards 1 mM acetylcholine are shown. Data are shown as the means and standard deviations of results from three biological replicates conducted in triplicate.

## Discussion

Acetylcholine is one of the key signaling molecules of life. It is best known as the primary neurotransmitter in the vertebrate peripheral nervous system, where it mediates signal transmission at the neuromuscular junction (Brown, 2019). In addition, many human tissues contain non-neuronal acetylcholine, mostly in epithelial cells (airways, alimentary tract, urogenital tract, epidermis), muscles and other mesothelial cells (pleura, pericardium), and endothelial and immune cells (Wessler *et al.*, 1999; Kummer *et al.*, 2008). The signaling function of non-neuronal acetylcholine modulates diverse processes, including immune and

inflammatory responses, wound healing and development of cancer, cardiovascular, respiratory, digestive and orthopedic diseases (Grando *et al.*, 2015; Mashimo *et al.*, 2021). Importantly, non-neuronal acetylcholine is also produced by bacteria, archaea, algae, protozoa, tubellariae and plants, suggesting an extremely early appearance of acetylcholine in evolution (Wessler *et al.*, 1999). Acetylcholine mediates inter-kingdom and inter-bacterial communication (Roshchina, 2016). It has, for example, been identified as a key regulator of the interaction between microbes and the human immune system (Weinstein *et al.*, 2015).

The acetylcholine-mediated inter-domain communication between bacteria and other kingdoms is bi-directional, and there are several reports indicating that bacteria perceive acetylcholine. For example, acetylcholine is not a chemoeffector for *E. coli*, but it inhibits chemotaxis to aspartate (Shinozawa and Fukunaga, 1989). In another study, acetylcholine was found to reduce chemotaxis of *P. fluorescens* to L-Leu (Chet *et al.*, 1973). However, the mode by which acetylcholine is perceived is unknown. In *B. subtilis*, the transcriptional regulator BmrR binds acetylcholine with significant affinity ( $K_D=6.6 \mu\text{M}$ ) to control the expression of the Bmr multidrug efflux pump (Bachas *et al.*, 2011). In *S. meliloti*, the solute-binding protein ChoX binds acetylcholine (Oswald *et al.*, 2008). In *Dickeya dadantii*, acetylcholine was identified as a competitive antagonist that interacts with a ligand-gated ion channel (Matilla *et al.*, 2021a). To the best of our knowledge, our data constitute the first report that bacteria sense acetylcholine as a strong chemoattractant via chemoreceptors. Because acetylcholine is a crucial signal molecule, it is reasonable to suggest that chemotaxis to acetylcholine promotes the virulence of *P. aeruginosa*.

Signal transduction consists of converting a signaling input into an output. Here we have used ITC to quantify the signaling input (Table 3) and three different approaches to quantify the PctD mediated signaling output, namely i) *P. aeruginosa* chemotaxis assays (Figures 24 and S15), ii) analysis of *E. coli* cells harboring a PctD-Tar chimera by FRET (Figure 26) and iii) microfluidics measurements (Figure S17). There was satisfactory agreement between these four datasets. Choline and acetylcholine showed high affinity binding, with  $K_D$  values of 2.6 and 23  $\mu\text{M}$ , respectively. It was shown that the  $K_D$  values of 60% of all characterized chemoreceptors are between 1 to 50  $\mu\text{M}$  (Matilla *et al.*, 2022a), indicating that the recognition of both chemoeffectors by PctD is in the same range as most chemoreceptors. In contrast, betaine bound with low affinity and carnitine binding could not be visualized by ITC (Table 3). In agreement with these data all three approaches to monitor the signaling output showed highly sensitive responses to choline and acetylcholine, whereas low sensitivity responses were observed for betaine and carnitine. The EC50 values derived from FRET experiments (legend to Figure 26) were well below the  $K_D$  values from the ITC binding studies (Table 3), which is an observation that has been made for other chemoreceptors (Reyes-Darias *et al.*, 2015d; Reyes-Darias *et al.*, 2015a) and is likely due to signal amplification in chemoreceptor arrays. It can thus be concluded that the magnitude of signaling input determines the magnitude of signaling output at PctD.

The threshold concentration of acetylcholine for chemotaxis was found to be 1  $\mu\text{M}$ , with a maximal response at 10  $\mu\text{M}$ . How do these parameters compare to physiological acetylcholine concentrations? *P. aeruginosa* is the primary etiological agent of ulcerative keratitis (Dannelly *et al.*, 2001). Acetylcholine concentrations of 100 to 150  $\mu\text{M}$  were detected within the corneal epithelium (Pesin and Candia, 1982), concentrations comparable to those at which strong

chemoattraction is observed (Figure 24). In many cases, chemotaxis is required for the initial steps of infection in which sites that are suitable for establishing infection are recognized and colonized. Once infection is established, chemotaxis is no longer essential, and transcription of chemotaxis and motility genes is downregulated (Matilla and Krell, 2017a). A possible involvement of the PctD chemoreceptor in virulence is supported by the downregulation of *pctD* transcript levels in human sputum (Cornforth *et al.*, 2018; Rossi *et al.*, 2018), human burn wound infections (Cornforth *et al.*, 2018), and mouse lung infection (Damron *et al.*, 2016) compared to the levels seen during *in vitro* growth.

Experiments are needed to establish whether other bacteria also possess acetylcholine receptors. Overall sequence similarity with LBDs of known ligand profile does not permit prediction of the ligand recognized. However, comparison of the three-dimensional structures of ligand-bound PctD-LBD and PacA-LBD identifies the amino acids uniquely involved in acetylcholine recognition. To identify potential acetylcholine-binding receptors in other species, precise models of dCache domains can be generated using AlphaFold (Jumper *et al.*, 2021) and inspected for the presence of these amino acids.

PctD was determined to bind acetylcholine, a central neurotransmitter and signal molecule. Interestingly, two PctD orthologs in *P. aeruginosa*, PctC and TlpQ, bind and mediate chemoattraction to other neurotransmitters. GABA is the preferred ligand for the PctC chemoreceptor ( $K_D=1.2 \mu\text{M}$ ) (Rico-Jiménez *et al.*, 2013a), and histamine binds TlpQ with a  $K_D$  of  $0.64 \mu\text{M}$ . *P. aeruginosa* exhibits attraction to concentrations of histamine as low as 500 nM (Corral-Lugo *et al.*, 2018). The three-dimensional structures of the LBDs of these three dCache family receptors complexed with their respective ligands have been solved (Figure 31). Acetylcholine, GABA and histamine are human neurotransmitters and signal molecules involved in inter-kingdom communication. Therefore, the existence of three chemoreceptors for their recognition by *P. aeruginosa* suggests a particular relevance of chemoattraction to these compounds. Chemoattraction to neurotransmitters has also been observed in *E. coli*. *E. coli* is strongly attracted to norepinephrine (Pasupuleti *et al.*, 2014), a response that requires the conversion of norepinephrine to dihydroxymandelic acid, which is then sensed by the LBD of the Tsr chemoreceptor (Pasupuleti *et al.*, 2014; Orr *et al.*, 2020). This chemotaxis response is of physiological relevance, as in enterohemorrhagic *E. coli* norepinephrine controls the expression of many virulence genes, a response mediated by the QseC sensor kinase (Clarke *et al.*, 2006; Sule *et al.*, 2017; Pasupuleti *et al.*, 2018).

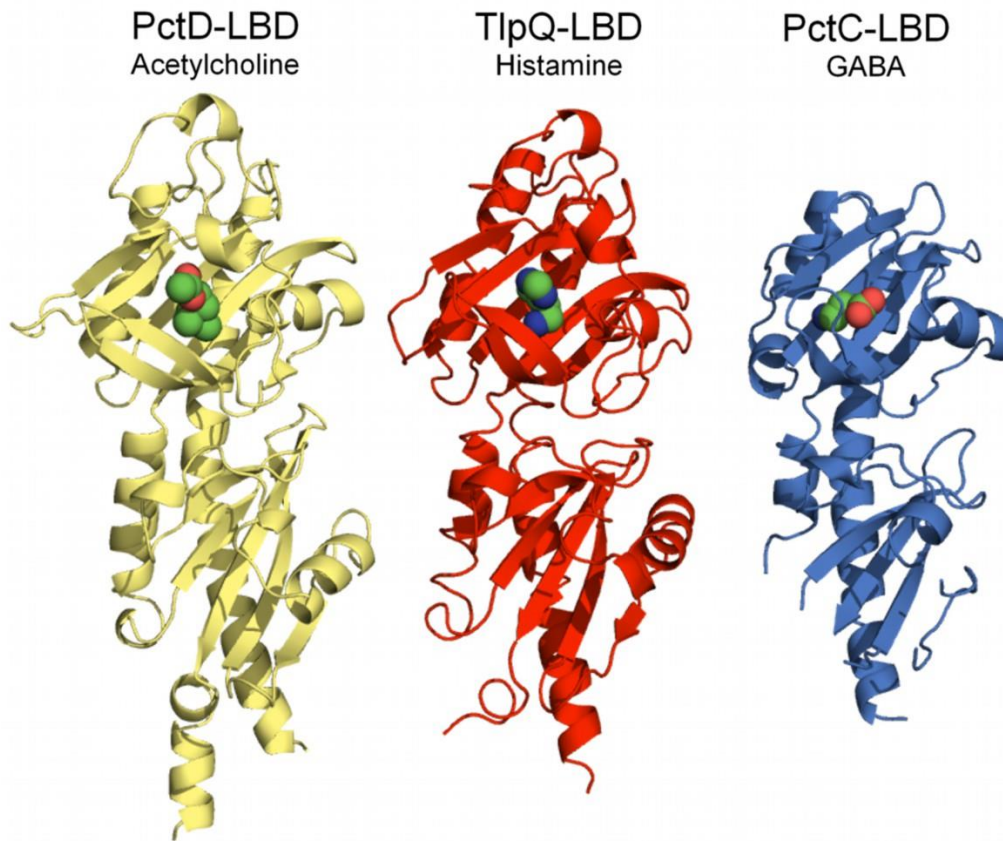


**Figure 31. The three dCache\_1 domain containing chemoreceptors of *P. aeruginosa* PAO1 that mediate chemotaxis to important neurotransmitters.** The 3D structures of the ligand binding domains of PctD in complex with acetylcholine (PDB ID 7PRR), TlpQ in complex with histamine (PDB ID 6FU4) (Corral-Lugo *et al.*, 2018) and PctC in complex with GABA (PDB ID 5LTV) (Rico-Jiménez *et al.*, 2013a) are shown. The respective  $K_D$  values are 23  $\mu\text{M}$ , 1.2  $\mu\text{M}$ , and 0.64  $\mu\text{M}$  (Rico-Jiménez *et al.*, 2013a; Corral-Lugo *et al.*, 2018).

We have tested other bacteria for chemotaxis to acetylcholine. Significant responses were seen with *Agrobacterium tumefaciens* and *Dickeya solani*, two plant pathogens (Figure 30). No chemotaxis to acetylcholine was observed in a number of other plant pathogens and non-pathogenic plant-associated species. Acetylcholine has been detected in many plant taxons and is considered to be a plant hormone (Roychoudhury, 2020). Within the plant, it is ubiquitously distributed, ranging from seeds and cotyledons to roots, shoots and leaves (Tretyn *et al.*, 1997). Acetylcholine regulates vital plant activities such as seed germination and plant growth. It mimics the action of red light, influencing leaf movement and membrane permeability to ions and modifying enzyme activities and metabolic processes (Roychoudhury, 2020). Acetylcholine concentrations in plants are typically in the lower  $\mu\text{M}$  range but can be as high as 100  $\mu\text{M}$  (Hartmann and Kilbinger, 1974; Tretyn *et al.*, 1997). Future investigations will be necessary to establish the physiological relevance of chemotaxis to acetylcholine in plant pathogens. Our study lays the foundation for studies to assess the phylogenetic spread of acetylcholine chemotaxis and to assess its physiological relevance in bacteria.

## Supplementary Material

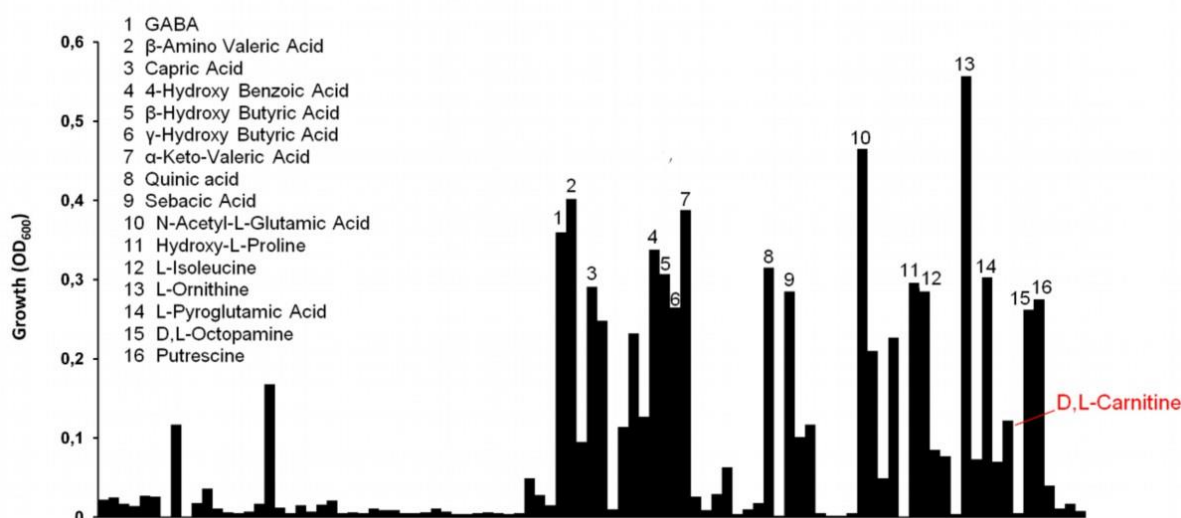


**Figure S 13. Growth experiments with *P. aeruginosa* PAO1.** Growth in M9 minimal medium supplemented with each of the compounds present in the Biolog compound array PM2A comprising carbon sources. Experiments were conducted in 96 well plates. The compounds that permit strongest growth are labelled. D,L-carnitine is the only quaternary amine in this compound array. The observation that D,L-carnitine permits growth as carbon source has prompted experiments to determine whether it is a chemoeffector. Data represent growth at 37 °C for 48 hours. Cells were grown at 37 °C using a Bioscreen Microbiological Growth Analyser (Oy Growth Curves Ab Ltd, Helsinki, Finland) under continuous shaking.



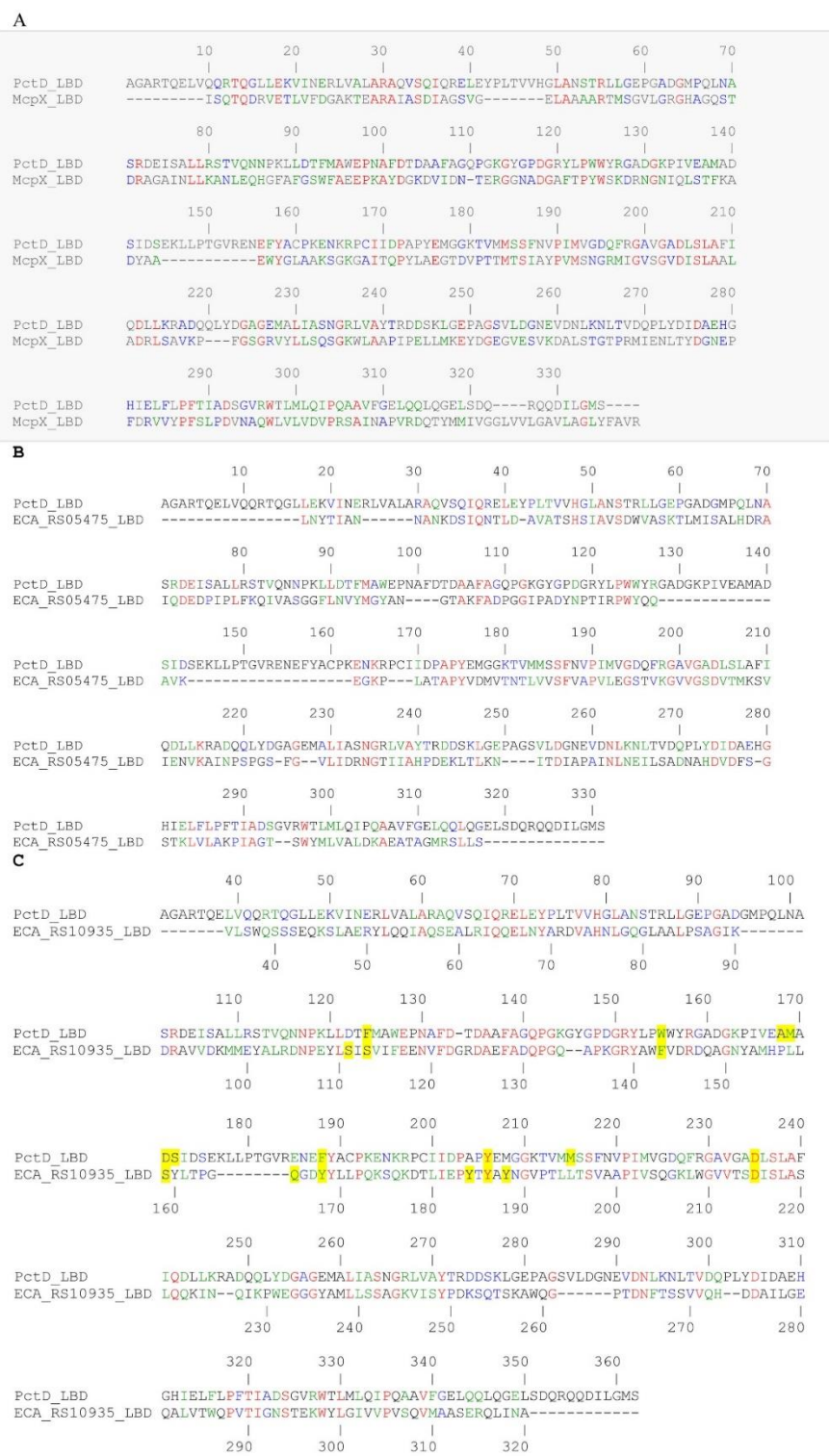


**Figure S 14. Sequence alignments of the ligand binding domains of *P. aeruginosa* PAO1 chemoreceptor PctD (PA4633) with *S. meliloti* McpX (A), *P. atrosepticum* SCRI1043 ECA\_RS05475 (B) and *P. atrosepticum* SCRI1043 chemoreceptor ECA\_RS10935 (PacA) (C). The alignment was done using the CLUSTALW algorithm of the npsa suite (Combet *et al.* (2000) Trends Biochem. Sci. 25, 147) using the GONNET weight matrix, a gap opening penalty of 10 and a gap extension penalty of 0.2. red: identical; green: highly similar; blue: weakly similar. The amino acids that interact in the PctD-LBD and PacA-LBD structures with the bound ligand are shaded in yellow.**



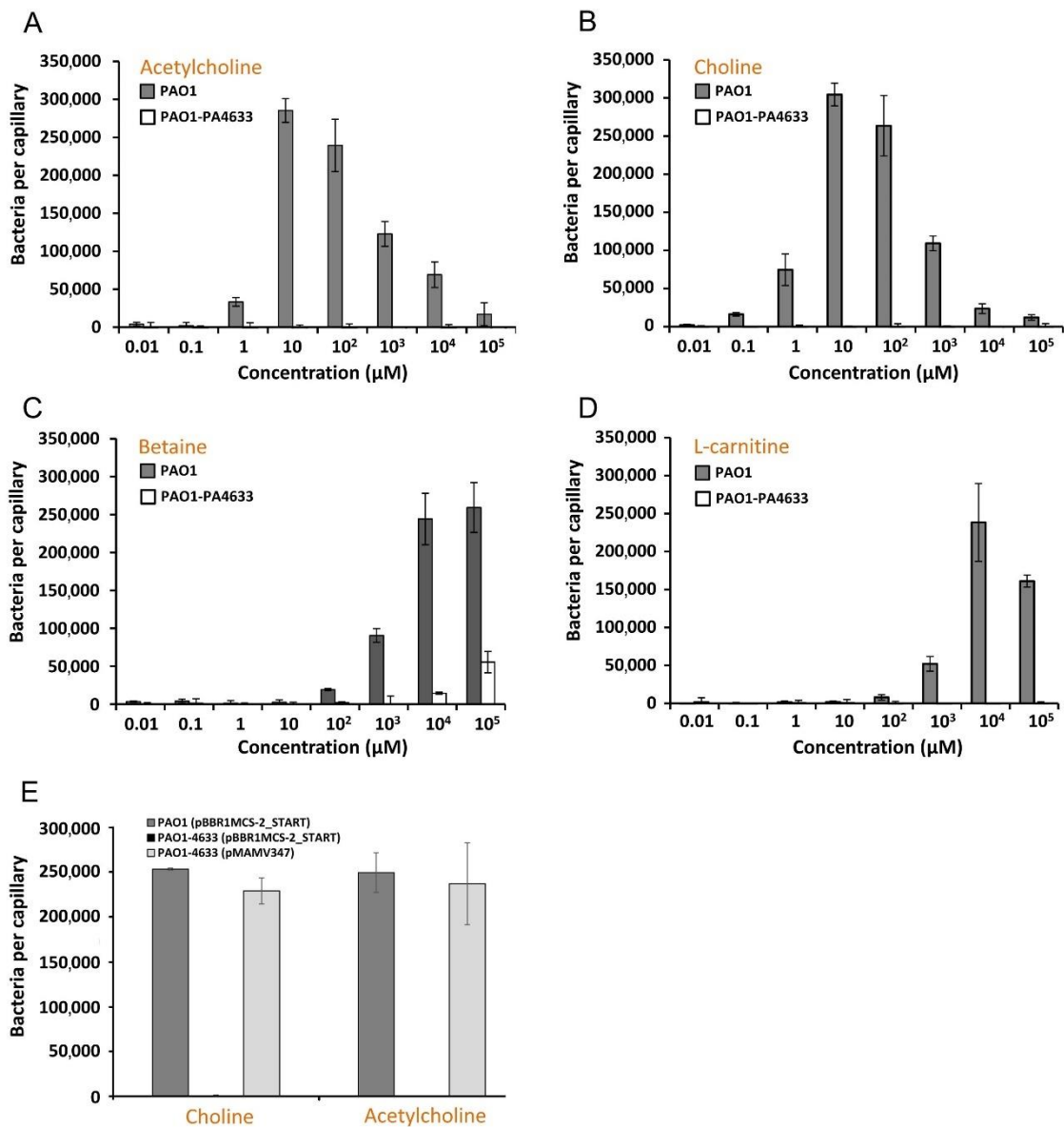


**Figure S 15. Quantitative capillary chemotaxis assays of *P. aeruginosa* PAO1, a mutant in *PA4633* (*pctD*) (A-D) and the mutant in *PA4633* harboring different plasmids for complementation (E). (A-D): Data have been corrected with the number of bacteria ( $7825 \pm 623$ ) that swam into buffer-containing capillaries. (E) The chemoeffector concentration was  $100 \mu\text{M}$ . Strains were complemented with the empty plasmid pBBR1MCS-2\_Start and its derivative containing the PA4633 encoding sequence (pMAMV347). Data have been corrected with the number of bacteria that swam into buffer-containing capillaries, namely  $23\,137 \pm 5\,179$  [PAO1 (pBBR1MCS2\_START)],  $16\,400 \pm 2\,969$  [PAO1-PA4633 (pBBR1MCS2\_START)] and  $8362 \pm 194$  [PAO1-PA4633 (pMAMV347)]. Data are means and standard deviations from three independent experiments conducted in triplicate.**

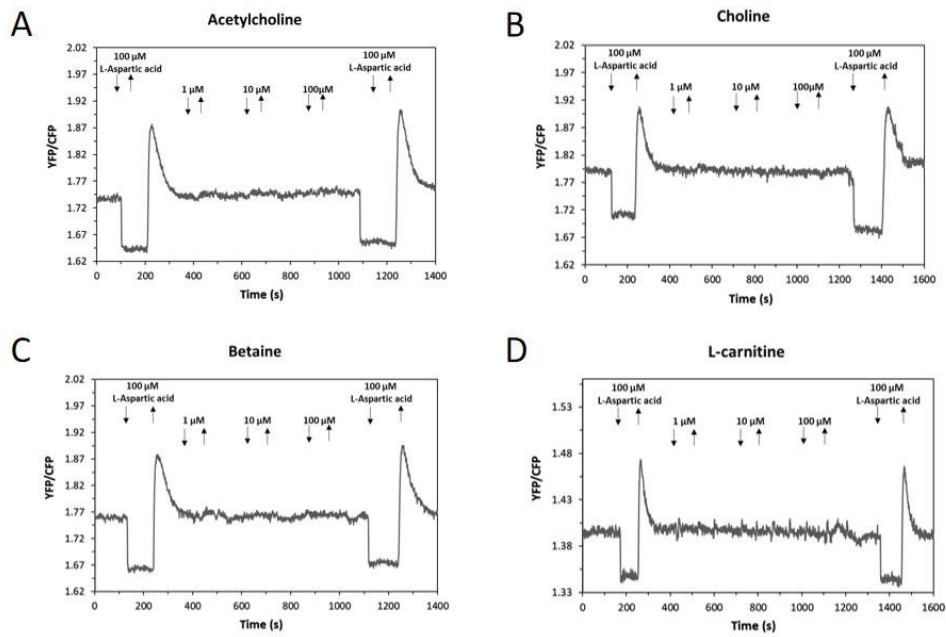


**Figure S 16. FRET measurements of the Tar response to PctD chemoeffectors.** Measurements were performed for receptorless *E. coli* cells expressing wildtype Tar as the sole receptor along with the FRET reporter plasmid. Cells were stimulated by the stepwise addition (down arrow) and subsequent removal (up arrow) of the indicated concentrations of acetylcholine (A), choline (B), betaine (C) and L-carnitine (D) in a flow chamber.

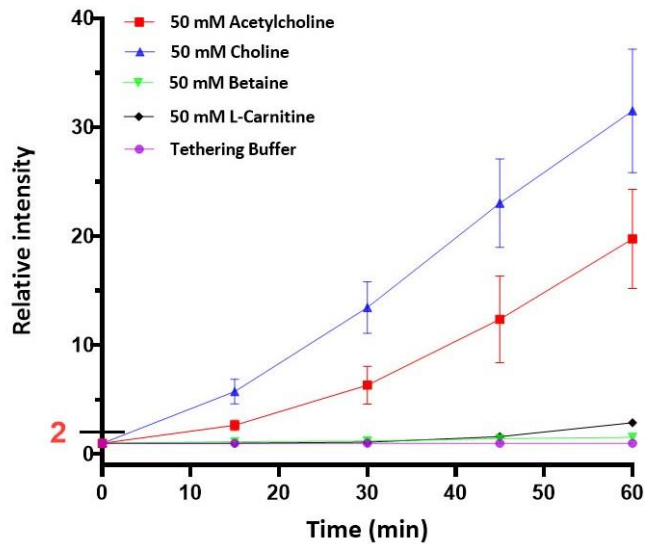


**Figure S 17. Microfluidic assay of the chemotactic response of *E. coli* strain UU1250 expressing PctD-Tar as the sole receptor.** Relative cell density (fluorescence intensity) in the observation channel over time in gradients of acetylcholine, choline, betaine, or L-carnitine with 50 mM in the source channel as indicated, or in a control channel with tethering buffer. Cell density in the observation channel before ligands stimulation ( $t=0$ ) was normalized to be one in each case. Error bars indicate standard deviation for three independent biological replicates.

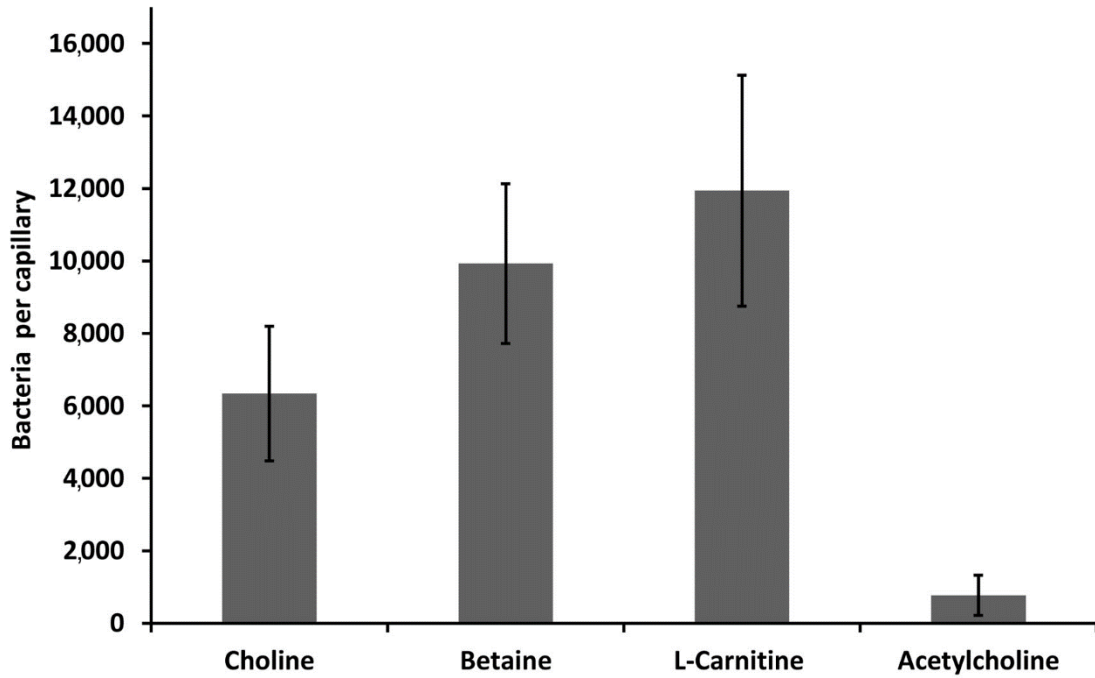


Figure S 18. Capillary chemotaxis assays of *P. atrosepticum* SCRI1043 to 1 mM choline, betaine, L-carnitine and acetylcholine. Data were corrected with the number of cells that swam into buffer containing capillaries ( $3424 \pm 417$ ). Data are means and standard deviations from triplicate analysis of three biological replicates.

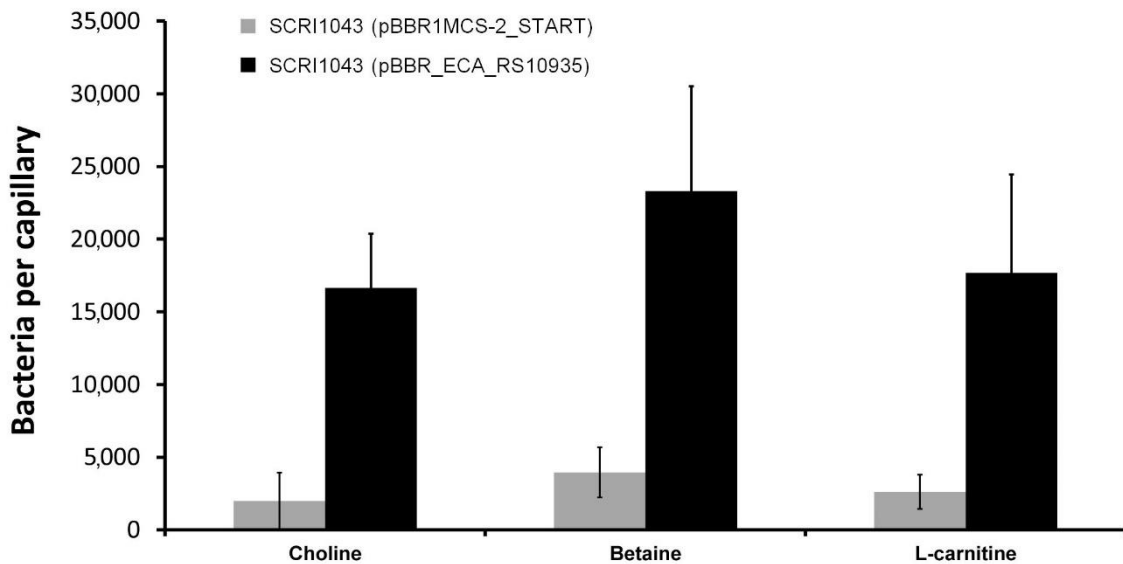


Figure S 19. Capillary chemotaxis assays of *P. atrosepticum* SCRI1043 containing the empty plasmid pBBR1MCS-2\_START and its derivative pBBR\_ECA\_RS10935 causing expression of chemoreceptor ECA\_RS10935 (PacA). Data have been corrected with the number of cells that swam into buffer-containing capillaries ( $530 \pm 233$  cells per capillary).

**Table S 9. Results from structural alignments of the PctD-LBD structure (in complex with acetylcholine) and the PacA-LBD structure (in complex with betaine) with structures deposited in the Protein Data Bank. Shown are the top 15 structures according to the Z-score. Alignments were made with the DALI server (Holm (2020) Methods Mol Biol. 2112, 29).**

PDB ID	Name	Sensor protein family	Ligands	Bacterial species	Z-score	rm sd	nres	% id
<b>PctD-LBD</b>								
6fu4	TlpQ	CR	Histamine, polyamines	<i>P. aeruginosa</i>	28.1	2.8	297	25
6pzj		CR	Unknown	<i>Leptospira interrogans</i>	24.8	2.4	264	26
3lib	mmHK1 S-Z3	SK	Unknown	<i>Methanosarcina mazei</i>	24.3	3.0	271	23
6d8v	McpX	CR	Quaternary amines	<i>Sinorhizobium meliloti</i>	23.5	3.6	270	19
4wy9	Tlp1	CR	Asp	<i>Campylobacter jejuni</i>	21.3	4.3	285	13
6e0a	TlpA	CR	Unknown	<i>Helicobacter pylori</i>	19.5	3.9	262	16
6mni	PscC	CR	Pro	<i>P. syringae</i>	18.7	3.3	259	13
5ere		ER		<i>Desulfohalobium retbaense</i>	18.0	3.9	540	12
5lt9	PctB	CR	Gln and other amino acids	<i>P. aeruginosa</i>	17.1	3.7	254	15
4xm q	Tlp3	CR	Amino acids and other compounds	<i>C. jejuni</i>	16.6	3.4	254	9
3lic	soHK1S -Z6	SK	Unknown	<i>Shewanella oneidensis</i>	15.7	4.4	265	18
3lid	vpHK1S -Z8	SK	Unknown	<i>Vibrio parahaemolyticus</i>	15.3	4.9	279	11
3lif	rpHK1S -Z16	SK	Unknown	<i>Rhodospseudomonas palustris</i>	15.2	3.5	243	12
3by9	DctB	SK	Succinate	<i>Vibrio cholerae</i>	14.6	3.8	259	9
4jgo	KinD	SK	Pyruvate, propionate, butyrate, autoinducer-2	<i>Bacillus subtilis</i>	14.4	3.7	210	9
<b>PacA-LBD</b>								
6pzj		CR	Unknown	<i>Leptospira interrogans</i>	28.0	2.3	264	22
3lib	mmHK1 S-Z3	SK	Unknown	<i>Methanosarcina mazei</i>	27.5	2.8	271	26

6fu4	TlpQ	CR	Histamine, polyamines	<i>P. aeruginosa</i>	27.0	2.3	297	26
6d8v	McpX	CR	Quaternary amines	<i>Sinorhizobium meliloti</i>	24.8	3.2	270	22
4wy9	Tlp1	CR	Asp	<i>Campylobacter jejuni</i>	21.5	4.4	285	13
3lic	soHK1S-Z6	SK	Unknown	<i>Shewanella oneidensis</i>	20.2	4.4	265	18
6e0a	TlpA	CR	Unknown	<i>Helicobacter pylori</i>	19.9	3.3	262	14
6mni	PscC	CR	Pro	<i>P. syringae</i>	19.7	3.1	259	19
5lt9	PctB	CR	Gln and other amino acids	<i>P. aeruginosa</i>	19.4	3.5	254	25
5ere		ER		<i>Desulfohalobium retbaense</i>	18.6	3.2	540	8
4xm q	Tlp3	CR	Amino acids and other compounds	<i>C. jejuni</i>	16.6	3.4	254	12
3lif	rpHK1S-Z16	SK	Unknown	<i>Rhodopseudomonas palustris</i>	16.3	3.3	243	13
7k5n		DC	Pro	<i>Aeromonas caviae</i>	16.3	3.7	238	20
2zbb	DctB	SK	Succinate	<i>Escherichia coli</i>	15.0	3.8	255	12
4jgo	KinD	SK	Pyruvate, propionate, butyrate, autoinduce r-2	<i>Bacillus subtilis</i>	14.4	3.6	210	11

CR: Chemoreceptor; SK: Sensor Kinase; ER: Extracellular Receptor; DC: Diguanylate Cyclase.

**Table S 10. Strains, plasmids and oligonucleotides used in Chapter 3.**

Strains and plasmids	Genotype or relevant characteristics <sup>a</sup>	Ref.
<b>Strains</b>		
<i>Escherichia coli</i> BL21(DE3)	F <sup>-</sup> <i>ompT gal dcm lon hsdS<sub>B</sub>(r<sub>B</sub><sup>-</sup>m<sub>B</sub><sup>-</sup>)</i> λ(DE3 [ <i>lacI lacUV5-T7p07 ind1 sam7 nin5</i> ]) [ <i>malB<sup>+</sup></i> ] <sub>K-12</sub> (λ <sup>S</sup> )	(Jeong <i>et al.</i> , 2009)
<i>E. coli</i> BL21-AI	F <sup>-</sup> <i>ompT hsdS<sub>B</sub> (r<sub>B</sub><sup>-</sup>m<sub>B</sub><sup>-</sup>) gal dcm araB::T7RNAP-tetA</i>	Invitrogen
<i>E. coli</i> DH5α	F <sup>-</sup> <i>endA1 glnV44 thi-1 recA1 relA1 gyrA96 deoR nupG purB20 φ80dlacZΔM15 Δ(lacZYA-argF)U169, hsdR17(r<sub>K</sub><sup>-</sup>m<sub>K</sub><sup>+</sup>), λ<sup>-</sup></i>	(Woodcock <i>et al.</i> , 1989)
<i>E. coli</i> CC118λpir	<i>araD Δ(ara, leu) ΔlacZ74 phoA20 galK thi-1 rspE rpoB argE recA1 λpir</i>	(Herrero <i>et al.</i> , 1990)
<i>E. coli</i> HH26	Mobilizing strain for conjugal transfer	(Kaniga <i>et al.</i> , 1991)
<i>E. coli</i> K12	F <sup>-</sup> lambda <sup>-</sup> <i>ilvG rfb-50 rph-1</i>	(Blattner <i>et al.</i> , 1997)
<i>E. coli</i> UU1250	Derivative of RP437, Δ <i>aerΔtsrΔ(tar-tap)Δtrg</i>	(Ames <i>et al.</i> , 2002)
<i>E. coli</i> VS181	Derivative of RP437; Δ( <i>cheYcheZ</i> )Δ <i>aerΔtsrΔ(tar-tap) Δtrg</i>	(Sourjik and Berg, 2004)
<i>Pseudomonas aeruginosa</i> PAO1	Wild type	(Stover <i>et al.</i> , 2000)
<i>P. aeruginosa</i> PAO1-PA4633	PAO1 transposon mutant <i>pa4633::ISlacZ/hah; Tc<sup>R</sup></i>	(Jacobs <i>et al.</i> , 2003)
<i>Pectobacterium atrosepticum</i> SCRI1043	Wild type, plant pathogen	(Bell <i>et al.</i> , 2004)
<i>P. atrosepticum</i> SCRI1043-ECA_RS10935	Deletion mutant of <i>ECA_RS10935</i>	This study
<i>Pantoea agglomerans</i> 9Rz4	Wild type, oilseed rape rhizosphere isolate	(Berg <i>et al.</i> , 2002)
<i>Serratia plymuthica</i> A153	Wild type, wheat rhizosphere isolate	(Matilla <i>et al.</i> , 2016)
<i>Pseudomonas stutzeri</i> AN10 PSC306	Wild type, polluted marine sediment isolate	(Brunet-Galmés <i>et al.</i> , 2012)
<i>Agrobacterium tumefaciens</i> C58	Wild-type, plant pathogen	(Wood <i>et al.</i> , 2001)
<i>Dickeya solani</i> MK10	Wild-type, plant pathogen	(Pritchard <i>et al.</i> , 2013)
<i>P. savastanoi</i> pv. <i>savastanoi</i> NCPPB 3335	Wild-type, plant pathogen	(Rodríguez-Palenzuela <i>et al.</i> , 2010)
<i>Pseudomonas putida</i> KT2440	Wild-type, non-pathogenic soil bacterium	(Espinosa-Urgel and Ramos, 2004)
<i>Salmonella enterica</i> sv. Typhimurium ATCC14028	Wild-type, human and animal pathogen	(Römling <i>et al.</i> , 1998)
<b>Plasmids</b>		
pET28b(+)	Km <sup>R</sup> , protein expression plasmid	Novagen
pET28_PA4633-LBD	Km <sup>R</sup> ; pET28b(+) derivative containing a DNA fragment encoding PA4633-LBD	This study
pET28_ECA_RS10935-LBD	Km <sup>R</sup> ; pET28b(+) derivative containing a DNA fragment encoding ECA_RS10935-LBD	This study
pBBR1MCS-2_START	Km <sup>R</sup> ; <i>oriRK2 mobRK2</i>	(Obranić <i>et al.</i> , 2013)
pBBR_ECA_RS10935	Km <sup>R</sup> ; a 2.0-kb PCR fragment containing the RS10935 gene cloned into the NdeI/EcoRI sites of pBBR1MCS-2_START	This study

pMAMV347	Km <sup>R</sup> ; a 2.2-kb PCR fragment containing the <i>pa4633</i> gene cloned into the NdeI/EcoRI sites of pBBR1MCS-2_START	This study
pKG116	Cm <sup>R</sup> ; Protein expression plasmid	(Burón-Barral <i>et al.</i> , 2006)
pVS1743	Cm <sup>R</sup> ; pKG116 derivative containing a DNA fragment encoding PctD [1-435]-Tar [267-553];	This study
pSB13	Cm <sup>R</sup> ; pKG116 derivative, Tar expression plasmid	(Bi <i>et al.</i> , 2018)
pVS88	Ap <sup>R</sup> ; CheY-EYFP / CheZ-ECFP expression plasmid	(Sourjik and Berg, 2004)
pOB30	Ap <sup>R</sup> ; GFP expression plasmid	(Bi <i>et al.</i> , 2016)
Oligonucleotides		
Name	Sequence (5'-3')	Purpose
PA4633-LBD-f	GGAATTCATATGGCCGGCGCGAACGCA	Construction of pET28_PA4633-LBD
PA4633-LBD-r	CCGCTCGAGTCACATGCCGAGGATATCCTGCT	
ECA_RS10935-LBD-f	CCGCGCGGCAGCCATATGAGCTGGCAGTCTAGT AGTGA	Construction of pET28_ECA_RS10935-LBD
ECA_RS10935-LBD-r	TCGACGGAGCTCGAATTCGGATCTCACAACCTGG CGCTCAGACG	
PA4633-NdeI-f	TAATCATATGAAGCTCAAGTCGATCCAGTT	Construction of pMAMV347
PA4633-EcoRI-r	TAATGAATTCCTGATAAGCCTGCTCGCCAAG	
1F-ECA_RS10935	TAATGCCATATGGCCAAACAATTAATAC	Construction of pBBR_ECA_RS10935
1R-ECA_RS10935	TAATGGATCCCCTTATGGTCGCCGGGTTAC	
PA4633-NdeI-f	AAACATATGATGAAGCTCAAGTCGATCCAG	Construction of pVS1743
PA4633-r	CCTTCGCGGACATGGCCGATCATGTTCTGCAGT TTG	
Tar-PA4633-f	GATCGCCATGTCCGCGAAGGTTTCAGAT	
Tar-BamHI-r	GGATCCTCAAATGTTTCCAGTTT	

**Table S 11. Crystallization conditions, data collection and refinement statistics of the PctD-LBD and PacA-LBD three-dimensional structures.**

	<b>PctD-LBD/choline</b>	<b>PctD-LBD/acetylcholine</b>	<b>PacA-LBD/betaine</b>
<b>Crystallization conditions</b>			
	30% (w/v) PEG 4K, 0.2 M NH <sub>4</sub> acetate, 0.1 M Na acetate, pH 4.6	30% (w/v) PEG 4K, 0.2 M NH <sub>4</sub> acetate, 0.1 M Na acetate, pH 4.6	30% (w/v) PEG 4K, 0.2 M Na acetate, 0.1 M Tris hydrochloride, pH 8.5
<b>Data collection</b>			
PDB ID.	7PRQ	7PRR	7PSG
Beam Line	ID23-1	Xaloc	ID30A-3
Space group	P 21 21 21	P 21 21 21	P 1 21 1
Unit cell			
a, b, c (Å)	56.14, 104.86, 118.60	62.29, 102.65, 104.85	80.78, 83.44, 94.91
ASU	2	2	4
Resolution (Å) *	59.3-2.0 (2.07-2.0)	47.48-1.8 (1.86-1.8)	39.99-1.91 (1.98-1.91)
Unique reflections *	47,974 (4,694)	62,195 (6,172)	91,902 (9,315)
Multiplicity *	4.5 (4.5)	4.5 (4.6)	2.9 (3.1)
Completeness (%) *	99.69 (99.62)	98.62 (99.42)	98.01 (98.75)
I/σ <sub>1</sub> *	11.25 (1.81)	12.00 (1.32)	10.95 (0.95)
Wilson B-factor	29.90	25.31	38.62
R <sub>merge</sub> (%) *	0.09827 (1.033)	0.08522 (0.9069)	0.05702 (1.211)
CC (1/2) *	0.998 (0.691)	0.998 (0.626)	0.998 (0.509)
<b>Refinement</b>			
R <sub>work</sub> /R <sub>free</sub> (%)	17.0 / 21.7	16.7 / 20.7	18.5 / 22.6
No. Atoms	5,368	5,517	8,894
Protein	5,005	4,984	8,443
Ligands	137	192	132
Solvent	312	455	395
B-factor (Å <sup>2</sup> )	43.95	36.09	53.94
R.m.s deviations			
Bond lengths (Å)	0.013	0.012	0.011
Bond angles (°)	1.26	1.08	1.33
Ramachandran (%)			
Favored (%)	97.24	97.56	97.93
Outliers (%)	0.00	0.00	0.00



## Chapter 4. Identification of three chemoreceptors for amino acids in *Pectobacterium atrosepticum* SCRI1043. Basis for broad-spectrum amino acid chemotaxis

---

*Published article*

**Three unrelated chemoreceptors provide *Pectobacterium atrosepticum* with a broad-spectrum amino acid sensing capability.**

Félix Velando<sup>1</sup>, Miguel A. Matilla<sup>1</sup>, Igor B. Zhulin<sup>2</sup>, Tino Krell<sup>1</sup>

<sup>1</sup>Department of Biotechnology and Environmental Protection, Estación Experimental del Zaidín, Consejo Superior de Investigaciones Científicas, Granada, Spain; <sup>2</sup>Department of Microbiology and Translational Data Analytics Institute, The Ohio State University, Columbus, Ohio, USA

**Microbial Biotechnology** (Published 25 March 2023); In press. doi: 10.1111/1751-7915.14255.

### Abstract

---

Amino acids are important nutrients and also serve as signals for diverse signal transduction pathways. Bacteria use chemoreceptors to recognize amino acid attractants and to navigate their gradients. In *Escherichia coli* two likely paralogous chemoreceptors Tsr and Tar detect 9 amino acids, whereas in *Pseudomonas aeruginosa* the paralogous chemoreceptors PctA, PctB, and PctC detect 18 amino acids. Here, we show that the phyto bacterium *Pectobacterium atrosepticum* uses the three non-homologous chemoreceptors PacA, PacB and PacC to detect 19 proteinogenic and several non-proteinogenic amino acids. PacB recognizes 18 proteinogenic amino acids as well as 8 non-proteinogenic amino acids. PacB has a ligand preference for the three branched chain amino acids L-leucine, L-valine and L-isoleucine. PacA detects L-proline next to several quaternary amines. The third chemoreceptor, PacC, is an ortholog of *E. coli* Tsr and the only one of the 36 *P. atrosepticum* chemoreceptors that is encoded in the cluster of chemosensory pathway genes. Surprisingly, in contrast to Tsr, which primarily senses serine, PacC recognizes aspartate as the major chemoeffector, but not serine. Our results demonstrate that bacteria use various strategies to sense a wide range of amino acids and that it takes more than one chemoreceptor to achieve this goal.

---

# Three unrelated chemoreceptors provide *Pectobacterium atrosepticum* with a broad-spectrum amino acid sensing capability

Félix Velando<sup>1</sup> | Miguel A. Matilla<sup>1</sup> | Igor B. Zhulin<sup>2</sup> | Tino Krell<sup>1</sup>

<sup>1</sup>Department of Biotechnology and Environmental Protection, Estación Experimental del Zaidín, Consejo Superior de Investigaciones Científicas, Granada, Spain

<sup>2</sup>Department of Microbiology and Translational Data Analytics Institute, The Ohio State University, Columbus, Ohio, USA

## Correspondence

Igor B. Zhulin, Department of Microbiology and Translational Data Analytics Institute, The Ohio State University, Columbus, Ohio, USA.

Email: joulaine.1@osu.edu

Tino Krell, Department of Biotechnology and Environmental Protection, Estación Experimental del Zaidín, Consejo Superior de Investigaciones Científicas, Granada, Spain.

Email: tino.krell@eez.csic.es

## Funding information

Consejería de Economía, Innovación, Ciencia y Empleo, Junta de Andalucía, Grant/Award Number: P18-FR-1621; Ministerio de Ciencia e Innovación, Grant/Award Number: PID2019-103972GA-I00 and PID2020-112812GB-I00; National Institutes of Health, Grant/Award Number: 1R35GM131760

## Abstract

Amino acids are important nutrients and also serve as signals for diverse signal transduction pathways. Bacteria use chemoreceptors to recognize amino acid attractants and to navigate their gradients. In *Escherichia coli* two likely paralogous chemoreceptors Tsr and Tar detect 9 amino acids, whereas in *Pseudomonas aeruginosa* the paralogous chemoreceptors PctA, PctB and PctC detect 18 amino acids. Here, we show that the phyto bacterium *Pectobacterium atrosepticum* uses the three non-homologous chemoreceptors PacA, PacB and PacC to detect 19 proteinogenic and several non-proteinogenic amino acids. PacB recognizes 18 proteinogenic amino acids as well as 8 non-proteinogenic amino acids. PacB has a ligand preference for the three branched chain amino acids L-leucine, L-valine and L-isoleucine. PacA detects L-proline next to several quaternary amines. The third chemoreceptor, PacC, is an ortholog of *E. coli* Tsr and the only one of the 36 *P. atrosepticum* chemoreceptors that is encoded in the cluster of chemosensory pathway genes. Surprisingly, in contrast to Tsr, which primarily senses serine, PacC recognizes aspartate as the major chemoeffector but not serine. Our results demonstrate that bacteria use various strategies to sense a wide range of amino acids and that it takes more than one chemoreceptor to achieve this goal.

## INTRODUCTION

Chemosensory signalling cascades are among the most sophisticated prokaryotic signal transduction systems. These cascades show a wide phylogenetic distribution and the corresponding signalling genes have been identified in about half of the sequenced bacterial genomes (Sanchis-López et al., 2021; Wuichet & Zhulin, 2010). Most of these cascades mediate chemotaxis, whereas others carry out alternative cellular functions or are associated with type IV pili-based motility

(Gumerov et al., 2021; Wuichet & Zhulin, 2010). Bacteria are able to perform chemotaxis to a wide range of different compounds. A large number of chemo effectors serve as growth substrates and chemotaxis enables cells to access nutrient sources (Matilla et al., 2022a). Other chemo effectors such as quorum sensing molecules (Zhang et al., 2020), plant and human hormones (Antunez-Lamas et al., 2009; Lopes & Sourjik, 2018; Rico-Jiménez et al., 2022) and neurotransmitters (Corral-Lugo et al., 2018; Pasupuleti et al., 2014) provide the bacterium with important information on its

This is an open access article under the terms of the [Creative Commons Attribution-NonCommercial-NoDerivs License](https://creativecommons.org/licenses/by-nc-nd/4.0/), which permits use and distribution in any medium, provided the original work is properly cited, the use is non-commercial and no modifications or adaptations are made.

© 2023 The Authors. *Microbial Biotechnology* published by Applied Microbiology International and John Wiley & Sons Ltd.

## Introduction

---

Chemosensory signaling cascades are among the most sophisticated prokaryotic signal transduction systems. These cascades show a wide phylogenetic distribution and the corresponding signaling genes have been identified in about half of the sequenced bacterial genomes (Wuichet and Zhulin, 2010; Sanchis-López *et al.*, 2021). Most of these cascades mediate chemotaxis, whereas others carry out alternative cellular functions or are associated with type IV pili-based motility (Wuichet and Zhulin, 2010; Gumerov *et al.*, 2021). Bacteria are able to perform chemotaxis to a wide range of different compounds. A large number of chemoeffectors serve as growth substrates and chemotaxis enables cells to access nutrient sources (Matilla *et al.*, 2022a). Other chemoeffectors such as quorum sensing molecules (Zhang *et al.*, 2020), plant and human hormones (Antunez-Lamas *et al.*, 2009; Lopes and Sourjik, 2018; Rico-Jiménez *et al.*, 2022) and neurotransmitters (Pasupuleti *et al.*, 2014; Corral-Lugo *et al.*, 2018) provide the bacterium with important information on its environment and chemotaxis to these compounds allows bacteria to find optimal environmental niches (Colin *et al.*, 2021).

The central feature of a chemosensory pathway is the ternary complex formed by the chemoreceptor, the CheA autokinase and the CheW coupling protein. In a canonical system, chemoeffector binding to the ligand binding domain (LBD) of the chemoreceptor generates a molecular stimulus that alters CheA autokinase activity and in turn transphosphorylation activity to the CheY response regulator. The phosphorylated form of CheY binds to the flagella motors to initiate random changes in swimming direction. Attractant stimuli suppress these movements to promote up-gradient travel. A sensory adaptation system matches the cell's detection sensitivity to ambient chemoeffector levels through reversible covalent modifications of chemoreceptor molecules, mediated by the CheR methyltransferase and CheB methylesterase (Parkinson *et al.*, 2015). In addition, some but not all chemosensory pathways employ auxiliary proteins like the alternative coupling protein CheV, the phosphatases CheC, CheZ and CheX or the CheD deamidase (Wuichet and Zhulin, 2010; Bi and Sourjik, 2018).

Bacteria encoding chemosensory pathways differ enormously in the number of chemoreceptor genes, ranging from one to ninety (Gumerov *et al.*, 2021). On average a bacterial genome contains 14 chemoreceptors (Lacal *et al.*, 2010b; Sanchis-López *et al.*, 2021) that frequently differ in their topology. Canonical transmembrane receptors that contain an extracytosolic LBD flanked by two transmembrane regions is the most prevalent type (Wuichet *et al.*, 2007), but there are also entirely cytosolic receptors, transmembrane receptors with a cytosolic LBD and receptors that lack a recognizable LBD (Ortega *et al.*, 2017a). Chemoreceptors employ almost 100 different LBD types (Ortega *et al.*, 2017a), of which most abundant are the four-helix bundle family (Ulrich and Zhulin, 2005) and the dCache\_1 family (Upadhyay *et al.*, 2016), which represent 17.6% and 15.5% of all chemoreceptor LBDs, respectively (Sanchis-López *et al.*, 2021). This diversity in the LBD type is reflected in the wide range of compounds that stimulate chemoreceptors. Chemoeffectors that stimulate chemoreceptors by direct binding to the LBDs include organic acids, amino acids, sugars, polyamines, quaternary amines, purines, metal cations, aromatic hydrocarbons, nitrate, oxygen, urea, c-di-GMP, autoinducer-2, inorganic phosphate or arsenate (Matilla *et al.*, 2022a). In addition, some chemoreceptors are activated

by the binding of chemoeffector-loaded solute binding proteins to the LBD and such mechanism was found, for example, to mediate chemotaxis to sugars, peptides, polyamines, amino acids or inorganic phosphate (Matilla *et al.*, 2021b).

Amino acids serve as important nutrients and signaling molecules, and bacteria evolved various chemoreceptors to detect amino acids. For example, in the model organism *Escherichia coli*, two chemoreceptors, Tsr and Tar, recognized L-serine and L-aspartate as major chemoattractants, respectively (Clarke and Koshland, 1979). Together, these two chemoreceptors enable *E. coli* to detect 9 amino acids (Hedblom and Adler, 1983). Tsr and Tar appear to be paralogs, because of their high sequence similarity. In a similar fashion, three paralogous chemoreceptors, PctA, PctB and PctC, enable *Pseudomonas aeruginosa* to sense 18 proteinogenic amino acids and gamma-aminobutyric acid (GABA) (Rico-Jiménez *et al.*, 2013a).

The goal of this study is to identify amino acid sensing chemoreceptors in *Pectobacterium atrosepticum*, which is among the top 10 most relevant plant pathogens (Mansfield *et al.*, 2012). Several studies have shown that chemotaxis is essential for an effective entry into plants and virulence of plant pathogens (Matilla and Krell, 2018b). This notion is also supported by the observation that plant pathogens contain more chemoreceptors than the average (Lacal *et al.*, 2010b; Matilla and Krell, 2018; Sanchis-López *et al.*, 2021). Data indicate that chemotaxis to compounds released by stomata and wounds enables efficient plant entry (Matilla and Krell, 2018). In other important plant pathogens like *Pseudomonas syringae* pv. *tomato* and *Pseudomonas syringae* pv. *tabaci* chemotaxis to proteinogenic amino acids and the non-proteinogenic amino acid GABA was found to be essential for bacterial virulence (Cerna-Vargas *et al.*, 2019; Tumewu *et al.*, 2020; Tumewu *et al.*, 2021; Santamaría-Hernando *et al.*, 2022). Remarkably, the application of an amino acid to the plant surface, masking existing compound gradients, reduced bacterial virulence, representing an alternative strategy to fight plant pathogens (Cerna-Vargas *et al.*, 2019).

The genome of *P. atrosepticum* strain SCRI1043 encodes 36 chemoreceptors that differ in topology and LBD type (Figure 32). Most prevalent are the 24 chemoreceptors that contain a four-helix bundle type LBD (Figure 32). So far, a single chemoreceptor, PacA, has been functionally characterized in SCRI1043 and was found to recognize different quaternary amines at its dCache\_1 type LBD causing chemoattraction (Matilla *et al.*, 2022b). Here, we report our strategy for searching for amino acid chemoreceptors in *P. atrosepticum* that resulted in the identification of three unrelated receptors that collectively enable this bacterium to detect 19 proteinogenic amino acids and various non-proteinogenic amino acids.

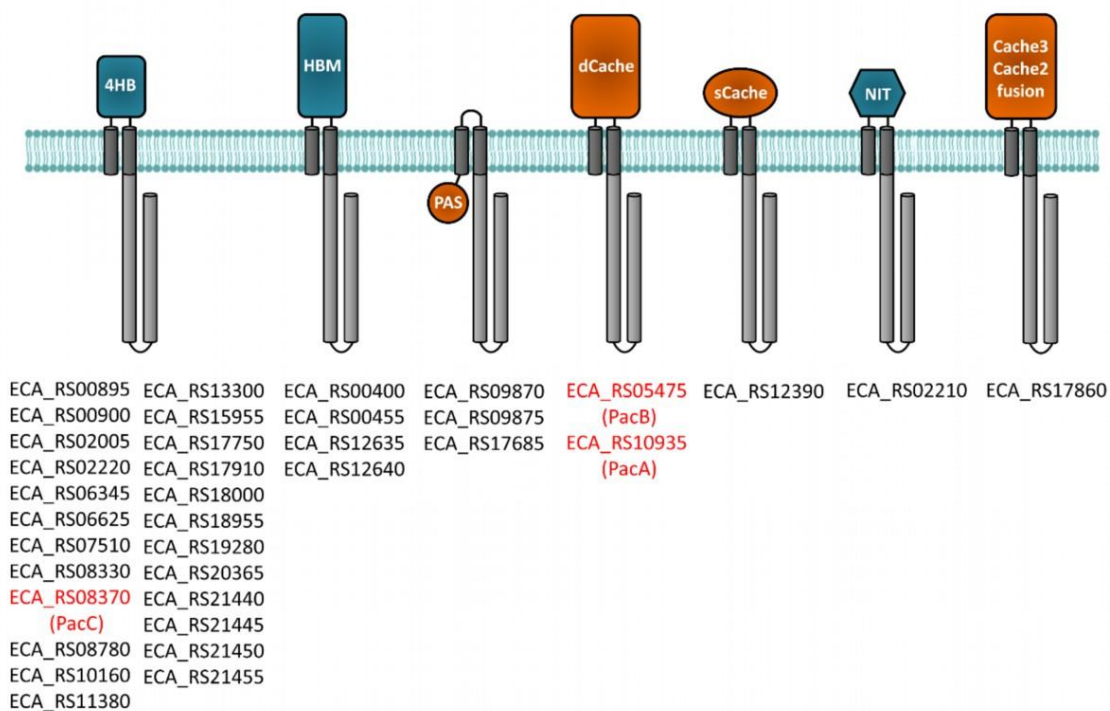


**Figure 32. The chemoreceptor repertoire of *Pectobacterium atrosepticum* SCRI1043.** Transmembrane regions have been predicted using the DAS algorithm (Cserzo *et al.*, 1997). The ligand binding domains (LBDs) have been annotated according to Pfam (Mistry *et al.*, 2021). Blue LBDs form parallel helix structures, whereas orange LBDs represent  $\alpha/\beta$  folds. The names of the chemoreceptors analyzed are colored in red.

## Materials and Methods

**Bacterial strains, plasmids and growth conditions:** Bacterial strains and plasmids used in this study are listed in Table S12. *P. atrosepticum* SCRI1043 and its derivative strains were routinely grown at 30 °C in Lisogeny Broth (5 g/l yeast extract, 10 g/l bacto tryptone, 5 g/l NaCl) or minimal medium (0.41 mM MgSO<sub>4</sub>, 7.56 mM (NH<sub>4</sub>)<sub>2</sub>SO<sub>4</sub>, 40 mM K<sub>2</sub>HPO<sub>4</sub>, 15 mM KH<sub>2</sub>PO<sub>4</sub>) supplemented with 0.2% (w/v) glucose as carbon source. *E. coli* strains were grown at 37 °C in LB. *E. coli* DH5 $\alpha$  was used as a host for gene cloning. Media for propagation of *E. coli*  $\beta$ 2163 were supplemented with 300 mM 2, 6-diaminopimelic acid. When appropriate, antibiotics were used at the following final concentrations (in  $\mu$ g/ml): kanamycin: 50; tetracycline: 10; streptomycin: 50; ampicillin: 100. Sucrose was added to a final concentration of 10% (w/v) when required to select derivatives that had undergone a second cross-over event during marker exchange mutagenesis.

**Generation of protein expression plasmids:** The DNA fragments encoding the LBDs of chemoreceptors PacB (ECA\_RS05475, amino acids 27-279) and PacC (ECA\_RS08370, amino acids 30-192) were PCR amplified from genomic DNA using the oligonucleotides listed in Table S13. The PCR products were digested with NdeI and BamHI, and cloned into pET28b(+) linearized with the same endonucleases. The generated plasmids were verified by DNA sequencing.

**Protein overexpression and purification:** For the overexpression of PacC-LBD and PacB-LBD, *E. coli* BL21(DE3) was transformed with plasmids pET28b-ECA\_RS05475-LBD and pET28b-

ECA\_RS08370-LBD, respectively. The resulting strains were grown under continuous shaking (200 rpm) at 30 °C in 2-liter Erlenmeyer flasks containing 500 ml LB medium supplemented with 50 µg/ml kanamycin. At an OD<sub>660</sub> of 0.6, protein expression was induced by the addition of 0.1 mM isopropyl β-D-1-thiogalactopyranoside. Growth was continued at 16 °C overnight before cell harvest by centrifugation at 10 000 x g for 30 min. Cell pellets were resuspended in buffer A (20 mM Tris/HCl, 500 mM NaCl, 5% (v/v) glycerol, 10 mM imidazole, 0.1 mM EDTA, pH 8.0) and broken by French press treatment at 1000 lb/in<sup>2</sup>. After centrifugation at 20 000 x g for 30 min, supernatants were loaded onto 5-ml HisTrap HP columns (Amersham Biosciences) equilibrated with buffer A and eluted with an imidazole gradient of 40–500 mM in the same buffer. All proteins were purified at 4 °C. Purified proteins were dialyzed overnight into the corresponding analysis buffers for immediate analysis.

*Differential Scanning Fluorimetry Based Thermal Shift Assays:* For ligand screening, the compound arrays PM1, PM2A (carbon sources), PM3B (nitrogen sources) and PM4A (phosphorous and sulphur sources) from Biolog (<https://www.biolog.com/>) were used. The composition of these compound arrays can be found at <https://www.biolog.com/wp-content/uploads/2020/04/00A-042-Rev-C-Phenotype-MicroArrays-1-10-Plate-Maps.pdf>.

Assays were carried out using a MyIQ2 Real-Time PCR instrument (BioRad, Hercules, CA, USA). Ligand solutions were prepared by dissolving the array compounds in 50 µl of Milli-Q water, which, according to the information provided by the manufacturer, corresponds to a concentration of 10–20 mM. Freshly purified proteins were dialyzed into the analysis buffer (as described in the section below). Experiments were conducted in 96-well plates and each assay mixture contained 20 µl of the dialyzed protein (at 20–40 µM), 2 µl of 62.5 × SYPRO™ orange (Life Technologies, Eugene, Oregon, USA) and 2.5 µl of the resuspended array compound to be tested or the equivalent amount of buffer in the ligand-free control. Samples were heated from 23 °C to 85 °C at a scan rate of 1 °C/min. The protein unfolding curves were monitored by detecting changes in SYPRO™ Orange fluorescence. The melting temperature (T<sub>m</sub>) values were determined using the first derivative values of the raw fluorescence data. The detailed experimental protocol of these assays can be retrieved from (Fernandez *et al.*, 2018).

*Isothermal titration calorimetry (ITC):* All experiments were conducted on a VP-microcalorimeter (MicroCal, Amherst, MA) at 25 °C. PacA-LBD was dialyzed into 5 mM Tris/HCl, 5 mM Pipes, 5 mM MES, pH 7.4, adjusted to 20 µM and titrated with 9.6 µl aliquots of a 2 mM L-proline solution. PacB-LBD was dialyzed into 5 mM Tris/HCl, 5 mM Pipes, 5 mM MES, 10% (v/v) glycerol, pH 8.0, adjusted to 30 µM and titrated with 9.6 µl aliquots of 1-2 mM amino acid solutions. PacC-LBD was dialyzed into 5 mM Tris/HCl, 5 mM Pipes, 5 mM MES, 10% (v/v) glycerol, pH 6.0, adjusted to 30 µM and titrated with 4.8-14.4 µl aliquots of 1-2 mM amino acid solutions. In case no binding was observed, experiments were repeated with the maximal possible syringe ligand concentration (solutions that caused dilution heats below 0.1 µcal/sec) that were in the range of 5 to 20 mM depending on the ligand. If necessary, the pH of the ligand solutions was adjusted to that of the dialysis buffer by the addition of concentrated HCl or NaOH. The mean enthalpies measured from the injection of the ligands into the buffer were subtracted from raw titration data prior to data analysis with the with the ‘One binding site model’ of the MicroCal version of ORIGIN.

*Construction of chemoreceptor mutant strains:* Chromosomal mutants defective in ECA\_RS05475 (*pacB*) and ECA\_RS08370 (*pacC*) of SCRI1043 were constructed by homologous

recombination using a derivative plasmid of the suicide vector pKNG101. The plasmids for the construction of the deletion mutants were generated by amplifying the up- and downstream flanking regions of the gene to be mutated, and primers used are listed in Table S13. The resulting PCR products were digested with enzymes described in Table S12 and ligated in a three-way ligation into pUC18Not, previously to be cloned into the suicide vector pKNG101. Plasmids were verified by PCR and DNA sequencing. The resulting plasmids pKNG101\_ΔECA\_RS08370 and pKNG101\_ΔECA\_RS05475 were transferred to *P. atrosepticum* SCRI1043 by biparental conjugation using *E. coli* β2163. All plasmids and mutations were confirmed by PCR and sequencing.

*Quantitative capillarity chemotaxis assays:* Overnight cultures of *P. atrosepticum* SCRI1043 were grown at 30 °C in minimal medium. At an OD<sub>660</sub> of 0.4-0.45, the cultures were washed twice with chemotaxis buffer (50 mM K<sub>2</sub>HPO<sub>4</sub>/KH<sub>2</sub>PO<sub>4</sub>, 20 μM EDTA and 0.05% (v/v) glycerol, pH 7.0) and diluted to an OD<sub>660</sub> of 0.1 in the same buffer. Subsequently, 230 μl of the resulting bacterial suspension were placed into the wells of 96-well plates. One-microliter capillary tubes (P1424, Microcaps; Drummond Scientific) were heat-sealed at one end and filled with either the chemotaxis buffer (negative control) or chemotaxis buffer containing the compounds to be assayed. The capillaries were immersed into the bacterial suspensions at its open end. After 30 min incubation at room temperature, the capillaries were removed from the bacterial suspensions, rinsed with sterile water and the content expelled into Eppendorf tubes containing 1 ml of 40 mM K<sub>2</sub>HPO<sub>4</sub>, 15 mM KH<sub>2</sub>PO<sub>4</sub>. Serial dilutions were plated onto minimal medium supplemented with 15 mM glucose as carbon source. The number of colony forming units was determined after 36 h incubation at 30 °C. In all cases, data were corrected with the number of cells that swam into buffer containing capillaries.

*Data sources and bioinformatics software:* BLAST searches were carried out against the NCBI RefSeq database using default parameters. Gene neighborhoods were identified using the MiST database (Gumerov *et al.*, 2020). Taxonomy information was retrieved from the Genome Taxonomy Database (Parks *et al.*, 2018). Identification of enterobacterial genomes containing chemotaxis genes was carried out by searching AnnoTree (Mendler *et al.*, 2019) with the Pfam CheW domain (Pfam accession PF01584) as a query. Multiple sequence alignments using full-length protein sequences were constructed using the MAFFT (v.7.310) L-INS-I algorithm (Kato and Standley, 2013). Maximum likelihood phylogenetic trees were built in MEGA (v.11) using the JTT substitution model (Kumar *et al.*, 2018).

## Results

---

### **PacB is a universal amino acid sensor with the widest range**

In a recent study we have identified a dCache subfamily, termed dCache\_1AA, that is present throughout the tree of life and that binds specifically amino acids (Gumerov *et al.*, 2022). This domain is characterized by a sequence motif that interacts with the bound amino acid. *P. atrosepticum* SCRI1043 has two dCache domain containing chemoreceptors (Figure 32). The inspection of their sequence has revealed that chemoreceptor ECA\_RS05475 contains this sequence motif (Figure S20), strongly suggesting that it is an amino acid responsive receptor. To identify the ligands recognized by ECA\_RS05475, we have cloned the DNA fragment encoding

its LBD into a protein expression vector and have submitted the purified protein to thermal shift assays. In these experiments the protein is brought in contact with compounds from compound libraries. Protein-compound mixtures are exposed to a temperature gradient and protein unfolding is recorded. The interaction of a ligand with the LBD typically delays thermal unfolding that can be quantified as an increase in the midpoint temperature of the protein unfolding transition ( $T_m$ ) (Fernandez *et al.*, 2018). The screening using the Biolog PM3B compound array, containing different nitrogen sources, resulted in the identification of 28 compounds that caused  $T_m$  increases greater than 3 °C (Figure 33A) that is considered a stringent cut-off for binding. Among these potential ligands were 18 proteinogenic amino acids. Amino acids with a negatively charged side chain, L-Asp and L-Glu, were the only amino acids that did not stabilize the protein. Furthermore, significant  $T_m$  shifts were observed for a D-amino acid (D-Ala), 8 other non-proteinogenic amino acids and ethanolamine (see the legend to Figure 33 for the full list).

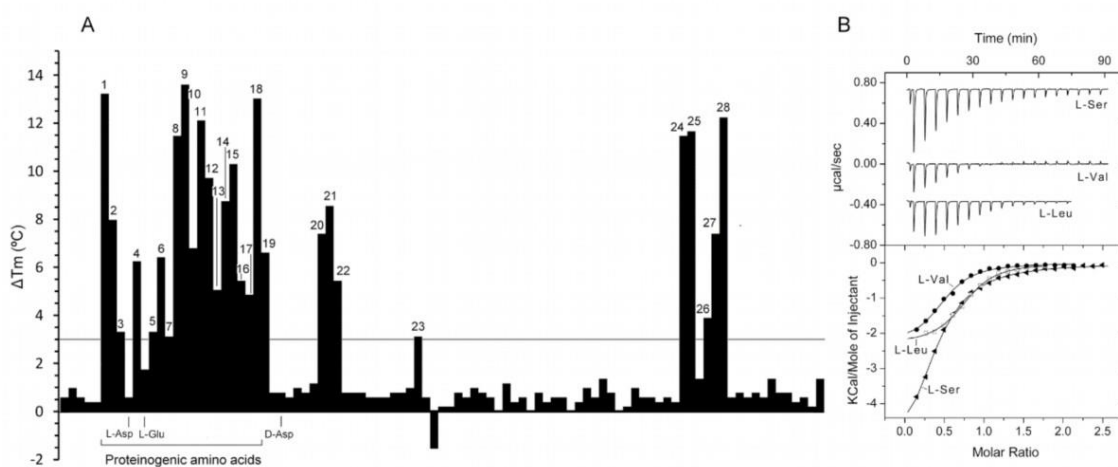


**Figure 33. PacB is a broad ligand range chemoreceptor.** (A) Thermal shift assays of PacB-LBD with the compounds of the Biolog array PM3B (different nitrogen sources). Shown are melting temperature ( $T_m$ ) changes with respect to the ligand-free protein. The compounds that caused  $T_m$  changes superior to 3 °C are labelled: 1: L-Ala, 2: L-Arg, 3: L-Asn, 4: L-Cys, 5: L-Gln, 6: Gly, 7: L-His, 8: L-Ile, 9: L-Leu, 10: L-Lys, 11: L-Met, 12: L-Phe, 13: L-Pro, 14: L-Ser, 15: L-Thr, 16: L-Trp, 17: L-Tyr, 18: L-Val, 19: D-Ala, 20: L-citrulline, 21: L-homoserine, 22: L-ornithine, 23: ethanolamine, 24: D,L- $\alpha$ -amino-butyric acid, 25:  $\gamma$ -amino-butyric acid, 26: D,L-amio-caprylic acid, 27:  $\delta$ -amino-N-valeric acid, 28:  $\alpha$ -amino-valeric acid. The grey line indicates a  $T_m$  shift of 3 °C, considered as stringent cut-off for binding. (B) Microcalorimetric titrations of 30  $\mu\text{M}$  PacB-LBD with 9.6  $\mu\text{l}$  aliquots of 1 mM ligand solutions. Upper panel: Raw titration data. Lower panel: Concentration-normalized and dilution heat-corrected raw data for the titration. The lines are the best fits with the “One binding site model” of the MicroCal version of ORIGIN.

The protein was subsequently submitted to microcalorimetric titrations to confirm binding and determine the binding parameters (Table 4). Dissociation constants ( $K_b$ ) could be derived for 14 proteinogenic amino acids. The failure to derive constants for the remaining 4 amino acids was most likely due to the fact that ITC only permits monitoring high-affinity interactions, which is due to the limitation in the syringe ligand concentration imposed by elevated dilution heats. However, lower affinity interactions can be detected by the thermal shift assay. This receptor has a clear preference for three branched chain amino acids (L-Val, L-Leu, L-Ile), that had  $K_b$  values between 1.4 to 3.1  $\mu\text{M}$  (Table 4, Figure 33B). To the best of our knowledge this is the first report of a chemoreceptor with ligand preference for the three branched chain amino acids.



This ligand group is then followed by other amino acids with an uncharged side chain, namely L-Ser, L-Met, L-Ala and L-Thr that bound with affinities between 6.8 to 14  $\mu\text{M}$  (Table 4, Figure 33B). Amino acids with a positively charged side chain, L-Arg and L-Lys, bound with comparatively low affinity ( $K_D$  of 35 and 36  $\mu\text{M}$ ). Of all ligands tested, L-Asn showed by far the lowest affinity with a  $K_D$  of 748  $\mu\text{M}$  (Table 4). As expected, ITC experiments failed to detect binding of the two amino acids that caused insignificant  $T_m$  increases, L-Asp and L-Glu. The ligand promiscuity of this receptor is illustrated by the binding of the non-proteinogenic amino acids GABA, amino-N-valeric acid, L-citrulline, L-homoserine and L-ornithine that bound to the LBD with  $K_D$  values ranging from 16 to 148  $\mu\text{M}$  (Table 4). To assess the functionality of the ECA\_RS05475 chemoreceptor we generated a deletion strain lacking this receptor and tested its chemotactic behaviors to L-Ala and L-Ser with quantitative capillary assays (Figure 34A). Both ligands were selected since initial experiments showed that they induced important chemotactic responses. We found that chemotaxis to L-Ala and L-Ser was significantly reduced in the mutant strain, but not entirely absent. The residual responses are presumably due to another chemoreceptor that detects the same chemoeffectors. Based on these results, we renamed ECA\_RS05475 as PacB (*Pectobacterium atrosepticum* chemoreceptor B).

**Table 4. Binding parameters derived from microcalorimetric titrations of the ligand binding domains of chemoreceptors PacA, PacB and PacC with different signal molecules.**

Protein	Compound	Thermal shift assay		ITC	
		$\Delta T_m$ (°C)	Binding	$K_D$ ( $\mu$ M)	$\Delta H$ (kcal/mol)
PacB-LBD	L-leucine	13.6	Binding	1.4 ± 0.2	-2.3 ± 0.0
	L-valine	13.0	Binding	1.5 ± 0.3	-2.0 ± 0.2
	L-isoleucine	11.5	Binding	3.1 ± 1.4	-3.5 ± 0.2
	L-serine	8.8	Binding	6.8 ± 0.7	-6.4 ± 0.4
	L-methionine	12.1	Binding	8.8 ± 1.2	-4.0 ± 0.4
	L-alanine	13.2	Binding	9.2 ± 2.2	-6.4 ± 0.6
	L-threonine	10.3	Binding	14 ± 0.6	-5.9 ± 0.1
	L-cysteine	6.8	Binding	30 ± 9.8	-18 ± 4.2
	Glycine	6.4	Binding	33 ± 5.9	-10 ± 0.7
	L-arginine	8.0	Binding	35 ± 2.0	-4.7 ± 0.1
	L-lysine	6.8	Binding	36 ± 2.2	-9.0 ± 0.4
	L-phenylalanine	9.7	Binding	41 ± 8.7	-1.4 ± 0.1
	L-tyrosine	4.9	Binding	50 ± 5.4	-3.6 ± 0.3
	L-asparagine	3.3	Binding	748 ± 30	-4.2 ± 0.1
	L-proline	5.1	Binding	No heats <sup>a</sup>	
	L-tryptophan	5.4	Binding	No heats <sup>a</sup>	
	L-glutamine	3.3	Binding	No heats <sup>a</sup>	
	L-histidine	3.1	Binding	No heats <sup>a</sup>	
	L-aspartate	0.6	No binding	No heats <sup>a</sup>	
	L-glutamate	1.8	No binding	No heats <sup>a</sup>	
	GABA	11.7	Binding	16 ± 1.5	-15 ± 1.3
	Amino-N-valeric acid	12.2	Binding	19 ± 8.9	-0.2 ± 0.1
	L-citrulline	7.4	Binding	25 ± 2.7	-3.0 ± 0.5
L-homoserine	8.6	Binding	87 ± 5.6	-17 ± 1.0	
L-ornithine	5.4	Binding	148 ± 10	-6.4 ± 0.4	
PacA-LBD	Betaine <sup>b</sup>	nd <sup>c</sup>		7.5 ± 0.1	-1.6 ± 0.2
	L-carnitine <sup>b</sup>	nd <sup>c</sup>		20 ± 2	-4.8 ± 0.7
	Choline <sup>b</sup>	nd <sup>c</sup>		113 ± 16	-1.9 ± 0.1
	L-proline	3.1	Binding	37 ± 1.1	-29 ± 4
PacC-LBD	D-aspartate	13.3	Binding	23 ± 2	-1.9 ± 0.1
	L-asparagine	8.6	Binding	65 ± 5	-0.6 ± 0.1
	L-aspartate	8.2	Binding	370 ± 82	-1.7 ± 0.6

<sup>a</sup>Under the experimental conditions used, namely the titration of 30  $\mu$ M protein with 5 to 20 mM ligand solutions.

<sup>b</sup>Data reported previously in (Matilla *et al.*, 2022a).

<sup>c</sup>Not determined.

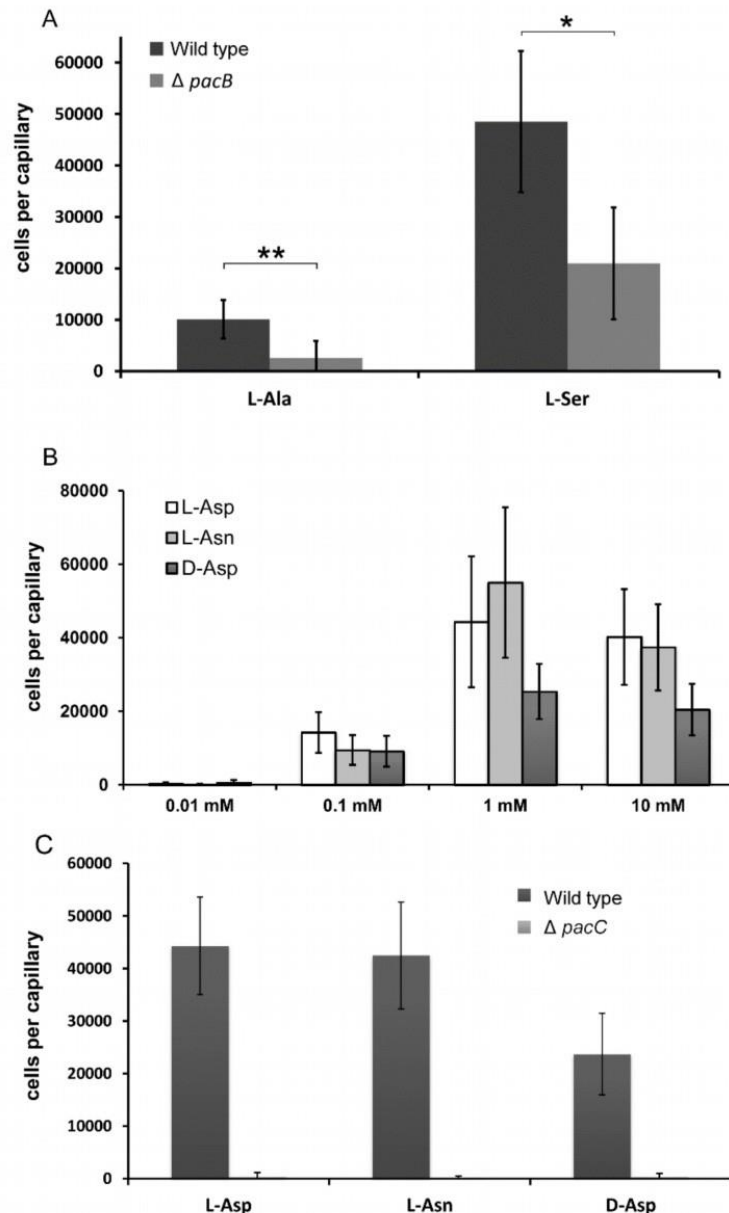


**Figure 34. Quantitative capillary chemotaxis assays of *Pectobacterium atrosepticum* SCRI1043 and mutants deficient in the PacB and PacC chemoreceptors. A)** Chemotaxis of the wt strain and a mutant in the *pacB* gene towards 1 mM of L-Ala and L-Ser. **B)** Chemotaxis of the wt strain to different concentrations of L-Asp, L-Asn and D-Asp. **C)** Chemotaxis of the wt strain and a mutant in the *pacC* gene towards 1 mM of the different chemoeffectors. The data have been corrected with the number of cells that swam into buffer-containing capillaries, namely  $1151 \pm 1065$  cells per capillary in the wild type,  $1088 \pm 440$  in the PacC mutant strain, and  $2293 \pm 580$  in the PacB mutant strain. \* $P < 0.05$ , \*\* $P < 0.01$  in Student's T-test.

### PacA binds and mediates chemotaxis to L-proline

We then searched for other chemoreceptors for amino acids. We have shown recently that PacA responds to the quaternary amines choline, betaine and L-carnitine (Matilla *et al.*, 2022b). However, studies from the Scharf laboratory revealed that the quaternary amine chemoreceptor McpX of *Sinorhizobium meliloti* also responds to L-proline (Webb *et al.*, 2017b), the only proteinogenic amino acid which is also a secondary amine. To determine whether PacA also binds L-proline, we conducted microcalorimetric studies using its individual LBD. Data

showed that L-proline bound to PacA-LBD with a  $K_D$  of 37  $\mu\text{M}$  (Figure 35, Table 4). In our previous study, we observed PacA mediated chemotaxis to quaternary amines by overexpressing its gene in *P. atrosepticum* from plasmid pBBR\_ECA\_RS10935 (Matilla *et al.*, 2022b). As shown in Figure S21, PacA overexpression caused an approximately 7-fold increase in chemotaxis to L-proline.

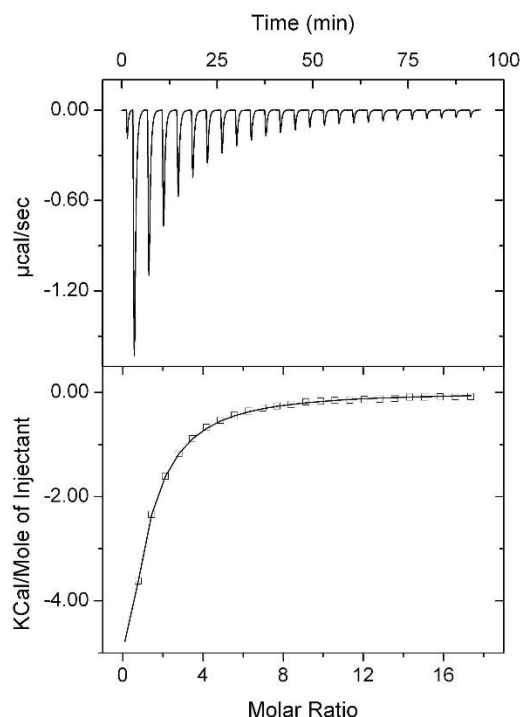


**Figure 35. Isothermal titration calorimetry study of the binding of L-proline to the LBD of *Pectobacterium atrosepticum* SCRI1043 chemoreceptor PacA.** Upper panel: Raw data for the titration of 20  $\mu\text{M}$  protein with 9.6  $\mu\text{l}$  aliquots of 2 mM L-proline. Lower panel: Concentration-normalized and dilution heat-corrected raw data for the titration. The continuous line is the best fit with the “One binding site model” of the MicroCal version of ORIGIN.

#### **PacC is the *Escherichia coli* Tsr ortholog mediating chemotaxis to aspartate and L-asparagine but not L-serine**

Chemotaxis to amino acids in *E. coli* is mediated by the Tar and Tsr chemoreceptors that possess a four-helix bundle type LBD. The chemosensory system in the family *Enterobacteriaceae* evolved vertically (Ortega and Zhulin, 2016), e.g. the CheA kinase of *P. atrosepticum* is orthologous to that of *E. coli*. In *E. coli*, the L-aspartate responsive chemoreceptor Tar is encoded in the chemosensory gene cluster containing *cheA* (Figure 36). Similarly, in *P. atrosepticum*, a single chemoreceptor, ECA\_RS08370, is encoded in the chemosensory gene cluster containing *cheA* (Gumerov *et al.*, 2020) (Figure 36). The ECA\_RS08370 receptor has a four-helix bundle LBD that shares 31 % sequence identity with Tar-LBD (Figure S22), suggesting that it might be a Tar ortholog. To test this idea, we performed a phylogenetic analysis of homologous chemoreceptors from representative genomes of *Enterobacteriaceae*, including *P. atrosepticum* (see Materials and Methods). We identified homologs of *E. coli* Tar, Tsr, and Tap chemoreceptors using BLAST searches against the set of representative *Enterobacteriaceae* genomes (Dataset S1), because a previous study reported that these three chemoreceptors belong to the same

cluster of orthologous groups (COG) (Ortega and Zhulin, 2016). We used *E. coli* Trg as an outgroup in the phylogenetic analysis, because it belongs to a different COG (Ortega and Zhulin, 2016). Sequences of identified homologs were aligned (Dataset S2), and a maximum likelihood tree was constructed from this multiple sequence alignment. The tree revealed a well-supported clade containing *E. coli* Tar and an adjacent clade containing *E. coli* Tsr and *P. atrosepticum* PacC (Figure 36A, Dataset S3), indicating that PacC is orthologous to Tsr. This was surprising, because *pacC* was located in the chemotaxis operon in the same position where *tar* is located in the *E. coli* chemotaxis operon. To further confirm that PacC is the Tsr ortholog, we analyzed chemotaxis gene clusters of all representative *Enterobacteriaceae* genomes in a phylogenomic context (Figure 36B). Taken together, the data shown in Figure 35 strongly suggests that, indeed, PacC is the Tsr ortholog and that Tar is the Tsr paralog, which originated in the evolutionary “newer” *Enterobacteriaceae* lineage (Figure 36B). Interestingly, upon *tsr* duplication, *tar* remained in the chemotaxis operon, whereas *tsr* moved elsewhere in the chromosome, and this pattern (as seen in *E. coli*) is fully conserved in this lineage (Figure 36B).

To investigate whether ECA\_RS08370 binds amino acids, we followed a similar strategy as for PacB and submitted its individual purified LBD to thermal shift assays using the Biolog compound arrays PM1, PM2A, PM3B and PM4A. Significant increases in  $T_m$  were observed for D-Asp, L-Asp, and L-Asn (Figure 37A). Microcalorimetric titrations showed that the protein bound preferentially D-aspartate ( $K_D=23 \mu\text{M}$ ) and L-asparagine ( $K_D=65 \mu\text{M}$ ), whereas L-aspartate binding occurred with significantly lower affinity ( $K_D=370 \mu\text{M}$ ) (Figure 37B, Table 4). Surprisingly, no binding heats were observed for a titration with L-Ser, the cognate ligand of Tsr. ECA\_RS08370 was renamed PacC (*Pectobacterium atrosepticum* chemoreceptor C). We have subsequently conducted quantitative capillary chemotaxis assays of *P. atrosepticum* SCRI1043 to the three ligands. Significant chemoattraction was observed for all three ligands (Figure 34B). The onset of response was in all cases at 0.1 mM and maximal responses were observed at 1 mM. To assess the role of PacC in this response we have generated the corresponding deletion mutant. This mutant failed to respond to these three ligands (Figure 34C) indicating that PacC is the sole chemoreceptor for these ligands under the experimental conditions used.

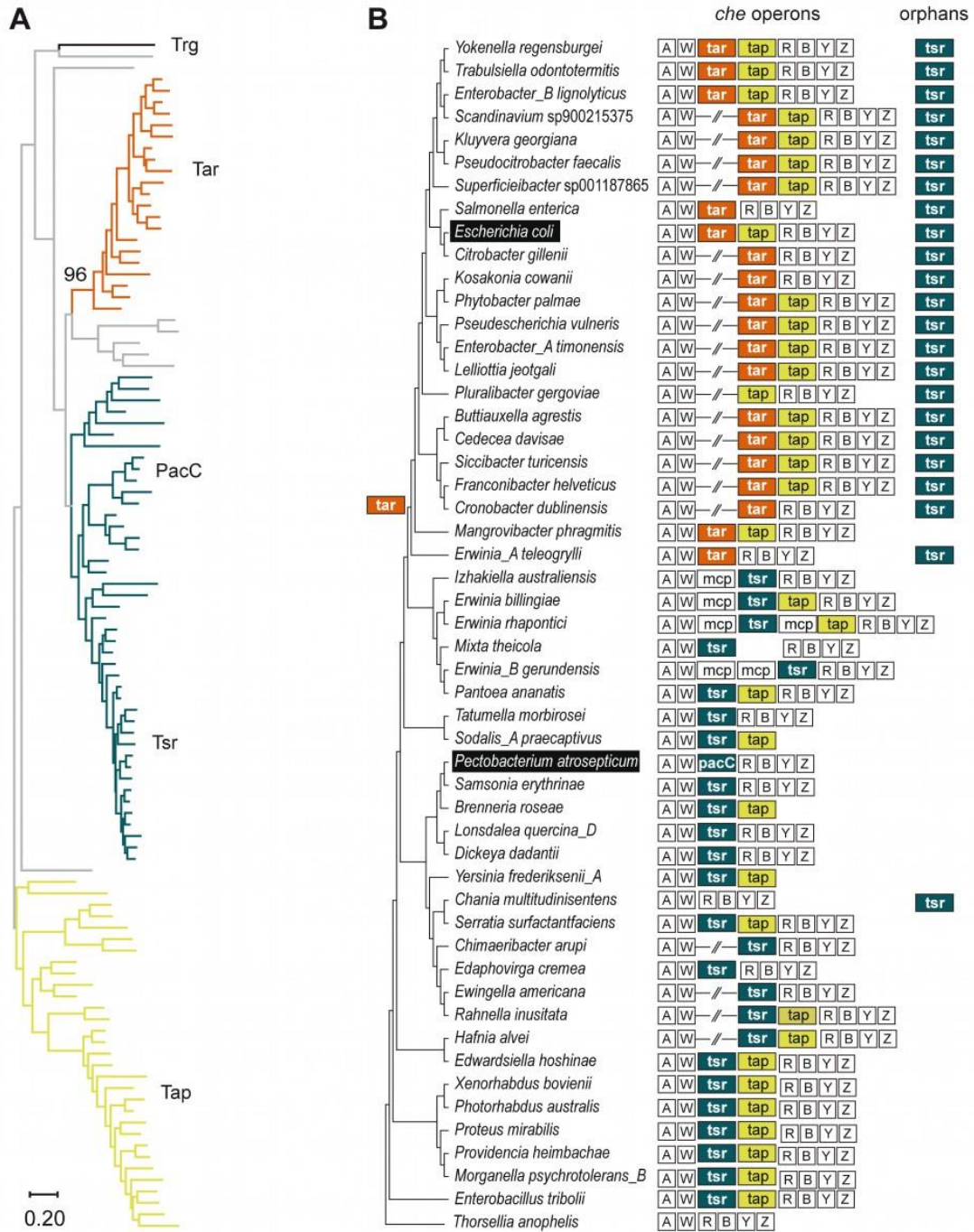


**Figure 36. PacC is a Tsr ortholog.** (A) A multiple likelihood tree of Tar, Tsr, and Tap homologs. Branches corresponding to *E. coli* Tar, Tsr, Tap, and Trg (outgroup) and *P. atrosepticum* PacC are labelled. Tar clade is shown in orange along with the percentage of bootstrap support (500 replications). Tsr clade containing PacC is shown in teal and the Tap cluster in yellow green. Branches with low bootstrap support and/or conflicting positions in other types of trees are shown in grey. The full version of the tree in Newick format and the underlying multiple sequence alignment are available as Datasets S3 and S2, respectively. (B) A guide genome tree (left panel) and genomic locations of *tar*, *tsr*, and *tap* genes (right panel) in representative *Enterobacteriaceae* genomes. Abbreviations: A, *cheA*; W, *cheW*; R, *cheR*; B, *cheB*; Y, *cheY*; Z, *cheZ*. Emergence of *tar* is shown on the corresponding internal branch of the genome tree. Accession numbers for all CheA, Tar, Tsr, and Tap homologs, genome accessions, and taxonomy information are available in Dataset S1.

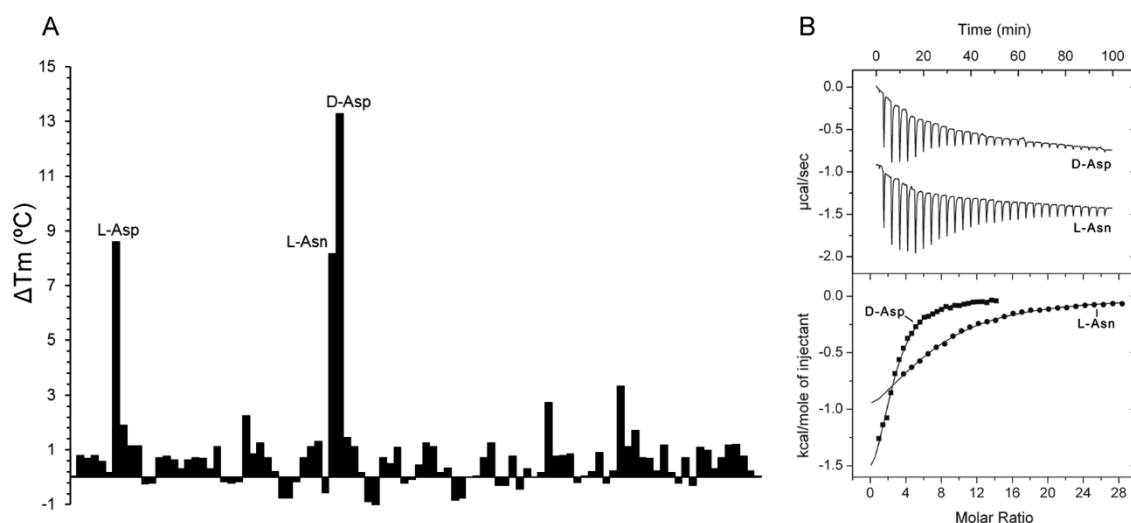


**Figure 37. The Tsr ortholog PacC binds aspartate and asparagine but not serine (A)** Thermal shift assays of PacC-LBD with the compounds of the Biolog array PM1 (different carbon sources). Shown are melting temperature ( $T_m$ ) changes with respect to the ligand-free protein. **(B)** Microcalorimetric titration of 30  $\mu\text{M}$  PacC-LBD with 9.6  $\mu\text{l}$  aliquots of 2 mM D-Asp and 4 mM L-Asn. Upper panel: Raw titration data. Lower panel: Concentration-normalized and dilution heat-corrected raw data of the raw titration data. The lines are the best fits with the “One binding site model” of the MicroCal version of ORIGIN.

## Discussion

Amino acids are of important nutritional value for many bacteria and are also central signal molecules throughout the Tree of Life. The latter notion is supported by our recent study showing that amino acid responsive dCache\_1 domains are present in a large number of bacterial receptor families such as chemoreceptors, sensor kinases, guanylate and diguanylate cyclases and phosphodiesterases or Ser/Thr kinases and phosphatases. These receptors carry out a multitude of different functions such as mediating chemotaxis, regulating gene expression or the control of different second messenger levels; but also in different eukaryotic and archaeal proteins (Gumerov *et al.*, 2022).

It is therefore not astonishing that bacteria have evolved the capacity to sense almost all proteinogenic amino acids (Taguchi *et al.*, 1997b; Oku *et al.*, 2012; Hida *et al.*, 2020). However, these broad sensing capacities have emerged via different mechanisms. We have established that in *P. aeruginosa* this capacity was due to the recent gene duplication and neofunctionalization of chemoreceptors leading to the three paralogous receptors, PctA, PctB and PctC, that possess complementary ligand specificities (Rico-Jiménez *et al.*, 2013a; Gavira *et al.*, 2020). Specifically, PctA is the ubiquitous amino acid sensor (Gumerov *et al.*, 2022), PctC originated from PctA duplication in the common ancestor of the *Pseudomonas* genus, and PctB emerged, via the most recent duplication, which occurred in the common ancestor of the *P. aeruginosa* species (Gavira *et al.*, 2020). In *P. atrosepticum*, broad sensing capacities are also provided by three chemoreceptors; however, they have different evolutionary trajectories. The PacB LBD belongs to the same subfamily of the universal amino acid sensor dCache\_1AA that

also contains the LBD of *P. aeruginosa* PctA. However, in contrast to PctB and PctC of *P. aeruginosa*, PacA and PacC of *P. atrosepticum* are not members of the dCache\_1AA subfamily. Indeed, PacC has an entirely different sensor domain fold - four helix bundle. Interestingly, the PacC/Tsr/Tar subfamily is dominant among *Enterobacteriaceae*, whereas members of PacA and PacB subfamilies show sporadic distribution (Dataset S1). This might be due to the fact that, in addition to sensing amino acids, Tsr transduces oxygen and redox signals that are critical for finding optimal conditions for maximal energy and growth (Rebbapragada *et al.*, 1997) - a functional aspect that potentially represents an evolutionary pressure for the dominance of the PacC/Tsr/Tar subfamily.

Of the 36 chemoreceptors of *P. atrosepticum* SCRI1043, PctC is the only receptor that is encoded in the signaling protein gene cluster. The order of genes in the chemosensory gene cluster in *E. coli* and *P. atrosepticum* is identical. However, phylogenetic analyses clearly show that PacC is an ortholog of Tsr, not of Tar, which is encoded in the *E. coli* chemosensory gene cluster. The term Tsr has been primed based on studies of *E. coli* and *Salmonella enterica* showing that this receptor specifically binds serine (Clarke and Koshland, 1979; Tajima *et al.*, 2011). We show here that the Tsr ortholog PacC does not bind serine, but instead binds D-/L-aspartate and L-asparagine. It is quite likely that, prior to the emergence of Tar, ancestral Tsr had a ligand profile similar to that of PacC. Upon duplication leading to emergence of Tar, the newly born paralog retained the ability to bind aspartate, whereas Tsr has neofunctionalized gaining serine binding ability. Investigating ligand specificity of Tsr orthologs from species close to the root of the *Enterobacteriaceae* genome tree should help validate this hypothesis.

Interestingly, PacC-LBD recognized preferentially D-Asp, a non-proteinogenic amino acid. This contrasts with data on amino acid chemoreceptors from phylogenetically very diverse bacteria like different Pseudomonads (Rico-Jiménez *et al.*, 2013a; Ud-Din *et al.*, 2020), *Sinorhizobium meliloti* (Webb *et al.*, 2017a), *Bacillus subtilis* (Glekas *et al.*, 2012), *Vibrio cholerae* (Nishiyama *et al.*, 2012) or *Campylobacter jejuni* (Rahman *et al.*, 2014) that bind the proteinogenic L-forms. However, the PscA chemoreceptors from the plant pathogens *P. syringae* pv. *tomato* and *P. syringae* pv. *actinidiae* were shown to recognize preferentially and with high affinity ( $K_D$  of 1-2  $\mu$ M) D-Asp (McKellar *et al.*, 2015; Cerna-Vargas *et al.*, 2019). Interestingly, the two D-Asp responsive receptors from *P. syringae* and PacC are non-homologous and belong to different receptor families. Whereas PacC binds its ligands at its four helix bundle domain, the *P. syringae* receptors employ dCache domains for signal recognition. Therefore, two receptor types have evolved in a convergent manner in plant pathogens to sense D-Asp. Since *P. atrosepticum* is also a plant pathogen, data thus suggest a particular relevance of chemoattraction to D-Asp in plant infection or virulence. In accordance with this hypothesis, chemotaxis mediated by the D-Asp responsive chemoreceptor PscA was found to be important for the virulence of *P. syringae* pv. *tomato* in tomato leaves (Cerna-Vargas *et al.*, 2019). Plants are able to synthesize D-Ser and D-Asp *de novo* by aspartate racemases, that showed a wide phylogenetic distribution in plants (Uda *et al.*, 2020), but the function of these D-amino acids in plants is unknown. An increase in the D-Asp concentration in *Arabidopsis thaliana* has been observed during germination and growth (Funakoshi *et al.*, 2008).

Other ligands recognized by PacC are L-Asp and L-Asn, showing a complementarity with the broad range PacB receptor. Whereas L-Asp is one of the two ligands that do not bind to PacB, L-Asn binds with much higher affinity to PacC as compared to PacB. A similar complementarity has



been observed for the *P. aeruginosa* chemoreceptors PctA and PctB. The latter receptor recognizes preferentially L-Gln corresponding to one of the three amino acids that are not recognized by the broad range PctA (Rico-Jiménez *et al.*, 2013a). There appears to be initial evidence for chemoreceptor complementarity for other compound classes. For example, the McpS chemoreceptor of *P. putida* KT2440 binds with high affinity most of the Krebs cycle intermediates, but citrate with relatively low affinity (Lacal *et al.*, 2010a). Citrate is highly abundant in the physiological habitats of this strain that was shown to be a metabolically-versatile saprophyte that is also able to colonize plant roots (Belda *et al.*, 2016). However, *P. putida* KT2440 was also shown to possess with McpQ a complementary chemoreceptor that recognizes exclusively citrate and citrate/malate complexes (Martín-Mora *et al.*, 2016b). Further studies will show to what degree complementarity in chemoreceptor function is a more general phenomenon.

## Supplementary material

MLKTRSRILAA**CSTIVVLSLVINT**FLNYTIANNANKDSIQNTLDAVATSHSIAVSDWVASKTLMISALH  
 DRAIQDEDP I PLFKQIVASGGFLNVYMGYANGTAKFADPGGIPAD**YNPTIRPWY**QQAVKEGKPLATAP**Y**V  
 DMVTNTLVVSFVAPVLEGSTVKGVVGS**D**VTMKSVIENVKAINPSPGSGVLI DRNGTIIAHPDEKLTLLKN  
 ITDIAPAINLNEILSADNAHDVDFSGSTKLV LAKPIAGTSWYMLVALDKAEATAGMRSLLS**TSVITLVII**  
**ALLGTLVIGFIIT**STLKRL LQIRDAMDDISNGNNDLTQRLPDEGHDEVAQIARSFNIFIDKISQVMMQIR  
 DISASLQVAADEISAGNNDLSARTE SAASSIQQTAASLEEISAAVTQSAGSAQQVNAKALLLSKDAGTGG  
 KVVSDVIVTMEEIVVASGKIGDIIGVIDGIAFQTNILALNAAVEAARAGEQGRGFAVVAGEVRS LAQRSA  
 QAAKEIKELIEATVSSVTSGSVQVRQASDTMNEIVSGVSTVSSVMSEITHAADEQMRGINEINKAVAQLD  
 SMVQQNAALVQESAAAASGALQSQAEEELNSVVGAFRV

**Figure S 20. Sequence of the ECA\_RS05475 (PacB) chemoreceptor of *P. atrosepticum* SCRI1043.** The transmembrane regions that flank the ligand binding domain are shown in green and the residues of the conserved amino acid binding motif of the amino acid specific dCache\_1AA domain, as identified in (Gumerov *et al.*, 2022), are in red.

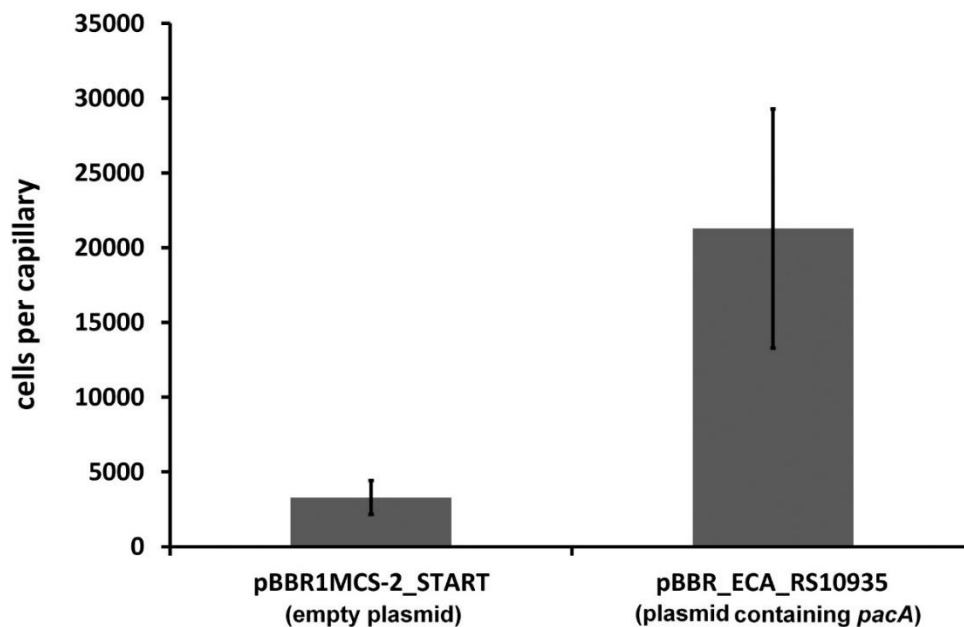


**Figure S 21. Quantitative chemotaxis capillary assays of *P. atrosepticum* SCRI1043 containing the empty plasmid pBBR1MCS-2\_START and plasmid pBBR\_ECA\_RS10935 (harboring the *pacA* gene) towards 1 mM L-proline.** The data have been corrected with the number of cells that swam into buffer-containing capillaries, namely  $530 \pm 233$  cells/capillary for pBBR1MCS-2\_START and  $347 \pm 183$  for pBBR\_ECA\_RS10935. Shown are means and standard deviation from three biological replicates conducted in triplicate.

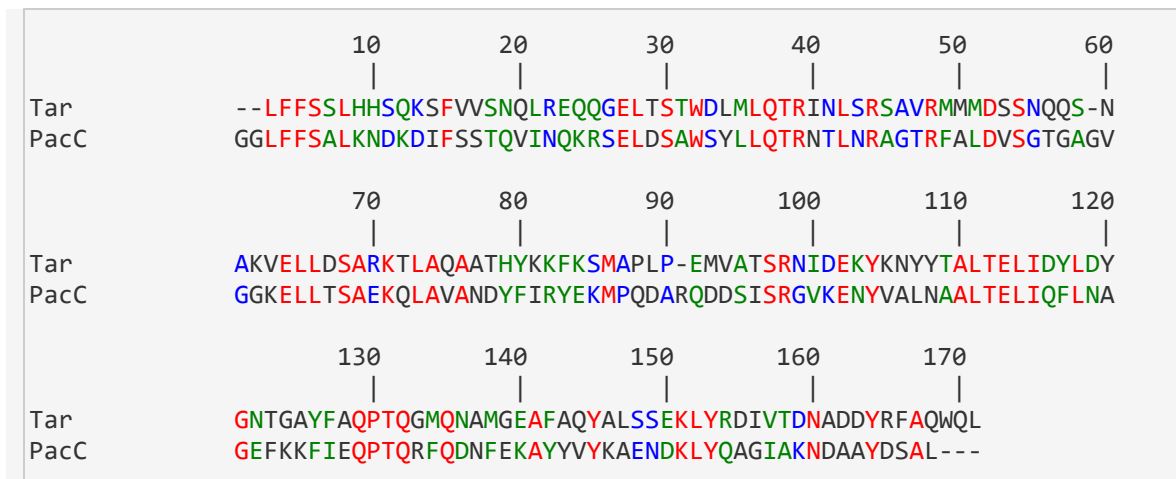


**Figure S 22. Sequence alignment of the ligand binding domains of the *E. coli* Tar and *P. atrosepticum* PacC (ECA\_RS08370) chemoreceptors.** The alignment was done using the CLUSTALW algorithm of the npsa suite (Combet *et al.*, 2000) using the GONNET weight matrix, a gap opening penalty of 10 and a gap extension penalty of 0.2. Red: identical; green: highly similar; blue: weakly similar. The overall sequence identity was 31 %.

**Table S 12. Strains and plasmids used in Chapter 4.**

Strains and plasmids	Genotype or relevant characteristics <sup>a</sup>	Reference
<b>Strains</b>		
<i>Escherichia coli</i> BL21(DE3)	F <sup>-</sup> <i>ompT gal dcm lon hsdS<sub>B</sub>(r<sub>B</sub><sup>-</sup>m<sub>B</sub><sup>-</sup>)</i> λ(DE3 [ <i>lacI lacUV5-T7p07 ind1 sam7 nin5</i> ]) [ <i>malB<sup>*</sup></i> ] <sub>K-12</sub> (λ <sup>S</sup> )	(Jeong <i>et al.</i> , 2009)
<i>E. coli</i> DH5α	F <sup>-</sup> <i>endA1 glnV44 thi-1 recA1 relA1 gyrA96 deoR nupG purB20 φ80dlacZΔM15 Δ(lacZYA-argF)U169, hsdR17(r<sub>K</sub><sup>-</sup>m<sub>K</sub><sup>+</sup>), λ<sup>-</sup></i>	(Woodcock <i>et al.</i> , 1989)
<i>E. coli</i> CC118λ <i>pir</i>	<i>araD Δ(ara, leu) ΔlacZ74 phoA20 galK thi-1 rspE rpoB argE recA1 λpir</i>	(Herrero <i>et al.</i> , 1990)
<i>E. coli</i> β2163	F- RP4-2-Tc::Mu <i>ΔdapA::(erm-pir)</i> ; Km <sup>R</sup> , Em <sup>R</sup>	(Demarre <i>et al.</i> , 2005)
<i>Pectobacterium atrosepticum</i> SCRI1043	Wild type strain	(Bell <i>et al.</i> , 2004)
<i>P. atrosepticum</i> SCRI1043 ΔECA_RS10935	SCRI1043 deletion mutant of <i>ECA_RS10935 (pacA)</i>	(Matilla <i>et al.</i> , 2022b)
<i>P. atrosepticum</i> SCRI1043 ΔECA_RS05475	SCRI1043 deletion mutant of <i>ECA_RS05475 (pacB)</i>	This study
<i>P. atrosepticum</i> SCRI1043 ΔECA_RS08370	SCRI1043 deletion mutant of <i>ECA_RS08370 (pacC)</i>	This study
<b>Plasmids</b>		
pET28b(+)	Km <sup>R</sup> ; protein expression plasmid	Novagen
pET28b-ECA_RS10935-LBD	Km <sup>R</sup> ; pET28b(+) derivative containing <i>ECA_RS10935 (pacA)</i> chemoreceptor gene	(Matilla <i>et al.</i> , 2022b)
pET28b-ECA_RS05475-LBD	Km <sup>R</sup> ; pET28b(+) derivative containing <i>ECA_RS05475 (pacB)</i> chemoreceptor gene	This study
pET28b-ECA_RS08370-LBD	Km <sup>R</sup> ; pET28b(+) derivative containing <i>ECA_RS08370 (pacC)</i> chemoreceptor gene	This study
pUC18Not	Ap <sup>R</sup> ; identical to pUC18 but with two NotI sites flanking pUC18 polylinker	(Herrero <i>et al.</i> , 1990)
pUC18_ΔECA_RS05475	Ap <sup>R</sup> ; 2.0-kb PCR product containing a 1.7-kb deletion of <i>ECA_RS05475</i> inserted into the EcoRI/PstI sites of pUC18Not	This study
pUC18_ΔECA_RS08370	Ap <sup>R</sup> ; 2.0-kb PCR product containing a 1.5-bp deletion of <i>ECA_RS08370</i> inserted into the EcoRI/PstI sites of pUC18Not	This study
pKNG101	Sm <sup>R</sup> ; <i>oriR6K mob sacBR</i>	(Kaniga <i>et al.</i> , 1991)
pKNG101_ΔECA_RS05475	Sm <sup>R</sup> ; 2.1-kb NotI fragment of pUC18_ΔECA_RS05475 was cloned at the same site in pKNG101. Construct for <i>ECA_RS05475</i> deletion	This study
pKNG101_ΔECA_RS08370	Sm <sup>R</sup> ; 2.1-kb NotI fragment of pUC18_ΔECA_RS08370 was cloned at the same site in pKNG101. Construct for <i>ECA_RS08370</i> deletion	This study
pBBR1MCS-2_START	Km <sup>R</sup> ; <i>oriRK2 mobRK2 lacZ</i>	(Obranic <i>et al.</i> , 2013)
pBBR_ECA_RS10935	Km <sup>R</sup> ; pBBR1MCS2_START derivative containing coding sequence for <i>ECA_RS10935</i>	(Matilla <i>et al.</i> , 2022b)

**Table S 13. Oligonucleotides used in Chapter 4:**

<b>Name</b>	<b>sequence (5'-3')</b>	<b>Purpose</b>
ECA_RS05475- NdeI-F	TAATCATATGCTTAATTACACCATAGCCAATAACGC	Construction of pET28b- ECA_RS05475- LBD
ECA_RS05475- BamHI-R	TAATGGATCCTCACAGAGAACGCATGCCAGC	
ECA_RS08370- NdeI-F	TAATCATATGTTTAGTGCATTAATAAATGATAAGGATATCTTC	Construction of pET28b- ECA_RS08370- LBD
ECA_RS08370- BamHI-R	TAATGGATCCTCACGCCGAGTCATACGCTG	
2F-BamHI ECA_RS05475	CTTGCGGCCTGTTGACCATGGATCCGCAATCACAGGCTGAAGAAC	Construction of deletion mutant in <i>ECA_RS05475</i>
2R-PstI ECA_RS05475	TAATCTGCAGTTACCGCCTAAGCCAGGATA	
1F-EcoRI ECA_RS05475	TAATGAATTCTATTGATGCGTCGCAGACAC	
1R-BamHI ECA_RS05475	TAATGGATCCTCGAACAGGCCGCAAGAATG	
1F-EcoRI ECA_RS08370	TAATGAATTCTGCCTTGTGGTCGATCAGT	Construction of deletion mutant in <i>ECA_RS08370</i>
1R-BamHI ECA_RS08370	TAATGGATCCACTCGGAACGCTTCTGGTTA	
2F-BamHI ECA_RS08370	TAATGGATCCATCGGTGAATGGCGGTAAGA	
2R-PstI-HF ECA_RS08370	TAATCTGCAGCAGCAAGTGTATCGCCAAT	



## Chapter 5. Identification of a receptor family that recognizes specifically phosphorylated compounds.

---

*To be published*

Félix Velando<sup>1</sup>, Roberta Genova<sup>1</sup>, Jiawei Xing<sup>2,3</sup>, Miguel A. Matilla<sup>1</sup>, Igor B. Zhulin<sup>2,3</sup>, Tino Krell<sup>1</sup>

<sup>1</sup>Department of Environmental Protection, Estación Experimental del Zaidín, Consejo Superior de Investigaciones Científicas; <sup>2</sup>Department of Microbiology, The Ohio State University, Columbus, OH 43210; <sup>3</sup>Translational Data Analytics Institute, The Ohio State University, Columbus, OH 43210.

### Abstract

---

Chemoreceptor-based signaling pathways are among the most sophisticated and complex bacterial signal transduction systems. Signaling is initiated by the recognition of chemoeffectors by chemoreceptors. We identify here chemoreceptor PacP from *Pectobacterium atrosepticum* that recognized at its sCache\_2 type sensor domain exclusively C3 phosphorylated compounds, namely glycerol 3-phosphate and glycerol 2-phosphate as well as the glycolysis intermediates glyceraldehyde 3-phosphate, dihydroxyacetone phosphate and 3-phosphoglycerate. Signal recognition at the PacP chemoreceptor resulted in a chemoattraction to these compounds. Other members of the C3 phosphorylated compounds responsive domain family were identified by bioinformatic analyses and verified by microcalorimetric titrations. These experiments showed that family members bound preferentially glycerol 3-phosphate (G3P), suggesting that chemoattraction to this compound was a major driving force in the evolution of this domain family. G3P is a central signal molecule in mammals, plants and bacteria. G3P levels in different plant exudates are increased in response to different stresses and infection and is a major signaling for generating systemic acquired resistance of plants. Further experiments will show to what degree these changes in the G3P exudate concentration will induce chemotaxis and alter the composition of the rhizo- or phyllosphere.

---

## Introduction

---

Bacteria contain many different receptor families that monitor the concentration of specific signals in the extracytoplasmic space (Galperin, 2018). Major families include histidine kinases; chemoreceptors; adenylate, diadenylate and diguanylate cyclases and certain cAMP, c-di-AMP and c-di-GMP phosphodiesterases; extracytoplasmic function sigma factors and Ser/Thr/Tyr protein kinases and phosphoprotein phosphatases. chemoreceptors, sensor histidine kinases, diguanylate cyclases and phosphodiesterases, The cellular responses mediated by these receptors are multiple and include different types of motility, changes in gene expression or alteration of a number of second messenger levels (Galperin, 2018). Hundreds of different sensor domains have evolved (Ortega *et al.*, 2017a; Gumerov *et al.*, 2020) and new sensor domains are regularly discovered (Elgamoudi *et al.*, 2021; Martín-Rodríguez *et al.*, 2022). The same type of sensor domain is frequently found in different signal transduction systems (Shu *et al.*, 2003; Ulrich and Zhulin, 2005), indicating that these domains have been exchanged and recombined with different during evolution. A major bottleneck in microbiology consists in the lacking information of signal molecules that interact with sensor domains and that stimulate receptors.

About half of the sequenced bacteria contain genes for chemoreceptors (Wuichet and Zhulin, 2010; Sanchis-López *et al.*, 2021), which are protein that stimulate chemosensory pathways. Most of these cascades mediate chemotaxis, whereas others carry out alternative cellular functions or are associated with type IV pili-based motility (Wuichet and Zhulin, 2010; Gumerov *et al.*, 2021). Chemotaxis is the directed, flagella driven swimming movement in gradients of chemoeffectors that are signals recognized by chemoreceptors. The primary motivation for chemotaxis is to access nutrient sources (Colin *et al.*, 2021). However, chemotaxis has also been observed for different signal molecules like quorum sensing molecules, hormones or neurotransmitters that provide the bacterium with useful information on their environment (Lopes and Sourjik, 2018; Zhang *et al.*, 2020; Santamaría-Hernando *et al.*, 2022). Chemoreceptors that have been reported for a number of different compound families including amino acids, organic acids, quaternary amines, polyamines, purine compounds, sugars, aromatic hydrocarbons, metal ions, inorganic anions or oxygen (Matilla *et al.*, 2022a).

Several studies have shown that chemotaxis is essential for an effective entry of plant pathogens into plants (Matilla and Krell, 2018b). This notion is also supported by the observation that plant pathogens contain more chemoreceptors than the average bacterium (Lacal *et al.*, 2010b; Matilla and Krell, 2018; Sanchis-López *et al.*, 2021). Data indicate that chemotaxis to compounds released by stomata and wounds enables efficient plant entry (Matilla and Krell, 2018b). In our laboratory we study the chemoreceptor based signal sensing by *Pectobacterium atrosepticum*, which is among the top 10 most relevant plant pathogens (Mansfield *et al.*, 2012). The genome of *P. atrosepticum* strain SCRI1043 encodes 36 chemoreceptors that differ in topology and LBD type (Gumerov *et al.*, 2020). Most prevalent are the 24 chemoreceptors that contain a four-helix bundle type LBD (Figure 12). So far, the function of only three chemoreceptors has been identified. PacA responds to different quaternary amines and proline (Matilla *et al.*, 2022b), whereas PacB and PacC are amino acid chemoreceptors (insert reference one available).

SCRI1043 contains a single chemoreceptor with a sCache\_2 (ECA\_RS12390) domain. This domain family is present in about 3 % of chemoreceptors (Sanchis-López *et al.*, 2021). A number of



chemoreceptors with a sCache\_2 sensor domain have been identified in phylogenetically diverse species. Most of these receptors recognize different C1 to C4 carboxylic acids (Pokkuluri *et al.*, 2013; García *et al.*, 2015; Brewster *et al.*, 2016; Martín-Mora *et al.*, 2018b; Compton *et al.*, 2018; Gasperotti *et al.*, 2020). In contrast, the sCache\_2 containing TlpB chemoreceptor of *Helicobacter pylori* recognizes urea and derivatives (Huang *et al.*, 2015; Hanyu *et al.*, 2019; Aguilar *et al.*, 2022). Here we show that chemoreceptor ECA\_RS12390 (McpP) binds specifically phosphorylated C3 compounds, among which 3 glycolysis intermediates. Bioinformatic analyses predicted 6 domains with a similar ligand profile in phylogenetically diverse species. Some of these predictions were verified experimentally. To the best of our knowledge, this is the first report on a domain family that binds specifically phosphorylated compounds.

## Materials and Methods

---

**Bacterial strains and growth conditions:** Bacterial strains used in this study are listed in Table S14. *P. atrosepticum* SCRI1043 and its derivative strains were routinely grown at 30 °C in Lisogeny Broth (5 g/l yeast extract, 10 g/l bacto tryptone, 5 g/l NaCl) or minimal medium (0.41 mM MgSO<sub>4</sub>, 7.56 mM (NH<sub>4</sub>)<sub>2</sub>SO<sub>4</sub>, 40 mM K<sub>2</sub>HPO<sub>4</sub>, 15 mM KH<sub>2</sub>PO<sub>4</sub>) supplemented with 0.2 % (w/v) glucose as carbon source. *E. coli* strains were grown at 37 °C in LB. When appropriate, antibiotics were used at the following final concentrations (in µg ml<sup>-1</sup>): kanamycin, 50, ampicillin, 100.

**Plasmids:** The DNA sequence for gene ECA\_RS12390 was amplified using primers ECA\_RS12390-NdeI-F and ECA\_RS12390-BamHI-R from genomic DNA of *P. atrosepticum* SCRI1043 and cloned into plasmid pBBR-MS2-START digested with NdeI and BamHI. The resulting plasmid was termed pBBR\_ECA\_RS12390. This plasmid was verified by PCR and sequencing the insert gene and its flanking regions, and subsequently transformed into *P. atrosepticum* SCRI1043 by electroporation. The pET28b(+) derivatives encoding the LBD of the different receptors analysed in this study (Table S14) were purchased from GeneScript. The sequences of the proteins analysed in this study are provided in Table S16.

**Protein overexpression and purification:** Plasmids for the overexpression of the different proteins were transformed into *E. coli* BL21 (DE3). The resulting strains were grown under continuous stirring (200 rpm) at 30 °C in 2-liter Erlenmeyer flasks containing 500 ml of LB medium supplemented with 50 µg/ml kanamycin. At an OD<sub>660</sub> of 0.5, protein expression was induced by the addition of 0.1 mM isopropyl β-D-1-thiogalactopyranoside (IPTG). Growth was continued at 16 °C overnight prior to cell harvest by centrifugation at 10 000 x g for 20 min. Cell pellets were resuspended in buffer A (Table S14) and subsequently broken by French press treatment at 62.5 lb/in<sup>2</sup>. After centrifugation at 20 000 x g for 30 min, supernatants were loaded onto 5-ml HisTrap HP columns (Amersham Biosciences) equilibrated with buffer A and eluted with a linear gradient of buffer B. All proteins were purified at 4 °C. Purified proteins were dialysed overnight into the corresponding analysis buffers (Table S14) for immediate analysis.

**Differential Scanning Fluorimetry-Based Thermal Shift Assays:** Assays were carried out using a MyIQ2 Real-Time PCR instrument (BioRad, Hercules, CA, USA). Ligand solutions were prepared by dissolving the array compounds in 50 µL of MilliQ water, which, according to the information provided by the manufacturer, corresponds to a concentration of 10–20 mM. Freshly purified proteins were dialyzed into the analysis buffer (as described later). Compound arrays PM1,

PM2A (carbon sources), PM3B (nitrogen sources) and PM4A (phosphorous and sulphur sources) from Biolog (<https://www.biolog.com/>) were used. The composition of these compound arrays can be found at [http://208.106.130.253/pdf/pm\\_lit/PM1-PM10.pdf](http://208.106.130.253/pdf/pm_lit/PM1-PM10.pdf). Experiments were conducted in 96-well plates and each assay mixture contained 20  $\mu$ l of the dialyzed protein (at 80–50  $\mu$ M), 2  $\mu$ l of 5 $\times$  SYPRO orange (Life Technologies, Eugene, Oregon, USA) and 2.5  $\mu$ l of the resuspended array compounds or the equivalent amount of buffer in the ligand-free control. Samples were heated from 23 to 85  $^{\circ}$ C using a scan rate of 1  $^{\circ}$ C/min. The protein unfolding curves were monitored by detecting changes in SYPRO Orange fluorescence. The  $T_m$  values were determined using the first derivative values of the raw fluorescence data.

*Isothermal titration calorimetry (ITC)*: All experiments were conducted on a VP-microcalorimeter (Microcal, Amherst, MA) at 15  $^{\circ}$ C for ECA\_RS12390-LBD and at 20  $^{\circ}$ C for the remaining proteins. Proteins were dialyzed into the analysis buffers specified in Table S15. Dialysed protein at a concentration of 30 to 80  $\mu$ M was placed into the sample cell and titrated with aliquots of ligand solutions (1 to 10 mM) freshly prepared in dialysis buffer. The mean enthalpies measured from the injection of the ligands into analysis buffer were subtracted from raw titration data prior to data analysis with the MicroCal version of ORIGIN. Data were fitted with the 'One binding site model' of ORIGIN.

*Quantitative capillarity chemotaxis assays*. Overnight cultures of *P. atrosepticum* SCRI1043 were grown at 30  $^{\circ}$ C in minimal medium. At an  $OD_{660}$  of 0.4-0.45, the cultures were washed twice with chemotaxis buffer (50 mM  $K_2HPO_4/KH_2PO_4$ , 20  $\mu$ M EDTA and 0.05% (v/v) glycerol, pH 7.0) and diluted to an  $OD_{660}$  of 0.1 in the same buffer. Subsequently, 230  $\mu$ l of the resulting bacterial suspension were placed into the wells of 96-well plates. One-microliter capillary tubes (P1424, Microcaps; Drummond Scientific) were heat-sealed at one end and filled with either the chemotaxis buffer (negative control) or chemotaxis buffer containing the compounds to be assayed. The capillaries were immersed into the bacterial suspensions at its open end. After 30 min at room temperature, the capillaries were removed from the bacterial suspensions, rinsed with sterile water and the content expelled into 1 ml of 40 mM  $K_2HPO_4$ , 15 mM  $KH_2PO_4$ . Serial dilutions were plated onto minimal medium supplemented with 15 mM glucose as carbon source. The number of colony forming units was determined after 36 h incubation at 30  $^{\circ}$ C. In all cases, data were corrected with the number of cells that swam into buffer containing capillaries.

*Protein target selection*. Molecular docking was performed on PacP and phosphorylated compounds using DiffDock with 10 inference steps (Corso, G. *et al.*, n.d.). Protein homologs of PacP (WP\_011094075.1) were collected from RefSeq using BLAST (E-value < 0.05) (O'Leary *et al.*, 2016). Sequences were aligned using MAFFT (Kato *et al.*, 2019) and reduced to 98% redundancy using Jalview (Waterhouse *et al.*, 2009). The sCache\_2 domain regions (WP\_011094075.1/1-203) from the aligned sequences were used for phylogenetic analysis. A maximum likelihood tree was constructed using MEGA with the JTT model and 100 bootstraps (Kumar *et al.*, 2018). The protein targets were selected from the phylogenetic tree based on the location and the key residue for ligand-binding.

## Results

### Chemoreceptor ECA\_RS12390 (PacP) binds exclusively phosphorylated C-3 compounds

To identify the ligands recognized by chemoreceptor ECA\_RS12390, its individual sensor domain was overexpressed in *E. coli* and purified by affinity chromatography. The protein was subsequently submitted to thermal shift assays based ligand screening using the Biolog compound arrays PM1, PM2, PM3B and PM4. This approach measures ligand-induced increases in the protein thermal stability, as quantified by the midpoint of the thermal unfolding transition ( $T_m$ ). Figure 38 shows the  $T_m$  changes induced by the 95 compounds of the PM4A compound array that contains different phosphorylated and sulfonated compounds. Significant increases were observed for glycerol 3-phosphate, carbamoylphosphate and 3-phosphoglycerate (Figure 38). No significant increases in  $T_m$  were recorded for the remaining compound arrays, including carboxylic acids that were shown to bind to other sCache\_2 domains (Pokkuluri *et al.*, 2013; García *et al.*, 2015; Brewster *et al.*, 2016; Martín-Mora *et al.*, 2018b; Compton *et al.*, 2018; Gasperotti *et al.*, 2020).

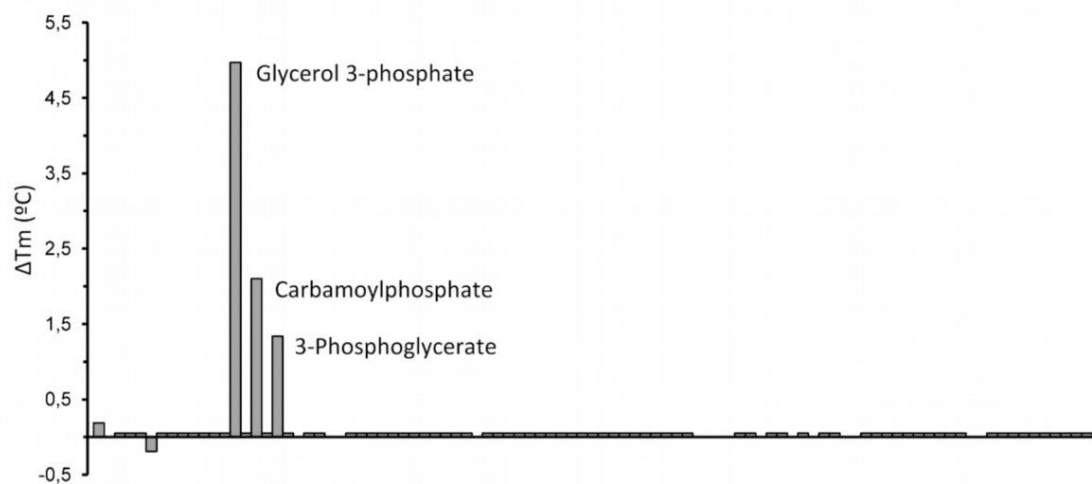


**Figure 38. Thermal shift assays of ECA\_RS12390 (PacP-LBD) with the compounds of the Biolog array PM4A (phosphorous and sulfur sources).** Shown are  $T_m$  changes with respect to the ligand-free protein.

We subsequently conducted Isothermal Titration Calorimetry binding studies to characterize these binding events. The titration of ECA\_RS12390-LBD with glycerol 3-phosphate (G3P) resulted in large exothermic heat changes (Figure 39A), and data analysis resulted in a dissociation constant of  $3.2 \pm 0.2 \mu\text{M}$  (Table 5). The binding of 3-phosphoglycerate occurred with significantly lower affinity ( $K_D = 88 \pm 5 \mu\text{M}$ ), whereas the titration with carbamoylphosphate did not result in binding heats. Due to the restriction of ligand dilution heats, ITC only permits monitoring higher affinity binding, indicating that carbamoylphosphate may bind with an affinity that is not detectable by ITC.

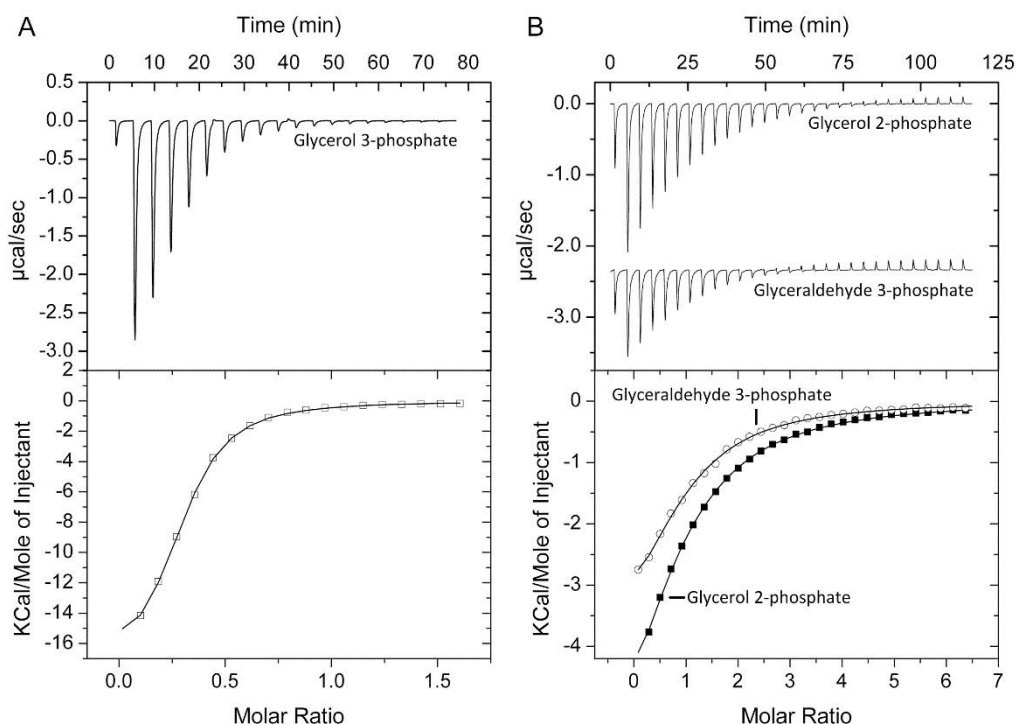


**Figure 39. Microcalorimetric titration of PacP-LBD with different phosphorylated compounds.** A) Titration of 80  $\mu\text{M}$  PacP-LBD with 8  $\mu\text{l}$  aliquots of 1 mM glycerol 3-phosphate. B) Titration of 80  $\mu\text{M}$  PacP-LBD with 8  $\mu\text{l}$  aliquots of 2 mM glycerol 2-phosphate and 2.5 mM glyceraldehyde 3-phosphate. Upper panels: Titration raw data. Lower panels: Concentration-normalized and dilution heat-corrected raw data of the raw titration data. The lines are the best fits with the “One binding site model” of the MicroCal version of ORIGIN.

**Table 5. Results of microcalorimetric binding studies of phosphorylated compounds to the LBDs of different chemoreceptors. Gal3P: glyceraldehyde 3-phosphate, DHAP: dihydroxyacetone phosphate, 3PG: 3-phosphoglycerate, G3P: glycerol 3-phosphate, G2P: glycerol 2-phosphate.**

Rec. No.	Acc. code	Species	$K_D$ ( $\mu\text{M}$ )				
			GAP	DHAP	3PG	G3P	G2P
1	WP_01109407 5.1	<i>P. atrosepticum</i> <sup>a</sup>	58 $\pm$ 2	13 $\pm$ 1	88 $\pm$ 5	3.2 $\pm$ 0.2	72 $\pm$ 2
2	WP_13615734 2.1	<i>Brenneria roseae</i> <sup>a</sup>	253 $\pm$ 11	99 $\pm$ 10	261 $\pm$ 17	11 $\pm$ 0.2	90 $\pm$ 3
3	WP_00646468 8.1	<i>Herbaspirillum frisingense</i> <sup>b</sup>	No binding	109 $\pm$ 14,4	No binding	33 $\pm$ 0,3	36 $\pm$ 2
4	WP_15828185 1.1	<i>Rivicola pingtungensis</i> <sup>c</sup>	100 $\pm$ 2	230 $\pm$ 9,9	926 $\pm$ 8	7 $\pm$ 0,2	60 $\pm$ 2
5	WP_02844467 8.1	<i>Chitinimonas koreensis</i> <sup>b</sup>	No binding	No binding	No binding	No binding	No binding
6	WP_17406224 8.1	<i>Agrobacterium larrymoorei</i> <sup>d</sup>	No binding	No binding	No binding	No binding	No binding
7	WP_01991537 5.1	<i>Methyloversatilis discipulorum</i> <sup>e</sup>	No binding	No binding	No binding	No binding	No binding

<sup>a</sup> belongs to the order *enterobacteriales*

<sup>b</sup> belongs to the order *burkholderiales*

<sup>c</sup> belongs to the order *neisseriales*

<sup>d</sup> belongs to the order *rhizobiales*

<sup>e</sup> belongs to the order *rhodocyclales*

Using ITC we then explored the binding of other compounds. No binding was observed for 2-phosphoglycerate. As shown in Figure 39B binding was also observed for glycerol 2-phosphate and glyceraldehyde 3-phosphate that bound with respective  $K_D$  values of  $72 \pm 2$  and  $58 \pm 2 \mu\text{M}$ . In addition, dihydroxyacetone phosphate showed high affinity binding with a  $K_D$  of  $13 \pm 1 \mu\text{M}$ . As previously mentioned, carboxylic acids are recognized by other sCache\_2 type sensor domains. However, microcalorimetric titrations with maximal concentrations of pyruvate and lactate did not reveal binding, confirming the results obtained by the thermal shift assays. The ligand spectrum of this receptor is summarized in Figure 40. This receptor thus binds specifically phosphorylated C3 compounds, which is to the best of our knowledge the first bacterial receptor that binds exclusively phosphorylated ligands. Three ligands, glyceraldehyde 3-phosphate, dihydroxyacetone phosphate and 3-phosphoglycerate are glycolysis intermediates (Figure 40). G3P is an intermediate that connects glycolysis, glycerol metabolism and triacylglycerol synthesis (Cronan, 2003; Nikel *et al.*, 2014). In addition, G3P homeostasis is important for growth and virulence factor synthesis in *P. aeruginosa* (Liu *et al.*, 2022b:1). Glycerol 2-phosphate can serve as sole phosphorous source for bacteria (Yang *et al.*, 2009). We have renamed ECA\_RS12390 PacP (*Pectobacterium atropeticum* chemoreceptor for phosphorylated compounds).

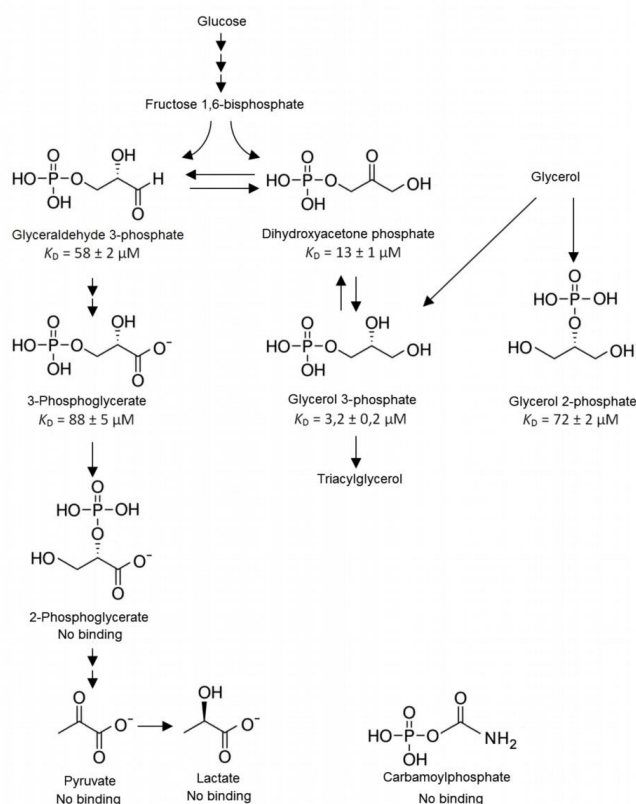


**Figure 40. Summary of binding studies to PacP-LBD.** Shown are the structures of ligands as well as their corresponding dissociation constants as derived from microcalorimetric titrations.

### PacP mediates chemoattraction to its chemoeffectors

We subsequently conducted quantitative capillary chemotaxis assays to determine whether the PacP ligands induce chemotaxis. However, analyses of the wild type strain resulted in only a very modest response. This was reminiscent to the weak chemotaxis that we observed for the PacA-mediated chemotaxis to choline (Matilla *et al.*, 2022b) that was due to a low receptor abundance under the experimental conditions used. In analogy to this study, we cloned the *pacP* sequence into plasmid pBBR1 that was then inserted into *P. atrosepticum*. As shown in Figure 41 the overexpression of the *pacP* gene resulted in a chemoattraction phenotype that was significantly higher than that of the strain containing the empty plasmid, indicating that the chemoattraction observed is due to the action of PacP.

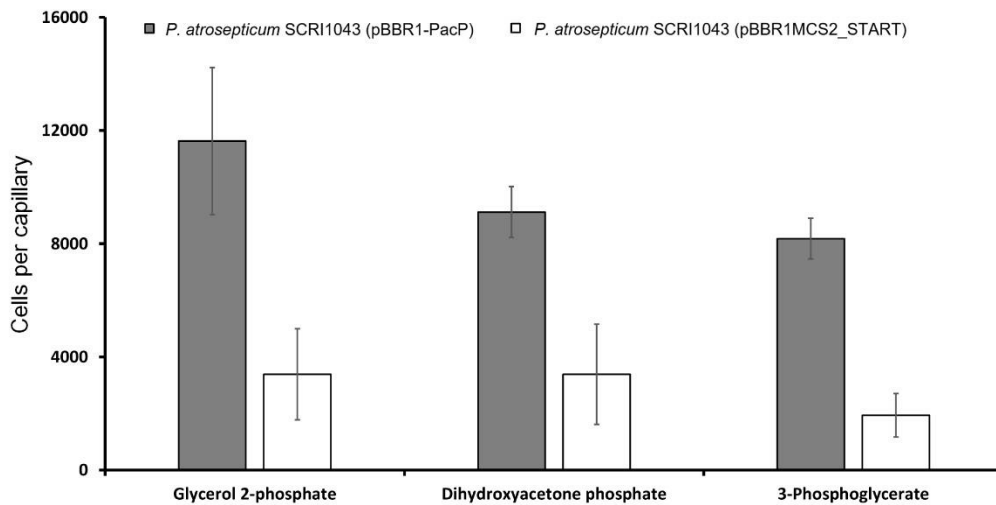
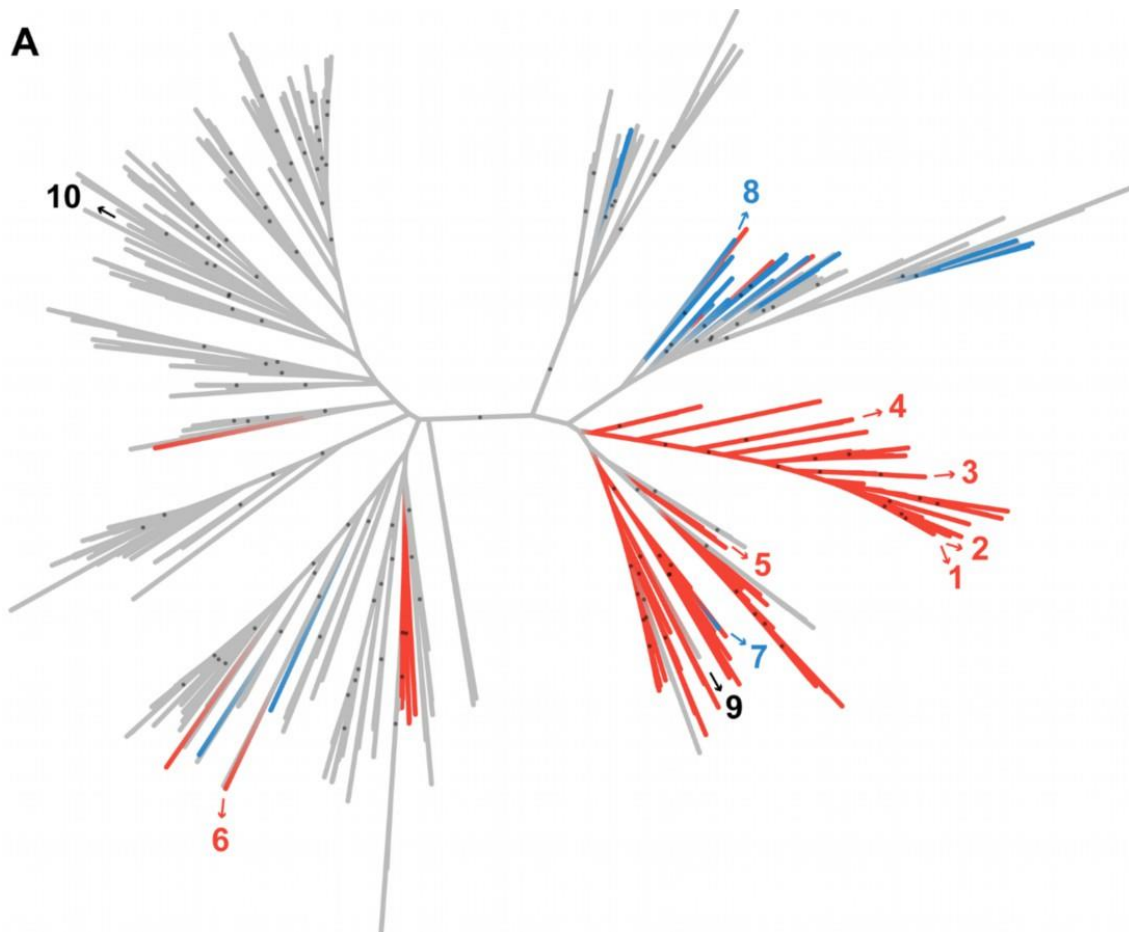


**Figure 41.** Capillary chemotaxis assays of *P. atrosepticum* SCRI1043 containing the empty plasmid pBBR1MCS-2\_START and its derivative pBBR1-PacP causing expression of chemoreceptor ECA\_RS12390 (PacP). Data have been corrected with the number of cells that swam into buffer-containing capillaries ( $614 \pm 839$  cells per capillary for pBBR1MCS-2\_START and  $541 \pm 758$  for pBBR1-PacP).

### Definition of the protein family

Molecular docking indicates that Arg105 in PacP is the key residue for phosphate-sensing (data not shown). To identify other chemoreceptors that also bind phosphorylated compounds, we collected 3,862 PacP homologs from the RefSeq protein database, from which 387 nonredundant sCache\_2 domains were used for phylogenetic analysis (Figure 42A). A major branch of the phylogenetic tree contains PacP (receptor 1) and its closely related homologs (receptors 2-4), all of which share conservation at the putative binding sites, including Arg105 (Figure 42A, 42B). We expect these homologs to bind phosphorylated compounds similarly to PacP.

To explore ligand-binding in distant homologs from other branches, we further selected two targets with conserved Arg (receptors 5 and 6), two targets with Arg to Lys substitutions (receptors 7 and 8), and two targets with Arg to Leu substitutions (receptors 9 and 10) (Figure 42A). We expect that the homologs without the key residue (receptors 9 and 10) will not bind phosphorylated compounds, whereas the remaining homologs with Arg or Lys (receptor 5-8) may bind the same ligands if Arg or Lys is the only determinant or may not bind these ligands if other residues are also required for binding (Figure 42B).



**B**

1) WP_011094075.1(PacP)	RYFF (9) YV <b>H</b> PNP <b>R</b> RIG (11) ER <b>Y</b> R (23) VE <b>K</b> L <b>Y</b> AV (12) GD <b>Y</b> I
2) WP_136157342.1	R <b>Y</b> FF (9) YV <b>H</b> PNP <b>R</b> RVG (11) ER <b>Y</b> R (23) VE <b>K</b> L <b>Y</b> AI (12) GD <b>Y</b> I
3) WP_006464688.1	N <b>Y</b> YF (9) YV <b>H</b> PNP <b>R</b> RVG (10) DR <b>Y</b> R (23) VQ <b>K</b> L <b>Y</b> AV (12) GA <b>Y</b> I
4) WP_158281851.1	R <b>Y</b> LW (9) LV <b>H</b> PNP <b>R</b> RVN (10) DE <b>Y</b> R (23) VG <b>K</b> L <b>Y</b> AL (12) GG <b>Y</b> L
5) WP_028444678.1	N <b>Y</b> FF (8) LI <b>H</b> PKTE <b>R</b> IG (15) AV <b>Y</b> A (25) LP <b>K</b> LNGV (12) GFFI
6) WP_174062248.1	G <b>Y</b> MF (8) MF <b>H</b> PDP <b>R</b> RVG (16) ELVR (22) FL <b>K</b> SSYA (12) GV <b>Y</b> V
7) WP_019915375.1	H <b>Y</b> MF (8) LA <b>H</b> VRKE <b>K</b> LG (15) QT <b>Y</b> R (23) LP <b>K</b> ISGV (12) GFFV
8) WP_028536266.1	D <b>Y</b> IF (8) LV <b>H</b> GNPD <b>K</b> EG (17) QT <b>Y</b> R (23) LP <b>K</b> ISGV (12) GV <b>F</b> V
9) WP_189529961.1	T <b>Y</b> IF (8) VV <b>H</b> PKTD <b>L</b> IG (16) EA <b>Y</b> E (23) VQ <b>K</b> LNGV (12) GV <b>Y</b> L
10) WP_028866120.1	N <b>Y</b> FW (8) IM <b>H</b> PVKP <b>Q</b> LA (17) EFVR (22) LE <b>K</b> ISYV (12) GI <b>Y</b> V

**Figure 42. PacP homologs.** (A) Maximum likelihood tree of sCache\_2 domains from PacP homologs. Protein targets selected for experimental analysis are labeled on the tree. Arg105 is proposed as the key residue for phosphate-sensing in PacP (receptor 1). Colored branches indicate sCache\_2 domains with different residues at this site: red, Arg; blue, Lys; gray, other residues. Dots indicate branches with bootstrap values not less than 70. (B) Multiple sequence alignment of experimentally studied protein targets. Putative binding sites for phosphorylated compounds are highlighted in yellow. The key binding site Arg105 or Lys105 (PacP numbering) is highlighted in red or blue, respectively.

### Experimental verification of ligand binding by family members

To verify these bioinformatic predictions we have selected three proteins, receptors 2 to 4 (Table 5), that were part of the major branch in the phylogenetic tree (Figure 42). In addition, we have selected three proteins (receptors 5 to 7 in Table 5) that had a substitution in the binding motif, such as the replacement of R105 by K. Furthermore, three proteins were selected (receptors 8 to 10 in Table 5) that did not possess the binding motif identified. All six proteins could be produced as soluble and stable proteins. Microcalorimetric titration with proteins from the major branch (receptors 2 to 4) all showed binding of phosphorylated compounds. Whereas receptors 2 and 4 bound all the five PacP ligands, receptor 3 bound only three of them, namely G3P, glycerol 2-phosphate and dihydroxyacetone phosphate (Table 5). Taken together PacP and receptors 2 to 4, a clear pattern in the molecular recognition was observed, since G3P was in all cases the ligand that showed highest affinity. This ligand preference is well illustrated by the microcalorimetric binding data of the 5 ligand that bound to receptor 4 (Figure 43). These data thus suggest that the receptor has primarily evolved to recognize preferentially this compound. In contrast, receptors 5 to 7, being further removed from the primary branch in the tree (Figure 42) failed to bind any of the 5 PacP ligands.

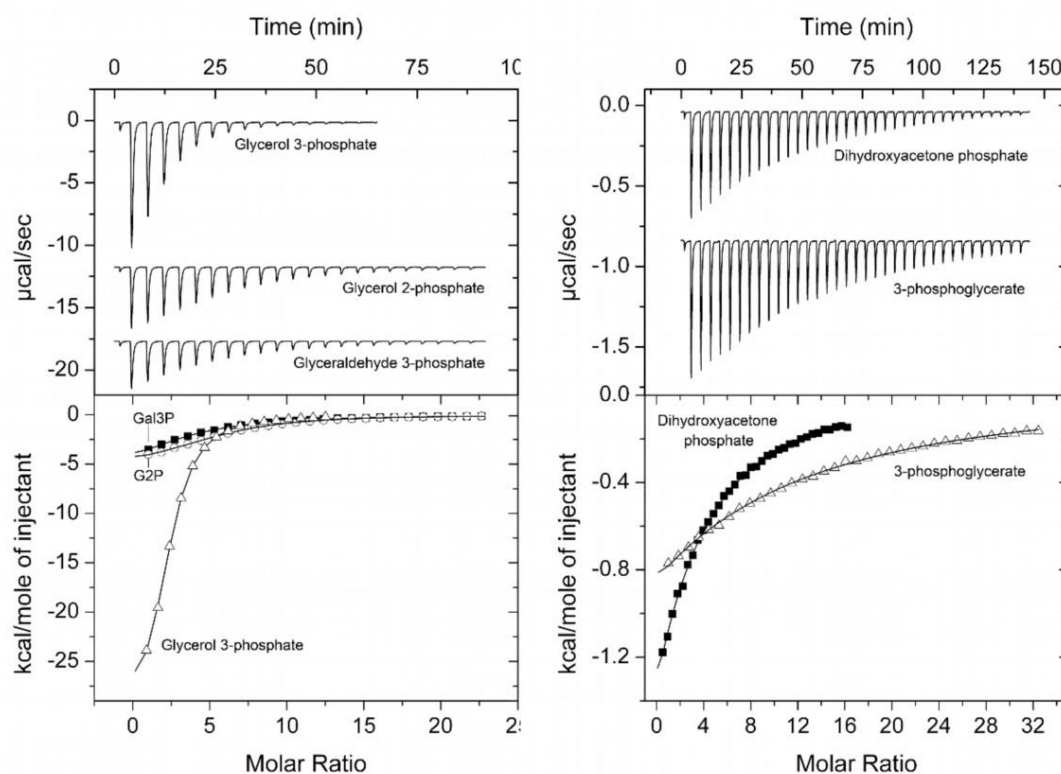


**Figure 43. Microcalorimetric titration of the Ligand Binding Domain of chemoreceptor WP\_158281851.1 from *Rivcola pingtungensis* with its different phosphorylated compounds. (A) Titration of 33 µM protein with 8 µl aliquots of 3 mM glycerol-3-phosphate, 5 mM glycerol 2-phosphate and 5 mM glyceraldehyde 3-phosphate. (B) Titration of 33 µM protein with 8 µl aliquots of 2.5 mM dihydroxyacetone phosphate and 5 mM 3-phosphoglycerate. Upper panels: Titration raw data. Lower panels: Concentration-normalized and dilution heat-corrected raw data of the raw titration data. The lines are the best fits with the “One binding site model” of the MicroCal version of ORIGIN. G2P: glycerol 2-phosphate; Gal3P: glyceraldehyde 3-phosphate.**



Other s\_Cache2 LBD-containing chemoreceptors have been found to bind organic acids (Alvarez-Ortega and Harwood, 2007; Oku *et al.*, 2014). Furthermore, molecular docking predicts PacP weak binding to acetate, pyruvate and propionate (data not shown). ITC Binding studies with the proteins that did not bind phosphorylated compounds showed they bound organic acids as well (Table 6). Both of the analyzed proteins bound malic acid, succinic acid and fumaric acid, different intermediate compounds of the Krebs cycle. These compounds have clear metabolic value. Thus, it is possible that the PacP family of chemoreceptors has evolved from a family of chemoreceptors containing S\_Cache 2 domains that recognize preferentially Krebs cycle intermediates. In a *Pab* SCRI1043, glycerol-2-phosphate can support growth, while dihydroxyacetone phosphate and glyceraldehyde-3-phosphate cannot (data not shown). G3P, the preferent ligand of the PacP family of proteins, probably is also able to support growth and the possible reason for the evolution of PacP homologues in plant-associated bacteria is dual; it permits host localization through recognition of a specific signal, which is also a compound with metabolic value for the bacteria.

**Table 6. Ligands identified for proteins with substitutions in the phosphorylated C3 compounds binding motif.**

	<b>Compound</b>	<b>ITC K<sub>D</sub> (μM)</b>
WP_028444678.1-LBD ( <i>Chitinimonas koreensis</i> )	<b>Citric acid</b>	10,3 ± 2
	<b>Fumaric acid</b>	67,6 ± 6,1
	<b>Succinic acid</b>	126,9 ± 4,7
	<b>Tricarballic acid</b>	14,5 ± 0,5
	<b>Malic acid</b>	61,3 ± 1,7
WP_174062248.1-LBD ( <i>Agrobacterium larrymoorei</i> )	<b>Succinic acid</b>	90 ± 4
	<b>Fumaric Acid</b>	90 ± 4
	<b>Malic Acid</b>	63 ± 0,5

## Discussion

Chemoreceptors have so far been shown to bind and mediate chemotaxis to a number of different compound families (Matilla *et al.*, 2022a). In this study we identify a chemoreceptor family that recognizes with C3 phosphorylated compounds a novel compound family, expanding thus the range of so far known chemoreceptor ligands. To the best of our knowledge this is the first report on a bacterial receptor family that recognizes specifically phosphorylated compounds and first evidence of chemotaxis to phosphorylated compounds. A significant number of sCache\_2 domain containing chemoreceptors recognized non-phosphorylated C3 compounds such as pyruvate and propionate (García *et al.*, 2015; Brewster *et al.*, 2016; Compton *et al.*, 2018). It would therefore be of interest to establish the evolutionary relationship between both receptor subfamilies.

In analogy to a number of other chemoeffectors such as acetylcholine, histamine or GABA (Colin *et al.*, 2021), there is evidence that the ligands identified in this study are of nutritional value but are also important signal molecules that mediate plant-bacteria interactions. Three of the ligands, glyceraldehyde 3-phosphate, dihydroxyacetone phosphate and 3-phosphoglycerate form part of the glycolysis pathway. We have identified in the past with McpS a chemoreceptor

for Krebs cycle intermediates (Lacal *et al.*, 2010a; Pineda-Molina *et al.*, 2012). In this context, it is thus not surprising that there are chemoreceptors for compounds that feed into the Krebs cycle. The nutritional values of the remaining phosphorylated compounds is evidenced by the fact that glycerol 2-phosphate and G3P can serve as sole phosphorous (Yang *et al.*, 2009) or carbon source (Stasi *et al.*, 2019) for bacteria. In addition, there are transporters for G3P that mediate the uptake of this compound (Huang *et al.*, 2003; Wuttge *et al.*, 2012). Furthermore, glycerolipids, major components of the biological membranes are synthesized from G3P (Ohshima *et al.*, 2008).

The domain family identified in this work bound preferentially G3P. This compound is a very important signal molecule in bacteria, human and plants. For example, in *P. aeruginosa*, glycerol-3-phosphate accumulation affected twitching motility, pyocyanine and exopolysaccharide biosynthesis, antibiotics resistance and oxidative stress tolerance (Liu *et al.*, 2022b). In mammalian cells, G3P levels regulated glycolysis and glucose oxidation, cellular redox and ATP production, gluconeogenesis, glycerolipid synthesis as well as fatty acid oxidation (Mugabo *et al.*, 2016). *P. atrosepticum* is a plant pathogen and two of the domains that bound phosphorylated C3 compounds were from plant-associated bacteria, *Brenneria roseae* (Brady *et al.*, 2014) and *Herbaspirillum frisingense* (Oliveira *et al.*, 2021). In this context it is important to note that G3P is among the most relevant plant signal molecules (Kachroo *et al.*, 2022). Of the 5 PacP ligands, metabolomics analysis showed that G3P is the only compound that could be detected in root exudates (Tawaraya *et al.*, 2014c; Tawaraya *et al.*, 2014a). There is evidence that G3P is a stress-related signal molecule. G3P levels in root extracts were also significantly increased in response to phosphate starvation (Tawaraya *et al.*, 2014b). Xu *et al.* have investigated changes in the root endosphere that were induced by drought (Xu *et al.*, 2018). Of the 114 compounds that were enriched in the drought treated endosphere, G3P was increased about 22 000-fold corresponding by far to the compound with the most significant increase. Further experiments showed that this increase was due to changes in the host and not the rhizosphere (Xu *et al.*, 2018). In addition to be a stress-related signal molecule, G3P is a critical inducer of systemic acquired resistance (SAR) in plants, since mutants defective in G3P synthesis are unable to induce SAR (Chanda *et al.*, 2008; Chanda *et al.*, 2011; Shine *et al.*, 2019a). Plant infection induces SAR by stimulating G3P biosynthesis via the upregulation of the G3P biosynthesis genes (Shine *et al.*, 2019b). G3P was found to accumulate at the site of infection but is also transported to distal tissues (Shine *et al.*, 2019b). Importantly, the SAR-mediated increases in the cellular levels of G3P also result in an accumulation of this compound in petiole and root exudates (Chanda *et al.*, 2011; Shine *et al.*, 2019a). In summary, drought stress as well as bacterial infection were found to increase G3P in different plant exudates. These increases will attract bacteria that perform chemotaxis towards G3P. Further studies will show to which degree stress-induced alteration in G3P plant exudate levels will cause the attraction of bacteria that perform G3P chemotaxis.

## Supplementary material

**Table S 14. Strain, plasmids and oligonucleotides used in Chapter 5.**

	Genotype or relevant characteristics <sup>a</sup>	Reference
<b>Strains</b>		
<i>Escherichia coli</i> DH5 $\alpha$	F <sup>-</sup> <i>endA1 glnV44 thi-1 recA1 relA1 gyrA96 deoR nupG purB20 <math>\phi</math>80dlacZ<math>\Delta</math>M15 <math>\Delta</math>(<i>lacZYA-argF</i>)U169, <i>hsdR17</i>(<i>r<sub>K</sub><sup>-</sup>m<sub>K</sub><sup>+</sup></i>), <math>\lambda</math><sup>-</sup></i>	(Woodcock <i>et al.</i> , 1989)
<i>Escherichia coli</i> BL21(DE3)	F <sup>-</sup> <i>ompT gal dcm lon hsdS<sub>B</sub></i> ( <i>r<sub>B</sub><sup>-</sup>m<sub>B</sub><sup>-</sup></i> ) $\lambda$ (DE3 [ <i>lacI lacUV5-T7p07 ind1 sam7 nin5</i> ]) [ <i>malB<sup>+</sup></i> ] <sub>K-12</sub> ( $\lambda$ <sup>S</sup> )	(Jeong <i>et al.</i> , 2009)
<i>Pectobacterium atrosepticum</i> SCRI1043	Wild type strain	(Bell <i>et al.</i> , 2004)
<b>Plasmids</b>		
pET28b(+)	Protein expression plasmid; Km <sup>R</sup>	Novagen
pET28b- ECA_ RS12390	Km <sup>R</sup> ; pET28b(+) derivative containing LBD from ECA_RS12390 chemorreceptor gene	This study
pBBR-MCS-2_START	Km <sup>R</sup> ; <i>mob lacZ alpha rep</i>	(Obranic <i>et al.</i> , 2013)
pBBR-ECA_RS12390	Km <sup>R</sup> ; pBBR-MS2-START derivative containing coding sequence for gene ECA_RS12390	This study
pET-28_PWC17178.1	Km <sup>R</sup> ; pET28b(+) derivative containing LBD from the PWC17178.1 gene from <i>Brenneria roseae</i>	This study
pET-28_WP_006464688.1	Km <sup>R</sup> ; pET28b(+) derivative containing LBD from the WP_006464688.1 gene from <i>Herbaspirillum frisingense</i>	This study
pET-28_WP_158281851.1	Km <sup>R</sup> ; pET28b(+) derivative containing LBD from the WP_158281851.1 gene from <i>Rivicola pingtungensis</i>	This study
pET28_WP_028444678.1	Km <sup>R</sup> ; pET28b(+) derivative containing LBD from the WP_028444678.1 gene from <i>Chitinimonas koreensis</i>	This study
pET28_WP_174062248.1	Km <sup>R</sup> ; pET28b(+) derivative containing LBD from the WP_174062248.1 gene from <i>Agrobacterium larrymoorei</i>	This study
pET28_WP_019915375.1	Km <sup>R</sup> ; pET28b(+) derivative containing LBD from the WP_019915375.1 gene from <i>Methyloversatilis discipulorum</i>	This study
pET28_WP_028536266.1	Km <sup>R</sup> ; pET28b(+) derivative containing LBD from the WP_028536266.1 gene from <i>Paludibacterium yongneupense</i>	This study
pET28_WP_189529961.1	Km <sup>R</sup> ; pET28b(+) derivative containing LBD from the gene WP_189529961.1 from <i>Paludibacterium paludism</i>	This study
pET28_WP_028866120.1	Km <sup>R</sup> ; pET28b(+) derivative containing LBD from the gene WP_028866120.1 from <i>Psychromonas aquimarina</i>	This study
<b>Oligonucleotides</b>		
ECA_RS12390-NdeI-F	TAATCATATGTGAAATTACGAACCAGAATTGCA	Cloning of ECA_RS05475 for overexpression
ECA_RS12390-BamHI-R	TAATGGATCCTTATCTTGCACCCAGCGCCA	Cloning of ECA_RS05475 for overexpression

**Table S 15. Composition and pH of purification and analysis buffers used for the different LBDs analysed in this study.**

Protein accession code	Purification Buffer		Dialysis buffer
	Buffer A	Buffer B	
WP_011095117	20 mM Tris/HCl, 500 mM NaCl, 5% (v/v) glycerol, 10 mM imidazole, 0.1 mM EDTA, pH 8.5	20 mM Tris/HCl, 500 mM NaCl, 5% (v/v) glycerol, 500 mM imidazole, 0.1 mM EDTA, pH 8.5	HEPES 20 mM NaCl 150 mM Glycerol 10%, pH 8.5
PWC17178	20 mM Tris/HCl, 500 mM NaCl, 5% (v/v) glycerol, 10 mM imidazole, 0.1 mM EDTA, pH 8.5	20 mM Tris/HCl, 500 mM NaCl, 5% (v/v) glycerol, 500 mM imidazole, 0.1 mM EDTA, pH 8.5	MES 5 mM PIPES 5 mM Tris-HCl 5 mM Glycerol 10%, pH 8.5
WP_006464688	20 mM Tris/HCl, 500 mM NaCl, 5% (v/v) glycerol, 10 mM imidazole, 0.1 mM EDTA, pH 6.5	20 mM Tris/HCl, 500 mM NaCl, 5% (v/v) glycerol, 500 mM imidazole, 0.1 mM EDTA, pH 6.5	K <sub>2</sub> HPO <sub>4</sub> 40mM, KH <sub>2</sub> PO <sub>4</sub> 40 mM Glycerol 5 % (v/v), pH 6.3
WP_158281851	20 mM Tris/HCl, 500 mM NaCl, 5% (v/v) glycerol, 10 mM imidazole, 0.1 mM EDTA, pH 6.5	20 mM Tris/HCl, 500 mM NaCl, 5% (v/v) glycerol, 500 mM imidazole, 0.1 mM EDTA, pH 6.5	K <sub>2</sub> HPO <sub>4</sub> 40mM, KH <sub>2</sub> PO <sub>4</sub> 40 mM Glycerol 5 %, pH 6.3
WP_028444678	20 mM Tris/HCl, 500 mM NaCl, 5% (v/v) glycerol, 10 mM imidazole, 0.1 mM EDTA, pH 8.5	20 mM Tris/HCl, 500 mM NaCl, 5% (v/v) glycerol, 500 mM imidazole, 0.1 mM EDTA, pH 8.5	MES 5 mM PIPES 5 mM Tris-HCl 5 mM NaCl 150 mM EDTA 1 mM Glycerol 10% (v/v), pH 7.4
WP_174062248	20 mM Tris/HCl, 500 mM NaCl, 5% (v/v) glycerol, 10 mM imidazole, 0.1 mM EDTA, pH 6.5	20 mM Tris/HCl, 500 mM NaCl, 5% (v/v) glycerol, 500 mM imidazole, 0.1 mM EDTA, pH 6.5	K <sub>2</sub> HPO <sub>4</sub> 100mM, KH <sub>2</sub> PO <sub>4</sub> 100 mM NaCl 200 mM EDTA 1 mM Glycerol 5% (v/v), pH 6.4
WP_019915375	20 mM Tris/HCl, 500 mM NaCl, 5% (v/v) glycerol, 10 mM imidazole, 0.1 mM EDTA, pH 8.5	20 mM Tris/HCl, 500 mM NaCl, 5% (v/v) glycerol, 500 mM imidazole, 0.1 mM EDTA, pH 8.5	K <sub>2</sub> HPO <sub>4</sub> 100mM, KH <sub>2</sub> PO <sub>4</sub> 100 mM NaCl 200 mM EDTA 1 mM Glycerol 5% (v/v), pH 8.5

**Table S 16. Amino acid sequence of the proteins purified for calorimetric studies, consisting of the LBDs predicted as PacP homologs plus an extension (coloured) containing the His Tag.**

WP_011095117 Ligand Binding Domain + His Tag	MGSSHHHHHHSSGLVPRGSHMNTLYNTMMSERTGQLSTLVELAHSAAQKAYE LEKSGQLSRDEAEKARTIGSFHQGDYFFVIRGYTNDVNYVHPNPKRIGIIDAN GGKEAGERYRASLQGNITIGTVIAEGTRPGQQNKVEKLYAVIKFEPWDWTIGYGD YIDDIQQTFWHNAL
PWC17178 Ligand Binding Domain + His Tag	MGSSHHHHHHSSGLVPRGSH TLYKSMMHERTSQ LSTLVELAHAAAQKSYDLEK SGQLSREEAENEAKRAIGSFHLNDRYFFVIRGFTNDVNYVHPNPKRVGIVDAKGG KEAGERYRAALQDNTIGTVIARGTRPGTTDEVEKLYAIVKFEPWDWIIGYGDYID DIQAFWRD
WP_006464688 Ligand Binding Domain + His Tag	MGSSHHHHHHSSGLVPRGSH TLRRTMMEERE AQLSLLVTLAKAAA EKAQAQE QAGKLTREQAQAQAKMVI GSFQKQNYFFVIRGYSDDFNYVHPNPKRVGIQDKT AKEDGDYRAALQGKEIGLLIAEGTRPNTTEKVQKLYAVTRFAPWDWTIGFGAYI DDINQAFYRN
WP_158281851 Ligand Binding Domain + His Tag	MGSSHHHHHHSSGLVPRGSH RANMISERQSQFGALVSQGKASLAFHKL EADG KLSREEAQLAKQAIASLHDGDRYLW/MRDNSNDVNLVHPNPKRVNHADPDAK KKGDEYRQAMQGVVEVGF LFSQGTRPGVEGNV GKLYALS LFPWNWIIGFGGYL DDIEQVFWQRAFTM
WP_028444678 Ligand Binding Domain + His Tag	MGSSHHHHHHSSGLVPRGSH QLRQTMMEERRGQITMLLGLAEGMLKQYQAL ETAGKLSREEAQRATQALGALRSEDNYFFARNGDNVMLIHPKTERIGKVDLGS KVPDGRYSTAVYAEALQQSNPALVVIQTERPKSKDKVLLPKLNGVLKFEPWQWT VGIGFFIDDIT
WP_174062248 Ligand Binding Domain + His Tag	MGSSHHHHHHSSGLVPRGSH QIKSSVNAIYEERYGMLRTQVQSSISILQSFYDKE KAGTLSREDAQKQAF AIVSSMKYVPDGYMFGYDYDVNMMFHPDPKRVGQNF KKGADSQGFAYRDELVRLARSGGGQVNF L GPKPGEQGDSFLKSSYAMAFEPW QIVVVTGVYVDDLQAQVRST
WP_019915375 Ligand Binding Domain + His Tag	MGSSHHHHHHSSGLVPRGSH EIRSTMMAEREARIVTLLKLSTGILQRYHEQEKA GTLTREQAQTHAREALLGLQSDDHYMFARSADDVLLAHRKEKLGQKDNGGV APDGRNTD VYREALAKADPAFVTVPAKKPGGSEALPKMNGVTHFAPWAWTL GTGFFVDDIEQAFKS



## GENERAL DISCUSSION

---

Considerable efforts are taking place to understand how bacteria sense, respond and adapt to environmental stimuli. In particular, in recent years, there has been a remarkable advance in the understanding of the mechanisms of chemotaxis in a wide variety of bacterial species (Manson, 2018; Watts *et al.*, 2019; Yang and Briegel, 2020; Gumerov *et al.*, 2021). In addition, the wealth of genomic data has permitted the *in silico* identification of thousands of chemoreceptors in understudied species. For instance, *P. atrosepticum* (*Pba*), the model species in this PhD thesis, has a wide repertoire of chemoreceptors. Exploration of this species has taken place in a wide range of topics, including the production of virulence determinants, transcriptional and post-transcriptional regulation, its CRISPR systems, prophages present in its genome, plant virulence, among others (Evans *et al.*, 2010; Pérez-Mendoza *et al.*, 2011; Bowden *et al.*, 2013; Richter and Fineran, 2013; Tan *et al.*, 2014; Panda *et al.*, 2016; Buttner *et al.*, 2018a; Buttner *et al.*, 2018b; Kang *et al.*, 2022). However, to our knowledge, before the start of this doctoral thesis, the mechanisms of chemotaxis had not been investigated in *Pba* in particular nor in bacteria of the genus *Pectobacterium* in general. Based on this gap in knowledge, the main purpose of this PhD thesis was to characterize the complex chemotactic system of *Pba* SCRI1043 – a model strain in plant pathology and the first soft rot pathogen to have its genome sequenced (Bell *et al.*, 2004). The genome of *Pba* SCRI1043 encodes 36 chemoreceptors with different types of sensing domains, suggesting that it is able to perform chemotaxis to a wide range of environmental signals. During the course of this thesis, I have described how the 9 different pentapeptides present at the carboxy-terminal end of 19 of the chemoreceptors bind the methyltransferase CheR\_Pec with different affinities and are not able to bind the methylesterase CheB\_Pec, at least in its unphosphorylated state. I have also resolved the 3D structure of CheB\_Pec. Furthermore, I have functionally characterized several chemoreceptors, namely PacA, PacB, PacC and PacP. During the time of this thesis, I also worked with other *Pba* SCRI1043 chemoreceptors, for example, by functionally characterizing the NIT-containing chemoreceptor (PacN) as a nitrate and nitrite sensor as well as the only chemoreceptor of *Pba* SCRI1043 containing a Cache3-Cache2 fusion domain as a specialized formate receptor (PacF). This work has been published (Monteagudo-Cascales *et al.*, 2023) or will be published independently from this thesis.

### **CheB methylesterases can be classified as pentapeptide-dependent and independent**

In *E. coli*, the pentapeptide present at the carboxy-terminal end of chemoreceptors Tar and Tsr binds CheB and enhances hydrolysis of chemoreceptor methylesters by this enzyme (Barnakov *et al.*, 2002). Thus, CheB binds not only to substrate side chains on the chemoreceptor cytoplasmic domains but also to the pentapeptide, and its methylesterase activity is dependent on both, its phosphorylation state and docking to the C-terminal pentapeptide (Barnakov *et al.*, 2001; Barnakov *et al.*, 2002). Furthermore, the pentapeptide position at the carboxy-terminal end of receptors seems important for efficient CheB activity, at least in *in vitro* models, although this effect is compensated *in vivo* and chemotaxis occurs even when the position of this pentapeptide is altered (Lai and Hazelbauer, 2005). In *E. coli*, assistance by pentapeptide-containing chemoreceptors for the adaptation of those chemoreceptors lacking pentapeptides

has been demonstrated, meaning that chemoreceptors with pentapeptides recruit and help the efficient methylation and demethylation by CheR and CheB, respectively, of proteins without these tethering sequences (Li and Hazelbauer, 2005). However, we have shown in this thesis that CheB\_Pec is different to its homologue from *E. coli* since it is unable to directly bind pentapeptide sequences in its unphosphorylated form. CheB from *E. coli* has a pentapeptide binding site that has been predicted to rest between its two domains, spanning the carboxy-terminal end of the receiver domain and the start of the linker that continues to the catalytic domain (Barnakov *et al.*, 2001). We found that the sequence corresponding to the pentapeptide binding site in *E. coli* is not conserved in the CheB\_Pec. Remarkably, the crystallization of CheB\_Pec (done in collaboration with Dr. Jose A. Gavira – IACT/CSIC) revealed that the region corresponding to the pentapeptide binding site of CheB of *S. enterica* serovar Typhimurium (Djordjevic *et al.*, 1998) is unstructured in CheB\_Pec, supporting that this is the molecular basis for the failure of CheB\_Pec to bind pentapeptides (Figure 18).

While unphosphorylated CheB from *E. coli* bound to the pentapeptide with low affinity ( $K_D$  values between 130 to 160  $\mu\text{M}$ ) (Barnakov *et al.*, 2002), phosphorylated CheB was shown to bind with an affinity of  $13 \pm 3 \mu\text{M}$ , an increase of 12- to 18-fold (Li *et al.*, 2021). In addition, molecular simulations revealed that a pentapeptide binding site in the CheB structure is only present in the activated, open state of the protein, thus resulting in selective binding of pentapeptides to activated CheB. Phosphorylation at CheB-P is short-lived because of a high rate of autodephosphorylation (Stewart, 1993). In our study, to investigate binding of pentapeptides to phosphorylated CheB\_Pec, we generated a phosphorylation mimic of CheB\_Pec using derivatization with beryllium fluoride. Our mimic of phosphorylated CheB\_Pec, however, did not bind pentapeptides, as is discussed throughout Chapter 1. Alternatively, in (Li *et al.*, 2021), a different strategy was followed, since a stable and functionally active mimic of phosphorylated CheB from *S. enterica* serovar Typhimurium was used. In this synthetic mimic, that was previously described (Saxl *et al.*, 2001), the aspartyl residue that is phosphorylated in the native protein is substituted by a cysteinyl residue. This residue is then modified by sodium thiophosphate, resulting in a stable adduct that harbors a negative charge causing protein activation similar to the phosphorylated form (Li *et al.*, 2021). We can't rule out that modifying CheB\_Pec using the protocol used by (Li *et al.*, 2021) would permit us to detect binding to pentapeptides. Alternatively, binding of CheB\_Pec to pentapeptides may be completely dependent on phosphorylation or it is too weak to be detected by microcalorimetry. Future studies may include the generation of CheB\_Pec that has been modified according to this protocol, which in turn would clarify this issue. However, the lack of conservation of the pentapeptide binding site at CheB\_Pec is a feature that, pending results of these new experiments, implies CheB\_Pec is indeed independent of pentapeptide-tethering. This is a common theme with CheR, where the existence of pentapeptide-dependent and independent proteins has been more clearly established (Perez and Stock, 2007; García-Fontana *et al.*, 2014; Batra *et al.*, 2016). Pentapeptide-independent methylesterases must exist, as demonstrated by species that do not contain a single chemoreceptor with a C-terminal pentapeptide. In the *Thermotoga maritima* CheB, independent of pentapeptide binding, surface electrostatic potential significantly differs compared to *E. coli* CheB, indicating different binding modes to chemoreceptors (Perez and Stock, 2007). A structure of *T. maritima* CheB has helped to define the interaction of the methylesterase with chemoreceptors using *in silico* docking analyses (Cho



*et al.*, 2011). Future studies will delve into the consequences of the inability of CheB\_Pec to bind pentapeptides. For example, does it provide an evolutionary advantage for *Pba*? To what degree do the chemotactic abilities of this strain depend on this regulatory feature? What effect would it have on the chemotactic properties of *Pba* to have a CheB that binds pentapeptides?

### **CheR\_Pec binding to pentapeptides as a potential mechanism of prioritizing chemotactic responses**

In the complex regulation of the activity of the chemosensory systems, a diversity of mechanisms that modify the output response has been reported over recent years (Roberts *et al.*, 2010; Colin and Sourjik, 2017; Waite *et al.*, 2018; Muok *et al.*, 2020b), adding to the established knowledge about the canonical chemotaxis system (Armitage, 1992; Parkinson *et al.*, 2015c). These mechanisms comprise variations in the set of proteins participating in these pathways in different species or in the functioning of the whole pathway or any of its parts. These regulatory mechanisms include: (i) the alternative arrangements that the chemosensory proteins can adopt in the sensory clusters at the supra-molecular level (Li and Hazelbauer, 2005; Muok *et al.*, 2020b); (ii) variations in the common signaling mechanisms like spontaneous fluctuations of the sensory modules or cell-to-cell differences in protein abundance that correlate to individual differences in chemotactic abilities between genetically identical individuals (Waite *et al.*, 2018); and (iii) presence of additional phosphatases (Muff and Ordal, 2008), additional proteins like CheV that in some cases replaces CheW function (Alexander *et al.*, 2010; Huang *et al.*, 2019b) or the ZomB protein that in some species acts as a motor brake influenced by CheY (Brenzinger *et al.*, 2018).

In the case of pentapeptides, variability in their sequences has been described before (Ortega and Krell, 2020). Positions 2 and 5 are conserved (Perez and Stock, 2007), whereas the rest of positions can have different residues. In *Pba* SCRI1043, nine different pentapeptide sequences were found; it has been established here that they all bind the methyltransferase CheR\_Pec, but affinities vary more than 12-fold, from 86 nM (GWTTF) to 1.04  $\mu$ M (NWTTF). Of note is that there is only a single amino acid change between the most and least affine pentapeptide. Moreover, performing quantitative immunoblot experiments, the cellular CheR\_Pec concentration has been found to range from  $1.4 \pm 0.3 \mu$ M to  $0.73 \pm 0.1 \mu$ M in exponential and stationary phase, respectively. This range is thus close to the affinities determined for the pentapeptides-CheR\_Pec interaction. It can therefore be hypothesized that pentapeptides with different sequences enable a selection of CheR\_Pec binding, depending on both CheR\_Pec intracellular concentration and binding affinity. This is very likely to have an effect on chemotactic performance, as the binding of the methyltransferase changes the rates of adaptation. Since we have shown that the cellular CheR\_Pec concentrations change during growth, these changes would consequently modulate the signaling output. In other words, the presence of different pentapeptides in a chemoreceptor has an effect in its net chemotactic output. Future experiments will be focused on adding or changing pentapeptides to functionally characterized chemoreceptors to verify this hypothesis.

### **PacA is a chemoreceptor that recognizes quaternary amines**

In Chapter 3, the dCache-containing LBD of the quaternary amine responsive chemoreceptor PctD of *P. aeruginosa* PAO1 was characterized at the biochemical and structural level. Since a homolog dCache domain-containing chemoreceptor, named PacA, was identified in *Pba* SCRI1043, I worked to find out if it bound the same ligands. PacA was shown to retain a similar ligand profile, binding L-carnitine, betaine, and choline, but strikingly it did not bind acetylcholine. We defined a motif that recognizes quaternary amines, which involves primarily hydrophobic interactions with aromatic residues. This contrasts with what is known about amino acid recognition, that is mostly mediated by establishing hydrogen bonds with the bound ligand (Gavira *et al.*, 2020; Gumerov *et al.*, 2022). Two conserved amino acids (Tyr and Asp) as well as two positions occupied by aromatic amino acids form the dCache motif for quaternary amines (Figure 29). On the other hand, the amino acids that coordinate the acetylcholine tail in PctD were not conserved in PacA (Figure 29), which represents the mechanism that results in the observed differences in ligand profile.

A recent work has reported the identification of the sequence motif that is specific for amine-sensing in dCache sensor domains, named dCache\_1AM (Cerna-Vargas *et al.*, 2023). Based on the structures described in Chapter 3 of this thesis, along with the McpX chemoreceptor structure from *Sinorhizobium meliloti* that also senses quaternary amines (Shrestha *et al.*, 2018), the most important interactions with the ligands, namely a cation- $\pi$  interaction with the  $\pi$ -system of aromatic residues in the ligand binding pocket, were identified, which in turn has led to the prediction of an amine-binding motif at dCache domains. This motif could be identified in more than 13,000 proteins from 8,000 bacterial and archaeal species. dCache\_1AM containing receptors were identified in all major receptor families including sensor kinases, chemoreceptors, receptors involved in second messenger homeostasis and Ser/Thr phosphatases. Interestingly, the authors observed that many dCache\_1AM domains are present in PAB, both beneficial and pathogenic. For example, an analysis of the species to which these predicted proteins belong shows that a large share can be classified as PAB (Figure 44).

The authors suggest that choline and acetylcholine are the main quaternary amine ligands recognized by dCache\_1AM-containing receptors, since other quaternary amines like betaine and L-carnitine were not common ligands for the proteins tested by thermal shift/ITC studies (Cerna-Vargas *et al.*, 2023). Notably, this motif in some proteins was not able to recognize quaternary amines, but binds other small biogenic amines, that can serve as substrates for aerobic and anaerobic growth, neurotransmitters or osmoprotectants (e.g. methylamine, ethylamine, ethylenediamine, dimethylamine, trimethylamine and ethanolamine). Subsequent binding studies performed with PacA-LBD demonstrated that it is also able to bind trimethylamine (Cerna-Vargas *et al.*, 2023), expanding the range of known ligands of this chemoreceptor.

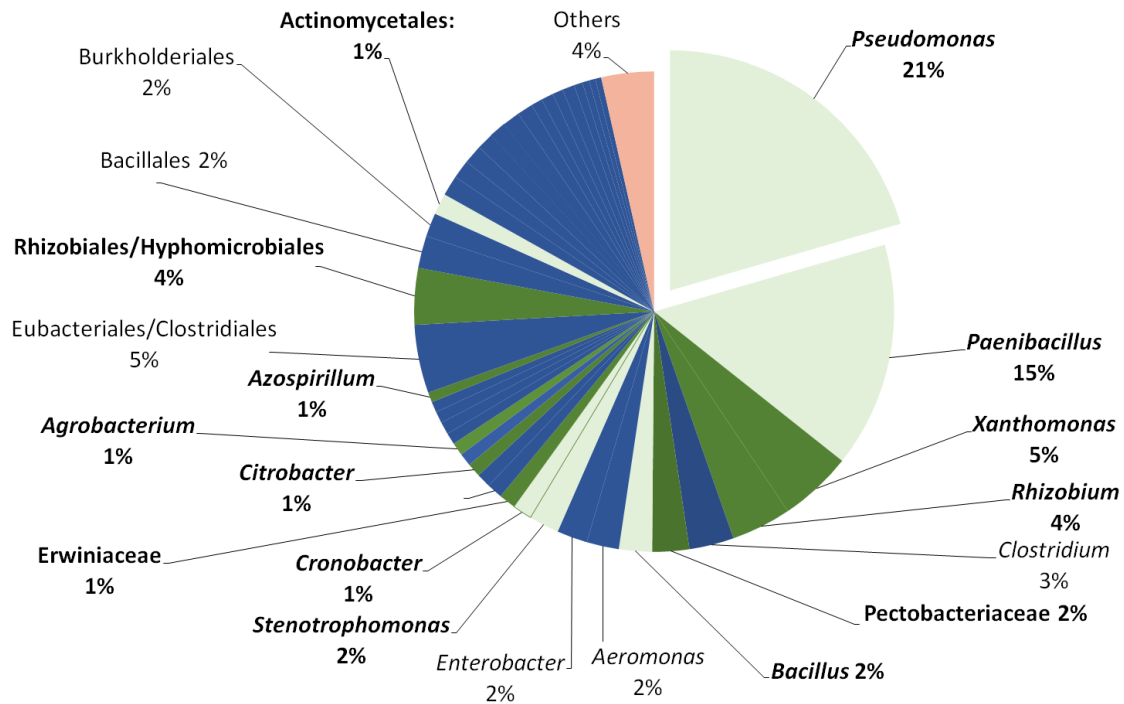


**Figure 44. Sector diagram with the percentage of predicted sequences with the dCache\_1AM motif according to their taxonomic classification.** Bacteria are grouped in genera, family or order depending on their sequence abundance. Taxonomic groups that are composed mainly of plant-associated bacteria are shown in green, while genera that contain both, plant associated bacteria and bacteria with other lifestyles are in light green. Bacteria not associated to plants are shown in blue. For clarity reasons, taxonomic units with less than 1% of the sequences are not named. Data have been generated by analyzing the bacterial species containing dCache\_1AM domains as reported by (Cerna-Vargas *et al.*, 2023).

The evolutionary origins of the dCache\_1AM domain have been investigated (Cerna-Vargas *et al.*, 2023). Of note is that there are several amino acids that are conserved in the binding motifs of the amino acid responsive dCache\_1AA and dCache\_1AM domains (Gumerov *et al.*, 2022). Similar ligand binding interfaces were observed by superimposition of ligand binding pockets of dCache\_1AA and dCache\_1AM. A phylogenetic tree using protein sequences of dCache\_1AA and dCache\_1AM from several bacterial and archaeal phyla showed that all dCache\_1AM sequences are found in a single branch derived from one of the branches of a more diverse set of dCache\_1AA sequences (Figure 45), indicating that the dCache\_1AM domain has evolved from an ancestral dCache\_1AA domain.

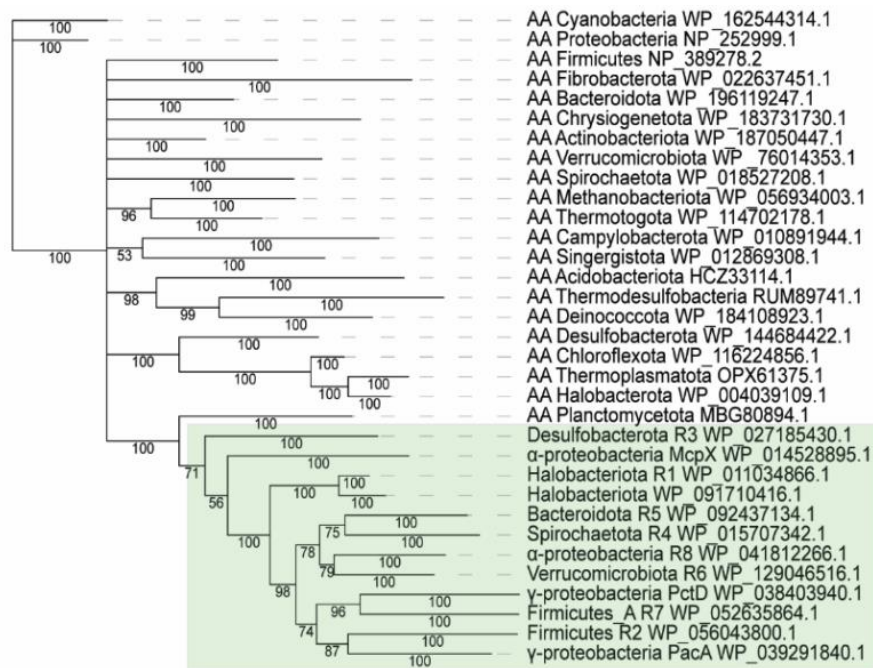


**Figure 45. Bayesian phylogenetic tree of amine and amino acid receptor sensory domains.** Amine receptors are shown in green background. Adapted from (Cerna-Vargas *et al.*, 2023).

In this Chapter 3, we also identified other plant pathogens that show chemotaxis towards acetylcholine (*Agrobacterium tumefaciens* and *Dickeya solanii*). This may suggest that chemotaxis to acetylcholine is potentially involved in virulence processes. We didn't look for chemotaxis towards quaternary amines other than acetylcholine in these other species, so we can't rule out other chemoreceptors similar to PacA (not able to bind acetylcholine) or even those only able to bind small amines are present. The importance of amine binding for plant pathogens is thus a field that can be further investigated. As indicated above, chemotaxis (and the chemoreceptor responsible of it) towards these quaternary amines has been investigated in the beneficial PAB, *Sinorhizobium meliloti* (Webb *et al.*, 2017b).

### ***Pba* SCRI1043 chemotaxis might be under tight regulation in laboratory conditions**

We must note that *in vivo* chemotaxis towards quaternary amines (e.g. betaine, choline, proline and carnitine) could only be demonstrated in *Pba* SCRI1043 by overexpressing the full chemoreceptor in a plasmid, suggesting that under our experimental conditions the *pacA* gene is not being expressed. Similar observations have been made with the PacP chemoreceptor (Chapter 5). These findings underlines the suitability of protein-based *in vitro* screening to explore the chemotactic repertoire of bacterial strains. Growth conditions in the lab can only mimic the conditions in their natural ecosystems to a point, so chemotaxis experiments may fail to identify ligands of some chemoreceptors. The overexpression of chemoreceptor genes thus provides evidence for protein functionality without gene regulatory effects that may mask phenotypes tightly regulated, for example, in bacterial strains with complex life cycles, as shown in this thesis.

Several articles investigate the regulation of gene expression in *Pba* (Toth *et al.*, 2006b; Evans *et al.*, 2010; Bowden *et al.*, 2013; Richter and Fineran, 2013; Gorshkov *et al.*, 2014; Tan *et al.*, 2014; Panda *et al.*, 2016; Gorshkov *et al.*, 2016; Deochand *et al.*, 2016; Gorshkov *et al.*, 2017; Gorshkov *et al.*, 2018; Bellieny-Rabelo *et al.*, 2019; Van Gijsegem *et al.*, 2021). The efficiency of this bacterium in plant colonization depends on its ability to persist effectively under various stress conditions (including nutrient deprivation) without compromising its virulence (Gorshkov *et al.*, 2017). To this end, gene expression should be tightly regulated by environmental signals. For example, pH and reactive oxygen species present in the plant apoplast are important for the regulation of the master regulator of virulence PecS (Deochand *et al.*, 2016; Deochand *et al.*, 2019). In this regard, a complex regulatory scheme may control the efficient expression of chemoreceptors in laboratory conditions. In *P. aeruginosa* PAO1, a strain that generally shows a larger magnitude of chemotactic responses than *Pba* (Matilla *et al.*, 2021a), the cellular abundance of many chemoreceptors can greatly vary with the growth condition and the amount of chemoreceptors did not correlate with the magnitude of chemotaxis to their cognate chemoeffectors (Matilla *et al.*, 2023). In *Pba*, under “starvation conditions” (i.e. transferring cells from an overnight culture in rich medium to a minimal medium without carbon source and incubating without aeration for four hours), several genes related to chemotaxis are up-regulated, including 21 of 36 genes for chemoreceptors along with the chemotactic signaling gene cluster (Gorshkov *et al.*, 2017). Notably, among the upregulated genes was *pacA*. Another chemoreceptor gene, *ECA\_RS02210*, is among the most up-regulated genes under these conditions (Gorshkov *et al.*, 2017), suggesting that chemotaxis towards specific plant signals can be only detectable under specific growth conditions. Moreover, our unpublished studies have shown that chemotaxis to formate in *Pba* SCRI1043 was only observed when cells were exposed to anaerobic conditions hours before performing the chemotaxis assays with this compound. No chemotaxis was observed under aerobic conditions whatsoever, confirming importance of growth conditions on the chemotactic response in *Pba*. In this case, we speculate the chemoreceptor responsible of recognizing formate is repressed in aerobic conditions, like the ones I have used in all the chemotaxis assays throughout this thesis, only becoming expressed when oxygen is removed. This anaerobic or microanaerobic conditions are probably encountered by bacteria in soil, so host localization and colonization of roots and tubers occurs in absence or with very low levels of oxygen. This may explain expression of chemoreceptors under these conditions.

### **Amino acids are probably the most important chemotactic signals in bacteria**

My work has also shown that PacB is an amino acid sensor with a wide range and that contains the recently described motif of the dCache\_1AA subfamily for amino acid binding (Gumerov *et al.*, 2022). PacB bound with high affinity 14 proteinogenic amino acids and 5 non-proteinogenic amino acids. Additionally, 4 other proteinogenic amino acids, 3 non-proteinogenic amino acids, one D-amino acid (D-Ala) and ethanolamine were found to bind PacB with lower affinity. Amino acids with a negatively charged side chain, L-Asp and L-Glu, were the only amino acids that did not show binding. PacB is the first chemoreceptor characterized with a clear preference for three branched chain amino acids (e.g. L-Val, L-Leu, L-Ile). The fact that chemotaxis in the *pacB* mutant was significantly reduced towards L-Ala and L-Ser, but not totally abolished, suggests the

existence of additional chemoreceptors with an overlapping ligand profile. In this thesis, I have shown that PacA binds and mediates chemotaxis to L-Pro as well as quaternary amines (Chapter 3) and that PacC binds and mediates chemotaxis to D-Asp, L-Asp and L-Asn. L-Asp and L-Asn are among the strongest elicitors of chemotaxis so far detected for this strain (unpublished data) and PacC is the sole chemoreceptor responsible of mediating chemotaxis towards these compounds under the experimental conditions used. This set of chemoreceptors dedicated to amino acid sensing adds to a growing perception of this type of signals as very important elicitors of bacterial chemotaxis. A very large number of the functionally characterized chemoreceptors were found to bind amino acids (Matilla *et al.*, 2022a), and several species, particularly those belonging to the *Pseudomonas* genus show a set of paralogous chemoreceptors to detect amino acid signals (Rico-Jiménez *et al.*, 2013a; McKellar *et al.*, 2015; Cerna-Vargas *et al.*, 2019; Gavira *et al.*, 2020; Tumewu *et al.*, 2021). In this thesis, a plant-associated enterobacterium was also shown to harbor a set of different chemoreceptors that enable chemotaxis towards different amino acids, including D-amino acids that may be present in their environment. However, in this case the chemoreceptors are not paralogous, suggesting convergent evolutionary events.

Genome-wide analysis of the SBPs present in *Pba* also supports the notion that amino acids are important signals, since from the 85 identified SBPs, almost 30% are predicted to be devoted to amino acid recognition (Figure 46), with an additional 20% predicted to be devoted to dipeptide/oligopeptide sensing. SBPs can interact with membrane-associated transporters but they can also interact specifically with chemoreceptors expanding their ligand range (Manson *et al.*, 1986; Björkman *et al.*, 1994; Zhang *et al.*, 1999; Hegde *et al.*, 2011; Rader *et al.*, 2011b; Rico-Jiménez *et al.*, 2016). Thus, the elevated number of amino acid-binding SBPs may be indicative of additional amino acid chemotaxis. We can thus hypothesize that the chemotaxis to certain ligands of PacB that I observed in the *pacB* mutant strain may be recognized by a different chemoreceptor that can potentially be stimulated by SBP binding, as reviewed in (Matilla *et al.*, 2021b). SBP-mediated stimulation of a dCache LBD-containing amino acid chemoreceptor has been reported previously in *Bacillus subtilis* (Glekas *et al.*, 2012).

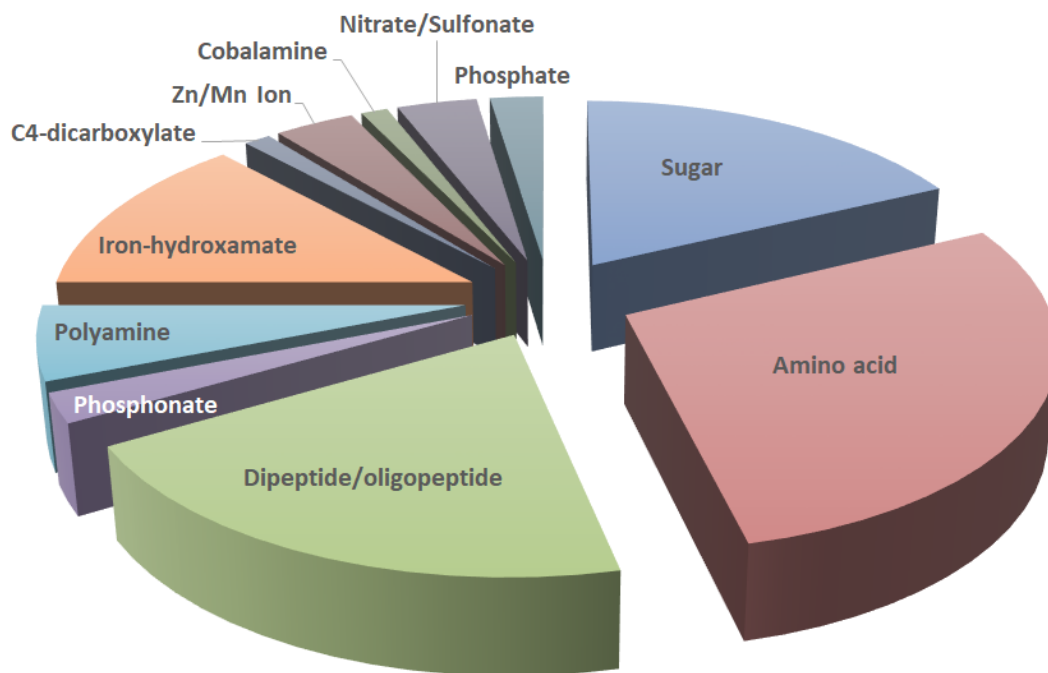


**Figure 46.** Sector diagram showing the percentage of the 85 identified SBPs in *P. atrosepticum* SCRI1043 genome predicted to recognize each class of ligands. Data extracted from *in silico* analyses undertaken in (Ortega *et al.*, 2022).

#### Several chemoreceptors evolve to recognize a wide set of amino acids

Bacteria are under selective pressures that require an adequate adaptation to their corresponding niches, especially in complex environments such as soil and water ecosystems, leaf surfaces and other natural contexts (Matilla and Krell, 2017a; Sanchis-López *et al.*, 2021a). Thus, during evolution, bacteria have evolved different strategies to recognize a variety of signals by sensor proteins (Matilla *et al.*, 2022a), including the acquisition or evolution of new chemoreceptors that are able to expand the overall chemoeffector range. This happens through at least two different mechanisms, namely either by horizontal gene transfer or gene duplication and neofunctionalization (Gavira *et al.*, 2020b). Neofunctionalization can occur because chemoreceptors have two clearly differentiated parts, the LBD and the signaling domain. Whereas the signaling domain is very conserved in sequence and evolutionarily fixed, LBDs have a different speed of evolution that frequently result in recognition of new types of ligands (Gavira *et al.*, 2020a; Gumerov *et al.*, 2021c). For example, PacB and PacC chemoreceptors have complementary ligand profiles with only minimal overlap. Since both receptors belong to different families (i.e. different types of LBD) it is thus likely that an evolutionary event has resulted in the acquisition of PacC/PacB at some point in this lineage, to expand the number of amino acids that were recognized. In collaboration with bio-informatician Prof. Igor Zhulin (Ohio State University, USA), we have investigated the evolutionary history of PacC. Our analyses showed that PacC is the *Escherichia coli* Tsr ortholog. This was unexpected, because the *pacC* gene was located in the chemotaxis operon in the same position as the *tar* gene in the *E. coli* chemotaxis operon. Our findings thus suggest that the *tsr* gene underwent a duplication event

in the *E. coli* lineage that resulted in the evolution of *tar*, which was followed by another event that ultimately transferred the *tsr* gene outside the signaling protein gene cluster.

Another question that has emerged during this thesis was the reason for *Pab* SCRI1043 chemotaxis to the non-proteinogenic amino acid D-aspartate. This amino acid is recognized with high affinity by the PacC chemoreceptor. Although proteins are solely composed of L-amino acids, their isomers occur widely in life (Du *et al.*, 2023). *Pab* SCRI1043 can use D-aspartate as sole carbon and nitrogen source to support growth (Figure 47), so it might be of interest for the bacteria to detect this amino acid. The other compounds this chemoreceptor binds are L-asparagine and L-aspartic, which *Pba* SCRI1043 can also use as nutrient sources (Figure 47). L-Aspartate, next to its abundance in apoplasts (Rico and Preston, 2008; Kumar *et al.*, 2017), appears to be an amino acid of particular relevance for bacteria since several other chemoreceptors have evolved that recognize this amino acid with high specificity, including both Tar homologues from *E. coli* and *S. enterica* serovar Typhimurium and PspTo-PscA from *P. syringae* pv. tomato, all of which bind L-aspartate with high preference (Slocum and Parkinson, 1985; Foster *et al.*, 1985; Milligan and Koshland, 1993; Mise, 2016). The PsPto-PscA chemoreceptor bound L-Asp, D-Asp and L-Glu (Cerna-Vargas *et al.*, 2019). Although the binding affinity of L-Asp and D-Asp to the individual LBD of PsPto-PscA was the same, the chemotaxis to D-Asp was higher than that to L-Asp. Importantly, the PsPto-PscA mutant strain showed reduced virulence in tomato plants (Cerna-Vargas *et al.*, 2019). Infection assays with the wild-type strain demonstrated that exposing the bacteria to saturating concentrations of D-Asp before inoculating the plants with the phytopathogen reduced bacterial virulence (Cerna-Vargas *et al.*, 2019). This was related with the inability of *P. syringae* pv. tomato to metabolize this compound, preventing the generation of gradients of this compound. These results may imply that D-aspartate is used by different plant pathogens as a host signal that facilitates locating the host by the pathogen. The function of D-Asp and other D-amino acids in plants is unclear, but free D-amino acids in the low percentage range are principal constituents of plants, and D-Asp has been detected in most vegetal sample analyzed by mass spectrometry (Brückner and Westhauser, 1994; Brückner and Westhauser, 2003).



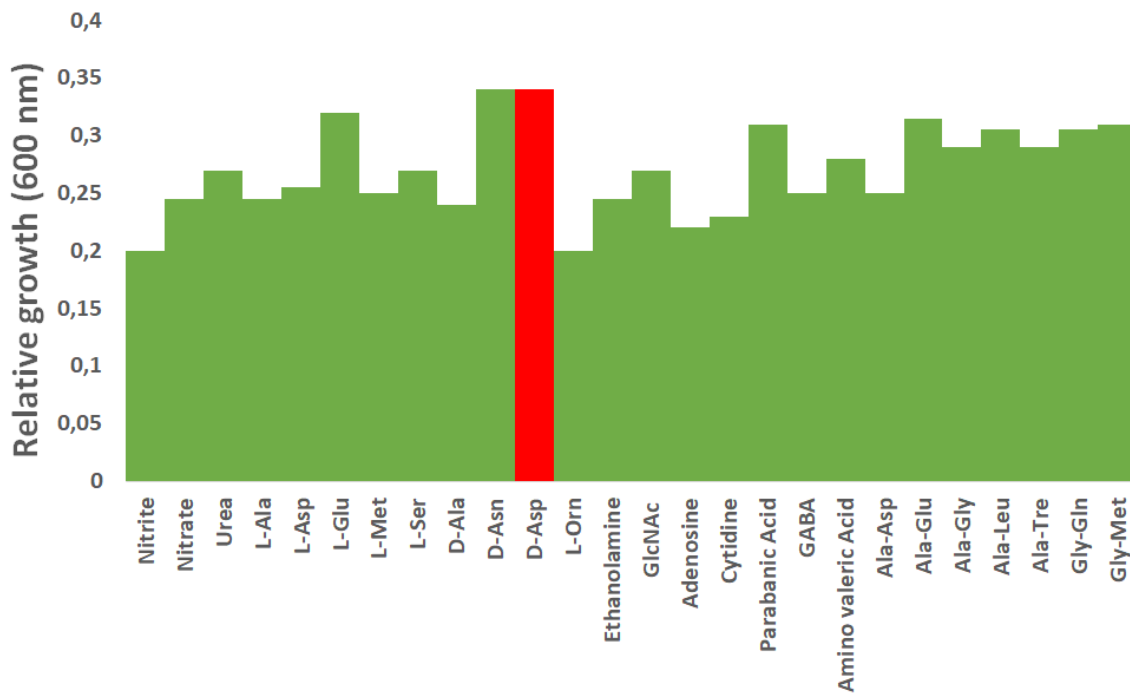


**Figure 47. Histogram representing some compounds that *P. atrosepticum* SCRI1043 can use as sole nitrogen source.** Shown is relative growth (OD<sub>600</sub>), obtained after normalization of the observed growth with the growth in a control sample without nitrogen source. The data point corresponding to D-Asp is highlighted in red. Data taken from García Montoya, F. (2018), “Characterization of the chemotactic properties of the phytopathogenic bacterium *Pectobacterium atrosepticum* SCRI1043”- Master project, Granada University.

To evaluate the role of chemotaxis in general and PacC in particular in the virulence of *Pba* SCRI1043, I performed experiments of plant leaf entry in its natural host, *Solanum tuberosum*, during a short stay at Prof. Emilia López-Solanilla (CBGP-Madrid) laboratory. Wild type *Pba* SCRI1043, a mutant deficient in chemotaxis ( $\Delta cheA$ ) and a deletion mutant in *pacC* were used for these studies (unpublished data). At cellular densities of inoculation of around  $2 \times 10^4$  CFU/mL, a defect in plant leaf entry was observed for the  $\Delta cheA$  mutant. The number of cells recovered from wound sites was consistently lower for the  $\Delta cheA$  mutant as compared to the WT (unpublished data). These assays thus showed that chemotaxis is important for plant entry, although the PacC chemoreceptor does not seem to play a key role in this process – at least under the conditions tested, which may be due to the number of chemoreceptors present in this strain. These experiments were performed under the notion that the related pathogen *Dickeya dadantii* is able to effectively infect plants through foliar entry (Gálvez-Roldán *et al.*, 2022), but there are differences between these phytopathogens, with virulence of *Pba* SCRI1043 clearly lower than that of *D. dadantii* 3937 in the experimental system used. For SRP in general, and *Pectobacterium* in particular, the main source of tuber infection is initiated in lenticels and the stolon end (Toth *et al.*, 2021). Disease development is mainly initiated from contaminated mother tubers under disease-inducing conditions, but SRP can also enter new host plants via the roots after persisting in the soil, water or insects (Toth *et al.*, 2021).

### **PacP is the first chemoreceptor that specifically recognized phosphorylated compounds**

*Pab* SCRI1043 presents taxis to the "usual" set of bacterial attractants, which act both as compounds of nutritional value and host signals, like some sugars, amino acids, organic acids, nitrate and amines (García Montoya, F. (2018), and this thesis). However, to our knowledge, recognition and taxis towards glycerol-3-phosphate (G3P) and other phosphorylated compounds has never been described before. Thus, PacP is the first chemoreceptor identified that binds exclusively phosphorylated compounds. Chemotaxis to G3P may be of particular relevance for PAB. In this regards, the concentration of this compound was shown to increase in plant exudates upon stress conditions as drought and bacterial infection (Tawaraya *et al.*, 2014a; Xu *et al.*, 2018; Shine *et al.*, 2019). Stress-induced alteration in G3P levels in plant exudates may chemotactically attract bacteria by sensing G3P. In this thesis, we could only demonstrate G3P chemotaxis by overexpression of the *pacP* gene, suggesting, as it happened before with PacA, that the chemoreceptor is poorly expressed under the experimental conditions tested. Future efforts are therefore necessary to identify the conditions under which this chemotaxis phenotype can be observed.

A number of chemoreceptors for organic acids have been reported in the literature that contain either a sCache or HBM domain (Alvarez-Ortega and Harwood, 2007; Gavira *et al.*, 2012; Oku *et al.*, 2014; Martín-Mora *et al.*, 2016b; Martín-Mora *et al.*, 2018b). Notably, we have shown in this thesis how the family of chemoreceptors homologous to PacP has likely arisen from sCache\_2 family members that bind primarily Krebs cycle intermediates like malate, citrate or fumarate. When looking for ligands of the LBDs of phylogenetically close chemoreceptors that failed to bind phosphorylated C3 compounds, we could demonstrate they bind diverse organic acids (Table 6). These proteins lacked some of the residues identified in the putative binding motif for C3 phosphorylated compounds (Figure 42). The PacP family is thus likely an evolutionary product of sCache\_2 domains that recognize other organic acids. Importantly, the PacP homologue were all present on a well-defined branch in the phylogenetic tree, facilitating in turn the identification of other family members. This branch is composed of Gammaproteobacteria, including plant-associated or freshwater bacteria belonging to the *Dickeya*, *Brenneria*, *Acidovorax*, *Herbaspirillum*, *Pantoea*, *Franconibacter*, *Comamonas*, *Variovorax*, *Rivincola*, *Undibacterium*, *Janthinobacterium* and *Chitinovorax* genera. Questions still remain concerning the evolution of the PacP family chemoreceptors in PAB. For example: which advantages get *Pectobacterium* from potentially detecting and moving towards phosphorylated C3 compounds like G3P? Is chemotaxis towards phosphorylated C3 compounds important for *Pba* virulence?

### **Concluding remarks**

Taking together the results of this thesis, considerable progress has been made in describing the chemotactic system of *Pba* - a bacterial phytopathogen of global relevance. Insights into two different features for some its chemoreceptor proteins were gained: (i) the function of their carboxy-terminal pentapeptides; and (ii) the sensing capabilities of their LBDs. Identification of the function of chemoreceptors of *Pba* has also increased knowledge of determinants of ligand recognition, laying the groundwork for the identification of ligands that are recognized by uncharacterised chemoreceptors in other species. Future research will involve the

characterization of the whole set of chemoeffectors of *Pba* SCRI1043. Together with this, advances are needed to understand the regulation of the chemotactic behavior of *Pba* SCRI1043 and its contribution to host localization, entry and/or virulence. In fact, this doctoral thesis has laid the foundations for a new doctoral thesis that is currently under development in the research group. Exploring chemotaxis, and more broadly, cell signaling on plant pathogens is an expanding research field, whose gaps of knowledge can be certainly reduced with current state-of-the-art techniques, including both laboratory work and bioinformatic approaches.



## CONCLUSIONS

---

1. *Pectobacterium atrosepticum* SCRI1043 has a chemosensory pathway that mediates chemotaxis and CheA, CheB and CheR are essential for its function.
2. *P. atrosepticum* SCRI1043 has 36 chemoreceptors, 19 of which present pentapeptides at their C-terminal end bearing 9 different sequences. All these pentapeptides are recognized by CheR\_Pec, whereas, under the conditions analysed, CheB-Pec lacks the ability to recognise these sequences.
3. Structure analysis revealed that the region that corresponds to the pentapeptide-binding site of *Escherichia coli* CheB is unstructured in CheB\_Pec. Given the very high identity between CheB\_Pec and CheB of *E. coli*, this feature represents, with high confidence, the reason for the failure of CheB\_Pec to recognize pentapeptides.
4. Affinities of CheR\_Pec for the different pentapeptides are in the nanomolar to lower micromolar range and vary 12-fold with only one amino acid substitution. The intracellular concentration of CheR\_Pec suffers variations during growth. These alterations can potentially alter the occupation of chemoreceptor by CheR, causing a modulation of the signaling output.
5. PacA and PctD from *P. aeruginosa* bind different quaternary amines. The capacity of PctD to bind acetylcholine is likely due to amino acids that recognize the acetate moiety.
6. The capacity of *P. atrosepticum* to respond to almost all proteinogenic amino acid is due to the action of at least three chemoreceptors with overlapping and partially complementary ligand profiles. These chemoreceptors are not paralogous, suggesting that they have been acquired by horizontal gene transfer.
7. PacC is a Tsr ortholog that binds L-Asn, D- and L-Asp, indicating that Tsr orthologs do not necessarily bind L-Ser, the ligand of *E. coli* Tar. Tsr homologs are the ancestral chemoreceptors from which the Tar chemoreceptor has evolved.
8. PacP is the first chemoreceptor that specifically binds phosphorylated compounds. The identification of a sequence motif present in the ligand binding site of PacP has enabled the prediction of homologous receptors with similar ligand profiles.
9. PacP-LBD is part of a subfamily of sensor domains that respond preferentially to glycerol 3-phosphate. The PacP subfamily has arisen from sCache\_2 LBD-containing chemoreceptors that bound organic acids like malate, fumarate, and citrate in a lineage of Gammaproteobacteria composed of plant-associated and fresh-water species.
10. Using standard laboratory conditions, *P. atrosepticum* SCRI1043 wild type cells present little or no chemotaxis to compounds that are ligands of some chemoreceptors described, like phosphorylated compounds, quaternary amines and some amino acids. This suggests that some chemoreceptors of this strain are under complex regulatory control and conducting *in vitro* screening of the individual sensor domains is a potent strategy to identify chemoeffectors that would not have been detected using microbiological approaches.



## REFERENCES

---

- Abril, M.A., Michan, C., Timmis, K.N., and Ramos, J.L. (1989) Regulator and enzyme specificities of the TOL plasmid-encoded upper pathway for degradation of aromatic hydrocarbons and expansion of the substrate range of the pathway. *J Bacteriol* 171: 6782–6790.
- Afonine, P.V., Grosse-Kunstleve, R.W., Echols, N., Headd, J.J., Moriarty, N.W., Mustyakimov, M., et al. (2012) Towards automated crystallographic structure refinement with phenix.refine. *Acta Crystallogr D Biol Crystallogr* 68: 352–367.
- Afonine, P.V., Mustyakimov, M., Grosse-Kunstleve, R.W., Moriarty, N.W., Langan, P., and Adams, P.D. (2010) Joint X-ray and neutron refinement with phenix.refine. *Acta Crystallogr D Biol Crystallogr* 66: 1153–1163.
- Aguilar, C., Pauzuolis, M., Pompaiah, M., Vafadarnejad, E., Arampatzi, P., Fischer, M., et al. (2022) *Helicobacter pylori* shows tropism to gastric differentiated pit cells dependent on urea chemotaxis. *Nat Commun* 13: 5878.
- Aguilar, P.S., Hernandez-Arriaga, A.M., Cybulski, L.E., Erazo, A.C., and Mendoza, D. de (2001) Molecular basis of thermosensing: a two-component signal transduction thermometer in *Bacillus subtilis*. *EMBO J* 20: 1681–1691.
- Airola, M.V., Sukomon, N., Samanta, D., Borbat, P.P., Freed, J.H., Watts, K.J., and Crane, B.R. (2013) HAMP domain conformers that propagate opposite signals in bacterial chemoreceptors. *PLoS Biol* 11: e1001479.
- Alexander, R.P., Lowenthal, A.C., Harshey, R.M., and Ottemann, K.M. (2010) CheV: CheW-like coupling proteins at the core of the chemotaxis signaling network. *Trends Microbiol* 18: 494–503.
- Alexander, R.P., and Zhulin, I.B. (2007) Evolutionary genomics reveals conserved structural determinants of signaling and adaptation in microbial chemoreceptors. *Proc Natl Acad Sci U S A* 104: 2885–2890.
- Allard-Massicotte, R., Tessier, L., Lécuyer, F., Lakshmanan, V., Lucier, J.-F., Garneau, D., et al. (2016) *Bacillus subtilis* Early Colonization of *Arabidopsis thaliana* Roots Involves Multiple Chemotaxis Receptors. *mBio* 7: e01664-16.
- Alvarez-Ortega, C., and Harwood, C.S. (2007) Identification of a malate chemoreceptor in *Pseudomonas aeruginosa* by screening for chemotaxis defects in an energy taxis-deficient mutant. *Appl Env Microbiol* 73: 7793–7795.
- Ames, P., Hunter, S., and Parkinson, J.S. (2016) Evidence for a Helix-Clutch Mechanism of Transmembrane Signaling in a Bacterial Chemoreceptor. *J Mol Biol* 428: 3776–3788.
- Ames, P., Studdert, C.A., Reiser, R.H., and Parkinson, J.S. (2002) Collaborative signaling by mixed chemoreceptor teams in *Escherichia coli*. *Proc Natl Acad Sci U S A* 99: 7060–7065.
- Ames, P., Zhou, Q., and Parkinson, J.S. (2014) HAMP domain structural determinants for signalling and sensory adaptation in Tsr, the *Escherichia coli* serine chemoreceptor. *Mol Microbiol* 91: 875–886.
- Amin, D.N., Taylor, B.L., and Johnson, M.S. (2006) Topology and boundaries of the aerotaxis receptor Aer in the membrane of *Escherichia coli*. *J Bacteriol* 188: 894–901.
- Anand, G.S., Goudreau, P.N., and Stock, A.M. (1998) Activation of methylesterase CheB: evidence of a dual role for the regulatory domain. *Biochemistry* 37: 14038–14047.

- Anand, G.S., and Stock, M.A. (2002) Kinetic basis for the stimulatory effect of phosphorylation on the methylesterase activity of CheB. *Biochemistry* 41,21: 6752-60.
- Anderson, T.F. (1951) Techniques for the preservation of three-dimensional structure in preparing specimens for the electron microscope. *Trans N Y Acad Sci* 13: 130–134.
- Antunez-Lamas, M., Cabrera, E., Lopez-Solanilla, E., Solano, R., González-Melendi, P., Chico, J.M., et al. (2009) Bacterial chemoattraction towards jasmonate plays a role in the entry of *Dickeya dadantii* through wounded tissues. *Mol Microbiol* 74: 662–671.
- Antúñez-Lamas, M., Cabrera-Ordóñez, E., López-Solanilla, E., Raposo, R., Trelles-Salazar, O., Rodríguez-Moreno, A., and Rodríguez-Palenzuela, P. (2009) Role of motility and chemotaxis in the pathogenesis of *Dickeya dadantii* 3937 (ex *Erwinia chrysanthemi* 3937). *Microbiology* 155: 434–442.
- Arizala, D., and Arif, M. (2019) Genome-wide analyses revealed remarkable heterogeneity in pathogenicity determinants, antimicrobial compounds, and CRISPR-Cas systems of complex phytopathogenic genus *Pectobacterium*. *Pathogens* 8: 247.
- Armitage, J.P. (1992) Bacterial motility and chemotaxis. *Sci Prog* 76: 451–477.
- Aroney, S.T.N., Poole, P.S., and Sánchez-Cañizares, C. (2021) Rhizobial Chemotaxis and Motility Systems at Work in the Soil. *Front Plant Sci* 12: 725338.
- Ashby, A.M., Watson, M.D., Loake, G.J., and Shaw, C.H. (1988) Ti plasmid-specified chemotaxis of *Agrobacterium tumefaciens* C58C1 toward vir-inducing phenolic compounds and soluble factors from monocotyledonous and dicotyledonous plants. *J Bacteriol* 170: 4181–4187.
- Bachas, S., Eginton, C., Gunio, D., and Wade, H. (2011) Structural contributions to multidrug recognition in the multidrug resistance (MDR) gene regulator, BmrR. *Proc Natl Acad Sci U S A* 108: 11046–11051.
- Baek, M., DiMaio, F., Anishchenko, I., Dauparas, J., Ovchinnikov, S., Lee, G.R., et al. (2021) Accurate prediction of protein structures and interactions using a three-track neural network. *Science* 373: 871–876.
- Barahona, E., Navazo, A., Yousef-Coronado, F., Aguirre de Cárcer, D., Martínez-Granero, F., Espinosa-Urgel, M., et al. (2010) Efficient rhizosphere colonization by *Pseudomonas fluorescens* f113 mutants unable to form biofilms on abiotic surfaces. *Env Microbiol* 12: 3185–3195.
- Barnakov, A.N., Barnakova, L.A., and Hazelbauer, G.L. (1999) Efficient adaptational demethylation of chemoreceptors requires the same enzyme-docking site as efficient methylation. *Proc Natl Acad Sci U S A* 96: 10667–10672.
- Barnakov, A.N., Barnakova, L.A., and Hazelbauer, G.L. (2001) Location of the receptor-interaction site on CheB, the methylesterase response regulator of bacterial chemotaxis. *J Biol Chem* 276: 32984–32989.
- Barnakov, A.N., Barnakova, L.A., and Hazelbauer, G.L. (2002) Allosteric enhancement of adaptational demethylation by a carboxyl-terminal sequence on chemoreceptors. *J Biol Chem* 277: 42151–42156.
- Baron, S., Afanjar, O., and Eisenbach, M. (2017) Methylation-independent adaptation in chemotaxis of *Escherichia coli* involves acetylation-dependent speed adaptation. *FEBS Lett* 591: 331–337.



- Bartelli, N.L., and Hazelbauer, G.L. (2011a) Direct evidence that the carboxyl-terminal sequence of a bacterial chemoreceptor is an unstructured linker and enzyme tether. *Protein Sci* 20: 1856–1866.
- Bashir, I., War, A.F., Rafiq, I., Reshi, Z.A., Rashid, I., and Shouche, Y.S. (2022) Phyllosphere microbiome: Diversity and functions. *Microbiol Res* 254: 126888.
- Batra, M., Sharma, R., Malik, A., Dhindwal, S., Kumar, P., and Tomar, S. (2016) Crystal structure of pentapeptide-independent chemotaxis receptor methyltransferase (CheR) reveals idiosyncratic structural determinants for receptor recognition. *J Struct Biol* 196: 364–374.
- Battley, E.H. (1988) *Escherichia Coli* and *Salmonella Typhimurium*. Cellular and Molecular Biology, Volume 1; Volume 2. Neidhardt F.C., Ingraham, J.L., Magasanik, B., Low, K.B., Schaechter, M., Umberger, H.E. *Q Rev Biol* 63: 463–464.
- Battye, T.G.G., Kontogiannis, L., Johnson, O., Powell, H.R., and Leslie, A.G.W. (2011) iMOSFLM: a new graphical interface for diffraction-image processing with MOSFLM. *Acta Crystallogr D Biol Crystallogr* 67: 271–281.
- Beals, K.A. (2019) Potatoes, Nutrition and Health. *Am J Potato Res* 96: 102–110.
- Bédard, E., Prévost, M., and Déziel, E. (2016) *Pseudomonas aeruginosa* in premise plumbing of large buildings. *MicrobiologyOpen* 5: 937–956.
- Bel Hadj Ahmed, A., Salah Abbassi, M., Rojo-Bezares, B., Ruiz-Roldán, L., Dhahri, R., Mehri, I., et al. (2020) Characterization of *Pseudomonas aeruginosa* isolated from various environmental niches: New STs and occurrence of antibiotic susceptible “high-risk clones.” *Int J Environ Health Res* 30: 643–652.
- Belda, E., Heck, R.G. van, Lopez-Sanchez, M.J., Cruveiller, S., Barbe, V., Fraser, C., et al. (2016) The revisited genome of *Pseudomonas putida* KT2440 enlightens its value as a robust metabolic chassis. *Env Microbiol* 18: 3403–3424.
- Bell, K.S., Sebahia, M., Pritchard, L., Holden, M.T., Hyman, L.J., Holeva, M.C., et al. (2004) Genome sequence of the enterobacterial phytopathogen *Erwinia carotovora* subsp. *atroseptica* and characterization of virulence factors. *Proc Natl Acad Sci U S A* 101: 11105–10.
- Belliény-Rabelo, D., Tanui, C.K., Miguel, N., Kwenda, S., Shyntum, D.Y., and Moleleki, L.N. (2019) Transcriptome and comparative genomics analyses reveal new functional insights on key determinants of pathogenesis and interbacterial competition in *Pectobacterium* and *Dickeya* spp. *Appl Env Microbiol* 85.
- Berg, G., Roskot, N., Steidle, A., Eberl, L., Zock, A., and Smalla, K. (2002) Plant-dependent genotypic and phenotypic diversity of antagonistic rhizobacteria isolated from different *Verticillium* host plants. *Appl Environ Microbiol* 68: 3328–3338.
- Berg, H.C., and Brown, D.A. (1972) Chemotaxis in *Escherichia coli* analysed by three-dimensional tracking. *Nature* 239: 500–504.
- Berke, A.P., Turner, L., Berg, H.C., and Lauga, E. (2008) Hydrodynamic attraction of swimming microorganisms by surfaces. *Phys Rev Lett* 101: 038102.
- Berman, H., Henrick, K., and Nakamura, H. (2003) Announcing the worldwide Protein Data Bank. *Nat Struct Biol* 10: 980.

- Besharova, O., Suchanek, V.M., Hartmann, R., Drescher, K., and Sourjik, V. (2016) Diversification of Gene Expression during Formation of Static Submerged Biofilms by *Escherichia coli*. *Front Microbiol* 7: 1568.
- Bi, S., Jin, F., and Sourjik, V. (2018) Inverted signaling by bacterial chemotaxis receptors. *Nat Commun* 9: 2927.
- Bi, S., and Lai, L. (2015) Bacterial chemoreceptors and chemoeffectors. *Cell Mol Life Sci* 72: 691–708.
- Bi, S., Pollard, A.M., Yang, Y., Jin, F., and Sourjik, V. (2016) Engineering Hybrid Chemotaxis Receptors in Bacteria. *ACS Synth Biol* 5: 989–1001.
- Bi, S., and Sourjik, V. (2018) Stimulus sensing and signal processing in bacterial chemotaxis. *Curr Opin Microbiol* 45: 22–29.
- Björkman, A.J., Binnie, R.A., Zhang, H., Cole, L.B., Hermodson, M.A., and Mowbray, S.L. (1994) Probing protein-protein interactions. The ribose-binding protein in bacterial transport and chemotaxis. *J Biol Chem* 269: 30206–30211.
- Blattner, F.R., Plunkett, G., Bloch, C.A., Perna, N.T., Burland, V., Riley, M., et al. (1997) The complete genome sequence of *Escherichia coli* K-12. *Science* 277: 1453–1462.
- Bond, S.R., and Naus, C.C. (2012) RF-Cloning.org: an online tool for the design of restriction-free cloning projects. *Nucleic Acids Res* 40: W209-213.
- Bowden, S.D., Eyres, A., Chung, J.C.S., Monson, R.E., Thompson, A., Salmond, G.P.C., et al. (2013) Virulence in *Pectobacterium atrosepticum* is regulated by a coincidence circuit involving quorum sensing and the stress alarmone, (p)ppGpp. *Mol Microbiol* 90: 457–471.
- Boyeldieu, A., Poli, J.-P., Ali Chaouche, A., Fierobe, H.-P., Giudici-Orticoni, M.-T., Méjean, V., and Jourlin-Castelli, C. (2022) Multiple detection of both attractants and repellents by the dCache-chemoreceptor SO\_1056 of *Shewanella oneidensis*. *FEBS J* 289: 6752–6766.
- Brady, C., Hunter, G., Kirk, S., Arnold, D., and Denman, S. (2014) Description of *Brenneria roseae* sp. nov. and two subspecies, *Brenneria roseae* subspecies *roseae* ssp. nov. and *Brenneria roseae* subspecies *americana* ssp. nov. isolated from symptomatic oak. *Syst Appl Microbiol* 37: 396–401.
- Brenzinger, S., Pecina, A., Mrusek, D., Mann, P., Völse, K., Wimmi, S., et al. (2018) ZomB is essential for flagellar motor reversals in *Shewanella putrefaciens* and *Vibrio parahaemolyticus*. *Mol Microbiol* 109: 694–709.
- Brewster, J.L., McKellar, J.L., Finn, T.J., Newman, J., Peat, T.S., and Gerth, M.L. (2016) Structural basis for ligand recognition by a Cache chemosensory domain that mediates carboxylate sensing in *Pseudomonas syringae*. *Sci Rep* 6: 35198.
- Briegel, A., Ortega, D.R., Huang, A.N., Oikonomou, C.M., Gunsalus, R.P., and Jensen, G.J. (2015) Structural conservation of chemotaxis machinery across Archaea and Bacteria. *Environ Microbiol Rep* 7: 414–419.
- Briegel, A., Ortega, D.R., Tocheva, E.I., Wuichet, K., Li, Z., Chen, S., et al. (2009) Universal architecture of bacterial chemoreceptor arrays. *Proc Natl Acad Sci U S A* 106: 17181–17186.
- Brown, D.A. (2019) Acetylcholine and cholinergic receptors. *Brain Neurosci Adv* 3: 2398212818820506.

- Brückner, H., and Westhauser, T. (1994) Chromatographic determination of D-amino acids as native constituents of vegetables and fruits. *Chromatographia* 39: 419–426.
- Brückner, H., and Westhauser, T. (2003) Chromatographic determination of L- and D-amino acids in plants. *Amino Acids* 24: 43–55.
- Brunet-Galmés, I., Busquets, A., Peña, A., Gomila, M., Nogales, B., García-Valdés, E., et al. (2012) Complete genome sequence of the naphthalene-degrading bacterium *Pseudomonas stutzeri* AN10 (CCUG 29243). *J Bacteriol* 194: 6642–6643.
- Bunkóczi, G., Echols, N., McCoy, A.J., Oeffner, R.D., Adams, P.D., and Read, R.J. (2013) Phaser.MRage: automated molecular replacement. *Acta Crystallogr D Biol Crystallogr* 69: 2276–2286.
- Burón-Barral, M. del C., Gosink, K.K., and Parkinson, J.S. (2006) Loss- and gain-of-function mutations in the F1-HAMP region of the *Escherichia coli* aerotaxis transducer Aer. *J Bacteriol* 188: 3477–3486.
- Burt, A., Cassidy, C.K., Stansfeld, P.J., and Gutsche, I. (2021) Alternative Architecture of the *E. coli* Chemosensory Array. *Biomolecules* 11: 495.
- Buschart, A., Sachs, S., Chen, X., Herglotz, J., Krause, A., and Reinhold-Hurek, B. (2012) Flagella mediate endophytic competence rather than act as MAMPS in rice-*Azoarcus* sp. strain BH72 interactions. *Mol Plant Microbe Interact* 25: 191–199.
- Buttimer, C., Hendrix, H., Lucid, A., Neve, H., Noben, J.-P., Franz, C., et al. (2018a) Novel N4-Like Bacteriophages of *Pectobacterium atrosepticum*. *Pharm Basel Switz* 11: 45.
- Buttimer, C., Lucid, A., Neve, H., Franz, C.M.A.P., O’Mahony, J., Turner, D., et al. (2018b) *Pectobacterium atrosepticum* Phage vB\_PatP\_CB5: A Member of the Proposed Genus “Phimunavirus.” *Viruses* 10: 394.
- Caffall, K.H., and Mohnen, D. (2009) The structure, function, and biosynthesis of plant cell wall pectic polysaccharides. *Carbohydr Res* 344: 1879–1900.
- Caiazza, N.C., Merritt, J.H., Brothers, K.M., and O’Toole, G.A. (2007) Inverse regulation of biofilm formation and swarming motility by *Pseudomonas aeruginosa* PA14. *J Bacteriol* 189: 3603–3612.
- Capra, E.J., and Laub, M.T. (2012) Evolution of two-component signal transduction systems. *Annu Rev Microbiol* 66: 325–347.
- Cassidy, C.K., Himes, B.A., Sun, D., Ma, J., Zhao, G., Parkinson, J.S., et al. (2020) Structure and dynamics of the *E. coli* chemotaxis core signaling complex by cryo-electron tomography and molecular simulations. *Commun Biol* 3: 24.
- Cerna-Vargas, J.P., Gumerov, V.M., Krell, T., and Zhulin, I.B. (2023) Amine recognizing domain in diverse receptors from bacteria and archaea evolved from the universal amino acid sensor. *BioRxiv Prepr Serv Biol* 2023.04.06.535858.
- Cerna-Vargas, J.P., Santamaría-Hernando, S., Matilla, M.A., Rodríguez-Herva, J.J., Daddaoua, A., Rodríguez-Palenzuela, P., et al. (2019) Chemoperception of Specific Amino Acids Controls Phytopathogenicity in *Pseudomonas syringae* pv. tomato. *MBio* 10,5 e01868-19.
- Chan, Y.-C., Wu, H.-P., and Chuang, D.-Y. (2009) Extracellular secretion of Carocin S1 in *Pectobacterium carotovorum* subsp. *carotovorum* occurs via the type III secretion system integral to the bacterial flagellum. *BMC Microbiol* 9: 181.

- Chanda, B., Venugopal, S.C., Kulshrestha, S., Navarre, D.A., Downie, B., Vaillancourt, L., et al. (2008) Glycerol-3-phosphate levels are associated with basal resistance to the hemibiotrophic fungus *Colletotrichum higginsianum* in *Arabidopsis*. *Plant Physiol* 147: 2017–2029.
- Chanda, B., Xia, Y., Mandal, M.K., Yu, K., Sekine, K.-T., Gao, Q., et al. (2011) Glycerol-3-phosphate is a critical mobile inducer of systemic immunity in plants. *Nat Genet* 43: 421–427.
- Charkowski, A., Sharma, K., Parker, M.L., Secor, G.A., and Elphinstone, J. (2020) Bacterial Diseases of Potato. In *The Potato Crop*. Campos, H., and Ortiz, O. (eds). *Springer International Publishing*, Cham. pp. 351–388.
- Charkowski, A.O., Lind, J., and Rubio-Salazar, I. (2014) Genomics of Plant-Associated Bacteria: The Soft Rot Enterobacteriaceae. In *Genomics of Plant-Associated Bacteria*. Gross, D.C., Lichens-Park, A., and Kole, C. (eds). *Springer Berlin Heidelberg*, Berlin, Heidelberg. pp. 37–58.
- Chatterjee, S., Almeida, R.P.P., and Lindow, S. (2008) Living in two worlds: the plant and insect lifestyles of *Xylella fastidiosa*. *Annu Rev Phytopathol* 46: 243–271.
- Chen, V.B., Arendall, W.B., Headd, J.J., Keedy, D.A., Immormino, R.M., Kapral, G.J., et al. (2010) MolProbity: all-atom structure validation for macromolecular crystallography. *Acta Crystallogr D Biol Crystallogr* 66: 12–21.
- Chervitz, S.A., and Falke, J.J. (1996) Molecular mechanism of transmembrane signaling by the aspartate receptor: a model. *Proc Natl Acad Sci U S A* 93: 2545–2550.
- Chesnokova, O., Coutinho, J.B., Khan, I.H., Mikhail, M.S., and Kado, C.I. (1997) Characterization of flagella genes of *Agrobacterium tumefaciens*, and the effect of a bald strain on virulence. *Mol Microbiol* 23: 579–590.
- Chet, I., Henis, Y., and Mitchell, R. (1973) Effect of biogenic amines and cannabinoids on bacterial chemotaxis. *J Bacteriol* 115: 1215–1218.
- Cheung, J., and Hendrickson, W.A. (2008) Crystal structures of C4-dicarboxylate ligand complexes with sensor domains of histidine kinases DcuS and DctB. *J Biol Chem* 283: 30256–30265.
- Cho, H., Wang, W., Kim, R., Yokota, H., Damo, S., Kim, S.H., et al. (2001) BeF(3)(-) acts as a phosphate analog in proteins phosphorylated on aspartate: structure of a BeF(3)(-) complex with phosphoserine phosphatase. *Proc Natl Acad Sci U S A* 98: 8525–8530.
- Cho, K.-H., Crane, B.R., and Park, S. (2011) An insight into the interaction mode between CheB and chemoreceptor from two crystal structures of CheB methyltransferase catalytic domain. *Biochem Biophys Res Commun* 411: 69–75.
- Chuang, D.-Y., Chien, Y.-C., and Wu, H.-P. (2007) Cloning and expression of the *Erwinia carotovora* subsp. *carotovora* gene encoding the low-molecular-weight bacteriocin carocin S1. *J Bacteriol* 189: 620–626.
- Clarke, M.B., Hughes, D.T., Zhu, C., Boedeker, E.C., and Sperandio, V. (2006) The QseC sensor kinase: a bacterial adrenergic receptor. *Proc Natl Acad Sci U S A* 103: 10420–10425.
- Clarke, S., and Koshland, D.E., Jr. (1979) Membrane receptors for aspartate and serine in bacterial chemotaxis. *J Biol Chem* 254: 9695–702.
- Coleman, M.D., Bass, R.B., Mehan, R.S., and Falke, J.J. (2005) Conserved glycine residues in the cytoplasmic domain of the aspartate receptor play essential roles in kinase coupling and on-off switching. *Biochemistry* 44: 7687–7695.

- Colin, R., Ni, B., Laganenka, L., and Sourjik, V. (2021) Multiple functions of flagellar motility and chemotaxis in bacterial physiology. *FEMS Microbiol Rev* 45,6: fuab038.
- Colin, R., and Sourjik, V. (2017) Emergent properties of bacterial chemotaxis pathway. *Curr Opin Microbiol* 39: 24–33.
- Collaborative Computational Project, Number 4 (1994) The CCP4 suite: programs for protein crystallography. *Acta Crystallogr D Biol Crystallogr* 50: 760–763.
- Collins, K.D., Lacal, J., and Ottemann, K.M. (2014) Internal sense of direction: sensing and signaling from cytoplasmic chemoreceptors. *Microbiol Mol Biol Rev* 78: 672–684.
- Combet, C., Blanchet, C., Geourjon, C., and Deléage, G. (2000) NPS@: network protein sequence analysis. *Trends Biochem Sci* 25: 147–150.
- Compton, K.K., Hildreth, S.B., Helm, R.F., and Scharf, B.E. (2018) *Sinorhizobium meliloti* Chemoreceptor McpV Senses Short-Chain Carboxylates via Direct Binding. *J Bacteriol* 200: e00519-18.
- Compton, K.K., and Scharf, B.E. (2021) Rhizobial Chemoattractants, the Taste and Preferences of Legume Symbionts. *Front Plant Sci* 12: 686465.
- Condinho, M., Carvalho, B., Cruz, A., Pinto, S.N., Arraiano, C.M., and Pobre, V. (2022) The role of RNA regulators, quorum sensing and c-di-GMP in bacterial biofilm formation. *FEBS Open Bio*: 10.1002/2211-5463.13389.
- Cornforth, D.M., Dees, J.L., Ibberson, C.B., Huse, H.K., Mathiesen, I.H., Kirketerp-Møller, K., et al. (2018) *Pseudomonas aeruginosa* transcriptome during human infection. *Proc Natl Acad Sci U S A* 115: E5125–E5134.
- Corral-Lugo, A., Matilla, M.A., Martín-Mora, D., Silva Jiménez, H., Mesa Torres, N., Kato, J., et al. (2018) High-affinity chemotaxis to histamine mediated by the TlpQ chemoreceptor of the human pathogen *Pseudomonas aeruginosa*. *MBio* 9,6 e01894-18.
- Corso, G., Stärk, H., Jing, B., Barzilay, R., and Jaakkola, T. DiffDock: Diffusion Steps, Twists, and Turns for Molecular Docking. *1048550/arXiv221001776*.
- Cosgrove, D.J. (1997) Assembly and enlargement of the primary cell wall in plants. *Annu Rev Cell Dev Biol* 13: 171–201.
- Cremer, J., Honda, T., Tang, Y., Wong-Ng, J., Vergassola, M., and Hwa, T. (2019) Chemotaxis as a navigation strategy to boost range expansion. *Nature* 575: 658–663.
- Cronan, J.E. (2003) Bacterial membrane lipids: where do we stand? *Annu Rev Microbiol* 57: 203–224.
- Crone, S., Vives-Flórez, M., Kvich, L., Saunders, A.M., Malone, M., Nicolaisen, M.H., et al. (2020) The environmental occurrence of *Pseudomonas aeruginosa*. *APMIS Acta Pathol Microbiol Immunol Scand* 128: 220–231.
- Crooks, G.E., Hon, G., Chandonia, J.M., and Brenner, S.E. (2004) WebLogo: a sequence logo generator. *Genome Res* 14: 1188–90.
- Cserző, M., Wallin, E., Simon, I., Heijne, G. von, and Elofsson, A. (1997) Prediction of transmembrane alpha-helices in prokaryotic membrane proteins: the dense alignment surface method. *Protein Eng* 10: 673–676.

- Czajkowski, R., Pérombelon, M.C.M., Jafra, S., Lojkowska, E., Potrykus, M., Wolf, J.M. van der, and Sledz, W. (2015) Detection, identification and differentiation of *Pectobacterium* and *Dickeya* species causing potato blackleg and tuber soft rot: a review. *Ann Appl Biol* 166: 18–38.
- Czajkowski, R., Pérombelon, M.C.M., Veen, J.A. van, and Wolf, J.M. van der (2011) Control of blackleg and tuber soft rot of potato caused by *Pectobacterium* and *Dickeya* species: a review: Control of *Dickeya* and *Pectobacterium* species in potato. *Plant Pathol* 60: 999–1013.
- Damron, F.H., Oglesby-Sherrouse, A.G., Wilks, A., and Barbier, M. (2016) Dual-seq transcriptomics reveals the battle for iron during *Pseudomonas aeruginosa* acute murine pneumonia. *Sci Rep* 6: 39172.
- Dannelly, K.H., Liu, Y., and Ghosh, S.K. (2001) *Pseudomonas aeruginosa* corneal infection affects cholinergic enzymes in rat lacrimal gland. *Arch Microbiol* 177: 47–53.
- Davidsson, P.R., Kariola, T., Niemi, O., and Palva, E.T. (2013) Pathogenicity of and plant immunity to soft rot pectobacteria. *Front Plant Sci* 4: 191.
- Dees, M.W., Lebecka, R., Perminow, J.I.S., Czajkowski, R., Grupa, A., Motyka, A., et al. (2017) Characterization of *Dickeya* and *Pectobacterium* strains obtained from diseased potato plants in different climatic conditions of Norway and Poland. *Eur J Plant Pathol* 148: 839–851.
- Demarre, G., Guérout, A.-M., Matsumoto-Mashimo, C., Rowe-Magnus, D.A., Marlière, P., and Mazel, D. (2005a) A new family of mobilizable suicide plasmids based on broad host range R388 plasmid (IncW) and RP4 plasmid (IncPalpha) conjugative machineries and their cognate *Escherichia coli* host strains. *Res Microbiol* 156: 245–255.
- Dennis, J.J., and Zylstra, G.J. (1998) Plasposons: modular self-cloning minitransposon derivatives for rapid genetic analysis of gram-negative bacterial genomes. *Appl Env Microbiol* 64: 2710–5.
- Deochand, D.K., Meariman, J.K., and Grove, A. (2016) pH-Dependent DNA Distortion and Repression of Gene Expression by *Pectobacterium atrosepticum* PecS. *ACS Chem Biol* 11: 2049–2056.
- Deochand, D.K., Pande, A., Meariman, J.K., and Grove, A. (2019) Redox Sensing by PecS from the Plant Pathogen *Pectobacterium atrosepticum* and Its Effect on Gene Expression and the Conformation of PecS-Bound Promoter DNA. *Biochemistry* 58: 2564–2575.
- Dhodary, B., Sampedro, I., Behroozian, S., Borza, V., Her, S., and Hill, J.E. (2022) The Arginine Catabolism-Derived Amino Acid L-ornithine Is a Chemoattractant for *Pseudomonas aeruginosa*. *Microorganisms* 10: 264.
- Djordjevic, S., Goudreau, P.N., Xu, Q., Stock, A.M., and West, A.H. (1998) Structural basis for methyltransferase CheB regulation by a phosphorylation-activated domain. *Proc Natl Acad Sci U S A* 95: 1381–1386.
- Djordjevic, S., and Stock, A.M. (1998) Chemotaxis receptor recognition by protein methyltransferase CheR. *Nat Struct Biol* 5: 446–450.
- Doorn, J. van, Vreeburg, P.J.M., Leeuwen, P.J. van, and Dees, R.H.L. (2011) The presence and survival of soft rot (*Erwinia*) in flower bulb production systems. *Acta Hort.* 886, 365-379.
- Du, S., Wey, M., and Armstrong, D.W. (2023) d-Amino acids in biological systems. *Chirality*, 10.1002/chir.23562.

- Dufour, Y.S., Gillet, S., Frankel, N.W., Weibel, D.B., and Emonet, T. (2016) Direct Correlation between Motile Behavior and Protein Abundance in Single Cells. *PLoS Comput Biol* 12: e1005041.
- Dunin-Horkawicz, S., and Lupas, A.N. (2010) Comprehensive analysis of HAMP domains: implications for transmembrane signal transduction. *J Mol Biol* 397: 1156–1174.
- Dupuis, B., Nkuriyingoma, P., and Van Gijsegem, F. (2021) Economic Impact of *Pectobacterium* and *Dickeya* Species on Potato Crops: A Review and Case Study. In *Plant Diseases Caused by Dickeya and Pectobacterium Species*. Van Gijsegem, F., Wolf, J.M. van der, and Toth, I.K. (eds). *Springer International Publishing*, Cham. pp. 263–282.
- Dwyer, M.A., and Hellinga, H.W. (2004) Periplasmic binding proteins: a versatile superfamily for protein engineering. *Curr Opin Struct Biol* 14: 495–504.
- Ehrhardt, M.K.G., Gerth, M.L., and Johnston, J.M. (2021) Structure of a double CACHE chemoreceptor ligand-binding domain from *Pseudomonas syringae* provides insights into the basis of proline recognition. *Biochem Biophys Res Commun* 549: 194–199.
- Elgamoudi, B.A., Andrianova, E.P., Shewell, L.K., Day, C.J., King, R.M., Taha, et al. (2021) The *Campylobacter jejuni* chemoreceptor Tlp10 has a bimodal ligand-binding domain and specificity for multiple classes of chemoeffectors. *Sci Signal* 14: eabc8521.
- El-Gebali, S., Mistry, J., Bateman, A., Eddy, S.R., Luciani, A., Potter, S.C., et al. (2019) The Pfam protein families database in 2019. *Nucleic Acids Res* 47: D427–D432.
- Elliott, K.T., and Dirita, V.J. (2008) Characterization of CetA and CetB, a bipartite energy taxis system in *Campylobacter jejuni*. *Mol Microbiol* 69: 1091–1103.
- Emsley, P., Lohkamp, B., Scott, W.G., and Cowtan, K. (2010) Features and development of Coot. *Acta Crystallogr D Biol Crystallogr* 66: 486–501.
- Erbse, A.H., and Falke, J.J. (2009) The core signaling proteins of bacterial chemotaxis assemble to form an ultrastable complex. *Biochemistry* 48: 6975–6987.
- Espinosa-Urgel, M., and Ramos, J.-L. (2004) Cell density-dependent gene contributes to efficient seed colonization by *Pseudomonas putida* KT2440. *Appl Environ Microbiol* 70: 5190–5198.
- Evans, P.R., and Murshudov, G.N. (2013) How good are my data and what is the resolution? *Acta Crystallogr D Biol Crystallogr* 69: 1204–1214.
- Evans, T.J., Coulthurst, S.J., Komitopoulou, E., and Salmond, G.P.C. (2010) Two mobile *Pectobacterium atrosepticum* prophages modulate virulence. *FEMS Microbiol Lett* 304: 195–202.
- Fagard, M., Dellagi, A., Roux, C., Périno, C., Rigault, M., Boucher, V., et al. (2007) *Arabidopsis thaliana* Expresses Multiple Lines of Defense to Counterattack *Erwinia chrysanthemi*. *Mol Plant-Microbe Interactions* 20: 794–805.
- Falke, J.J., and Hazelbauer, G.L. (2001) Transmembrane signaling in bacterial chemoreceptors. *Trends Biochem Sci* 26: 257–265.
- Feng, H., Lv, Y., Krell, T., Fu, R., Liu, Y., Xu, Z., et al. (2022) Signal binding at both modules of its dCache domain enables the McpA chemoreceptor of *Bacillus velezensis* to sense different ligands. *Proc Natl Acad Sci U S A* 119: e2201747119.

- Feng, H., Zhang, N., Fu, R., Liu, Y., Krell, T., Du, W., et al. (2019) Recognition of dominant attractants by key chemoreceptors mediates recruitment of plant growth-promoting rhizobacteria. *Env Microbiol* 21: 402–415.
- Feng, X., Baumgartner, J.W., and Hazelbauer, G.L. (1997) High- and low-abundance chemoreceptors in *Escherichia coli*: differential activities associated with closely related cytoplasmic domains. *J Bacteriol* 179: 6714–20.
- Feng, X., Lilly, A.A., and Hazelbauer, G.L. (1999) Enhanced function conferred on low-abundance chemoreceptor Trg by a methyltransferase-docking site. *J Bacteriol* 181: 3164–71.
- Fernandez, M., Ortega, A., Rico-Jimenez, M., Martin-Mora, D., Daddaoua, A., Matilla, M.A., and Krell, T. (2018) High-Throughput Screening to Identify Chemoreceptor Ligands. *Methods Mol Biol* 1729: 291–301.
- Fernández-Llamosas, H., Díaz, E., and Carmona, M. (2021) Motility, adhesion and c-di-GMP influence the endophytic colonization of rice by *Azoarcus* sp. CIB. *Microorganisms* 9: 554.
- Ferrández, A., Hawkins, A.C., Summerfield, D.T., and Harwood, C.S. (2002) Cluster II che genes from *Pseudomonas aeruginosa* are required for an optimal chemotactic response. *J Bacteriol* 184: 4374–4383.
- Flack, C.E., and Parkinson, J.S. (2018) A zipped-helix cap potentiates HAMP domain control of chemoreceptor signaling. *Proc Natl Acad Sci U S A* 115: E3519–E3528.
- Flemming, H.-C., and Wuertz, S. (2019) Bacteria and archaea on Earth and their abundance in biofilms. *Nat Rev Microbiol* 17: 247–260.
- Foster, D.L., Mowbray, S.L., Jap, B.K., and Koshland, D.E. (1985) Purification and characterization of the aspartate chemoreceptor. *J Biol Chem* 260: 11706–11710.
- Fulcher, N.B., Holliday, P.M., Klem, E., Cann, M.J., and Wolfgang, M.C. (2010) The *Pseudomonas aeruginosa* Chp chemosensory system regulates intracellular cAMP levels by modulating adenylate cyclase activity. *Mol Microbiol* 76: 889–904.
- Funakoshi, M., Sekine, M., Katane, M., Furuchi, T., Yohda, M., Yoshikawa, T., and Homma, H. (2008) Cloning and functional characterization of *Arabidopsis thaliana* D-amino acid aminotransferase-D-aspartate behavior during germination. *FEBS J* 275: 1188–1200.
- Gabadinho, J., Beteva, A., Guijarro, M., Rey-Bakaikoa, V., Spruce, D., Bowler, M.W., et al. (2010) MxCuBE: a synchrotron beamline control environment customized for macromolecular crystallography experiments. *J Synchrotron Radiat* 17: 700–707.
- Galperin, M.Y. (2004) Bacterial signal transduction network in a genomic perspective. *Environ Microbiol* 6: 552–567.
- Galperin, M.Y. (2006) Structural classification of bacterial response regulators: diversity of output domains and domain combinations. *J Bacteriol* 188: 4169–4182.
- Galperin, M.Y. (2010) Diversity of structure and function of response regulator output domains. *Curr Opin Microbiol* 13: 150–159.
- Galperin, M.Y. (2018) What bacteria want. *Env Microbiol* 20: 4221–4229.
- Gálvez-Roldán, C., Cerna-Vargas, J.P., Rodríguez Herva, J.J., Krell, T., Santamaria-Hernando, S., and López-Solanilla, E. (2022) A NIT sensor domain containing chemoreceptor is required for a successful entry and virulence of *Dickeya dadantii* 3937 in potato plants. *Phytopathology* 113,3: 390-399.



- Gao, R., and Stock, A.M. (2009) Biological insights from structures of two-component proteins. *Annu Rev Microbiol* 63: 133–154.
- García, D., Orillard, E., Johnson, M.S., and Watts, K.J. (2017) Gas Sensing and Signaling in the PAS-Heme Domain of the *Pseudomonas aeruginosa* Aer2 Receptor. *J Bacteriol* 199: e00003-17.
- García, D., Watts, K.J., Johnson, M.S., and Taylor, B.L. (2016) Delineating PAS-HAMP interaction surfaces and signalling-associated changes in the aerotaxis receptor Aer. *Mol Microbiol* 100: 156–172.
- García, V., Reyes-Darias, J.-A., Martín-Mora, D., Morel, B., Matilla, M.A., and Krell, T. (2015a) Identification of a Chemoreceptor for C2 and C3 Carboxylic Acids. *Appl Environ Microbiol* 81: 5449–5457.
- García-Fontana, C., Corral Lugo, A., and Krell, T. (2014) Specificity of the CheR2 methyltransferase in *Pseudomonas aeruginosa* is directed by a C-terminal pentapeptide in the McpB chemoreceptor. *Sci Signal* 7: ra34.
- García-Fontana, C., Reyes-Darias, J.A., Muñoz-Martínez, F., Alfonso, C., Morel, B., Ramos, J.L., and Krell, T. (2013) High specificity in CheR methyltransferase function: CheR2 of *Pseudomonas putida* is essential for chemotaxis, whereas CheR1 is involved in biofilm formation. *J Biol Chem* 288: 18987–18999.
- García-Fontana, C., Vílchez, J.I., González-Requena, M., González-López, J., Krell, T., Matilla, M.A., and Manzanera, M. (2019) The involvement of McpB chemoreceptor from *Pseudomonas aeruginosa* PAO1 in virulence. *Sci Rep* 9: 13166.
- Gardina, P.J., Bormans, A.F., and Manson, M.D. (1998) A mechanism for simultaneous sensing of aspartate and maltose by the Tar chemoreceptor of *Escherichia coli*. *Mol Microbiol* 29: 1147–1154.
- Garita-Cambroner, J., Palacio-Bielsa, A., López, M.M., and Cubero, J. (2016) Comparative Genomic and Phenotypic Characterization of Pathogenic and Non-Pathogenic Strains of *Xanthomonas arboricola* Reveals Insights into the Infection Process of Bacterial Spot Disease of Stone Fruits. *PLoS One* 11: e0161977.
- Garvis, S., Munder, A., Ball, G., Bentzmann, S. de, Wiehlmann, L., Ewbank, J.J., et al. (2009) *Caenorhabditis elegans* semi-automated liquid screen reveals a specialized role for the chemotaxis gene *cheB2* in *Pseudomonas aeruginosa* virulence. *PLoS Pathog* 5: e1000540.
- Gasperotti, A.F., Karina Herrera Seitz, M., Balmaceda, R.S., Prosa, L.M., Jung, K., and Studdert, C.A. (2020) Direct binding of benzoate derivatives to two chemoreceptors with Cache sensor domains in *Halomonas titanicae* KHS3. *Mol Microbiol* 115: 672–683.
- Gavira, J.A., Gumerov, V.M., Rico-Jiménez, M., Petukh, M., Upadhyay, A.A., Ortega, A., et al. (2020) How Bacterial Chemoreceptors Evolve Novel Ligand Specificities. *mBio* 11: e03066-19.
- Gavira, J.A., Lacal, J., Ramos, J.L., García-Ruiz, J.M., Krell, T., and Pineda-Molina, E. (2012) Crystallization and crystallographic analysis of the ligand-binding domain of the *Pseudomonas putida* chemoreceptor McpS in complex with malate and succinate. *Acta Crystallogr Sect F Struct Biol Cryst Commun* 68: 428–431.
- Gavira, J.A., Matilla, M.A., Fernández, M., and Krell, T. (2021) The structural basis for signal promiscuity in a bacterial chemoreceptor. *FEBS J* 288: 2294–2310.

- Gavira, J.A., Ortega, Á., Martín-Mora, D., Conejero-Muriel, M.T., Corral-Lugo, A., Morel, B., et al. (2018) Structural basis for polyamine binding at the dCACHE domain of the McpU chemoreceptor from *Pseudomonas putida*. *J Mol Biol* 430: 1950–1963.
- Glekas, G.D., Mulhern, B.J., Kroc, A., Duelfer, K.A., Lei, V., Rao, C.V., and Ordal, G.W. (2012) The *Bacillus subtilis* chemoreceptor McpC senses multiple ligands using two discrete mechanisms. *J Biol Chem* 287: 39412–8.
- Goers Sweeney, E., Henderson, J.N., Goers, J., Wreden, C., Hicks, K.G., Foster, J.K., et al. (2012) Structure and proposed mechanism for the pH-sensing *Helicobacter pylori* chemoreceptor TlpB. *Structure* 20: 1177–1188.
- González-Ramírez, L.A., Ruiz-Martínez, C.R., Estremera-Andújar, R.A., Nieves-Marrero, C.A., García-Caballero, A., Gavira, J.A., et al. (2017) Efficient Screening Methodology for Protein Crystallization Based on the Counter-Diffusion Technique. *Cryst Growth Des* 17: 6780–6786.
- Gorshkov, V., Daminova, A., Ageeva, M., Petrova, O., Gogoleva, N., Tarasova, N., and Gogolev, Y. (2014) Dissociation of a population of *Pectobacterium atrosepticum* SCRI1043 in tobacco plants: formation of bacterial emboli and dormant cells. *Protoplasts* 251: 499–510.
- Gorshkov, V., Gubaev, R., Petrova, O., Daminova, A., Gogoleva, N., Ageeva, M., et al. (2018) Transcriptome profiling helps to identify potential and true molecular switches of stealth to brute force behavior in *Pectobacterium atrosepticum* during systemic colonization of tobacco plants. *Eur J Plant Pathol* 152: 957–976.
- Gorshkov, V., Kwenda, S., Petrova, O., Osipova, E., Gogolev, Y., and Moleleki, L.N. (2017) Global Gene Expression Analysis of Cross-Protected Phenotype of *Pectobacterium atrosepticum*. *PLoS One* 12: e0169536.
- Gorshkov, V.Y., Daminova, A.G., Mikshina, P.V., Petrova, O.E., Ageeva, M.V., Salnikov, V.V., et al. (2016) Pathogen-induced conditioning of the primary xylem vessels - a prerequisite for the formation of bacterial emboli by *Pectobacterium atrosepticum*. *Plant Biol* 18: 609–617.
- Grando, S.A., Kawashima, K., Kirkpatrick, C.J., Kummer, W., and Wessler, I. (2015) Recent progress in revealing the biological and medical significance of the non-neuronal cholinergic system. *Int Immunopharmacol* 29: 1–7.
- Grognot, M., and Taute, K.M. (2021) More than propellers: how flagella shape bacterial motility behaviors. *Curr Opin Microbiol* 61: 73–81.
- Gude, S., Pinçe, E., Taute, K.M., Seinen, A.-B., Shimizu, T.S., and Tans, S.J. (2020) Bacterial coexistence driven by motility and spatial competition. *Nature* 578: 588–592.
- Guhaniyogi, J., Robinson, V.L., and Stock, A.M. (2006) Crystal structures of beryllium fluoride-free and beryllium fluoride-bound CheY in complex with the conserved C-terminal peptide of CheZ reveal dual binding modes specific to CheY conformation. *J Mol Biol* 359: 624–645.
- Gumerov, V.M., Andrianova, E.P., Matilla, M.A., Page, K.M., Monteagudo-Cascales, E., Dolphin, A.C., et al. (2022) Amino acid sensor conserved from bacteria to humans. *Proc Natl Acad Sci U S A* 119: e2110415119.
- Gumerov, V.M., Andrianova, E.P., and Zhulin, I.B. (2021) Diversity of bacterial chemosensory systems. *Curr Opin Microbiol* 61: 42–50.

- Gumerov, V.M., Ortega, D.R., Adebali, O., Ulrich, L.E., and Zhulin, I.B. (2020) MiST 3.0: an updated microbial signal transduction database with an emphasis on chemosensory systems. *Nucleic Acids Res* 48: D459–D464.
- Gushchin, I., Melnikov, I., Polovinkin, V., Ishchenko, A., Yuzhakova, A., Buslaev, P., et al. (2017) Mechanism of transmembrane signaling by sensor histidine kinases. *Science* 356,6342: eaah6345.
- Hadjidemetriou, K., Kaur, S., Cassidy, C.K., and Zhang, P. (2022) Mechanisms of *E. coli* chemotaxis signaling pathways visualized using cryoET and computational approaches. *Biochem Soc Trans* 50: 1595–1605.
- Haefele, D.M., and Lindow, S.E. (1987) Flagellar motility confers epiphytic fitness advantages upon *Pseudomonas syringae*. *Appl Env Microbiol* 53: 2528–2533.
- Hanyu, H., Engevik, K.A., Matthis, A.L., Ottemann, K.M., Montrose, M.H., and Aihara, E. (2019) *Helicobacter pylori* Uses the TlpB Receptor To Sense Sites of Gastric Injury. *Infect Immun* 87: e00202-19.
- Hartmann, E., and Kilbinger, H. (1974) Occurrence of light-dependent acetylcholine concentrations in higher plants. *Experientia* 30: 1397–1398.
- Hauben, L., Moore, E.R., Vauterin, L., Steenackers, M., Mergaert, J., Verdonck, L., and Swings, J. (1998) Phylogenetic position of phytopathogens within the Enterobacteriaceae. *Syst Appl Microbiol* 21: 384–397.
- Hazelbauer, G.L. (2012) Bacterial chemotaxis: the early years of molecular studies. *Annu Rev Microbiol* 66: 285–303.
- Hazelbauer, G.L., Falke, J.J., and Parkinson, J.S. (2008a) Bacterial chemoreceptors: high-performance signaling in networked arrays. *Trends Biochem Sci* 33: 9–19.
- Hazelbauer, G.L., and Lai, W.-C. (2010) Bacterial chemoreceptors: providing enhanced features to two-component signaling. *Curr Opin Microbiol* 13: 124–132.
- Hedblom, M.L., and Adler, J. (1983) Chemotactic response of *Escherichia coli* to chemically synthesized amino acids. *J Bacteriol* 155: 1463–6.
- Hegde, M., Englert, D.L., Schrock, S., Cohn, W.B., Vogt, C., Wood, T.K., et al. (2011) Chemotaxis to the quorum-sensing signal AI-2 requires the Tsr chemoreceptor and the periplasmic LsrB AI-2-binding protein. *J Bacteriol* 193: 768–773.
- Hemsley, A., Arnheim, N., Toney, M.D., Cortopassi, G., and Galas, D.J. (1989) A simple method for site-directed mutagenesis using the polymerase chain reaction. *Nucleic Acids Res* 17: 6545–6551.
- Henry, J.T., and Crosson, S. (2011) Ligand-binding PAS domains in a genomic, cellular, and structural context. *Annu Rev Microbiol* 65: 261–286.
- Herrera Seitz, M.K., Frank, V., Massazza, D.A., Vaknin, A., and Studdert, C.A. (2014) Bacterial chemoreceptors of different length classes signal independently. *Mol Microbiol* 93: 814–822.
- Herrero, M., Lorenzo, V. de, and Timmis, K.N. (1990) Transposon vectors containing non-antibiotic resistance selection markers for cloning and stable chromosomal insertion of foreign genes in gram-negative bacteria. *J Bacteriol* 172: 6557–6567.

- Hickman, J.W., Tifrea, D.F., and Harwood, C.S. (2005) A chemosensory system that regulates biofilm formation through modulation of cyclic diguanylate levels. *Proc Natl Acad Sci U S A* 102: 14422–14427.
- Hida, A., Oku, S., Kawasaki, T., Nakashimada, Y., Tajima, T., and Kato, J. (2015) Identification of the *mcpA* and *mcpM* genes, encoding methyl-accepting proteins involved in amino acid and l-malate chemotaxis, and involvement of McpM-mediated chemotaxis in plant infection by *Ralstonia pseudosolanacearum* (formerly *Ralstonia solanacearum* phylotypes I and III). *Appl Environ Microbiol* 81: 7420–7430.
- Hida, A., Oku, S., Miura, M., Matsuda, H., Tajima, T., and Kato, J. (2020) Characterization of methyl-accepting chemotaxis proteins (MCPs) for amino acids in plant-growth-promoting rhizobacterium *Pseudomonas protegens* CHA0 and enhancement of amino acid chemotaxis by MCP genes overexpression. *Biosci Biotechnol Biochem* 84: 1948–1957.
- Hida, A., Oku, S., Nakashimada, Y., Tajima, T., and Kato, J. (2017) Identification of boric acid as a novel chemoattractant and elucidation of its chemoreceptor in *Ralstonia pseudosolanacearum* Ps29. *Sci Rep* 7: 8609.
- Hida, A., Tajima, T., and Kato, J. (2019) Two citrate chemoreceptors involved in chemotaxis to citrate and/or citrate-metal complexes in *Ralstonia pseudosolanacearum*. *J Biosci Bioeng* 127: 169–175.
- Hinton, J.C.D., Sidebotham, J.M., Hyman, L.J., Pérombelon, M.C.M., and Salmond, G.P.C. (1989) Isolation and characterisation of transposon-induced mutants of *Erwinia carotovora* subsp. *atroseptica* exhibiting reduced virulence. *Mol Gen Genet* MGG 217: 141–148.
- Hong, C.S., Shitashiro, M., Kuroda, A., Ikeda, T., Takiguchi, N., Ohtake, H., and Kato, J. (2004) Chemotaxis proteins and transducers for aerotaxis in *Pseudomonas aeruginosa*. *FEMS Microbiol Lett* 231: 247–252.
- Hong, Y., Huang, Z., Guo, L., Ni, B., Jiang, C.-Y., Li, X.-J., et al. (2019) The ligand-binding domain of a chemoreceptor from *Comamonas testosteroni* has a previously unknown homotrimeric structure. *Mol Microbiol* 112: 906–917.
- Hosking, E.R., Vogt, C., Bakker, E.P., and Manson, M.D. (2006) The *Escherichia coli* MotAB proton channel unplugged. *J Mol Biol* 364: 921–937.
- Huang, J.Y., Sweeney, E.G., Sigal, M., Zhang, H.C., Remington, S.J., Cantrell, M.A., et al. (2015) Chemodetection and Destruction of Host Urea Allows *Helicobacter pylori* to Locate the Epithelium. *Cell Host Microbe* 18: 147–56.
- Huang, Y., Lemieux, M.J., Song, J., Auer, M., and Wang, D.-N. (2003) Structure and mechanism of the glycerol-3-phosphate transporter from *Escherichia coli*. *Science* 301: 616–620.
- Huang, Y., Liu, C.L., Wang, H., Guan, T., Liu, L., and Yu, S. (2019a) Bioinformatic analysis of the complete genome sequence of *Pectobacterium carotovorum* subsp. *brasiliense* BZA12 and candidate effector screening. *J Plant Pathol* 101: 39–49.
- Huang, Z., Ni, B., Jiang, C.-Y., Wu, Y.-F., He, Y.-Z., Parales, R.E., and Liu, S.-J. (2016) Direct sensing and signal transduction during bacterial chemotaxis toward aromatic compounds in *Comamonas testosteroni*. *Mol Microbiol* 101: 224–237.
- Huang, Z., Pan, X., Xu, N., and Guo, M. (2019b) Bacterial chemotaxis coupling protein: Structure, function and diversity. *Microbiol Res* 219: 40–48.

- Huang, Z., Wang, Y.-H., Zhu, H.-Z., Andrianova, E.P., Jiang, C.-Y., Li, D., et al. (2019c) Cross Talk between Chemosensory Pathways That Modulate Chemotaxis and Biofilm Formation. *mBio* 10: e02876-18.
- Hugouvieux-Cotte-Pattat, N., Blot, N., and Reverchon, S. (2001) Identification of TogMNAB, an ABC transporter which mediates the uptake of pectic oligomers in *Erwinia chrysanthemi* 3937. *Mol Microbiol* 41: 1113–1123.
- Hulko, M., Berndt, F., Gruber, M., Linder, J.U., Truffault, V., Schultz, A., et al. (2006) The HAMP domain structure implies helix rotation in transmembrane signaling. *Cell* 126: 929–940.
- Ichinose, Y., Taguchi, F., and Mukaiyama, T. (2013) Pathogenicity and virulence factors of *Pseudomonas syringae*. *J Gen Plant Pathol* 79: 285–296.
- Iglewski, B.H. (1996) *Pseudomonas*. In Medical Microbiology. Baron, S. (ed.). University of Texas Medical Branch at Galveston, Galveston (TX).
- Igo, M.M., Ninfa, A.J., Stock, J.B., and Silhavy, T.J. (1989) Phosphorylation and dephosphorylation of a bacterial transcriptional activator by a transmembrane receptor. *Genes Dev* 3: 1725–1734.
- Imelio, J.A., Trajtenberg, F., and Buschiazzo, A. (2021) Allostery and protein plasticity: the keystones for bacterial signaling and regulation. *Biophys Rev* 13: 943–953.
- Incardona, M.-F., Bourenkov, G.P., Levik, K., Pieritz, R.A., Popov, A.N., and Svensson, O. (2009) EDNA: a framework for plugin-based applications applied to X-ray experiment online data analysis. *J Synchrotron Radiat* 16: 872–879.
- Inda, M.E., Vandenbranden, M., Fernández, A., Mendoza, D. de, Ruyschaert, J.-M., and Cybulski, L.E. (2014) A lipid-mediated conformational switch modulates the thermosensing activity of DesK. *Proc Natl Acad Sci U S A* 111: 3579–3584.
- Jacobs, M.A., Alwood, A., Thaipisuttikul, I., Spencer, D., Haugen, E., Ernst, S., et al. (2003) Comprehensive transposon mutant library of *Pseudomonas aeruginosa*. *Proc Natl Acad Sci U S A* 100: 14339–14344.
- Jahn, C.E., Willis, D.K., and Charkowski, A.O. (2008) The Flagellar Sigma Factor FliA Is Required for *Dickeya dadantii* Virulence. *Mol Plant-Microbe Interactions* 21: 1431–1442.
- Jean, S.-S., Chang, Y.-C., Lin, W.-C., Lee, W.-S., Hsueh, P.-R., and Hsu, C.-W. (2020) Epidemiology, Treatment, and Prevention of Nosocomial Bacterial Pneumonia. *J Clin Med* 9: 275.
- Jeong, H., Barbe, V., Lee, C.H., Vallenet, D., Yu, D.S., Choi, S.-H., et al. (2009) Genome sequences of *Escherichia coli* B strains REL606 and BL21(DE3). *J Mol Biol* 394: 644–652.
- Johnson, K.S., Elgamoudi, B.A., Jen, F.E.-C., Day, C.J., Sweeney, E.G., Pryce, M.L., et al. (2021) The dCache chemoreceptor TlpA of *Helicobacter pylori* binds multiple attractant and antagonistic ligands via distinct sites. *MBio* 12: e0181921.
- Johnson, K.S., and Ottemann, K.M. (2018) Colonization, localization, and inflammation: the roles of *H. pylori* chemotaxis in vivo. *Curr Opin Microbiol* 41: 51–57.
- Jonkheer, E.M., Brankovics, B., Houwers, I.M., Wolf, J.M. van der, Bonants, P.J.M., Vreeburg, R.A.M., et al. (2021) The *Pectobacterium* pangenome, with a focus on *Pectobacterium brasiliense*, shows a robust core and extensive exchange of genes from a shared gene pool. *BMC Genomics* 22: 265.
- Jumper, J., Evans, R., Pritzel, A., Green, T., Figurnov, M., Ronneberger, O., et al. (2021) Highly accurate protein structure prediction with AlphaFold. *Nature* 596: 583–589.

- Kabbara, S., Hérivaux, A., Dugé de Bernonville, T., Courdavault, V., Clastre, M., Gastebois, A., et al. (2019) Diversity and evolution of sensor histidine kinases in eukaryotes. *Genome Biol Evol* 11: 86–108.
- Kabsch, W. (2010) XDS. *Acta Crystallogr D Biol Crystallogr* 66: 125–132.
- Kachroo, A., Liu, H., Yuan, X., Kurokawa, T., and Kachroo, P. (2022) Systemic acquired resistance-associated transport and metabolic regulation of salicylic acid and glycerol-3-phosphate. *Essays Biochem* 66: 673–681.
- Källberg, M., Wang, H., Wang, S., Peng, J., Wang, Z., Lu, H., and Xu, J. (2012) Template-based protein structure modeling using the RaptorX web server. *Nat Protoc* 7: 1511–1522.
- Kang, C.-I., Kim, S.-H., Kim, H.-B., Park, S.-W., Choe, Y.-J., Oh, M.-D., et al. (2003) *Pseudomonas aeruginosa* bacteremia: risk factors for mortality and influence of delayed receipt of effective antimicrobial therapy on clinical outcome. *Clin Infect Dis Off Publ Infect Dis Soc Am* 37: 745–751.
- Kang, J.E., Hwang, S., Yoo, N., Kim, B.S., and Chung, E.-H. (2022) A resveratrol oligomer, hopeaphenol suppresses virulence activity of *Pectobacterium atrosepticum* via the modulation of the master regulator, FlhDC. *Front Microbiol* 13: 999522.
- Kaniga, K., Delor, I., and Cornelis, G.R. (1991) A wide-host-range suicide vector for improving reverse genetics in gram-negative bacteria: inactivation of the *blaA* gene of *Yersinia enterocolitica*. *Gene* 109: 137–141.
- Kato, J., Nakamura, T., Kuroda, A., and Ohtake, H. (1999) Cloning and characterization of chemotaxis genes in *Pseudomonas aeruginosa*. *Biosci Biotechnol Biochem* 63: 155–161.
- Katoh, K., Rozewicki, J., and Yamada, K.D. (2019) MAFFT online service: multiple sequence alignment, interactive sequence choice and visualization. *Brief Bioinform* 20: 1160–1166.
- Katoh, K., and Standley, D.M. (2013) MAFFT multiple sequence alignment software version 7: improvements in performance and usability. *Mol Biol Evol* 30: 772–80.
- Keegstra, J.M., Carrara, F., and Stocker, R. (2022) The ecological roles of bacterial chemotaxis. *Nat Rev Microbiol* 20: 491–504.
- Keegstra, J.M., Kamino, K., Anquez, F., Lazova, M.D., Emonet, T., and Shimizu, T.S. (2017) Phenotypic diversity and temporal variability in a bacterial signaling network revealed by single-cell FRET. *Elife* 6; e27455.
- Kehry, M.R., Doak, T.G., and Dahlquist, F.W. (1985) Sensory adaptation in bacterial chemotaxis: regulation of demethylation. *J Bacteriol* 163: 983–990.
- Kelley, L.A., Mezulis, S., Yates, C.M., Wass, M.N., and Sternberg, M.J.E. (2015) The Phyre2 web portal for protein modeling, prediction and analysis. *Nat Protoc* 10: 845–858.
- Khan, M.F., Machuca, M.A., Rahman, M.M., Koç, C., Norton, R.S., Smith, B.J., and Roujeinikova, A. (2020) Structure-activity relationship study reveals the molecular basis for specific sensing of hydrophobic amino acids by the *Campylobacter jejuni* chemoreceptor Tlp3. *Biomolecules* 10: 744.
- Kim, H., and Farrand, S.K. (1998) Opine catabolic loci from *Agrobacterium* plasmids confer chemotaxis to their cognate substrates. *Mol Plant Microbe Interact* 11: 131–143.
- Kim, H.-E., Shitashiro, M., Kuroda, A., Takiguchi, N., Ohtake, H., and Kato, J. (2006) Identification and characterization of the chemotactic transducer in *Pseudomonas aeruginosa* PAO1 for positive chemotaxis to trichloroethylene. *J Bacteriol* 188: 6700–6702.

- Kim, H.-S., Thammarat, P., Lommel, S.A., Hogan, C.S., and Charkowski, A.O. (2011) *Pectobacterium carotovorum* Elicits Plant Cell Death with DspE/F but the *P. carotovorum* DspE Does Not Suppress Callose or Induce Expression of Plant Genes Early in Plant–Microbe Interactions. *Mol Plant-Microbe Interactions* 24: 773–786.
- Kim, K.K., Yokota, H., and Kim, S.H. (1999) Four-helical-bundle structure of the cytoplasmic domain of a serine chemotaxis receptor. *Nature* 400: 787–792.
- Kitanovic, S., Ames, P., and Parkinson, J.S. (2011) Mutational analysis of the control cable that mediates transmembrane signaling in the *Escherichia coli* serine chemoreceptor. *J Bacteriol* 193: 5062–5072.
- Knights, H.E., Jorriin, B., Haskett, T.L., and Poole, P.S. (2021) Deciphering bacterial mechanisms of root colonization. *Env Microbiol Rep* 13: 428–444.
- Koshland, D.E. (1974) Chemotaxis as a model for sensory systems. *FEBS Lett* 40: suppl:S3-9.
- Koshland, D.E. (1981) Biochemistry of sensing and adaptation in a simple bacterial system. *Annu Rev Biochem* 50: 765–782.
- Koskella, B. (2020) The phyllosphere. *Curr Biol CB* 30: R1143–R1146.
- Kumar, S., Stecher, G., Li, M., Knyaz, C., and Tamura, K. (2018) MEGA X: Molecular Evolutionary Genetics Analysis across Computing Platforms. *Mol Biol Evol* 35: 1547–1549.
- Kumar, V., Sharma, A., Kaur, R., Thukral, A.K., Bhardwaj, R., and Ahmad, P. (2017) Differential distribution of amino acids in plants. *Amino Acids* 49: 821–869.
- Kumar Verma, R., Samal, B., and Chatterjee, S. (2018) *Xanthomonas oryzae* pv. *oryzae* chemotaxis components and chemoreceptor Mcp2 are involved in the sensing of constituents of xylem sap and contribute to the regulation of virulence-associated functions and entry into rice. *Mol Plant Pathol* 19: 2397–2415.
- Kummer, W., Lips, K.S., and Pfeil, U. (2008) The epithelial cholinergic system of the airways. *Histochem Cell Biol* 130: 219–234.
- Kwenda, S., Motlolometsi, T.V., Birch, P.R.J., and Moleleki, L.N. (2016) RNA-seq Profiling Reveals Defense Responses in a Tolerant Potato Cultivar to Stem Infection by *Pectobacterium carotovorum* ssp. *brasiliense*. *Front Plant Sci* 7: 1905.
- Lacal, J., Alfonso, C., Liu, X., Parales, R.E., Morel, B., Conejero-Lara, F., et al. (2010a) Identification of a chemoreceptor for tricarboxylic acid cycle intermediates: differential chemotactic response towards receptor ligands. *J Biol Chem* 285: 23126–36.
- Lacal, J., García-Fontana, C., Muñoz-Martínez, F., Ramos, J.-L., and Krell, T. (2010b) Sensing of environmental signals: classification of chemoreceptors according to the size of their ligand binding regions. *Env Microbiol* 12: 2873–2884.
- Laganenka, L., Colin, R., and Sourjik, V. (2016) Chemotaxis towards autoinducer 2 mediates autoaggregation in *Escherichia coli*. *Nat Commun* 7: 12984.
- Laganenka, L., and Sourjik, V. (2018) Autoinducer 2-dependent *Escherichia coli* biofilm formation is enhanced in a dual-species coculture. *Appl Env Microbiol* 84,5 e02638-17.
- Lai, W.-C., and Hazelbauer, G.L. (2005) Carboxyl-terminal extensions beyond the conserved pentapeptide reduce rates of chemoreceptor adaptational modification. *J Bacteriol* 187: 5115–5121.

- Laskowski, R.A., Jabłońska, J., Pravda, L., Vařeková, R.S., and Thornton, J.M. (2018) PDBsum: Structural summaries of PDB entries. *Protein Sci Publ Protein Soc* 27: 129–134.
- Laskowski, R.A., MacArthur, M.W., Moss, D.S., and Thornton, J.M. (1993) PROCHECK: a program to check the stereochemical quality of protein structures. *J Appl Crystallogr* 26: 283–291.
- Laskowski, R.A., and Swindells, M.B. (2011) LigPlot+: multiple ligand-protein interaction diagrams for drug discovery. *J Chem Inf Model* 51: 2778–2786.
- Laub, M.T. (2010) The Role of Two-Component Signal Transduction Systems in Bacterial Stress Responses. In *Bacterial Stress Responses*. pp. 45–58.
- Lauffenburger, D., Aris, R., and Keller, K. (1982) Effects of cell motility and chemotaxis on microbial population growth. *Biophys J* 40: 209–219.
- Lazova, M.D., Butler, M.T., Shimizu, T.S., and Harshey, R.M. (2012) *Salmonella* chemoreceptors McpB and McpC mediate a repellent response to L-cystine: a potential mechanism to avoid oxidative conditions. *Mol Microbiol* 84: 697–711.
- Le Moual, H., Quang, T., and Koshland, D.E. (1997) Methylation of the *Escherichia coli* chemotaxis receptors: intra- and interdimer mechanisms. *Biochemistry* 36: 13441–13448.
- Leonard, S., Hommais, F., Nasser, W., and Reverchon, S. (2017) Plant-phytopathogen interactions: bacterial responses to environmental and plant stimuli. *Environ Microbiol* 19: 1689–1716.
- Li, J., Li, G., and Weis, R.M. (1997) The serine chemoreceptor from *Escherichia coli* is methylated through an inter-dimer process. *Biochemistry* 36: 11851–11857.
- Li, M., and Hazelbauer, G.L. (2004) Cellular stoichiometry of the components of the chemotaxis signaling complex. *J Bacteriol* 186: 3687–3694.
- Li, M., and Hazelbauer, G.L. (2005) Adaptational assistance in clusters of bacterial chemoreceptors. *Mol Microbiol* 56: 1617–1626.
- Li, M., and Hazelbauer, G.L. (2006) The carboxyl-terminal linker is important for chemoreceptor function. *Mol Microbiol* 60: 469–479.
- Li, M., and Hazelbauer, G.L. (2020) Methyltransferase CheR binds to its chemoreceptor substrates independent of their signaling conformation yet modifies them differentially. *Protein Sci* 29: 443–454.
- Li, M., Khursigara, C.M., Subramaniam, S., and Hazelbauer, G.L. (2011) Chemotaxis kinase CheA is activated by three neighbouring chemoreceptor dimers as effectively as by receptor clusters. *Mol Microbiol* 79: 677–685.
- Li, M., Xu, X., Zou, X., and Hazelbauer, G.L. (2021) A Selective Tether Recruits Activated Response Regulator CheB to Its Chemoreceptor Substrate. *mBio* 12: e0310621.
- Li, X., Fleetwood, A.D., Bayas, C., Bilwes, A.M., Ortega, D.R., Falke, J.J., et al. (2013) The 3.2 Å resolution structure of a receptor: CheA:CheW signaling complex defines overlapping binding sites and key residue interactions within bacterial chemosensory arrays. *Biochemistry* 52: 3852–3865.
- Lin, L.N., Li, J., Brandts, J.F., and Weis, R.M. (1994) The serine receptor of bacterial chemotaxis exhibits half-site saturation for serine binding. *Biochemistry* 33: 6564–6570.
- Liu, J., Hu, B., Morado, D.R., Jani, S., Manson, M.D., and Margolin, W. (2012) Molecular architecture of chemoreceptor arrays revealed by cryoelectron tomography of *Escherichia coli* minicells. *Proc Natl Acad Sci U S A* 109: E1481-8.



- Liu, X., Zhang, R., and Yuan, J. (2022a) Suppression of cell-cell variation by cooperative interaction of phosphatase and response regulator. *Biophys J* 121: 319–326.
- Liu, Y., Sun, W., Ma, L., Xu, R., Yang, C., Xu, P., et al. (2022b) Metabolic Mechanism and Physiological Role of Glycerol 3-Phosphate in *Pseudomonas aeruginosa* PAO1. *mBio* e0262422.
- Lopes, J.G., and Sourjik, V. (2018) Chemotaxis of *Escherichia coli* to major hormones and polyamines present in human gut. *ISME J* 12: 2736–2747.
- López-Redondo, M.L., Moronta, F., Salinas, P., Espinosa, J., Cantos, R., Dixon, R., et al. (2010) Environmental control of phosphorylation pathways in a branched two-component system. *Mol Microbiol* 78: 475–489.
- Luu, R.A., Kootstra, J.D., Nesteryuk, V., Brunton, C.N., Parales, J.V., Ditty, J.L., and Parales, R.E. (2015) Integration of chemotaxis, transport and catabolism in *Pseudomonas putida* and identification of the aromatic acid chemoreceptor PcaY. *Mol Microbiol* 96: 134–147.
- Ma, X., Schloop, A., Swingle, B., and Perry, K.L. (2018) *Pectobacterium* and *Dickeya* Responsible for Potato Blackleg Disease in New York State in 2016. *Plant Dis* 102: 1834–1840.
- Machuca, M.A., Johnson, K.S., Liu, Y.C., Steer, D.L., Ottemann, K.M., and Roujeinikova, A. (2017) *Helicobacter pylori* chemoreceptor TlpC mediates chemotaxis to lactate. *Sci Rep* 7: 14089.
- Machuca, M.A., Liu, Y.C., Beckham, S.A., Gunzburg, M.J., and Roujeinikova, A. (2016) The crystal structure of the tandem-PAS sensing domain of *Campylobacter jejuni* chemoreceptor Tlp1 suggests indirect mechanism of ligand recognition. *J Struct Biol* 194: 205–213.
- Macnab, R.M., and Koshland Jr, D.E. (1972) The gradient-sensing mechanism in bacterial chemotaxis. *Proc Natl Acad Sci U S A* 69: 2509–2512.
- Maddox, D.A., and Harrison, M.D. (1988) Presence and population dynamics of *Erwinia carotovora* in irrigation water in south central Colorado. *J Appl Bacteriol* 64: 169–182.
- Mansfield, J., Genin, S., Magori, S., Citovsky, V., Sriariyanum, M., Ronald, P., et al. (2012) Top 10 plant pathogenic bacteria in molecular plant pathology. *Mol Plant Pathol* 13: 614–629.
- Manson, M.D. (2018) The Diversity of Bacterial Chemosensing. *Methods Mol Biol Clifton NJ* 1729: 3–6.
- Manson, M.D., Blank, V., Brade, G., and Higgins, C.F. (1986) Peptide chemotaxis in *E. coli* involves the Tap signal transducer and the dipeptide permease. *Nature* 321: 253–256.
- Mao, H., Cremer, P.S., and Manson, M.D. (2003) A sensitive, versatile microfluidic assay for bacterial chemotaxis. *Proc Natl Acad Sci U S A* 100: 5449–5454.
- Martínez-García, E., Nikel, P.I., Chavarría, M., and Lorenzo, V. de (2014) The metabolic cost of flagellar motion in *Pseudomonas putida* KT2440. *Environ Microbiol* 16: 291–303.
- Martín-Mora, D., Fernández, M., Velando, F., Ortega, Á., Gavira, J.A., Matilla, M.A., and Krell, T. (2018a) Functional annotation of bacterial signal transduction systems: Progress and challenges. *Int J Mol Sci* 19: 3755.
- Martín-Mora, D., Ortega, Á., Matilla, M.A., Martínez-Rodríguez, S., Gavira, J.A., and Krell, T. (2019) The molecular mechanism of nitrate chemotaxis via direct ligand binding to the PilJ domain of McpN. *MBio* 10: e02334-18.
- Martín-Mora, D., Ortega, Á., Pérez-Maldonado, F.J., Krell, T., and Matilla, M.A. (2018b) The activity of the C4-dicarboxylic acid chemoreceptor of *Pseudomonas aeruginosa* is controlled by chemoattractants and antagonists. *Sci Rep* 8: 2102.

- Martín-Mora, D., Ortega, A., Reyes-Darias, J.A., García, V., López-Farfán, D., Matilla, M.A., and Krell, T. (2016) Identification of a Chemoreceptor in *Pseudomonas aeruginosa* That Specifically Mediates Chemotaxis Toward  $\alpha$ -Ketoglutarate. *Front Microbiol* 7: 1937.
- Martín-Mora, D., Reyes-Darias, J.-A., Ortega, Á., Corral-Lugo, A., Matilla, M.A., and Krell, T. (2016b) McpQ is a specific citrate chemoreceptor that responds preferentially to citrate/metal ion complexes. *Environ Microbiol* 18: 3284–3295.
- Martín-Rodríguez, A.J., Higdon, S.M., Thorell, K., Tellgren-Roth, C., Sjöling, Å., Galperin, M.Y., et al. (2022) Comparative Genomics of Cyclic di-GMP Metabolism and Chemosensory Pathways in *Shewanella algae* Strains: Novel Bacterial Sensory Domains and Functional Insights into Lifestyle Regulation. *mSystems* 7: e0151821.
- Masduki, A., Nakamura, J., Ohga, T., Umezaki, R., Kato, J., and Ohtake, H. (1995) Isolation and characterization of chemotaxis mutants and genes of *Pseudomonas aeruginosa*. *J Bacteriol* 177: 948–952.
- Mashimo, M., Moriwaki, Y., Misawa, H., Kawashima, K., and Fujii, T. (2021) Regulation of Immune Functions by Non-Neuronal Acetylcholine (ACh) via Muscarinic and Nicotinic ACh Receptors. *Int J Mol Sci* 22: 6818.
- Matilla, M.A., Drew, A., Udaondo, Z., Krell, T., and Salmond, G.P.C. (2016) Genome Sequence of *Serratia plymuthica* A153, a Model Rhizobacterium for the Investigation of the Synthesis and Regulation of Haterumalides, Zeamine, and Andrimid. *Genome Announc* 4: e00373-16.
- Matilla, M.A., Genova, R., Martín-Mora, D., Maaß, S., Becher, D., and Krell, T. (2023) The Cellular Abundance of Chemoreceptors, Chemosensory Signaling Proteins, Sensor Histidine Kinases, and Solute Binding Proteins of *Pseudomonas aeruginosa* Provides Insight into Sensory Preferences and Signaling Mechanisms. *Int J Mol Sci* 24: 1363.
- Matilla, M.A., and Krell, T. (2018) The effect of bacterial chemotaxis on host infection and pathogenicity. *FEMS Microbiol Rev* 42,1: 10.1093/femsre/fux052.
- Matilla, M.A., and Krell, T. (2017) Chemoreceptor-based signal sensing. *Curr Opin Biotechnol* 45: 8–14.
- Matilla, M.A., and Krell, T. (2022) Noncanonical Sensing Mechanisms for *Bacillus subtilis* Chemoreceptors. *J Bacteriol* 204: e0002722.
- Matilla, M.A., Martín-Mora, D., Gavira, J.A., and Krell, T. (2021a) *Pseudomonas aeruginosa* as a Model To Study Chemosensory Pathway Signaling. *Microbiol Mol Biol Rev* 85: e00151-20.
- Matilla, M.A., Martín-Mora, D., and Krell, T. (2020) The use of isothermal titration calorimetry to unravel chemotactic signalling mechanisms. *Environ Microbiol* 22: 3005–3019.
- Matilla, M.A., Ortega, Á., and Krell, T. (2021b) The role of solute binding proteins in signal transduction. *Comput Struct Biotechnol J* 19: 1786–1805.
- Matilla, M.A., Velando, F., Martín-Mora, D., Monteagudo-Cascales, E., and Krell, T. (2022a) A catalogue of signal molecules that interact with sensor kinases, chemoreceptors and transcriptional regulators. *FEMS Microbiol Rev* 46: fuab043.
- Matilla, M.A., Velando, F., Tajuelo, A., Martín-Mora, D., Xu, W., Sourjik, V., et al. (2022b) Chemotaxis of the human pathogen *Pseudomonas aeruginosa* to the neurotransmitter acetylcholine. *mBio* e0345821.
- Matthews, B.W. (1968) Solvent content of protein crystals. *J Mol Biol* 33: 491–497.

- McCarter-Zorner, N.J., Franc, G.D., Harrison, M.D., Michaud, J.E., Quinn, C.E., Sells, I.A., and Graham, D.C. (1984) Soft rot *Erwinia* bacteria in surface and underground waters in southern Scotland and in Colorado, United States. *J Appl Bacteriol* 57: 95–105.
- McClune, C.J., Alvarez-Buylla, A., Voigt, C.A., and Laub, M.T. (2019) Engineering orthogonal signalling pathways reveals the sparse occupancy of sequence space. *Nature* 574: 702–706.
- McKellar, J.L., Minnell, J.J., and Gerth, M.L. (2015) A high-throughput screen for ligand binding reveals the specificities of three amino acid chemoreceptors from *Pseudomonas syringae* pv. actinidiae. *Mol Microbiol* 96: 694–707.
- Mears, P.J., Koirala, S., Rao, C.V., Golding, I., and Chemla, Y.R. (2014) *Escherichia coli* swimming is robust against variations in flagellar number. *Elife* 3: e01916.
- Mehan, R.S., White, N.C., and Falke, J.J. (2003) Mapping out regions on the surface of the aspartate receptor that are essential for kinase activation. *Biochemistry* 42: 2952–2959.
- Mendler, K., Chen, H., Parks, D.H., Lobb, B., Hug, L.A., and Doxey, A.C. (2019) AnnoTree: visualization and exploration of a functionally annotated microbial tree of life. *Nucleic Acids Res* 47: 4442–4448.
- Milburn, M.V., Privé, G.G., Milligan, D.L., Scott, W.G., Yeh, J., Jancarik, J., et al. (1991) Three-dimensional structures of the ligand-binding domain of the bacterial aspartate receptor with and without a ligand. *Science* 254: 1342–1347.
- Milligan, D.L., and Koshland, D.E. (1993) Purification and characterization of the periplasmic domain of the aspartate chemoreceptor. *J Biol Chem* 268: 19991–19997.
- Milo, R., Jorgensen, P., Moran, U., Weber, G., and Springer, M. (2010) BioNumbers--the database of key numbers in molecular and cell biology. *Nucleic Acids Res* 38: D750–753.
- Minamino, T., Kinoshita, M., and Namba, K. (2019) Directional switching mechanism of the bacterial flagellar motor. *Comput Struct Biotechnol J* 17: 1075–1081.
- Mise, T. (2016) Structural Analysis of the Ligand-Binding Domain of the Aspartate Receptor Tar from *Escherichia coli*. *Biochemistry* 55: 3708–3713.
- Mistry, J., Chuguransky, S., Williams, L., Qureshi, M., Salazar, G.A., Sonnhammer, E.L.L., et al. (2021) Pfam: The protein families database in 2021. *Nucleic Acids Res* 49: D412–D419.
- Moleki, L.N., Pretorius, R.G., Tanui, C.K., Mosina, G., and Theron, J. (2017) A quorum sensing-defective mutant of *Pectobacterium carotovorum* ssp. *brasiliense* 1692 is attenuated in virulence and unable to occlude xylem tissue of susceptible potato plant stems. *Mol Plant Pathol* 18: 32–44.
- Monteagudo-Cascales, E., Ortega, Á., Velando, F., Morel, B., Matilla, M.A., and Krell, T. (2023) Study of NIT domain-containing chemoreceptors from two global phytopathogens and identification of NIT domains in eukaryotes. *Mol Microbiol* mmi.15069.
- Morata, L., Cobos-Trigueros, N., Martínez, J.A., Soriano, A., Almela, M., Marco, F., et al. (2012) Influence of multidrug resistance and appropriate empirical therapy on the 30-day mortality rate of *Pseudomonas aeruginosa* bacteremia. *Antimicrob Agents Chemother* 56: 4833–4837.
- Morgan, R., Kohn, S., Hwang, S.-H., Hassett, D.J., and Sauer, K. (2006) BdlA, a chemotaxis regulator essential for biofilm dispersion in *Pseudomonas aeruginosa*. *J Bacteriol* 188: 7335–7343.
- Muff, T.J., and Ordal, G.W. (2008) The diverse CheC-type phosphatases: chemotaxis and beyond. *Mol Microbiol* 70: 1054–1061.

- Mugabo, Y., Zhao, S., Seifried, A., Gezzar, S., Al-Mass, A., Zhang, D., et al. (2016) Identification of a mammalian glycerol-3-phosphate phosphatase: Role in metabolism and signaling in pancreatic  $\beta$ -cells and hepatocytes. *Proc Natl Acad Sci U S A* 113: E430-439.
- Mulholland, V., Hinton, J.C., Sidebotham, J., Toth, I.K., Hyman, L.J., Pérombelon, M.C., et al. (1993) A pleiotropic reduced virulence (Rvi-) mutant of *Erwinia carotovora* subspecies *atroseptica* is defective in flagella assembly proteins that are conserved in plant and animal bacterial pathogens. *Mol Microbiol* 9: 343–356.
- Muok, A.R., Briegel, A., and Crane, B.R. (2020a) Regulation of the chemotaxis histidine kinase CheA: A structural perspective. *Biochim Biophys Acta Biomembr* 1862: 183030.
- Muok, A.R., Ortega, D.R., Kurniyati, K., Yang, W., Maschmann, Z.A., Sidi Mabrouk, A., et al. (2020b) Atypical chemoreceptor arrays accommodate high membrane curvature. *Nat Commun* 11: 5763.
- Murshudov, G.N., Skubák, P., Lebedev, A.A., Pannu, N.S., Steiner, R.A., Nicholls, R.A., et al. (2011) REFMAC5 for the refinement of macromolecular crystal structures. *Acta Crystallogr D Biol Crystallogr* 67: 355–367.
- Neumann, S., Grosse, K., and Sourjik, V. (2012) Chemotactic signaling via carbohydrate phosphotransferase systems in *Escherichia coli*. *Proc Natl Acad Sci U S A* 109: 12159–12164.
- Neumann, S., Hansen, C.H., Wingreen, N.S., and Sourjik, V. (2010) Differences in signalling by directly and indirectly binding ligands in bacterial chemotaxis. *EMBO J* 29: 3484–3495.
- Nguyen, A.H., Tomita, T., Hirota, M., Sato, T., and Kamio, Y. (1999) A simple purification method and morphology and component analyses for carotovoricin Er, a phage-tail-like bacteriocin from the plant pathogen *Erwinia carotovora* Er. *Biosci Biotechnol Biochem* 63: 1360–1369.
- Ni, B., Colin, R., Link, H., Endres, R.G., and Sourjik, V. (2020) Growth-rate dependent resource investment in bacterial motile behavior quantitatively follows potential benefit of chemotaxis. *Proc Natl Acad Sci U S A* 117: 595–601.
- Ni, B., Huang, Z., Fan, Z., Jiang, C.-Y., and Liu, S.-J. (2013) *Comamonas testosteroni* uses a chemoreceptor for tricarboxylic acid cycle intermediates to trigger chemotactic responses towards aromatic compounds. *Mol Microbiol* 90: 813–823.
- Nikel, P.I., Kim, J., and Lorenzo, V. de (2014) Metabolic and regulatory rearrangements underlying glycerol metabolism in *Pseudomonas putida* KT2440. *Environ Microbiol* 16: 239–254.
- Nishiyama, S., Suzuki, D., Itoh, Y., Suzuki, K., Tajima, H., Hyakutake, A., et al. (2012) Mlp24 (McpX) of *Vibrio cholerae* implicated in pathogenicity functions as a chemoreceptor for multiple amino acids. *Infect Immun* 80: 3170–8.
- Nishiyama, S., Takahashi, Y., Yamamoto, K., Suzuki, D., Itoh, Y., Sumita, K., et al. (2016) Identification of a *Vibrio cholerae* chemoreceptor that senses taurine and amino acids as attractants. *Sci Rep* 6: 20866.
- Obranić, S., Babić, F., and Maravić-Vlahoviček, G. (2013) Improvement of pBBR1MCS plasmids, a very useful series of broad-host-range cloning vectors. *Plasmid* 70: 263–267.
- Ohshima, N., Yamashita, S., Takahashi, N., Kuroishi, C., Shiro, Y., and Takio, K. (2008) *Escherichia coli* cytosolic glycerophosphodiester phosphodiesterase (UgpQ) requires Mg<sup>2+</sup>, Co<sup>2+</sup>, or Mn<sup>2+</sup> for its enzyme activity. *J Bacteriol* 190: 1219–1223.

- Oku, S., Komatsu, A., Nakashimada, Y., Tajima, T., and Kato, J. (2014) Identification of *Pseudomonas fluorescens* Chemotaxis Sensory Proteins for Malate, Succinate, and Fumarate, and Their Involvement in Root Colonization. *Microbes Environ* 29: 413–419.
- Oku, S., Komatsu, A., Tajima, T., Nakashimada, Y., and Kato, J. (2012) Identification of chemotaxis sensory proteins for amino acids in *Pseudomonas fluorescens* Pf0-1 and their involvement in chemotaxis to tomato root exudate and root colonization. *Microbes Environ* 27: 462–469.
- Okumura, H., Nishiyama, S., Sasaki, A., Homma, M., and Kawagishi, I. (1998) Chemotactic adaptation is altered by changes in the carboxy-terminal sequence conserved among the major methyl-accepting chemoreceptors. *J Bacteriol* 180: 1862–1868.
- O’Leary, N.A., Wright, M.W., Brister, J.R., Ciufu, S., Haddad, D., McVeigh, R., et al. (2016) Reference sequence (RefSeq) database at NCBI: current status, taxonomic expansion, and functional annotation. *Nucleic Acids Res* 44: D733-745.
- Oliveira, W.K., Ávila, H.L., Tadra, M.Z., Cardoso, R.L., Fadel-Pichet, C.M.T., Souza, E.M. de, et al. (2021) High Genomic Identity between Clinical and Environmental Strains of *Herbaspirillum frisingense* Suggests Pre-Adaptation to Different Hosts and Intrinsic Resistance to Multiple Drugs. *Antibiot Basel Switz* 10: 1409.
- O’Neal, L., Baraquet, C., Suo, Z., Dreifus, J.E., Peng, Y., Raivio, T.L., et al. (2022) The Wsp system of *Pseudomonas aeruginosa* links surface sensing and cell envelope stress. *Proc Natl Acad Sci U S A* 119: e2117633119.
- Orillard, E., and Watts, K.J. (2021) Deciphering the Che2 chemosensory pathway and the roles of individual Che2 proteins from *Pseudomonas aeruginosa*. *Mol Microbiol* 115: 222–237.
- Orr, A.A., Yang, J., Sule, N., Chawla, R., Hull, K.G., Zhu, M., et al. (2020) Molecular Mechanism for Attractant Signaling to DHMA by *E. coli* Tsr. *Biophys J* 118: 492–504.
- Ortega, Á., and Krell, T. (2014) The HBM domain: introducing bimodularity to bacterial sensing. *Protein Sci* 23: 332–336.
- Ortega, Á., and Krell, T. (2020) Chemoreceptors with C-terminal pentapeptides for CheR and CheB binding are abundant in bacteria that maintain host interactions. *Comput Struct Biotechnol J* 18: 1947–1955.
- Ortega, Á., Matilla, M.A., and Krell, T. (2022) The Repertoire of Solute-Binding Proteins of Model Bacteria Reveals Large Differences in Number, Type, and Ligand Range. *Microbiol Spectr* 10: e0205422.
- Ortega, Á., Zhulin, I.B., and Krell, T. (2017a) Sensory repertoire of bacterial chemoreceptors. *Microbiol Mol Biol Rev* 81,4: e00033-17.
- Ortega, D.R., Fleetwood, A.D., Krell, T., Harwood, C.S., Jensen, G.J., and Zhulin, I.B. (2017b) Assigning chemoreceptors to chemosensory pathways in *Pseudomonas aeruginosa*. *Proc Natl Acad Sci U S A* 114: 12809–12814.
- Ortega, D.R., Yang, W., Subramanian, P., Mann, P., Kjær, A., Chen, S., et al. (2020) Repurposing a chemosensory macromolecular machine. *Nat Commun* 11: 2041.
- Ortega, D.R., and Zhulin, I.B. (2016) Evolutionary Genomics Suggests That CheV Is an Additional Adaptor for Accommodating Specific Chemoreceptors within the Chemotaxis Signaling Complex. *PLoS Comput Biol* 12: e1004723.

- Ostovar, G., Naughton, K.L., and Boedicker, J.Q. (2020) Computation in bacterial communities. *Phys Biol* 17: 061002.
- Oswald, C., Smits, S.H.J., Höing, M., Sohn-Bösser, L., Dupont, L., Le Rudulier, D., et al. (2008) Crystal structures of the choline/acetylcholine substrate-binding protein ChoX from *Sinorhizobium meliloti* in the liganded and unliganded-closed states. *J Biol Chem* 283: 32848–32859.
- Painter, J., and Merritt, E.A. (2006a) TLSMD web server for the generation of multi-group TLS models. *J Appl Crystallogr* 39: 109–111.
- Painter, J., and Merritt, E.A. (2006b) Optimal description of a protein structure in terms of multiple groups undergoing TLS motion. *Acta Crystallogr D Biol Crystallogr* 62: 439–450.
- Panda, P., Vanga, B.R., Lu, A., Fiers, M., Fineran, P.C., Butler, R., et al. (2016) *Pectobacterium atrosepticum* and *Pectobacterium carotovorum* Harbor Distinct, Independently Acquired Integrative and Conjugative Elements Encoding Coronafacic Acid that Enhance Virulence on Potato Stems. *Front Microbiol* 7: 397.
- Parke, D., Ornston, L.N., and Nester, E.W. (1987) Chemotaxis to plant phenolic inducers of virulence genes is constitutively expressed in the absence of the Ti plasmid in *Agrobacterium tumefaciens*. *J Bacteriol* 169: 5336–5338.
- Parkinson, J.S., Hazelbauer, G.L., and Falke, J.J. (2015) Signaling and sensory adaptation in *Escherichia coli* chemoreceptors: 2015 update. *Trends Microbiol* 23: 257–266.
- Parks, D.H., Chuvochina, M., Waite, D.W., Rinke, C., Skarshewski, A., Chaumeil, P.A., and Hugenholtz, P. (2018) A standardized bacterial taxonomy based on genome phylogeny substantially revises the tree of life. *Nat Biotechnol* 36: 996–1004.
- Pasupuleti, S., Sule, N., Cohn, W.B., MacKenzie, D.S., Jayaraman, A., and Manson, M.D. (2014) Chemotaxis of *Escherichia coli* to norepinephrine (NE) requires conversion of NE to 3,4-dihydroxymandelic acid. *J Bacteriol* 196: 3992–4000.
- Pasupuleti, S., Sule, N., Manson, M.D., and Jayaraman, A. (2018) Conversion of Norepinephrine to 3,4-Dihydroxymandelic Acid in *Escherichia coli* Requires the QseBC Quorum-Sensing System and the FearR Transcription Factor. *J Bacteriol* 200: e00564-17.
- Perez, E., and Stock, A.M. (2007) Characterization of the *Thermotoga maritima* chemotaxis methylation system that lacks pentapeptide-dependent methyltransferase CheR:MCP tethering. *Mol Microbiol* 63: 363–378.
- Pérez-Mendoza, D., Coulthurst, S.J., Humphris, S., Campbell, E., Welch, M., Toth, I.K., and Salmond, G.P.C. (2011) A multi-repeat adhesin of the phytopathogen, *Pectobacterium atrosepticum*, is secreted by a Type I pathway and is subject to complex regulation involving a non-canonical diguanylate cyclase: Complex regulation of a *Pectobacterium* type I-secreted adhesin. *Mol Microbiol* 82: 719–733.
- Perkins, A., Tudorica, D.A., Amieva, M.R., Remington, S.J., and Guillemin, K. (2019) *Helicobacter pylori* senses bleach (HOCl) as a chemoattractant using a cytosolic chemoreceptor. *PLoS Biol* 17: e3000395.
- Pérombelon, M.C.M. (2002) Potato diseases caused by soft rot *erwinias*: an overview of pathogenesis. *Plant Pathol* 51: 1–12.
- Pesin, S.R., and Candia, O.A. (1982) Acetylcholine concentration and its role in ionic transport by the corneal epithelium. *Invest Ophthalmol Vis Sci* 22: 651–659.

- Petrova, O.E., Cherny, K.E., and Sauer, K. (2015) The diguanylate cyclase GcbA facilitates *Pseudomonas aeruginosa* biofilm dispersion by activating BdlA. *J Bacteriol* 197: 174–187.
- Petrova, O.E., and Sauer, K. (2012) PAS domain residues and prosthetic group involved in BdlA-dependent dispersion response by *Pseudomonas aeruginosa* biofilms. *J Bacteriol* 194: 5817–5828.
- Pham, H.T., and Parkinson, J.S. (2011) Phenol sensing by *Escherichia coli* chemoreceptors: a nonclassical mechanism. *J Bacteriol* 193: 6597–6604.
- Pineda-Molina, E., Reyes-Darias, J.-A., Lacal, J., Ramos, J.L., García-Ruiz, J.M., Gavira, J.A., and Krell, T. (2012) Evidence for chemoreceptors with bimodular ligand-binding regions harboring two signal-binding sites. *Proc Natl Acad Sci U S A* 109: 18926–18931.
- Pokkuluri, P.R., Dwulit-Smith, J., Duke, N.E., Wilton, R., Mack, J.C., Bearden, J., et al. (2013) Analysis of periplasmic sensor domains from *Anaeromyxobacter dehalogenans* 2CP-C: structure of one sensor domain from a histidine kinase and another from a chemotaxis protein. *Microbiologyopen* 2: 766–77.
- Porter, S.L., and Armitage, J.P. (2002) Phosphotransfer in *Rhodobacter sphaeroides* chemotaxis. *J Mol Biol* 324: 35–45.
- Pritchard, L., Humphris, S., Baeyen, S., Maes, M., Van Vaerenbergh, J., Elphinstone, J., et al. (2013) Draft Genome Sequences of Four *Dickeya dianthicola* and Four *Dickeya solani* Strains. *Genome Announc* 1: e00087-12.
- Raan, S. du, Coutinho, T.A., and Waals, J.E. van der (2016) Cardinal temperature differences, determined in vitro, between closely related species and subspecies of pectinolytic bacteria responsible for blackleg and soft rot on potatoes. *Eur J Plant Pathol* 144: 361–369.
- Rader, B.A., Wreden, C., Hicks, K.G., Sweeney, E.G., Ottemann, K.M., and Guillemin, K. (2011a) *Helicobacter pylori* perceives the quorum-sensing molecule AI-2 as a chemorepellent via the chemoreceptor TlpB. *Microbiol Read Engl* 157: 2445–2455.
- Rahman, H., King, R.M., Shewell, L.K., Semchenko, E.A., Hartley-Tassell, L.E., Wilson, J.C., et al. (2014) Characterisation of a multi-ligand binding chemoreceptor CcmL (Tlp3) of *Campylobacter jejuni*. *PLoS Pathog* 10: e1003822.
- Rahme, L.G., Ausubel, F.M., Cao, H., Drenkard, E., Goumnerov, B.C., Lau, G.W., et al. (2000) Plants and animals share functionally common bacterial virulence factors. *Proc Natl Acad Sci U S A* 97: 8815–8821.
- Raina, J.-B., Fernandez, V., Lambert, B., Stocker, R., and Seymour, J.R. (2019) The role of microbial motility and chemotaxis in symbiosis. *Nat Rev Microbiol* 17: 284–294.
- Ramos-González, M.I., and Molin, S. (1998) Cloning, sequencing, and phenotypic characterization of the *rpoS* gene from *Pseudomonas putida* KT2440. *J Bacteriol* 180: 3421–3431.
- Rapun-Araiz, B., Haag, A.F., De Cesare, V., Gil, C., Dorado-Morales, P., Penades, J.R., and Lasa, I. (2020) Systematic Reconstruction of the Complete Two-Component Sensorial Network in *Staphylococcus aureus*. *mSystems* 5: e00511-20.
- Rather, M.A., Gupta, K., and Mandal, M. (2021) Microbial biofilm: formation, architecture, antibiotic resistance, and control strategies. *Braz J Microbiol Publ Braz Soc Microbiol* 52: 1701–1718.
- Rebbapragada, A., Johnson, M.S., Harding, G.P., Zuccarelli, A.J., Fletcher, H.M., Zhulin, I.B., and Taylor, B.L. (1997) The Aer protein and the serine chemoreceptor Tsr independently sense

- intracellular energy levels and transduce oxygen, redox, and energy signals for *Escherichia coli* behavior. *Proc Natl Acad Sci U S A* 94: 10541–6.
- Reyes-Darias, J.A., García, V., Rico-Jiménez, M., Corral-Lugo, A., Lesouhaitier, O., Juárez-Hernández, D., et al. (2015a) Specific gamma-aminobutyrate chemotaxis in pseudomonads with different lifestyle. *Mol Microbiol* 97: 488–501.
- Reyes-Darias, J.A., Yang, Y., Sourjik, V., and Krell, T. (2015b) Correlation between signal input and output in PctA and PctB amino acid chemoreceptor of *Pseudomonas aeruginosa*. *Mol Microbiol* 96: 513–525.
- Richter, C., and Fineran, P.C. (2013) The subtype I-F CRISPR-Cas system influences pathogenicity island retention in *Pectobacterium atrosepticum* via crRNA generation and Csy complex formation. *Biochem Soc Trans* 41: 1468–1474.
- Rico, A., and Preston, G.M. (2008) *Pseudomonas syringae* pv. tomato DC3000 uses constitutive and apoplast-induced nutrient assimilation pathways to catabolize nutrients that are abundant in the tomato apoplast. *Mol Plant-Microbe Interact* MPMI 21: 269–282.
- Rico-Jiménez, M., Muñoz-Martínez, F., García-Fontana, C., Fernandez, M., Morel, B., Ortega, A., et al. (2013a) Paralogous chemoreceptors mediate chemotaxis towards protein amino acids and the non-protein amino acid gamma-aminobutyrate (GABA). *Mol Microbiol* 88: 1230–1243.
- Rico-Jiménez, M., Muñoz-Martínez, F., Krell, T., Gavira, J.A., and Pineda-Molina, E. (2013b) Purification, crystallization and preliminary crystallographic analysis of the ligand-binding regions of the PctA and PctB chemoreceptors from *Pseudomonas aeruginosa* in complex with amino acids. *Acta Crystallogr Sect F Struct Biol Cryst Commun* 69: 1431–1435.
- Rico-Jiménez, M., Reyes-Darias, J.A., Ortega, Á., Díez Peña, A.I., Morel, B., and Krell, T. (2016) Two different mechanisms mediate chemotaxis to inorganic phosphate in *Pseudomonas aeruginosa*. *Sci Rep* 6: 28967.
- Rico-Jiménez, M., Roca, A., Krell, T., and Matilla, M.A. (2022) A bacterial chemoreceptor that mediates chemotaxis to two different plant hormones. *Environ Microbiol* 24: 3580–3597.
- Río-Álvarez, I., Muñoz-Gómez, C., Navas-Vásquez, M., Martínez-García, P.M., Antúnez-Lamas, M., Rodríguez-Palenzuela, P., and López-Solanilla, E. (2015) Role of *Dickeya dadantii* 3937 chemoreceptors in the entry to *Arabidopsis* leaves through wounds. *Mol Plant Pathol* 16: 685–698.
- Rivera-Chávez, F., Winter, S.E., Lopez, C.A., Xavier, M.N., Winter, M.G., Nuccio, S.-P., et al. (2013) *Salmonella* uses energy taxis to benefit from intestinal inflammation. *PLoS Pathog* 9: e1003267.
- Roberts, M.A.J., Papachristodoulou, A., and Armitage, J.P. (2010) Adaptation and control circuits in bacterial chemotaxis. *Biochem Soc Trans* 38: 1265–1269.
- Robin, X., Haas, J., Gumienny, R., Smolinski, A., Tauriello, G., and Schwede, T. (2021) Continuous Automated Model EvaluatiOn (CAMEO)-Perspectives on the future of fully automated evaluation of structure prediction methods. *Proteins* 89: 1977–1986.
- Rodríguez-Palenzuela, P., Matas, I.M., Murillo, J., López-Solanilla, E., Bardaji, L., Pérez-Martínez, I., et al. (2010) Annotation and overview of the *Pseudomonas savastanoi* pv. *savastanoi* NCPPB 3335 draft genome reveals the virulence gene complement of a tumour-inducing pathogen of woody hosts. *Environ Microbiol* 12: 1604–1620.



- Römling, U., Bian, Z., Hammar, M., Sierralta, W.D., and Normark, S. (1998) Curli fibers are highly conserved between *Salmonella typhimurium* and *Escherichia coli* with respect to operon structure and regulation. *J Bacteriol* 180: 722–731.
- Roshchina, V.V. (2016) New Trends and Perspectives in the Evolution of Neurotransmitters in Microbial, Plant, and Animal Cells. *Adv Exp Med Biol* 874: 25–77.
- Rossi, E., Falcone, M., Molin, S., and Johansen, H.K. (2018) High-resolution in situ transcriptomics of *Pseudomonas aeruginosa* unveils genotype independent patho-phenotypes in cystic fibrosis lungs. *Nat Commun* 9: 3459.
- Roychoudhury, A. (2020) Neurotransmitter Acetylcholine Comes to the Plant Rescue. *J Mol Cell Biol Forecast* 3 (1).
- Salek, M.M., Carrara, F., Fernandez, V., Guasto, J.S., and Stocker, R. (2019) Bacterial chemotaxis in a microfluidic T-maze reveals strong phenotypic heterogeneity in chemotactic sensitivity. *Nat Commun* 10: 1877.
- Sambrook, J., Fritsch, E.F., and Maniatis, T. (1989) Molecular Cloning: A Laboratory Manual, 2nd edn. *Cold Spring Harbor Laboratory Press*, New York, NY, USA.
- Sanchis-López, C., Cerna-Vargas, J.P., Santamaría-Hernando, S., Ramos, C., Krell, T., Rodríguez-Palenzuela, P., et al. (2021a) Prevalence and Specificity of Chemoreceptor Profiles in Plant-Associated Bacteria. *mSystems* 6: e0095121.
- Santamaría-Hernando, S., López-Maroto, Á., Galvez-Roldán, C., Munar-Palmer, M., Monteagudo-Cascales, E., Rodríguez-Herva, J.-J., et al. (2022) *Pseudomonas syringae* pv. tomato infection of tomato plants is mediated by GABA and I-Pro chemoperception. *Mol Plant Pathol* 23: 1433–1445.
- Saxl, R.L., Anand, G.S., and Stock, A.M. (2001) Synthesis and biochemical characterization of a phosphorylated analogue of the response regulator CheB. *Biochemistry* 40: 12896–12903.
- Schrödinger, L. (2010) The PyMOL Molecular Graphics System, Version 1.3r1.
- Schweinitzer, T., Mizote, T., Ishikawa, N., Dudnik, A., Inatsu, S., Schreiber, S., et al. (2008) Functional characterization and mutagenesis of the proposed behavioral sensor TlpD of *Helicobacter pylori*. *J Bacteriol* 190: 3244–3255.
- Schweizer, H.P. (1992) Allelic exchange in *Pseudomonas aeruginosa* using novel ColE1-type vectors and a family of cassettes containing a portable oriT and the counter-selectable *Bacillus subtilis* sacB marker. *Mol Microbiol* 6: 1195–1204.
- Segall, J.E., Block, S.M., and Berg, H.C. (1986) Temporal comparisons in bacterial chemotaxis. *Proc Natl Acad Sci U S A* 83: 8987–8991.
- Sena-Vélez, M., Ferragud, E., Redondo, C., Graham, J.H., and Cubero, J. (2022) Chemotactic responses of *Xanthomonas* with different host ranges. *Microorganisms* 11: 43.
- Shine, M.B., Gao, Q.-M., Chowda-Reddy, R.V., Singh, A.K., Kachroo, P., and Kachroo, A. (2019a) Glycerol-3-phosphate mediates rhizobia-induced systemic signaling in soybean. *Nat Commun* 10: 5303.
- Shine, M.B., Xiao, X., Kachroo, P., and Kachroo, A. (2019b) Signaling mechanisms underlying systemic acquired resistance to microbial pathogens. *Plant Sci Int J Exp Plant Biol* 279: 81–86.
- Shinozawa, T., and Fukunaga, S. (1989) Acetylcholine inhibition of *Escherichia coli* chemotaxis for aspartate. *Microbiol Immunol* 33: 689–692.

- Shrestha, M., Compton, K.K., Mancl, J.M., Webb, B.A., Brown, A.M., Scharf, B.E., and Schubot, F.D. (2018) Structure of the sensory domain of McpX from *Sinorhizobium meliloti*, the first known bacterial chemotactic sensor for quaternary ammonium compounds. *Biochem J* 475: 3949–3962.
- Shu, C.J., Ulrich, L.E., and Zhulin, I.B. (2003) The NIT domain: a predicted nitrate-responsive module in bacterial sensory receptors. *Trends Biochem Sci* 28: 121–4.
- Shu, R., Yuan, C., Liu, B., Song, Y., Hou, L., Ren, P., et al. (2022) PAS domain-containing chemoreceptors influence the signal sensing and intestinal colonization of *Vibrio cholerae*. *Genes Basel* 13: 2224.
- Si, G., Yang, W., Bi, S., Luo, C., and Ouyang, Q. (2012) A parallel diffusion-based microfluidic device for bacterial chemotaxis analysis. *Lab Chip* 12: 1389–1394.
- Silversmith, R.E. (2010) Auxiliary phosphatases in two-component signal transduction. *Curr Opin Microbiol* 13: 177–183.
- Sindeldecker, D., and Stoodley, P. (2021) The many antibiotic resistance and tolerance strategies of *Pseudomonas aeruginosa*. *Biofilm* 3: 100056.
- Skelsey, P., Humphris, S.N., Campbell, E.J., and Toth, I.K. (2018) Threat of establishment of non-indigenous potato blackleg and tuber soft rot pathogens in Great Britain under climate change. *PLoS One* 13: e0205711.
- Slocum, M.K., and Parkinson, J.S. (1985) Genetics of methyl-accepting chemotaxis proteins in *Escherichia coli*: null phenotypes of the tar and tap genes. *J Bacteriol* 163: 586–594.
- Somavanshi, R., Ghosh, B., and Sourjik, V. (2016) Sugar Influx Sensing by the Phosphotransferase System of *Escherichia coli*. *PLoS Biol* 14: e2000074.
- Sourjik, V., and Berg, H.C. (2002a) Receptor sensitivity in bacterial chemotaxis. *Proc Natl Acad Sci U S A* 99: 123–127.
- Sourjik, V., and Berg, H.C. (2002b) Binding of the *Escherichia coli* response regulator CheY to its target measured in vivo by fluorescence resonance energy transfer. *Proc Natl Acad Sci U S A* 99: 12669–12674.
- Sourjik, V., and Berg, H.C. (2004) Functional interactions between receptors in bacterial chemotaxis. *Nature* 428: 437–441.
- Sourjik, V., Vaknin, A., Shimizu, T.S., and Berg, H.C. (2007) In vivo measurement by FRET of pathway activity in bacterial chemotaxis. *Methods Enzymol* 423: 365–391.
- Starkey, M., Hickman, J.H., Ma, L., Zhang, N., De Long, S., Hinz, A., et al. (2009) *Pseudomonas aeruginosa* rugose small-colony variants have adaptations that likely promote persistence in the cystic fibrosis lung. *J Bacteriol* 191: 3492–3503.
- Stasi, R., Neves, H.I., and Spira, B. (2019) Phosphate uptake by the phosphonate transport system PhnCDE. *BMC Microbiol* 19: 79.
- Stephenson, K., and Hoch, J.A. (2002) Evolution of signalling in the sporulation phosphorelay. *Mol Microbiol* 46: 297–304.
- Stewart, R.C. (1993) Activating and inhibitory mutations in the regulatory domain of CheB, the methyl-esterase in bacterial chemotaxis. *J Biol Chem* 268: 1921–1930.

- Stover, C.K., Pham, X.Q., Erwin, A.L., Mizoguchi, S.D., Warrenner, P., Hickey, M.J., et al. (2000) Complete genome sequence of *Pseudomonas aeruginosa* PAO1, an opportunistic pathogen. *Nature* 406: 959–964.
- Studdert, C.A., and Parkinson, J.S. (2004) Crosslinking snapshots of bacterial chemoreceptor squads. *Proc Natl Acad Sci U S A* 101: 2117–2122.
- Studdert, C.A., and Parkinson, J.S. (2005) Insights into the organization and dynamics of bacterial chemoreceptor clusters through in vivo crosslinking studies. *Proc Natl Acad Sci U S A* 102: 15623–15628.
- Suchanek, V.M., Esteban-López, M., Colin, R., Besharova, O., Fritz, K., and Sourjik, V. (2020) Chemotaxis and cyclic-di-GMP signalling control surface attachment of *Escherichia coli*. *Mol Microbiol* 113: 728–739.
- Sule, N., Pasupuleti, S., Kohli, N., Menon, R., Dangott, L.J., Manson, M.D., and Jayaraman, A. (2017) The Norepinephrine Metabolite 3,4-Dihydroxymandelic Acid Is Produced by the Commensal Microbiota and Promotes Chemotaxis and Virulence Gene Expression in Enterohemorrhagic *Escherichia coli*. *Infect Immun* 85: e00431-17.
- Sun, Z., Liu, Q., Qu, G., Feng, Y., and Reetz, M.T. (2019) Utility of B-Factors in Protein Science: Interpreting Rigidity, Flexibility, and Internal Motion and Engineering Thermostability. *Chem Rev* 119: 1626–1665.
- Swain, K.E., and Falke, J.J. (2007) Structure of the conserved HAMP domain in an intact, membrane-bound chemoreceptor: a disulfide mapping study. *Biochemistry* 46: 13684–13695.
- Swain, K.E., Gonzalez, M.A., and Falke, J.J. (2009) Engineered socket study of signaling through a four-helix bundle: evidence for a yin-yang mechanism in the kinase control module of the aspartate receptor. *Biochemistry* 48: 9266–9277.
- Szurmant, H., Bunn, M.W., Cho, S.H., and Ordal, G.W. (2004) Ligand-induced conformational changes in the *Bacillus subtilis* chemoreceptor McpB determined by disulfide crosslinking in vivo. *J Mol Biol* 344: 919–928.
- Taguchi, K., Fukutomi, H., Kuroda, A., Kato, J., and Ohtake, H. (1997) Genetic identification of chemotactic transducers for amino acids in *Pseudomonas aeruginosa*. *Microbiol Read Engl* 143 (Pt 10): 3223–3229.
- Taha, Elgamoudi, B.A., Andrianova, E.P., Haselhorst, T., Day, C.J., Hartley-Tassell, L.E., et al. (2022) Diverse sensory repertoire of paralogous chemoreceptors Tlp2, Tlp3, and Tlp4 in *Campylobacter jejuni*. *Microbiol Spectr* 10: e0364622.
- Tajima, H., Imada, K., Sakuma, M., Hattori, F., Nara, T., Kamo, N., et al. (2011) Ligand specificity determined by differentially arranged common ligand-binding residues in bacterial amino acid chemoreceptors Tsr and Tar. *J Biol Chem* 286: 42200–42210.
- Takahashi, Y., Nishiyama, S.-I., Sumita, K., Kawagishi, I., and Imada, K. (2019) Calcium Ions Modulate Amino Acid Sensing of the Chemoreceptor Mlp24 of *Vibrio cholerae*. *J Bacteriol* 201: e00779-18.
- Tan, H., West, J.A., Ramsay, J.P., Monson, R.E., Griffin, J.L., Toth, I.K., and Salmond, G.P.C. (2014) Comprehensive overexpression analysis of cyclic-di-GMP signalling proteins in the phytopathogen *Pectobacterium atrosepticum* reveals diverse effects on motility and virulence phenotypes. *Microbiol Read Engl* 160: 1427–1439.

- Tanui, C.K., Shyntum, D.Y., Sedibane, P.K., Bellieny-Rabelo, D., and Moleleki, L.N. (2021) *Pectobacterium brasiliense* 1692 chemotactic responses and the role of methyl-accepting chemotactic proteins in ecological fitness. *Front Plant Sci* 12: 650894.
- Tawarayama, K., Horie, R., Saito, S., Wagatsuma, T., Saito, K., and Oikawa, A. (2014a) Metabolite Profiling of Root Exudates of Common Bean under Phosphorus Deficiency. *Metabolites* 4: 599–611.
- Tawarayama, K., Horie, R., Shinano, T., Wagatsuma, T., Saito, K., and Oikawa, A. (2014b) Metabolite profiling of soybean root exudates under phosphorus deficiency. *Soil Sci Plant Nutr* 60: 679–694.
- Taylor, B.L., Zhulin, I.B., and Johnson, M.S. (1999) Aerotaxis and other energy-sensing behavior in bacteria. *Annu Rev Microbiol* 53: 103–128.
- Tecon, R., and Or, D. (2017) Biophysical processes supporting the diversity of microbial life in soil. *FEMS Microbiol Rev* 41: 599–623.
- Tohidifar, P., Bodhankar, G.A., Pei, S., Cassidy, C.K., Walukiewicz, H.E., Ordal, G.W., et al. (2020) The unconventional cytoplasmic sensing mechanism for ethanol chemotaxis in *Bacillus subtilis*. *MBio* 11,5 e02177-20.
- Toth, I.K. (2022) Microbe Profile: *Pectobacterium atrosepticum*: an enemy at the door. *Microbiology* 168 ,8: 10.1099/mic.0.001221.
- Toth, I.K., Barny, M., Brurberg, M.B., Condemine, G., Czajkowski, R., Elphinstone, J.G., et al. (2021) *Pectobacterium* and *Dickeya*: Environment to Disease Development. In *Plant Diseases Caused by Dickeya and Pectobacterium Species*. Van Gijsegem, F., Wolf, J.M. van der, and Toth, I.K. (eds). *Springer International Publishing*, Cham. pp. 39–84.
- Toth, I.K., Bell, K.S., Holeva, M.C., and Birch, P.R. (2003) Soft rot erwiniae: from genes to genomes. *Mol Plant Pathol* 4: 17–30.
- Toth, I.K., and Birch, P.R. (2005) Rotting softly and stealthily. *Curr Opin Plant Biol* 8: 424–429.
- Toth, I.K., Pritchard, L., and Birch, P.R.J. (2006) Comparative genomics reveals what makes an enterobacterial plant pathogen. *Annu Rev Phytopathol* 44: 305–336.
- Toth, I.K., Thorpe, C.J., Bentley, S.D., Mulholland, V., Hyman, L.J., Perombelon, M.C., and Salmond, G.P. (1999) Mutation in a gene required for lipopolysaccharide and enterobacterial common antigen biosynthesis affects virulence in the plant pathogen *Erwinia carotovora* subsp. *atroseptica*. *Mol Plant-Microbe Interact* MPMI 12: 499–507.
- Tretyn, A., Łukasiewicz-Rutkowska, H., and Kopcewicz, J. (1997) Isolation, purification and identification of acetylcholine in *Pharbitis nil* seedlings. *Acta Physiol Plant* 19: 303–309.
- Trueba, F.J., and Woldringh, C.L. (1980) Changes in cell diameter during the division cycle of *Escherichia coli*. *J Bacteriol* 142: 869–878.
- Tumewu, S.A., Matsui, H., Yamamoto, M., Noutoshi, Y., Toyoda, K., and Ichinose, Y. (2020) Requirement of  $\gamma$ -Aminobutyric Acid Chemotaxis for Virulence of *Pseudomonas syringae* pv. *tabaci* 6605. *Microbes Env* 35: ME20114.
- Tumewu, S.A., Matsui, H., Yamamoto, M., Noutoshi, Y., Toyoda, K., and Ichinose, Y. (2021) Identification of chemoreceptor proteins for amino acids involved in host plant infection in *Pseudomonas syringae* pv. *tabaci* 6605. *Microbiol Res* 253: 126869.

- Tunchai, M., Hida, A., Oku, S., Nakashimada, Y., Nikata, T., Tajima, T., and Kato, J. (2017a) Negative chemotaxis of *Ralstonia pseudosolanacearum* to maleate and identification of the maleate chemosensory protein. *J Biosci Bioeng* 124: 647–652.
- Tunchai, M., Hida, A., Oku, S., Nakashimada, Y., Tajima, T., and Kato, J. (2017b) Identification and characterization of chemosensors for d-malate, unnatural enantiomer of malate, in *Ralstonia pseudosolanacearum*. *Microbiol Read Engl* 163: 233–242.
- Tunchai, M., Hida, A., Oku, S., Tajima, T., and Kato, J. (2021) Chemotactic disruption as a method to control bacterial wilt caused by *Ralstonia pseudosolanacearum*. *Biosci Biotechnol Biochem* 85: 697–702.
- Turner, L., Ryu, W.S., and Berg, H.C. (2000) Real-time imaging of fluorescent flagellar filaments. *J Bacteriol* 182: 2793–2801.
- Uda, K., Edashige, Y., Nishimura, R., Shikano, Y., Matsui, T., Radkov, A.D., and Moe, L.A. (2020) Distribution and evolution of the serine/aspartate racemase family in plants. *Phytochemistry* 169: 112164.
- Ud-Din, A., Khan, M.F., and Roujeinikova, A. (2020) Broad Specificity of Amino Acid Chemoreceptor CtaA of *Pseudomonas fluorescens* Is Afforded by Plasticity of Its Amphipathic Ligand-Binding Pocket. *Mol Plant Microbe Interact* 33: 612–623.
- Ulrich, L.E., Koonin, E.V., and Zhulin, I.B. (2005) One-component systems dominate signal transduction in prokaryotes. *Trends Microbiol* 13: 52–56.
- Ulrich, L.E., and Zhulin, I.B. (2005) Four-helix bundle: a ubiquitous sensory module in prokaryotic signal transduction. *Bioinformatics* 21 Suppl 3: iii45-8.
- Umemura, T., Matsumoto, Y., Ohnishi, K., Homma, M., and Kawagishi, I. (2002) Sensing of cytoplasmic pH by bacterial chemoreceptors involves the linker region that connects the membrane-spanning and the signal-modulating helices. *J Biol Chem* 277: 1593–1598.
- Upadhyay, A.A., Fleetwood, A.D., Adebali, O., Finn, R.D., and Zhulin, I.B. (2016) Cache Domains That are Homologous to, but Different from PAS Domains Comprise the Largest Superfamily of Extracellular Sensors in Prokaryotes. *PLoS Comput Biol* 12: e1004862.
- Vagin, A., and Teplyakov, A. (2010) Molecular replacement with MOLREP. *Acta Crystallogr D Biol Crystallogr* 66: 22–25.
- Vaknin, A., and Berg, H.C. (2006) Osmotic stress mechanically perturbs chemoreceptors in *Escherichia coli*. *Proc Natl Acad Sci U S A* 103: 592–596.
- Van Gijsegem, F., Hugouvieux-Cotte-Pattat, N., Kraepiel, Y., Lojkowska, E., Moleleki, L.N., Gorshkov, V., and Yedidia, I. (2021) Molecular Interactions of *Pectobacterium* and *Dickeya* with Plants. In *Plant Diseases Caused by Dickeya and Pectobacterium Species*. Van Gijsegem, F., Wolf, J.M. van der, and Toth, I.K. (eds). *Springer International Publishing*, Cham. pp. 85–147.
- Velando, F., Gavira, J.A., Rico-Jimenez, M., Matilla, M.A., and Krell, T. (2020) Evidence for Pentapeptide-Dependent and Independent CheB Methylsterases. *Int J Mol Sci* 21: E8459.
- Velankar, S., Alhroub, Y., Best, C., Caboche, S., Conroy, M.J., Dana, J.M., et al. (2012) PDBe: Protein Data Bank in Europe. *Nucleic Acids Res* 40: D445-452.
- Vladimirov, N., and Sourjik, V. (2009) Chemotaxis: how bacteria use memory. *Biol Chem* 390: 1097–1104.

- Wadhams, G.H., and Armitage, J.P. (2004) Making sense of it all: bacterial chemotaxis. *Nat Rev Mol Cell Biol* 5: 1024–1037.
- Waite, A.J., Frankel, N.W., and Emonet, T. (2018) Behavioral Variability and Phenotypic Diversity in Bacterial Chemotaxis. *Annu Rev Biophys* 47: 595–616.
- Walker, T.S., Bais, H.P., Déziel, E., Schweizer, H.P., Rahme, L.G., Fall, R., and Vivanco, J.M. (2004) *Pseudomonas aeruginosa*-plant root interactions. Pathogenicity, biofilm formation, and root exudation. *Plant Physiol* 134: 320–331.
- Waterhouse, A., Bertoni, M., Bienert, S., Studer, G., Tauriello, G., Gumienny, R., et al. (2018) SWISS-MODEL: homology modelling of protein structures and complexes. *Nucleic Acids Res* 46: W296–W303.
- Waterhouse, A.M., Procter, J.B., Martin, D.M., Clamp, M., and Barton, G.J. (2009) Jalview Version 2--a multiple sequence alignment editor and analysis workbench. *Bioinformatics* 25: 1189–91.
- Watts, K.J., Johnson, M.S., and Taylor, B.L. (2011) Different conformations of the kinase-on and kinase-off signaling states in the Aer HAMP domain. *J Bacteriol* 193: 4095–4103.
- Watts, K.J., Vaknin, A., Fuqua, C., and Kazmierczak, B.I. (2019) New twists and turns in Bacterial Locomotion and Signal Transduction. *J Bacteriol* 201,20 e00439-19.
- Webb, B.A., Compton, K.K., Del Campo, J.S.M., Taylor, D., Sobrado, P., and Scharf, B.E. (2017a) *Sinorhizobium meliloti* Chemotaxis to Multiple Amino Acids Is Mediated by the Chemoreceptor McpU. *Mol Plant Microbe Interact* 30: 770–777.
- Webb, B.A., Karl Compton, K., Castañeda Saldaña, R., Arapov, T.D., Keith Ray, W., Helm, R.F., and Scharf, B.E. (2017b) *Sinorhizobium meliloti* chemotaxis to quaternary ammonium compounds is mediated by the chemoreceptor McpX. *Mol Microbiol* 103: 333–346.
- Weinstein, L.I., Revuelta, A., and Pando, R.H. (2015) Catecholamines and acetylcholine are key regulators of the interaction between microbes and the immune system. *Ann N Y Acad Sci* 1351: 39–51.
- Wessler, I., Kirkpatrick, C.J., and Racké, K. (1999) The cholinergic “pitfall”: acetylcholine, a universal cell molecule in biological systems, including humans. *Clin Exp Pharmacol Physiol* 26: 198–205.
- West, A.H., Martinez-Hackert, E., and Stock, A.M. (1995) Crystal structure of the catalytic domain of the chemotaxis receptor methylesterase, CheB. *J Mol Biol* 250: 276–290.
- Whitchurch, C.B., Leech, A.J., Young, M.D., Kennedy, D., Sargent, J.L., Bertrand, J.J., et al. (2004) Characterization of a complex chemosensory signal transduction system which controls twitching motility in *Pseudomonas aeruginosa*. *Mol Microbiol* 52: 873–893.
- Whitman, W.B., Coleman, D.C., and Wiebe, W.J. (1998) Prokaryotes: the unseen majority. *Proc Natl Acad Sci U S A* 95: 6578–6583.
- Willett, J.W., and Kirby, J.R. (2011) CrdS and CrdA comprise a two-component system that is cooperatively regulated by the Che3 chemosensory system in *Myxococcus xanthus*. *MBio* 2,4 e00110-11.
- Williams, C.J., Headd, J.J., Moriarty, N.W., Prisant, M.G., Videau, L.L., Deis, L.N., et al. (2018) MolProbity: More and better reference data for improved all-atom structure validation. *Protein Sci Publ Protein Soc* 27: 293–315.
- Winn, M.D., Ballard, C.C., Cowtan, K.D., Dodson, E.J., Emsley, P., Evans, P.R., et al. (2011) Overview of the CCP4 suite and current developments. *Acta Crystallogr D Biol Crystallogr* 67: 235–242.

- Wolf, J.M. van der, Acuña, I., De Boer, S.H., Brurberg, M.B., Cahill, G., Charkowski, A.O., et al. (2021) Diseases Caused by *Pectobacterium* and *Dickeya* Species Around the World. In Plant Diseases Caused by *Dickeya* and *Pectobacterium* Species. Van Gijsegem, F., Wolf, J.M. van der, and Toth, I.K. (eds). *Springer International Publishing*, Cham. pp. 215–261.
- Wood, D.W., Setubal, J.C., Kaul, R., Monks, D.E., Kitajima, J.P., Okura, V.K., et al. (2001) The genome of the natural genetic engineer *Agrobacterium tumefaciens* C58. *Science* 294: 2317–2323.
- Woodcock, D.M., Crowther, P.J., Doherty, J., Jefferson, S., DeCruz, E., Noyer-Weidner, M., et al. (1989) Quantitative evaluation of *Escherichia coli* host strains for tolerance to cytosine methylation in plasmid and phage recombinants. *Nucleic Acids Res* 17: 3469–3478.
- Wu, H., Kato, J., Kuroda, A., Ikeda, T., Takiguchi, N., and Ohtake, H. (2000) Identification and characterization of two chemotactic transducers for inorganic phosphate in *Pseudomonas aeruginosa*. *J Bacteriol* 182: 3400–3404.
- Wu, J., Li, J., Li, G., Long, D.G., and Weis, R.M. (1996) The receptor binding site for the methyltransferase of bacterial chemotaxis is distinct from the sites of methylation. *Biochemistry* 35: 4984–4993.
- Wu, R., Gu, M., Wilton, R., Babnigg, G., Kim, Y., Pokkuluri, P.R., et al. (2013) Insight into the sporulation phosphorelay: crystal structure of the sensor domain of *Bacillus subtilis* histidine kinase, KinD. *Protein Sci Publ Protein Soc* 22: 564–576.
- Wuichet, K., Alexander, R.P., and Zhulin, I.B. (2007) Comparative genomic and protein sequence analyses of a complex system controlling bacterial chemotaxis. *Methods Enzym* 422: 1–31.
- Wuichet, K., and Zhulin, I.B. (2010) Origins and diversification of a complex signal transduction system in prokaryotes. *Sci Signal* 3: ra50.
- Wuttge, S., Bommer, M., Jäger, F., Martins, B.M., Jacob, S., Licht, A., et al. (2012) Determinants of substrate specificity and biochemical properties of the sn-glycerol-3-phosphate ATP binding cassette transporter (UgpB-AEC2) of *Escherichia coli*. *Mol Microbiol* 86: 908–920.
- wwPDB consortium, Burley, S.K., Berman, H.M., Bhikadiya, C., Bi, C., Chen, L., et al. (2019) Protein Data Bank: the single global archive for 3D macromolecular structure data. *Nucleic Acids Res* 47: D520–D528.
- Xie, L., Altindal, T., Chattopadhyay, S., and Wu, X.-L. (2011) From the Cover: Bacterial flagellum as a propeller and as a rudder for efficient chemotaxis. *Proc Natl Acad Sci U S A* 108: 2246–2251.
- Xin, X.-F., and He, S.Y. (2013) *Pseudomonas syringae* pv. tomato DC3000: a model pathogen for probing disease susceptibility and hormone signaling in plants. *Annu Rev Phytopathol* 51: 473–498.
- Xu, K., Wang, L., Xiong, D., Chen, H., Tong, X., Shao, X., et al. (2022) The Wsp chemosensory system modulates c-di-GMP-dependent biofilm formation by integrating DSF quorum sensing through the WspR-RpfG complex in *Lyso bacter*. *NPJ Biofilms Microbiomes* 8: 97.
- Xu, L., Naylor, D., Dong, Z., Simmons, T., Pierroz, G., Hixson, K.K., et al. (2018) Drought delays development of the sorghum root microbiome and enriches for monoderm bacteria. *Proc Natl Acad Sci U S A* 115: E4284–E4293.
- Xu, L., Xin, L., Zeng, Y., Yam, J.K., Ding, Y., Venkataramani, P., et al. (2016) A cyclic di-GMP-binding adaptor protein interacts with a chemotaxis methyltransferase to control flagellar motor switching. *Sci Signal* 9: ra102.

- Xu, N., Wang, M., Yang, X., Xu, Y., and Guo, M. (2020) In silico analysis of the chemotactic system of *Agrobacterium tumefaciens*. *Microb Genom* 6,11: mgen000460.
- Yang, K., Wang, M., and Metcalf, W.W. (2009) Uptake of glycerol-2-phosphate via the ugp-encoded transporter in *Escherichia coli* K-12. *J Bacteriol* 191: 4667–4670.
- Yang, S., Peng, Q., San Francisco, M., Wang, Y., Zeng, Q., and Yang, C.-H. (2008) Type III Secretion System Genes of *Dickeya dadantii* 3937 Are Induced by Plant Phenolic Acids. *PLoS ONE* 3: e2973.
- Yang, W., Alvarado, A., Glatter, T., Ringgaard, S., and Briegel, A. (2018) Baseplate variability of *Vibrio cholerae* chemoreceptor arrays. *Proc Natl Acad Sci U S A* 115: 13365–13370.
- Yang, W., and Briegel, A. (2020) Diversity of Bacterial Chemosensory Arrays. *Trends Microbiol* 28: 68–80.
- Yao, J., and Allen, C. (2007) The plant pathogen *Ralstonia solanacearum* needs aerotaxis for normal biofilm formation and interactions with its tomato host. *J Bacteriol* 189: 6415–6424.
- Ye, J., Gao, M., Zhou, Q., Wang, H., Xu, N., and Guo, M. (2021) The only chemoreceptor encoded by the operon affects the chemotactic response of *Agrobacterium* to various chemoeffectors. *Microorganisms* 9: 1923.
- Yi, X., and Weis, R.M. (2002) The receptor docking segment and S-adenosyl-L-homocysteine bind independently to the methyltransferase of bacterial chemotaxis. *Biochim Biophys Acta* 1596: 28–35.
- Yu, D., Ma, X., Tu, Y., and Lai, L. (2015) Both piston-like and rotational motions are present in bacterial chemoreceptor signaling. *Sci Rep* 5: 8640.
- Zatakia, H.M., Arapov, T.D., Meier, V.M., and Scharf, B.E. (2018) Cellular Stoichiometry of Methyl-Accepting Chemotaxis Proteins in *Sinorhizobium meliloti*. *J Bacteriol* 200: e00614-17.
- Zhang, L., Li, S., Liu, X., Wang, Z., Jiang, M., Wang, R., et al. (2020) Sensing of autoinducer-2 by functionally distinct receptors in prokaryotes. *Nat Commun* 11: 5371.
- Zhang, Y., Gardina, P.J., Kuebler, A.S., Kang, H.S., Christopher, J.A., and Manson, M.D. (1999) Model of maltose-binding protein/chemoreceptor complex supports intrasubunit signaling mechanism. *Proc Natl Acad Sci U S A* 96: 939–944.
- Zhao, R., Collins, E.J., Bourret, R.B., and Silversmith, R.E. (2002) Structure and catalytic mechanism of the *E. coli* chemotaxis phosphatase CheZ. *Nat Struct Biol* 9: 570–575.
- Zhulin, I.B. (2016) Classic Spotlight: Genetics of *Escherichia coli* Chemotaxis. *J Bacteriol* 198: 3041.
- Zhulin, I.B., Nikolskaya, A.N., and Galperin, M.Y. (2003) Common extracellular sensory domains in transmembrane receptors for diverse signal transduction pathways in bacteria and archaea. *J Bacteriol* 185: 285–294.
- Zschiedrich, C.P., Keidel, V., and Szurmant, H. (2016) Molecular Mechanisms of Two-Component Signal Transduction. *J Mol Biol* 428: 3752–3775.



